

TABLE OF CONTENTS

	Page
INTRODUCTION	1
CHAPTER 1 BACKGROUND AND LITERATURE SURVEY	4
CHAPTER 2 THEORY	11
2.1 General.....	11
2.2 Theoretical analysis of reflection from a flat wall	13
2.3 Reflection from other surfaces.....	32
2.4 Summary and evaluation of analysis results.....	35
CHAPTER 3 EXPERIMENTAL RESULTS.....	38
3.1 General.....	38
3.2 Experimental results.....	39
3.2.1 Measurement methods	39
3.2.2 Results.....	42
3.2.3 Summary and analysis of experimental results.....	80
CHAPTER 4 APPLICATIONS.....	81
4.1 Propagation models for practical channels	81
4.2 Estimation of link availability.....	82
4.3 Example of outage area prediction	87
CHAPTER 5 EFFECTS OF SINGLE DOMINANT REFLECTION ON SIGNAL MODULATION.....	96
5.1 General.....	96
5.2 Mathematical models of modulated signals.....	98
5.3 Delay and doppler effects	99
5.4 Effect of reflections on modulated signals.....	100
5.5 Effects of single dominant reflection on signal spectrum.....	104
5.6 Effects of single dominant reflection on receiver synchronization	105

5.6.1	Aspects of synchronization	105
5.6.2	Steady state timing and carrier recovery phase errors due to single reflection.....	109
5.7	Direct sequence spread spectrum systems	111
5.8	OFDM systems	113
5.9	Performance of other receivers	116
CONCLUSIONS.....		120
ANNEX	QPSK TIMING AND CARRIER RECOVERY SIMULATIONS.....	123
REFERENCES		165

LIST OF FIGURES

		Page
Figure 2.1	Propagation model.	14
Figure 2.2	Vertical electric field magnitude, 10m × 10 m wall.	22
Figure 2.3	Vertical electric field magnitude, 10 m × 20 m wall.	23
Figure 2.4	Vertical electric field magnitude, 20m × 10 m wall.	24
Figure 2.5	Planar X-Y electric field distribution, 10m × 10m wall. X scale in m, wall extends from x = 6 to 16; Y scale in m from top, wall located at y = -3.	25
Figure 2.6	Vertical electric field magnitude, 10 m × 10 m wall, ground reflection. Red: direct field, Black: reflected field.	30
Figure 2.7	Vertical electric field magnitude, 10 m × 20 m wall, ground reflection. Red: direct field, Black: reflected field.	31
Figure 2.8	Vertical electric field magnitude, 20 m × 10 m wall, ground reflection. Red: direct field, Black: reflected field.	32
Figure 3.1	Experimental link configuration.	40
Figure 3.2	QPSK receiver.	41
Figure 3.3	Binary FM receiver.	41
Figure 3.4	Distribution of error rates, suburban and rural links.	43
Figure 3.5	Mobile close to a building.	44
Figure 3.6	RF spectrum (18 February 2005).	45
Figure 3.7	RF spectrum (18 February 2005).	46
Figure 3.8	IF spectrum (18 February 2005).	47
Figure 3.9	IF spectrum (18 February 2005).	48
Figure 3.10	IF spectrum (18 February 2005).	49
Figure 3.11	Spectrum analysis (a & b).	52

Figure 3.12	Spectrum analysis (a & b).....	53
Figure 3.13	Spectrum analysis (a & b).....	54
Figure 3.14	Spectrum analysis (a & b).....	55
Figure 3.15	Spectrum analysis (a & b).....	56
Figure 3.16	RF level variation with time, slow random variations (18 February 2005).	59
Figure 3.17	RF level variation with time, random variations (18 February 2005).	60
Figure 3.18	RF level variation with time, small single reflection (18 February 2005).....	61
Figure 3.19	RF level variation with time, small single reflection (18 February 2005).....	62
Figure 3.20	IF level variation with time (18 February 2005).....	63
Figure 3.21	IF level variation with time (18 February 2005).....	64
Figure 3.22	IF level variation with time (18 February 2005).....	65
Figure 3.23	IF level variation with time (18 February 2005).....	66
Figure 3.24	IF level variation with time (18 February 2005).....	67
Figure 3.25	IF level variation with time (18 February 2005).....	68
Figure 3.26	IF level variation with time (18 February 2005).....	69
Figure 3.27	Transmitted pulses (reference) (23 December 2004).....	71
Figure 3.28	Transmitted pulse spectrum (23 December 2004).	72
Figure 3.29	Received pulse (23 December 2004).	73
Figure 3.30	Received pulse (23 December 2004).	74
Figure 3.31	Received pulse (23 December 2004).	75
Figure 3.32	Received pulse (23 December 2004).	76
Figure 3.33	Received pulse (23 December 2004).	77
Figure 3.34	Received pulse (23 December 2004).	78
Figure 3.35	Received pulse (23 December 2004).	79

Figure 4.1	Reflection delay geometry.....	84
Figure 4.2	Outage area estimation.....	86
Figure 4.3	Test route of the mobile (© Google 2009).....	88
Figure 4.4	Magnified mobile route 1 (© Google 2009).....	90
Figure 4.5	Magnified mobile route 2 (© Google 2009).....	91
Figure 4.6	Magnified mobile route 3 (© Google 2009).....	92
Figure 4.7	Magnified mobile route 4 (© Google 2009).....	93
Figure 4.8	Magnified mobile route 5 (© Google 2009).....	94
Figure 5.1	Standard receiver model.....	102
Figure 5.2	Typical timing recovery function for QPSK.....	106
Figure 5.3	QPSK constellation.....	108
Figure A.1	Delay 0.0 symbols. a) average carrier phase error; b) received signal power; c) average timing phase error; d) peak timing phase detector output.....	123
Figure A.2	Delay 0.0 symbols. a) average carrier phase error; b) received signal power; c) average timing phase error; d) peak timing phase detector output.....	124
Figure A.3	Delay 0.1 symbols. a) average carrier phase error; b) received signal power; c) average timing phase error; d) peak timing phase detector output.....	125
Figure A.4	Delay 0.1 symbols. a) average carrier phase error; b) received signal power; c) average timing phase error; d) peak timing phase detector output.....	126
Figure A.5	Delay 0.2 symbols. a) average carrier phase error; b) received signal power; c) average timing phase error; d) peak timing phase detector output.....	127
Figure A.6	Delay 0.2 symbols. a) average carrier phase error; b) received signal power; c) average timing phase error; d) peak timing phase detector output.....	128

Figure A.7 Delay 0.3 symbols. a) average carrier phase error; b) received signal power; c) average timing phase error; d) peak timing phase detector output. 129

Figure A.8 Delay 0.3 symbols. a) average carrier phase error; b) received signal power; c) average timing phase error; d) peak timing phase detector output. 130

Figure A.9 Delay 0.4 symbols. a) average carrier phase error; b) received signal power; c) average timing phase error; d) peak timing phase detector output. 131

Figure A.10 Delay 0.4 symbols. a) average carrier phase error; b) received signal power; c) average timing phase error; d) peak timing phase detector output. 132

Figure A.11 Delay 0.5 symbols. a) average carrier phase error; b) received signal power; c) average timing phase error; d) peak timing phase detector output. 133

Figure A.12 Delay 0.5 symbols. a) average carrier phase error; b) received signal power; c) average timing phase error; d) peak timing phase detector output. 134

Figure A.13 Delay 0.6 symbols. a) average carrier phase error; b) received signal power; c) average timing phase error; d) peak timing phase detector output. 135

Figure A.14 Delay 0.6 symbols. a) average carrier phase error; b) received signal power; c) average timing phase error; d) peak timing phase detector output. 136

Figure A.15 Delay 0.7 symbols. a) average carrier phase error; b) received signal power; c) average timing phase error; d) peak timing phase detector output. 137

Figure A.16 Delay 0.7 symbols. a) average carrier phase error; b) received signal power; c) average timing phase error; d) peak timing phase detector output. 138

Figure A.17 Delay 0.8 symbols. a) average carrier phase error; b) received signal power; c) average timing phase error; d) peak timing phase detector output. 139

Figure A.18 Delay 0.8 symbols. a) average carrier phase error; b) received signal power; c) average timing phase error; d) peak timing phase detector output. 140

Figure A.19	Delay 0.9 symbols. a) average carrier phase error; b) received signal power; c) average timing phase error; d) peak timing phase detector output.	141
Figure A. 20	Delay 0.9 symbols. a) average carrier phase error; b) received signal power; c) average timing phase error; d) peak timing phase detector output.	142
Figure A.21	Delay 1.0 symbols. a) average carrier phase error; b) received signal power; c) average timing phase error; d) peak timing phase detector output.	143
Figure A.22	Delay 1.0 symbols. a) average carrier phase error; b) received signal power; c) average timing phase error; d) peak timing phase detector output.	144
Figure A.23	Delay 1.1 symbols. a) average carrier phase error; b) received signal power; c) average timing phase error; d) peak timing phase detector output.	145
Figure A.24	Delay 1.1 symbols. a) average carrier phase error; b) received signal power; c) average timing phase error; d) peak timing phase detector output.	146
Figure A.25	Delay 1.2 symbols. a) average carrier phase error; b) received signal power; c) average timing phase error; d) peak timing phase detector output.	147
Figure A.26	Delay 1.2 symbols. a) average carrier phase error; b) received signal power; c) average timing phase error; d) peak timing phase detector output.	148
Figure A.27	Delay 1.3 symbols. a) average carrier phase error; b) received signal power; c) average timing phase error; d) peak timing phase detector output.	149
Figure A.28	Delay 1.3 symbols. a) average carrier phase error; b) received signal power; c) average timing phase error; d) peak timing phase detector output.	150
Figure A.29	Delay 1.4 symbols. a) average carrier phase error; b) received signal power; c) average timing phase error; d) peak timing phase detector output.	151
Figure A.30	Delay 1.4 symbols. a) average carrier phase error; b) received signal power; c) average timing phase error; d) peak timing phase detector output.	152

Figure A.31	Delay 1.5 symbols. a) average carrier phase error; b) received signal power; c) average timing phase error; d) peak timing phase detector output.	153
Figure A.32	Delay 1.5 symbols. a) average carrier phase error; b) received signal power; c) average timing phase error; d) peak timing phase detector output.	154
Figure A.33	Delay 1.6 symbols. a) average carrier phase error; b) received signal power; c) average timing phase error; d) peak timing phase detector output.	155
Figure A.34	Delay 1.6 symbols. a) average carrier phase error; b) received signal power; c) average timing phase error; d) peak timing phase detector output.	156
Figure A.35	Delay 1.7 symbols. a) average carrier phase error; b) received signal power; c) average timing phase error; d) peak timing phase detector output.	157
Figure A.36	Delay 1.7 symbols. a) average carrier phase error; b) received signal power; c) average timing phase error; d) peak timing phase detector output.	158
Figure A.37	Delay 1.8 symbols. a) average carrier phase error; b) received signal power; c) average timing phase error; d) peak timing phase detector output.	159
Figure A.38	Delay 1.8 symbols. a) average carrier phase error; b) received signal power; c) average timing phase error; d) peak timing phase detector output.	160
Figure A.39	Delay 1.9 symbols. a) average carrier phase error; b) received signal power; c) average timing phase error; d) peak timing phase detector output.	161
Figure A.40	Delay 1.9 symbols. a) average carrier phase error; b) received signal power; c) average timing phase error; d) peak timing phase detector output.	162
Figure A.41	Delay 2.0 symbols. a) average carrier phase error; b) received signal power; c) average timing phase error; d) peak timing phase detector output.	163
Figure A.42	Delay 2.0 symbols. a) average carrier phase error; b) received signal power; c) average timing phase error; d) peak timing phase detector output.	164

LIST OF ABBREVIATIONS AND ACRONYMS

AGC	Automatic gain control
BPSK	Binary phase shift keying
CDMA	Code division multiple access
CW	Continuous wave
dB	Decibel
DC	Direct current (refers to zero frequency)
DS	Direct sequence
DSSS	Direct sequence spread spectrum
FFT	Fast Fourier transform
GO	Geometric optics
IDFT	Inverse discrete Fourier transform
IF	Intermediate frequency
Km	Kilometre
Km/hr	Kilometres per hour
LAN	Local area network
LOS	Line of sight
Mb/s	Megabits per second
MHz	Megahertz
MLSD	Maximum likelihood sequence detector
μ s	Microsecond
OFDM	Orthogonal frequency division multiplexing
PO	Physical optics
QAM	Quadrature amplitude modulation
QPSK	Quaternary phase shift keying
RAKE	Type of receiver for a direct sequence spread spectrum signal
RF	Radio frequency
RCS	Radar cross section
SUI	Stanford University interim model

UTD	Unified theory of diffraction
UWB	Ultra wideband
WiMAX	Worldwide interoperability for microwave access (a wireless technology)

LIST OF SYMBOLS

H	height of a reflecting wall
W	width of a reflecting wall
a	height of base station antenna
b	height of mobile antenna
r	distance from base station to mobile
$\rho_g, \rho_{g1}, \rho_{g2}$	ground plane reflection coefficients
ρ_w	wall reflection coefficient
E	electric field
E_i	incident electric field
E_s	scattered electric field
E_{SZ}	scattered electric field in z direction
S	scattering matrix
λ	wavelength
j	square root of -1
d	distance from scatterer or reflector to receiver
d_0	near zone distance
σ_R	radar cross section
P_{D0}	scattered power density
P_{Di}	incident power density
Z_0	wave impedance of free space
A	area
H_t	tangential magnetic field
H_i	incident magnetic field
J	current density
x, y, z	rectangular coordinate system
I	current
l	length of current element
R	distance from radiating element
θ	angle from the vertical of the vector from the base station to the mobile

$\Delta x, \Delta y, \Delta z$	increments of x, y, z
a_c	radius of circular flat plate
C, S	Fresnel integrals
P	transmitted power
G	base station antenna gain
R_1, R_2	distances from base station and base station image to mobile respectively
R_3, R_4	distances from base station and its image to a wall element
R_5, R_6	distances of a wall element and its image respectively to the mobile antenna
σ	ground conductivity
η	electrical parameter of ground
$\rho_{g1}, \rho_{g2}, \rho_{g3}$	reflection coefficients of ground
ρ_w	reflection coefficient of wall
ω	radian frequency
ξ, ξ_r	permittivity and relative permittivity respectively
θ_1	angle from the vertical of the vector from the base station image to the mobile
θ_5	angle from vertical to vector from base station image to mobile unit
θ_6	angle from vertical to vector from wall image to mobile unit
h	height of a rectangular surface
w	width of a rectangular surface
ρ	general reflection coefficient
r_1, r_2	principal radii of curvature of reflected wavefront
r_{S1}, r_{S2}	principal radii of curvature of reflective surface
A_S	attenuation of reflected wave due to surface roughness
σ_S	rms surface roughness
γ	grazing angle
V	lowpass power spectrum
V_1	complete power spectrum
f	frequency
f_0	carrier frequency
U	lowpass autocorrelation function

U_1	autocorrelation function
U_p	inphase part of U_1
U_q	quadrature part of U_1
τ	delay
x_b	amplitude modulation
y_b	autocorrelation function of y_b
U_{yb}	total signal
t	time
t_i	delay of i^{th} component
i	index variable
t_0, t_1, t_2	delay of components 0, 1, 2
a_i	amplitude of i^{th} component
a_0, a_1, a_2	amplitude of components 0, 1, 2
β	phase modulation
φ_i	phase shift of i^{th} component
b	relative amplitude of reflection
R_b	distance of base station from reflecting wall
R_m	distance from reflecting wall to mobile
R_{bm}	distance from base station to mobile
θ_r	reflection angle
ΔR	difference in distance between direct and reflected components
c	speed of light
R_s	symbol rate
p	in-phase component
q	quadrature component
s	signal waveform
z	analytic signal
a_{pn}	amplitude of n^{th} symbol in in-phase part
a_{qn}	amplitude of n^{th} symbol in quadrature part
n	index variable

T	symbol period
u	pulse shape as a function of time
z_l	delayed analytic signal
r_{tr}	distance which a ray travels from transmitter to receiver
v	velocity
θ_r	carrier phase shift associated with distance r
f_d	Doppler frequency shift
r_r	received signal containing reflections
a_{rn}	complex signal amplitude of n th reflection
f_{dn}	Doppler frequency shift of n th reflection
θ_{0n}	carrier phase shift of n th reflection
$\Delta\tau_n$	relative delay of n th reflection
Δf_n	relative frequency shift of n th reflection
$\Delta\theta_n$	relative carrier phase shift of n th reflection
R_r	Fourier transform of r_r
P	Fourier transform of p
Q	Fourier transform of q
F	channel frequency response
α_0	amplitude of direct signal component in frequency domain
α_1	amplitude of reflected signal component in frequency domain
P_d	phase detector function
K_d	phase detector constant
R_c	chip rate of DS waveform

INTRODUCTION

This thesis proposes a model for near line-of-sight propagation between a base station and a moving vehicle for a broadband communication channel. Such conditions occur on short range links in suburban and semi-rural areas. For this type of link, there is little or no obstruction of the direct path but there can still be considerable multipath due to scattering from buildings. The objective is to provide a better understanding of the communications environment for this type of link and to provide guidance for the design of system components which will optimize the performance e.g. minimize the error rate of the channel.

The motivation for this work was a series of measurements of radio performance in mobile applications conducted in a suburban area. The waveforms were simple robust types such as QPSK and the data rates were of the order of 1 Mb/s. The range was short and line-of-sight conditions were usually satisfied. Received signal levels were very high; well above the receiver noise thresholds. However, multipath was a significant problem, as expected. The initial measurements of this series indicated that the channel was either good, with no errors or very bad with high error rates. This good/bad channel behaviour was mentioned by several authors but no explanation was found in the literature. A theoretical investigation was then conducted and further testing was performed to validate the theoretical conclusions and to characterize the effects of the multipath on the signal waveforms. This thesis documents the results of this work and enables a better understanding of this type of channel.

This thesis presents a number of new contributions to the analysis and understanding of multipath channels.

- 1) It provides an analysis and validation of an important issue for near line of sight conditions when multipath is present:
 - a) Multipath is only significant in a near zone close to building walls
 - b) Size of the near zone is related to wall area and wavelength
 - c) Outside of the near zone, reflection amplitude falls off rapidly
 - d) Inside near zone, there is a single dominant reflection when buildings are isolated.

- 2) It analyzes reflection from building walls with ground reflections, using physical optics for wall reflection.
- 3) Based on the near zone concept, it derives a method to predict the regions where signal outages are likely for classical coherent receivers.
- 4) It shows that, when reflection delay is less than symbol period, there are serious signal degradations which are very difficult to compensate.
- 5) It provides a simulation of effects of a single dominant reflection on phase errors of timing recovery and carrier recovery circuits for a classical QPSK coherent receiver.

The thesis starts with a background and literature survey, followed by four major chapters treating the subject of near line-of-sight propagation. The second chapter is a theoretical analysis of the near line-of-sight channel which exists in suburban and semi-rural areas. The analysis considers reflections from the flat walls of buildings. It is shown that the amplitude of reflected signals is significant only in a near zone close to the building wall and that, outside that zone, the amplitude of the reflected signal falls off rapidly. This implies that the multipath model will consist of the desired signal and a single dominant reflection.

The next chapter describes the results of experimental measurements on a suburban and a semi-rural channel to determine whether the theoretical model is a good representation of the behaviour of such channels. It is found that bad channel conditions usually show the characteristics of a single dominant reflection.

The fourth chapter provides a methodology to find the locations which will produce the potentially bad channel conditions and hence to estimate the percentage of time for which a link between a base station and a mobile will have an outage. The theoretical analysis shows that, when the mobile is within a near zone close to the wall, the reflected signal will be similar in magnitude to the direct signal. The size of this near zone is determined approximately by the cross-section of the wall area in the direction of propagation of the reflection and a near zone distance which is a function of the wall area and the signal wavelength. It is important to note that these areas of poor performance (due to multipath) in

front of building walls will have large signal values when the distance to the base station is small. Thus, coverage models would show these areas to have good signals because they have line-of-sight or near line-of-sight. These results are the main contributions of this thesis project. They explain the reasons for the presence of areas of low and high multipath interference. It is believed that, although the physics behind this analysis is well known, it has not been explicitly applied to the modelling of multipath effects in mobile communications.

The fifth chapter analyzes the effects of a single dominant reflection on several typical signal waveforms, QPSK, direct sequence spread spectrum and OFDM. Much of the analysis concentrates on the timing and carrier recovery functions of QPSK for the specific channel conditions studied here. It is found that, when the reflected signal amplitude approaches that of the desired signal, it is likely that synchronization will be lost. This is in accord with the experimental observations. The chapter concludes with a brief consideration of the performance of more general receiver structures in the presence of multipath.

Finally the thesis findings are summarized in the conclusions.

CHAPTER 1

BACKGROUND AND LITERATURE SURVEY

As part of this thesis, the electromagnetic propagation environment, effects and communication strategies for near line-of-sight conditions in suburban and semi-rural areas has been investigated. In this situation, the link lengths are not very long and the receiver can often see the transmission antenna or the “direct” path is only slightly obstructed with a small amount of diffraction loss. However, the transmitting and receiving antennas are close to buildings or other reflecting structures. The resulting reflections produce a strong multipath interference which distorts the received signal. This condition is typical of mobile wireless communications.

The wireless multipath environment has been extensively studied for many years, both theoretically and experimentally, as documented in the literature to be cited below. The present work tries to extend the existing body of knowledge to explain several features of the observed multipath behaviour which have not, in our opinion, been sufficiently explored before. In addition, it tries to relate the observed multipath to the geometry of the scattering structure. Building reflections are modelled as reflections from flat walls. This model has been analyzed before, as noted in the literature references below, but the analyses are used here to explain several basic features of multipath behaviour which the author believes have not been emphasized in the literature.

The basic equation of electromagnetic propagation between two antennas is the free space loss equation [1], which states that, in a free space environment, the received power is inversely proportional to the square of the distance or, equivalently that the electric field is inversely proportional to the distance. Propagation loss equations for other conditions where there is reflection from the surface of the earth or diffraction loss due to obstructions have been developed by numerous authors, such as Bullington [2], Egli [3] and Deygout [4]. The reflection equations are typically those due to Fresnel, as documented by many standard

electromagnetic theory textbooks such as Balanis [5]. These reflection equations are for flat surfaces of infinite extent but are commonly used for most applications since they represent a limiting case. The diffraction equations are based on the diffraction loss due to knife edges, documented, for example in Balanis [5] or McNamara et al [6].

Note that there is also a great deal of information on propagation loss over a spherical earth [2] but this is not considered here because the link lengths are short and earth curvature is not a dominant effect for the paths being analyzed. Also not considered here are fading effects due to atmospheric multipath propagation [7, 8], although fading due to multipath reflections from buildings are a key part of the present work.

The multipath propagation in wireless channels has been extensively studied, both theoretically and experimentally. Lee [9] is an early text which summarizes the basic propagation studies as well as analyzing the effects of multipath on modulated signals. A recent comprehensive text for multipath propagation is Bertoni [10], which describes both theoretical and experimental characterizations of such channels. Durgin [11] treats the analysis of general multipath channels which can vary in time, frequency and position.

The multipath in urban areas is mainly due to scattering from buildings. The analysis must consider both reflection and diffraction effects. In this context, reflection means both specular reflection and scattering in non-specular directions. Reflections can be analyzed using geometric optics, GO, and ray tracing [6] or physical optics, PO, [10, 5], also referred to as Fresnel-Kirchhoff analysis. Diffraction is usually treated by means of the Uniform Theory of Diffraction (UTD) [12, 6] in the wireless propagation literature. Most analyses of multipath use a combination of GO and UTD [12, 13, 14, 15, 16, 17, 18, 19 20, 21, 22].

PO does not seem to be often used for multipath propagation analysis because it requires the integration of a field over the surface of a building, which is computationally intensive. However, Al-Nuaimi and Ding [23, 24] use this approach to model the reflections from

buildings by treating the buildings as flat plates. Also, Gutierrez et al [25] have recently used PO for urban coverage analysis.

Many of the theoretical analyses referenced above [12 to 22] also contain some measurements to validate the analysis approach since the analysis usually contains approximations due to the complexity of the problem.

Another way to characterize the analyses is as either deterministic or statistical i.e. treating either fixed geometries or classes of structures with some random features or parameters. Most of the analyses above combine these approaches by treating certain canonical structures but with random features to account for aspects of the structures which are either not known or not known accurately enough. Accuracy becomes an issue especially when the wavelength is small.

An important aspect of reflection and scattering from structures is the question of near field and far field scattering. Using GO and ray tracing automatically assumes near field reflection, which raises the question of the size of the near field region. Bertoni [10] uses a Fresnel zone criterion to establish a near zone distance within which a GO analysis is valid. However, this analysis is incomplete, as will be shown later in the present work. Al-Nuaimi and Ding [24] show an example of reflected field behaviour in the near zone but provide little additional explanation. Some references for near zone scattering also exist [26, 27] but the geometries which are treated are not useful for the present application.

There also exist numerous purely experimental investigations of wireless communication channels which measure and characterize multipath conditions observed in real channels. An early experimental study is that made by Cox [28]. Later studies have included the work on the Stanford University Interim (SUI) model [29] and Saleh and Valenzuela for indoor channels [30]. These studies characterize the results in terms of statistical distributions of model parameters.

As a result of the experimental and theoretical work, numerous models have been proposed and documented in the literature for propagation in the urban and suburban environment. They are statistical models and were intended for use by the wireless cellular industry and, more recently, providers of wireless LAN's and broadband wireless access systems. Examples are the Stanford University Interim (SUI) Models [29]. Some models treat the angle of arrival of multipath components e.g. the Lee Model (ring of scatterers) [31], the Geometrically Based Single Bounce Circular Model [32] and the Geometrically Based Single Bounce Elliptical Model [31, 32]. For line-of-sight links, the Rummler Model [33], which is a simple 3-ray multipath model, is often used to characterize dispersive fading.

It has been noted by several authors that the multipath channel seems to have two states: either good or very bad [34]. This has also been observed in the experimental portion of the present work. The purpose of this thesis project is to study this effect in more detail.

PO is based on placing equivalent currents on a reflecting surface to generate the reflected fields. A radiation equation is then integrated over the surface to calculate the fields at any point. This is formulated in a mathematical way by, for example, Balanis [5]. It should be noted that GO assumes that the wavelength is effectively zero while PO assumes that the wavelength is small relative to the dimensions of the structure.

The radiated field at a point in space can be calculated as an integral of field quantities over a surface. This is based on Huygen's principle, a basic principle of wave propagation, which states that any wavefront can be considered as a surface of secondary sources of radiation. This approach is described by Born and Wolf [35]. This method is also used by Beckmann and Spizzichino to calculate the scattered fields from rough surfaces [36]. The fields at the surface of a reflecting object are approximated by using the Kirkhoff approximation [35], which assumes that the reflected field at a point on a surface equals the incident field multiplied by the Fresnel reflection coefficient for the plane surface which is tangent to the point. This is the same assumption as that used in GO (as well as PO) to approximate the

reflected field at the surface [6]. An integral is then used to calculate the scattered field for any point in space.

It should be noted that several approximations are commonly used in scattering problems. The first is geometric optics (GO) [5, 6], which assumes that the wavelength of the incident waves is zero and that the waves behave as rays. A better approximation is physical optics (PO) [5], which assumes that the wavelength is finite but much smaller than the dimensions of the scattering object. In this work, PO is used along with the Kirkhoff approximation.

Another approach used for scattering calculations is that from the radar field where radar cross sections (RCS) are calculated [37]. In this approach the scattered field is related to the incident field through a scattering matrix [38, 39]. The RCS represents the equivalent area which receives the incident power density and re-radiates it uniformly in all directions. These relationships are designed to enable the calculation of the detectability of a radar target but they are general concepts which can be applied to any scattering problem.

A closely related problem is the calculation of the near field of an antenna in free space, particularly for an aperture antenna. It is well known that the field near an antenna is large, very complex and very variable with location [40]. However, beyond a certain distance, the field falls off inversely with distance. For an aperture antenna, such as a parabolic reflector, the radiated power near the antenna is mostly contained in a cylinder whose cross-section is that of the antenna aperture [40]. The peak power density for a paraboloidal reflector is roughly four times the transmitted power divided by the aperture area [40]. Beyond a certain distance (which depends on the aperture area and the wavelength), the field falls off inversely with the distance [41]. This behaviour defines two regions: the near field and the far field of the antenna.

Another closely related problem is the so-called Fresnel diffraction through an aperture. Diffraction is traditionally referred to as Fraunhofer for the far field and Fresnel for the near field [35]. In the far field, the rays to the field point are all considered as parallel and, for

equal distances, the field varies only with the azimuth and elevation angles. For a fixed direction, the field varies inversely with distance. In the near field, the rays to the field point are not parallel and the field variation with location is more complex and it is mostly confined to a cross-section which is the same as the aperture, as in the case of the near field of an antenna.

The present work shows that a similar behaviour occurs with the scattering of waves from structures, particularly flat walls of buildings. The implication is that, for areas where building density is not too high, the scattered fields will be significant near buildings and small elsewhere, corresponding to “good” and “bad” areas respectively. In such a case, only a single reflection will be significant. Therefore this work investigates some of the effects of a single reflection on signal demodulation for several simple modulation types such as QPSK. The analytical methods for characterizing signals in the presence of multipath is based on the work of Durgin [11].

For QPSK, timing and carrier recovery are investigated for the case of a single dominant reflection. Timing and carrier recovery for typical coherent demodulators are well known [42, 43, 44]. Typical methods of timing and carrier recovery are described by Proakis [42]. A tutorial review of timing and carrier recovery is given by Franks [45].

Direct sequence spread spectrum (DSSS) modulation is also a well known technique which is used to reject jamming, interference and multipath. A basic description is given by Dixon [46]. An advanced treatment of DSSS is given by Simon et al [47]. RAKE receivers for DS systems are described and analyzed by Proakis [42]. In the present work, a brief analysis is given to show how DSSS can mitigate the effects of reflections.

OFDM systems have also been the subject of a great deal of research because they are recognized to offer good performance in the presence of multipath. A typical text is Schulze [48].

The references cited above for modulation and demodulation techniques are mainly textbooks with good treatments of the relevant topics. Innumerable other references are available on these subjects. In the present work, the main emphasis is on the characteristics and modelling of the propagation. Brief analyses of the effects on the demodulation of different types of signals are given to show the main effects of the multipath.

CHAPTER 2

THEORY

2.1 General

This thesis proposes a model for the propagation between a base station and a moving vehicle for a broadband communication channel for which near line-of-sight conditions exist. Such conditions occur on short range links in suburban and semi-rural areas. For this type of link, there is little or no obstruction of the direct path but there can still be considerable multipath due to scattering from buildings. The objective is to provide a better understanding of the communications environment for this type of link and to provide guidance for the design of system components which will optimize the performance e.g. minimize the error rate of the channel.

It has been often reported that worst case signal strength variations have been observed in near line of sight situations for a so-called 'very bad channel'. In this thesis we show that a reflector such as a building can induce periodic deep fades. This can occur in an area close to the building whose size depends on the size of the building. In contrast to the usual Rayleigh or Rician distribution, these periodic fades are more frequent, nearly deterministic and, if the mobile moves along the building, the conditions may persist for long durations. This fade periodicity can induce a severe and long outage period if it has not been accounted for in the system design. Since the local area over which a bad channel exists depends on the size of the building producing the reflection, the overall fraction of the operating area which will exhibit poor channel characteristics will be a function of the building density.

It is well known that mobility inherently involves a great deal of multipath. The received signal consists of a 'direct path component' and delayed reflected components. The latter are reflected or scattered from various structures, mainly buildings. If the direct component is the largest, there will be interference only from delayed reflections. This is called the

minimum phase case. If a reflected component is the largest, there will be interference from both precursors and delayed components. This is called the non-minimum phase case.

The multipath phenomenon has been the subject of many books and papers, as indicated in the literature survey of Chapter 1. In this work, the emphasis is on building reflections. In the suburban or semi-rural environment, buildings are smaller and less numerous than in urban areas. In this environment, many links are line-of-sight but there can be significant reflections. There are also scattered and diffracted components but these are usually much smaller than reflections. In this context, reflections are components scattered in the specular direction while other scattered components are not in the specular direction. Diffracted components are those which are not in the line of sight. Diffraction losses are generally quite high. For example, a wave which grazes a knife edge but still has a line-of-sight has a 6 dB diffraction loss [8]. Losses for non-line-of sight cases are generally much higher. Similarly, scattering losses in non-specular directions for flat reflectors are also high, as will be shown.

A number of models have been used in the literature to treat reflections. The first is the geometric optics model, which assumes a building wall has a reflection coefficient. Reflected waves are analyzed using ray tracing. However, ray optics can only be used to a certain distance from the building. Bertoni [10] establishes this distance based on the building width being equal to a Fresnel zone for the reflection geometry. The building height is not considered since it is assumed to be much greater than the width (typical of an urban geometry). Beyond this distance, Bertoni [10] states that scattering theory must be used. The scattered field falls off inversely with distance from the building in this region. Al-Nuaimi and Ding [23, 24] provide a more complete analysis of scattering from building walls based on the Fresnel-Kirchhoff integral and note the differences between the near zone and far zone (scattering region). However, their analysis is done in the context of interference signals scattered from buildings and they also do not consider the impact of ground reflections. In the present work, an analysis of multipath due to building reflections is analyzed using mainly physical optics methods. The reflected fields at the surface are calculated using geometric optics. Equivalent currents are then assigned to the surface and

radiation formulas used to predict the scattered fields by integrating over the surface. All of these analysis methods are approximations but the surface integral methods provide important insights into the multipath channels caused by building reflections.

Section 2.2 below gives a theoretical analysis, performed by the author as part of this research project, of the propagation on short range links with multipath, mostly using physical optics for the wall reflection, and summarizes the key results. Section 3 proposes a channel model and discusses some applications.

2.2 Theoretical analysis of reflection from a flat wall

a) Propagation geometry

The types of areas considered in this study contain buildings on relatively flat terrain. When these reflectors are not present, the usual models (line-of-sight and ground reflections) prevail. When these isolated buildings are present however, the nature of the channel is significantly modified and should be taken into account at a system level. It is the typical very bad channel [34]. In the suburban case, most buildings are not as large as those in a downtown type of environment and consist of individual family houses, apartment buildings and moderately sized office buildings. For the rural case, the buildings consist of single houses and small clusters of farm buildings. Thus, we study the propagation model illustrated in **Figure 2.1**. A base station with an antenna on a 20 m mast is located on level ground and is transmitting to a vehicle having an antenna mounted at a height of 2 m. A building is located near the vehicle. The building, vehicle and base station are all in line to simplify the calculations. The antennas are vertically polarized. The distance between the base station and the mobile is up to 10 km. The building is modelled as a plane reflecting wall of height H and width W . The ground is also considered as a plane reflector. The communication link is a continuous full duplex link and the link frequencies are around 300 MHz. The data rates are considered to be of the order of 1 Mb/s.

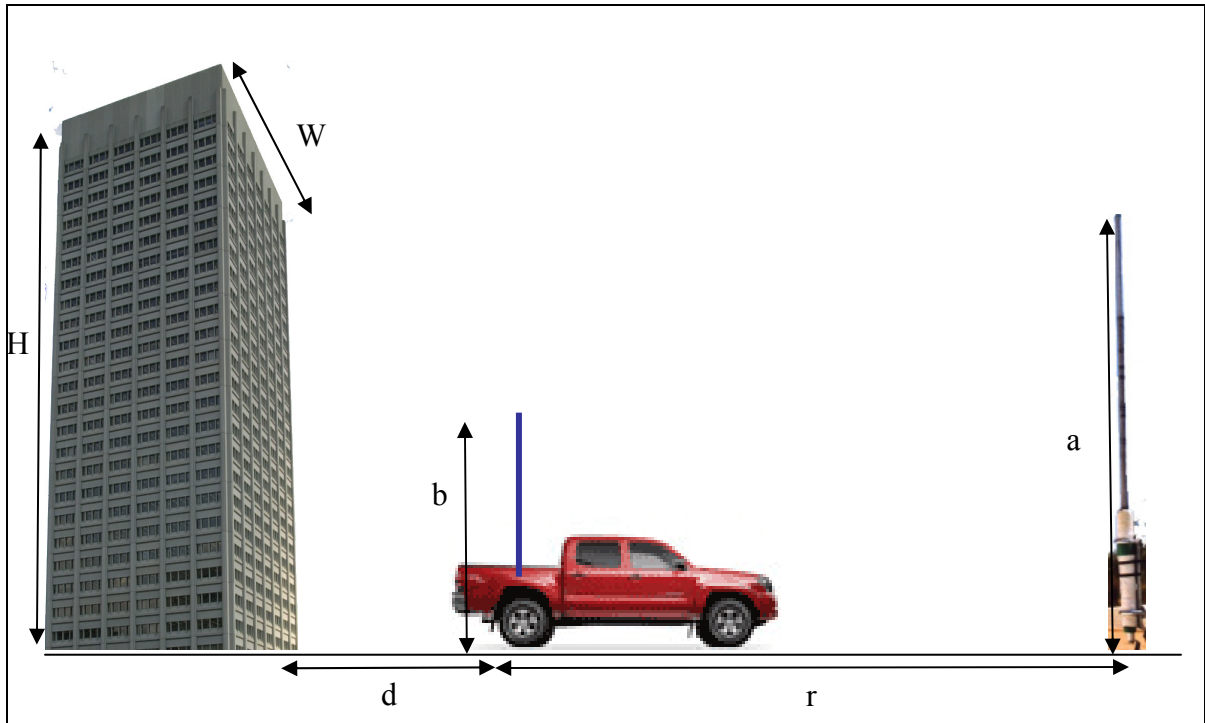


Figure 2.1 Propagation model.

The ground plane has a reflection coefficient ρ_g . When the wall dimensions are much larger than a wavelength, it can be considered as approximately an infinite reflecting plane characterized by a reflection coefficient ρ_w for a region very close to the wall. This approximation is valid for this case since a typical wall will be at least $10\text{m} \times 10\text{m}$ and the wavelength will be about 1m .

b) Simplified geometric optics model, no ground reflection

In a first analysis, we consider the case of no ground reflection, with the base station and vehicle antennas aligned with the center of the reflecting wall. Let the incident electric field at the wall be \mathbf{E}_i and the scattered field be \mathbf{E}_s . This field will be almost parallel to the wall since the base station is considered to be far away. If the wall is considered to be infinite, the reflected field will be $\mathbf{E}_s = \rho_w \mathbf{E}_i$ close to the wall. In practice, if the reflecting surface and the principal radii of curvature at the reflecting point are much larger than the wavelength,

geometric optics may be used to calculate the reflected field close to the surface using the Fresnel reflection coefficient and the principal radii of curvature [5].

However, the size of the wall is finite and the field must start to drop at some distance. In the radar literature, the scattered field at large distances is characterized by the equation:

$$\mathbf{E}_s = \frac{\exp(-j \cdot \frac{2 \cdot \pi \cdot d}{\lambda})}{d} \mathbf{S} \cdot \mathbf{E}_i \quad (2.1)$$

where λ is the wavelength, d is the distance from the reflector and \mathbf{S} is a scattering matrix [38, 39]. \mathbf{E}_i and \mathbf{E}_s are electric field vectors with orthogonal polarization components. In this study, since we are considering only vertical polarization, it is not necessary to use field vectors. These quantities are thus reduced to complex scalars. The matrix \mathbf{S} then becomes a scalar S . It should be noted that, at large distances, the scattered field is attenuated as $1/d$ where d is the distance from the reflector.

The magnitude of S can be derived from the radar cross section of the reflector. The radar cross section σ is defined as the equivalent surface area which collects the power of the incident wave and re-radiates it uniformly in all directions [37]. Thus, if the incident power density at the target is P_{Di} , the scattered power density P_{Do} in a particular direction at a distance d in the far field is given by:

$$P_{Do} = P_{Di} \frac{\sigma}{4 \cdot \pi \cdot d^2} \quad (2.2)$$

The power density for a plane wave is given by

$$P_D = \frac{|\mathbf{E}|^2}{Z_o} \quad (2.3)$$

where Z_o is the impedance of free space. For a perfectly reflecting flat plate of area A whose dimensions are much larger than a wavelength, the radar cross section is given by [37]:

$$\sigma_R = \frac{4 \cdot \pi \cdot A^2}{\lambda^2} \quad (2.4)$$

because the area A collects the incident power and also acts as an aperture antenna of area A which re-radiates it. The gain of such an aperture antenna is approximately $4\pi A/\lambda^2$ as long as the dimensions are much larger than a wavelength.

Using Equations (2.1) to (2.4), it can be shown that,

$$\sigma_R = 4 \cdot \pi \cdot |S|^2 \quad (2.5)$$

where S is the required scattering parameter [39]. In this study, we are interested in vertically polarized transmission and reception so that only this component will be used. Thus, for a perfect reflector, the scattering parameter for a flat plate is given by:

$$S = \frac{A}{\lambda} \quad (2.6)$$

For a real reflector with a reflection coefficient ρ_w , it will be assumed that:

$$S = \rho_w \frac{A}{\lambda} \quad (2.7)$$

The scattered field at large distances is therefore given by:

$$E_s = \frac{\exp(-j \cdot \frac{2 \cdot \pi \cdot d}{\lambda})}{d} \rho_w \cdot \frac{A}{\lambda} E_i \quad (2.8)$$

The case which is considered here is backscatter for broadside incidence. However, the equation is also valid for oblique scattering but the area A is interpreted as the projected area perpendicular to the direction of wave propagation (or reflection).

Since the field close to the surface is given by $\rho_w \cdot E_i$ and the far field by Equation (2.8), a near field/far field transition distance, referred to here as the near zone distance, can be defined such that these two quantities are equal. This gives a near zone distance of:

$$d_o = \frac{A}{\lambda} \quad (2.9)$$

Within this distance, the field is taken as constant. At greater distances, the field drops off as $1/d$. For many surfaces, the reflection coefficient is close to -1 , particularly if the surfaces are conductive. Therefore, this simplified model states that, near reflecting structures, the reflected field will be of the same order as the incident field but that, beyond the near zone distance of Equation (2.9), the scattered field diminishes with distance. If the distance r from the base station to the mobile is much greater than the distance d of the mobile from the reflector, the field from the base station at the mobile will be about the same as the incident field at the reflector. Therefore, within the near zone distance from the reflector, the reflected field will be of the same order as the desired field. As the vehicle moves, the total field will vary rapidly as the desired field is cancelled or reinforced. However, when the vehicle is several times the near zone distance away from the reflector, the scattered field will have only a small effect. The near zone concept has not been used in the propagation and multipath literature and Equation (2.9) is one of the main new contributions of this work.

The near zone distance given by Equation (2.9) depends on the size of the structure. For example, for a wall of width 10 m and height 10 m, the near zone distance is 100 m for a wavelength of 1 m. For a 20 m by 20 m wall, it is 400 m. In urban areas with large buildings, the near zone distances are much larger than in suburban or rural areas. However, Equation (2.9) gives only a rough idea of the near zone distance because the beamwidth of the scattered far field may be different in the azimuth and elevation planes. For a height H and width W , the azimuthal beamwidth is approximately λ/W while the elevation beamwidth is λ/H [5].

c) Physical optics model, no ground reflection

The simplified model presented in Section a) gives a constant field within the near zone. However, it is known that the near field of an aperture antenna, although roughly constant, varies significantly with location in a very complex way [41]. Therefore, a more precise scattering model using the physical optics approximation is required here. This approach assumes that the reflected field near the reflecting surface is given by $\rho_w \cdot E_i$. However, the

field at any other point is obtained by evaluating an integral over the reflecting surface. In Beckmann and Spizzichino [36], this integral is the Helmholtz Integral. An equivalent approach replaces the reflecting surface by an equivalent current sheet whose surface current density is derived from the reflected fields. The latter approach is used here. This method does not take into account any edge effects. The reflected fields are assumed to be discontinuous at the edges of the reflecting surface, which is not realistic. However, Balanis [5] states that the method is fairly accurate for calculating scattered fields in directions not far away from the direction of specular reflection.

The electromagnetic fields at any point can be determined if either the tangential electric or magnetic fields are specified over the surface enclosing the point [5]. In this case, this is the reflecting surface as all other surfaces are at infinity. Then, the surface can be replaced by either a magnetic or electric current sheet whose current density is derived from the tangential field. This surface current density has units of A/m. The sheet is divided into small current elements, whose radiated fields are summed by integration. Here, we will use the tangential magnetic field H_t , whose equivalent current density is:

$$J = 2 \cdot H_t \quad (2.10)$$

because the sheet is assumed to be a perfect conductor. In this case, a plane wave strikes the reflector at broadside incidence. E_i is parallel to the surface and the corresponding magnetic field H_i is perpendicular to E_i and also parallel to the surface. The reflected electric field at the surface is given by $\rho_w \cdot E_i$ and the reflected magnetic field by $\rho_w \cdot E_i / Z_o$. Therefore, the equivalent current density is:

$$J = 2 \cdot \rho_w \cdot \frac{E_i}{Z_o} \quad (2.11)$$

Assume that the reflecting wall is located in the x-z plane and its center is at the origin. The direction of the current elements is vertical. The radiated field at a distance R from a vertical current element, assuming a far field condition, is [10]:

$$E_{\theta} = j \cdot Z_o \cdot I \cdot l \frac{\exp(-j \cdot \frac{2 \cdot \pi \cdot R}{\lambda}) \cdot \sin(\theta)}{2 \cdot \lambda \cdot R} \quad (2.12)$$

where R is the distance to the field point, I is the current, l is the length of the current element and θ is the angle from the vertical to the radius vector. The electric field is in the θ direction.

The far field radiation formula is used here because, once the distance to the field point is a few wavelengths away from the wall, the near field terms for a current element will not cause an appreciable error. The resulting calculated fields in the near zone of the wall will be sufficiently accurate.

Using Equation (2.12), the contributions from each current element are summed to produce the total field. Each contribution is also multiplied by $\sin(\theta)$ because the receiving antenna is vertical. Since $I = J \Delta x$ and $l = \Delta z$, the summation can be written as a double integral over the wall area using (2.12) and substituting (2.11):

$$E_{sz} = j \cdot \rho_w \cdot E_i \iint \frac{\exp(-j \cdot \frac{2 \cdot \pi \cdot R}{\lambda}) \sin^2(\theta)}{\lambda \cdot R} dx \cdot dz \quad (2.13)$$

In this equation, E_i is the incident electric field (assumed parallel to the wall) and E_{sz} is the vertical component of the scattered field. R is the distance from a point on the wall to the point where the field is measured. The Equation (2.13) has been derived by the author based on the principles of scattering analysis described in [5].

The integral (2.13) is evaluated numerically below. However, it is useful to evaluate it analytically, which can be done approximately for certain cases. If the outline of the surface is simple, such as a circle or rectangle, and the field point is far from the surface and on the surface center line, the $\sin^2(\theta)$ term goes to 1 and the integral is identical to that for Fresnel diffraction through an aperture of the same size [35, 49]. The incident wave is assumed to be

plane. The integral has been evaluated approximately by Schelkunoff [49]. If the surface is circular with radius a_C , it can be shown [49] that the absolute value of the reflected field is:

$$|E_{sz}| = 2 \cdot \rho_w \cdot E_i \cdot \left| \sin\left(\frac{\pi \cdot a_C^2}{2 \cdot \lambda \cdot d}\right) \right| \quad (2.14)$$

where d is the distance from the center of the surface to the field point. The field magnitude oscillates between 0 and $2 \cdot \rho_w E_i$ for $d \leq a_C^2/\lambda$. For $d > \pi a_C^2/\lambda$, $|E_{sz}| \approx \rho_w \cdot E_i \cdot \frac{\pi \cdot a_C^2}{\lambda \cdot d}$.

Thus, Equation (2.9) gives the correct near zone distance and the field at large distances falls off as $1/d$, as required by Equation (2.1) or (2.8). The zeros and peaks of this function correspond to Fresnel zones [49, 35] for which the distances from the center of the surface to the field point and the edge to the field point differ by an integral number of half wavelengths. The first peak at $d = a_C^2/\lambda$ corresponds to the case where the surface fills the first Fresnel zone. The field contribution of each of the first few Fresnel zones is approximately the same but with alternating signs. This produces the deep nulls at certain distances.

The above expression is not valid for small d i.e. points very close to the surface. A numerical evaluation of Equation (2.13) for a circular surface shows that, as d decreases, the field oscillations become smaller and the field approaches $\rho_w E_i$ as required. For a surface of radius 5 m and wavelength of 1 m, it is found that the field is approximately constant when the field point is within a few meters of the surface while the first peak occurs at 25 m and the near zone distance is at about 78 m.

Schelkunoff [49] also evaluates the magnitude of the integral for a rectangular surface. For a width w and height h , the reflected field magnitude is given by:

$$|E_{sz}| = 2 \cdot \rho_w \cdot E_i \cdot \sqrt{\left[C^2\left(\frac{w}{\sqrt{2 \cdot \lambda \cdot d}}\right) + S^2\left(\frac{w}{\sqrt{2 \cdot \lambda \cdot d}}\right) \right] \cdot \left[C^2\left(\frac{h}{\sqrt{2 \cdot \lambda \cdot d}}\right) + S^2\left(\frac{h}{\sqrt{2 \cdot \lambda \cdot d}}\right) \right]} \quad (2.15)$$

where C and S are Fresnel integrals, sometimes represented as a Cornu spiral [49] and tabulated in [1]. The width and height occur in separate factors. It can be shown that, for large distances, $|E_{SZ}| \approx \rho_w \cdot E_i \cdot \frac{w \cdot h}{\lambda \cdot d}$. Also, if h and w are not too different, a reasonable approximation for the near zone distance is $h \cdot w / \lambda$, which shows that Equation (2.7) for the near zone distance is again approximately valid. If h or w is much smaller, a better approximation of the near zone distance is the smaller of w^2 / λ and h^2 / λ . The far field falls as $1/d$.

Again, when d becomes much smaller than the near zone distance, the approximations break down and the Equation (2.13) must be evaluated numerically. It is found, as shown in the following paragraphs, that the field variations are smaller than for the circular plate and there are no deep nulls. This is because the rectangular shape does not correspond to distinct Fresnel zones.

Equation (2.13) has been evaluated numerically for three wall sizes: 10 m wide \times 10 m high, 10 m wide \times 20 m high and 20 m wide \times 10 m high. The increments dx and dz were taken as 0.05 m and the integral was approximated by summation. The fields opposite the center of the wall have been plotted as a function of distance from the wall. These results are shown in **Figures 2.2, 2.3 and 2.4**. The numerical evaluation and the graphing of the results in **Figures 2.2, 2.3 and 2.4** have been performed by the author. The fields are normalized to the nominal reflected field $\rho_w \cdot E_i$.

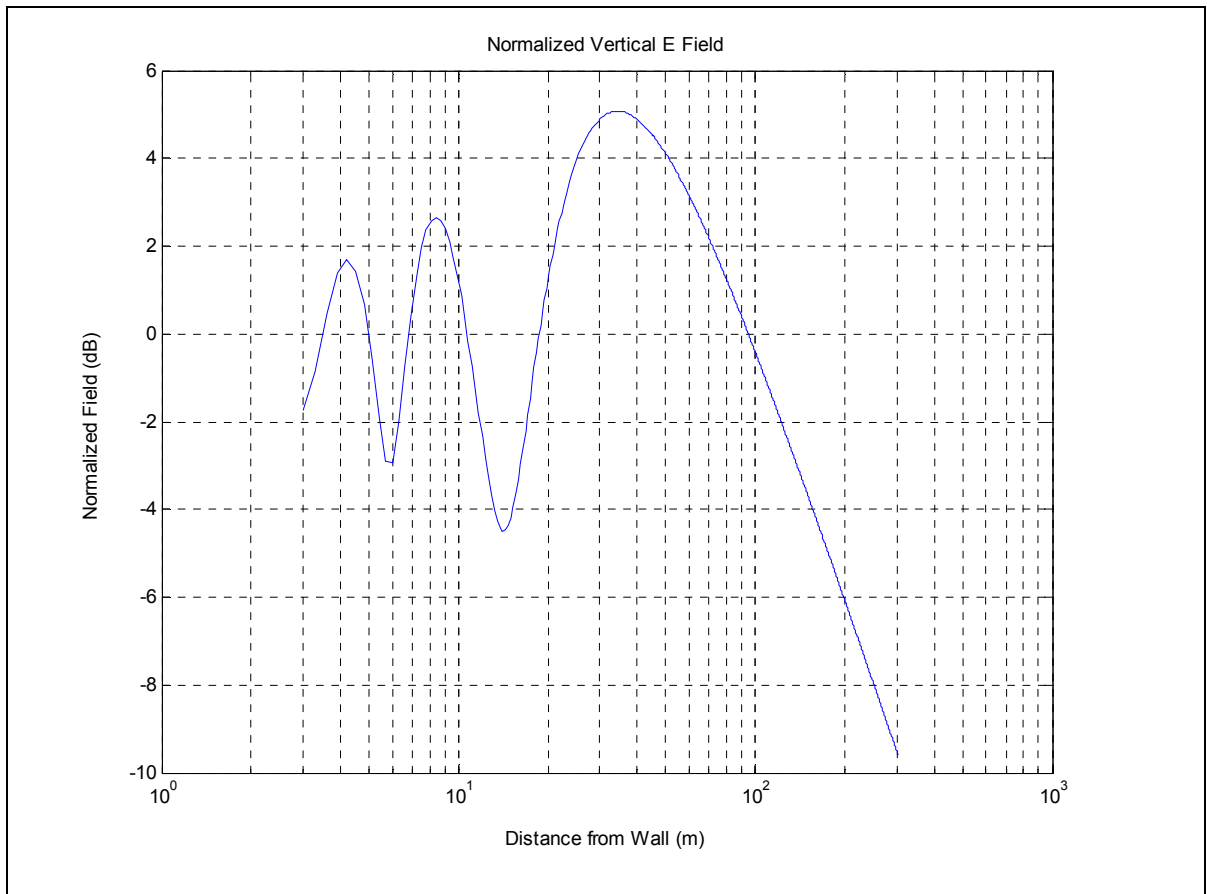


Figure 2.2 Vertical electric field magnitude, 10m × 10 m wall.

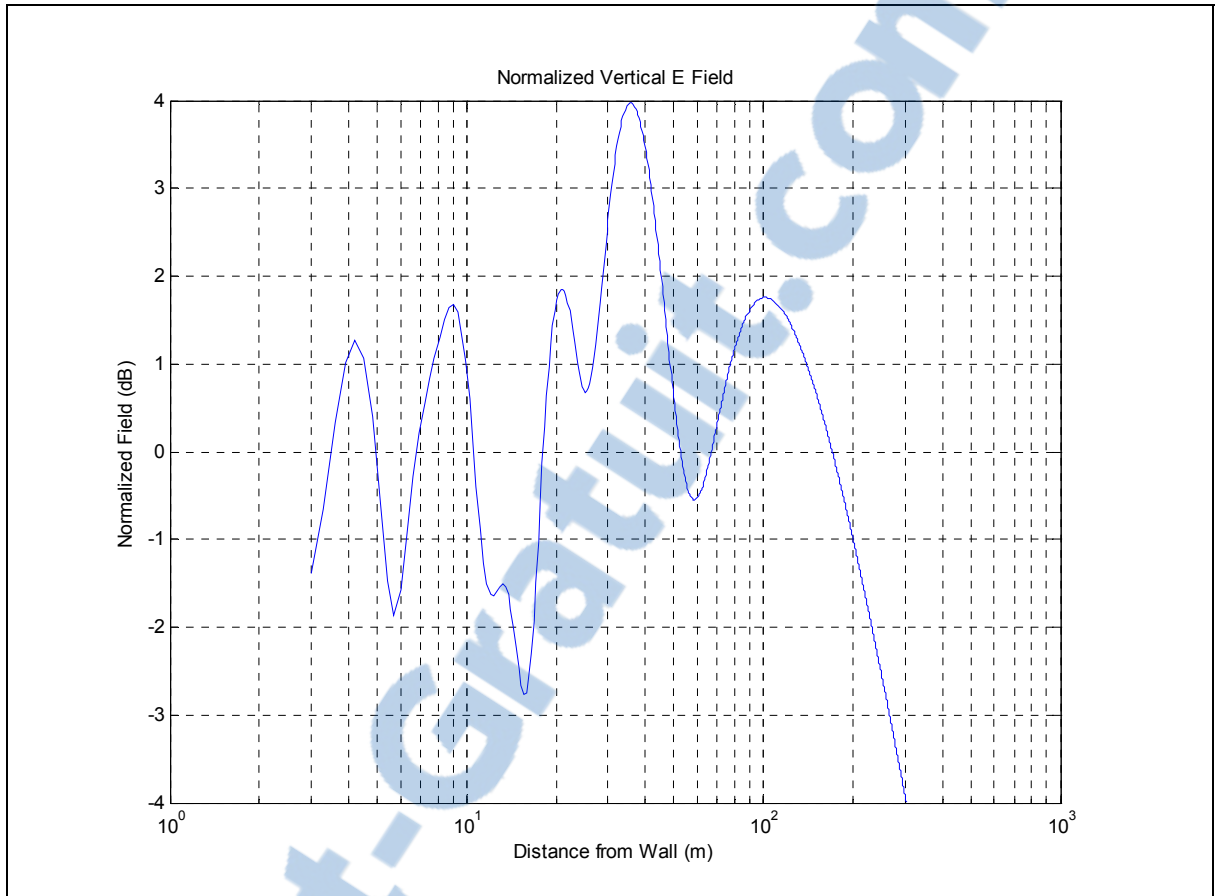


Figure 2.3 Vertical electric field magnitude, 10 m × 20 m wall.

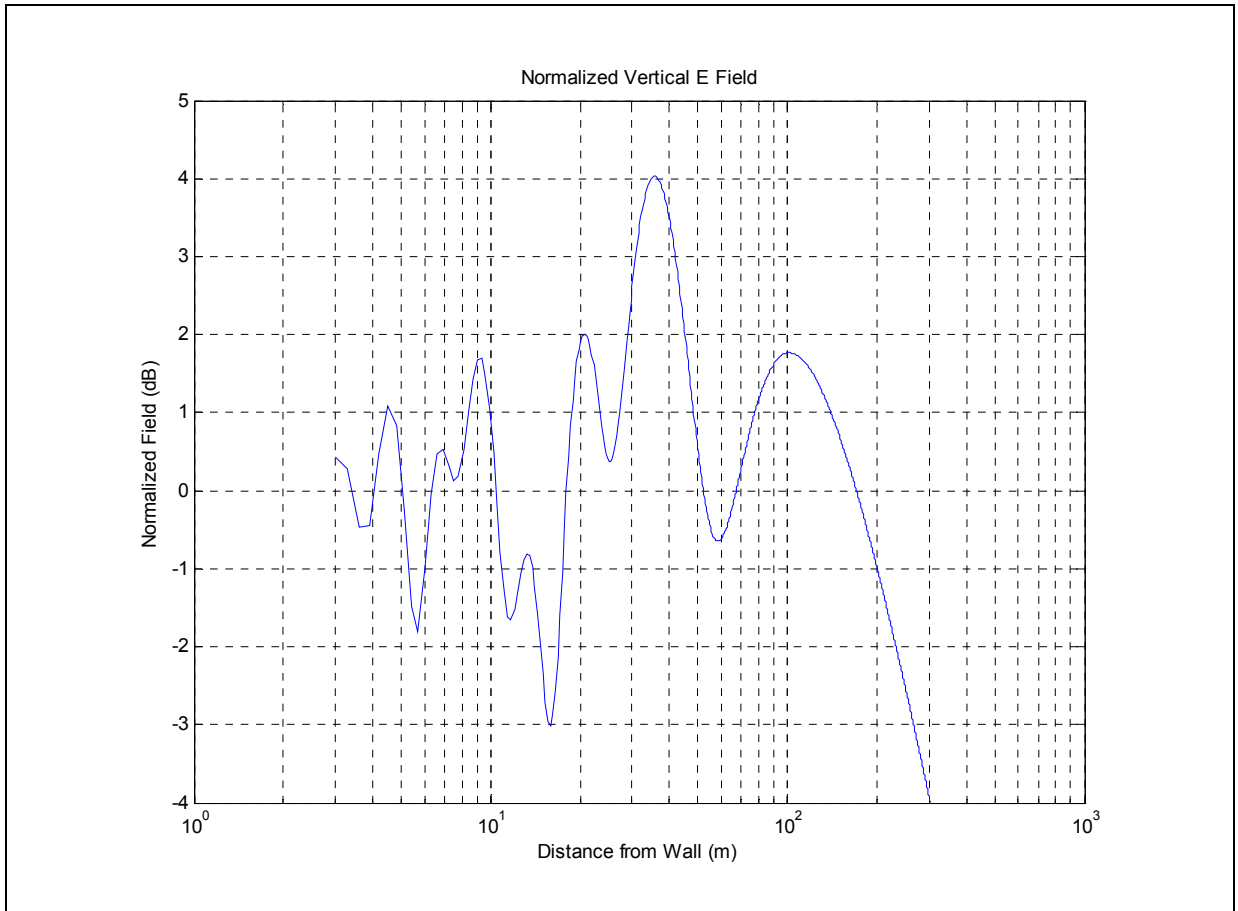


Figure 2.4 Vertical electric field magnitude, 20m × 10 m wall.

The electric field values oscillate around the nominal expected values but are complex functions of position. The near zone distances are approximately in agreement with Equation (9). The simulated values are 95, 170 and 170 m whereas Equation (9) gives the corresponding values of 100, 200 and 200 m. Beyond the near zone distance, the fields fall off as $1/d$ where d is the distance from the reflector. If the wall reflection coefficient is greater than 0.5, there are many locations within the near zone where the reflected field will be of the same order as the incident field at the wall and the desired field at the mobile unit.

In order to establish the horizontal extent of the near zone, Equation (2.13) was evaluated at discrete points on the horizontal plane which passes through the center of the wall for a wall size of 10m x 10m. The result is shown in **Figure 2.5**, where blue represents areas of low

field and dark red represents areas of the highest field. The example shown in **Figure 2.5** corresponds to **Figure 2.2** above. **Figure 2.5** has also been obtained by the author.

It is clear that, close to the wall, the field is mostly confined to a cylinder whose cross-section is the wall shape. The peak field occurs at about 40 m from the wall and, after about 100 m, the field declines rapidly and spreads out as required for the far field. The peak field is about 5 dB above the nominal reflected field and drops to 6 dB below the nominal reflected field at 200 m from the wall.

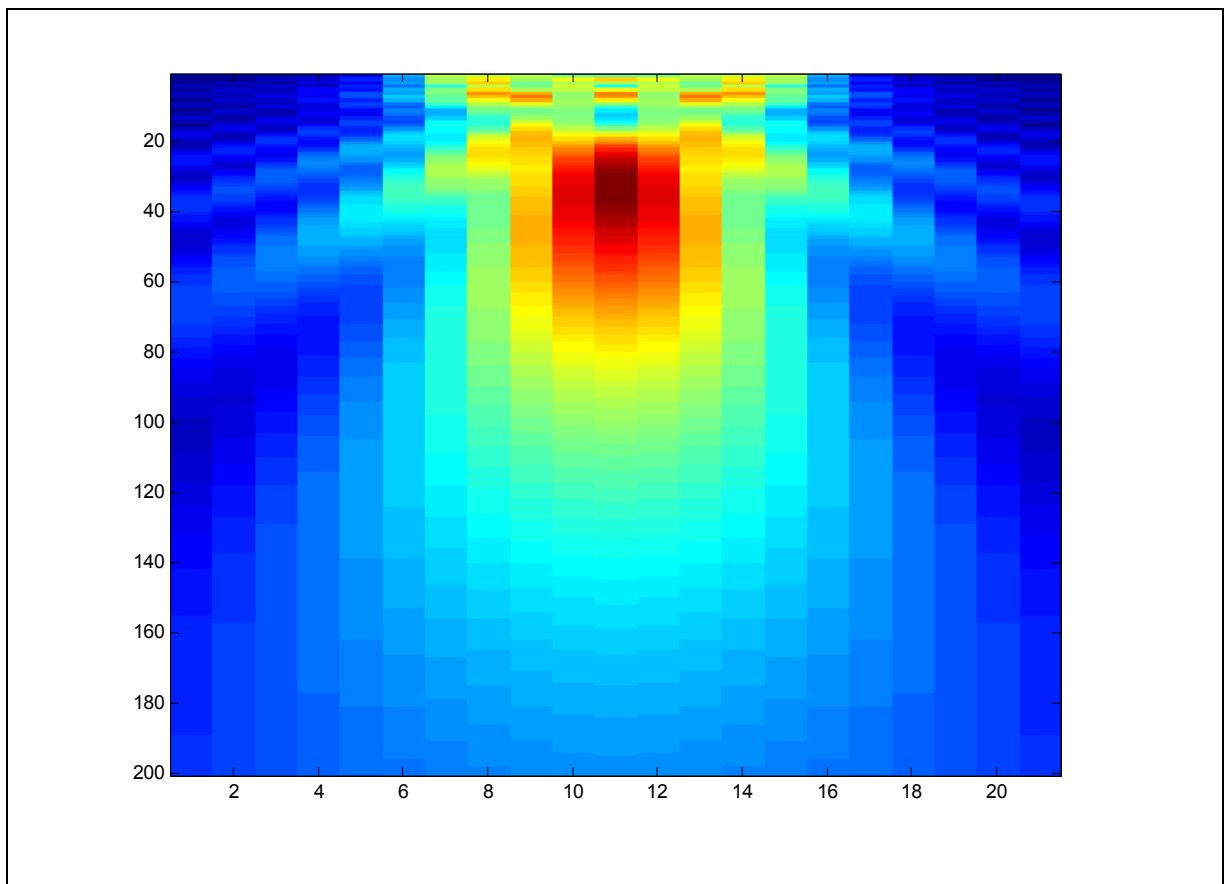


Figure 2.5 Planar X-Y electric field distribution, 10m \times 10m wall. X scale in m, wall extends from $x = 6$ to 16; Y scale in m from top, wall located at $y = -3$.

The preceding results are consistent with the results of Al-Nuaimi and Ding [23, 24]. Reflection amplitudes are significant in the near zone but fall off with distance beyond this zone. The results also permit an evaluation of the use of geometric optics and its limitations. Bertoni [10] states that ray methods can be used to predict reflected fields out to a distance from the building at which the building width represents a Fresnel zone width, and that, for larger distances, scattering models must be used. He ignores the effects of the building height, presumably because building heights in urban areas are often much greater than their width. For the case of the 10 m x 10 m wall, this Fresnel zone width represents a distance of 25 m. However, the field is not constant within this distance; it reaches a peak at about 30 m and oscillates strongly as the distance is decreased. It only reaches a value close to the field predicted by geometric optics at a distance of a few meters from the wall. Thus, geometric optics gives only a rough indication of reflected fields near buildings. The limitation on the distance means that, beyond this point, the field begins to fall off, which is equivalent to saying that scattering models must be used beyond this point.

The objective of the present work is to emphasize the importance of the near zone effects for multipath channel models. The use of geometric optics does not highlight these effects.

A further effect, which is not studied in detail in this work, is the variation of the phase with distance from the wall. The use of geometric optics implies that the phase varies linearly with distance from the wall. However, there are oscillatory phase variations which are correlated to the amplitude variations. They may be of importance for certain applications.

d) Physical optics model with ground reflections

At this point, we return to the original propagation model of **Figure 2.1**, which includes a flat ground plane. The methods of Part c) are adapted to this configuration. The reflection of the base station signal from the ground plane is modelled by assuming a second signal coming from an image below the ground plane, the field being multiplied by a reflection coefficient ρ_g for a vertically polarized wave. The desired electric field at the mobile is calculated using

the geometric optics theory. The incident electric field at each point of the wall is also calculated using geometric optics. The incident fields at the wall are assumed to be parallel to the wall, which is a valid approximation (for the wall sizes considered here) if the base station is at least 500 m from the wall. Equivalent current elements are calculated for each wall element using Equation (2.11), where the incident field is the sum of a direct field and a ground reflected field. The reflection coefficient for the wall is that for broadside incidence. The fields radiated by the wall current elements consist of a direct field to the mobile and a ground reflected field, which is assumed to come from an image of the current element below the ground plane and is multiplied by a ground reflection coefficient for a vertically polarized wave. The vertical component of the field at the mobile location is calculated.

The desired field at the mobile is given by:

$$E_d = \sqrt{\frac{P \cdot G \cdot Z_o}{4 \cdot \pi}} \cdot \left(\frac{\exp(-j \cdot \frac{2 \cdot \pi \cdot R_1}{\lambda})}{R_1} + \rho_{g1} \cdot \frac{\exp(-j \cdot \frac{2 \cdot \pi \cdot R_2}{\lambda})}{R_2} \right) \quad (2.16)$$

where $R_1 = \sqrt{(a-b)^2 + r^2}$, $R_2 = \sqrt{(a+b)^2 + r^2}$

$$\rho_{g1} = \frac{\eta \cos(\theta_1) - \sqrt{\eta - \sin^2(\theta_1)}}{\eta \cos(\theta_1) + \sqrt{\eta - \sin^2(\theta_1)}}$$

$\eta = \epsilon_r \cdot (1 + \frac{\sigma}{j \cdot \omega \epsilon})$ for the ground

σ : ground conductivity

ϵ, ϵ_r : permittivity and relative permittivity respectively

θ_j : angle from vertical to vector from image to mobile unit

P : transmitted power

G : base station antenna gain

It is assumed that both field components are perpendicular to the ground, which is a valid approximation as long as the mobile is at least 500 m from the base station for the antenna

heights considered here. The incident electric field at any point on the wall surface is similarly given by:

$$E_i = \sqrt{\frac{P \cdot G \cdot Z_o}{4 \cdot \pi}} \cdot \left(\frac{\exp(-j \cdot \frac{2 \cdot \pi \cdot R_3}{\lambda})}{R_3} + \rho_{g2} \cdot \frac{\exp(-j \cdot \frac{2 \cdot \pi \cdot R_4}{\lambda})}{R_4} \right) \quad (2.17)$$

where $R_3 = \sqrt{(a-z)^2 + (r+d)^2 + x^2}$, $R_4 = \sqrt{(a+z)^2 + (r+d)^2 + x^2}$

and (x,z) are the coordinates of the point on the wall. The reflection coefficient ρ_{g2} is given by a formula similar to that of ρ_{g1} except that the angle is that between the vertical and the vector from the base station image to the point on the wall. Equations (2.16) and (2.17) have been derived by the author based on the methods of [5].

The field reflected from the wall can then be written, in an analogous manner to Equation (2.13), as:

$$E_s = j \cdot \rho_w \iint E_i \frac{\exp(-j \cdot \frac{2 \cdot \pi \cdot R_5}{\lambda} \cdot \sin^2(\theta_5))}{\lambda R_5} dx \cdot dz + \quad (2.18)$$

$$j \cdot \rho_w \iint \rho_{g3} \cdot E_i \frac{\exp(-j \cdot \frac{2 \cdot \pi \cdot R_6}{\lambda} \cdot \sin^2(\theta_6))}{\lambda R_6} dx \cdot dz$$

where $R_5 = \sqrt{(b-z)^2 + d^2 + x^2}$, $R_6 = \sqrt{(b+z)^2 + d^2 + x^2}$

$$\sin(\theta_5) = \sqrt{\frac{d^2 + x^2}{R_5}}, \quad \sin(\theta_6) = \sqrt{\frac{d^2 + x^2}{R_6}}$$

$$\rho_{g3} = \frac{\eta \cos(\theta_6) - \sqrt{\eta - \sin^2(\theta_6)}}{\eta \cos(\theta_6) + \sqrt{\eta - \sin^2(\theta_6)}}$$

and ρ_w is the reflection coefficient of the wall.

The angles θ_5 and θ_6 are the angles from the vertical to the vectors from a wall point and its image to the mobile. They must be taken into account here because the mobile may be close to the wall. Equation (2.18) has been derived by the author.

Equation (2.18) can be evaluated numerically in the same way as Equation (2.13) as a summation. This evaluation has been done, by the author, for the same three cases as for **Figures 2.2, 2.3 and 2.4** to obtain the results shown in **Figures 2.6, 2.7 and 2.8**. For these calculations, the ground parameters have been chosen for typical ground. The wall parameters have been chosen for a relative permittivity of 10 and zero conductivity. Many other parameter values could be chosen but it is believed that the general nature of the results would not change. In particular for small ground reflection angles, the ground reflection coefficient is usually close to -1 . The wall parameters produce a reflection coefficient which is about 0.5. A reflection coefficient of 0.5 is consistent with that used by Constantinu [12]. The scattered electric field is directly proportional to the reflection coefficient.

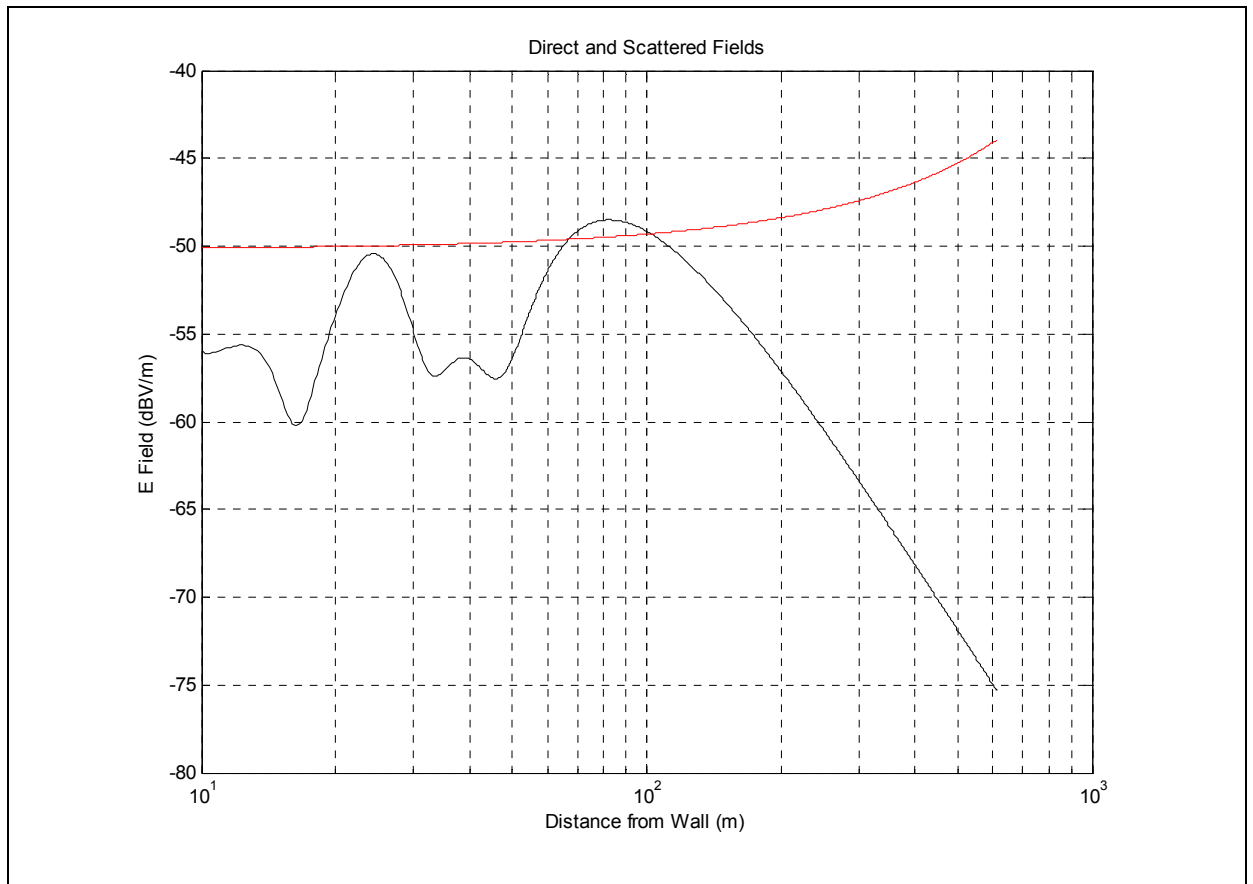


Figure 2.6 Vertical electric field magnitude, $10 \text{ m} \times 10 \text{ m}$ wall, ground reflection.
Red: direct field, Black: reflected field.

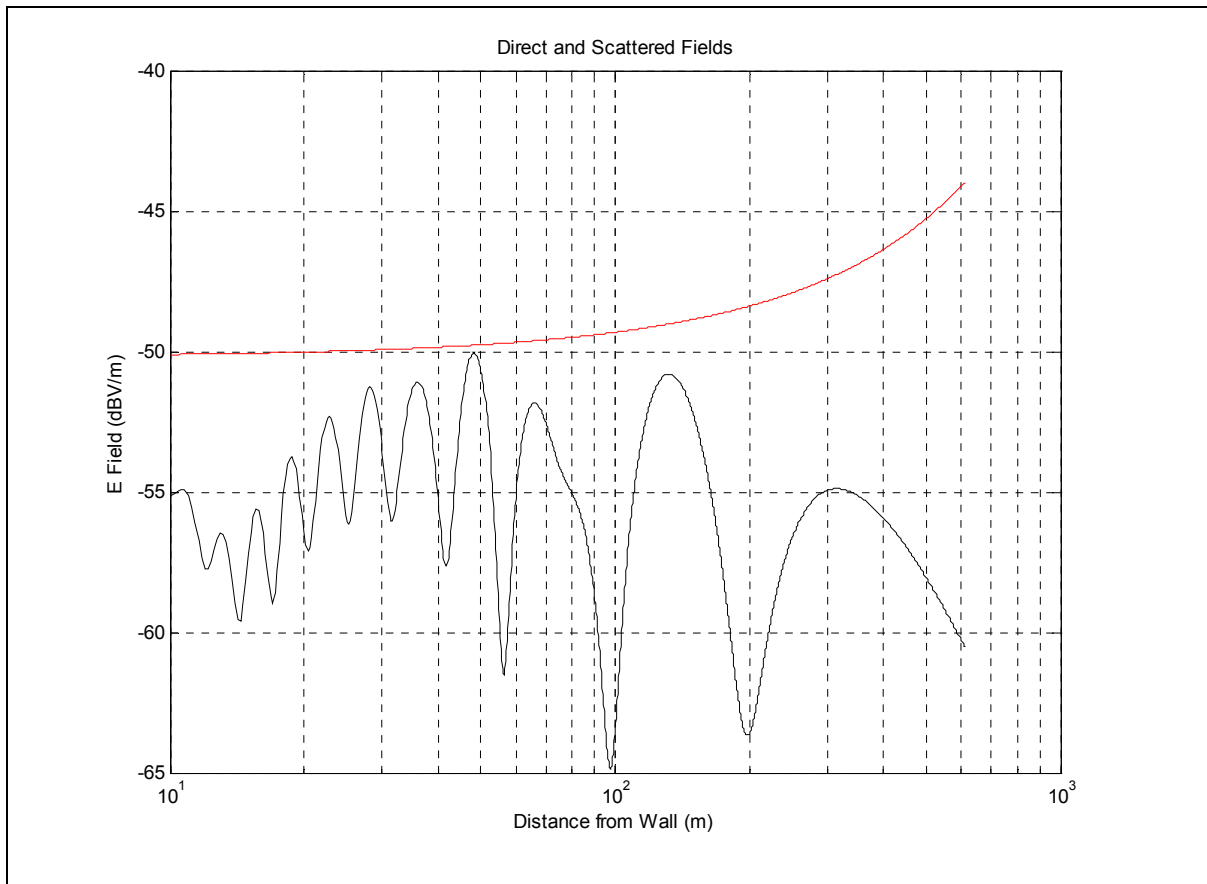


Figure 2.7 Vertical electric field magnitude, 10 m × 20 m wall, ground reflection. Red: direct field, Black: reflected field.

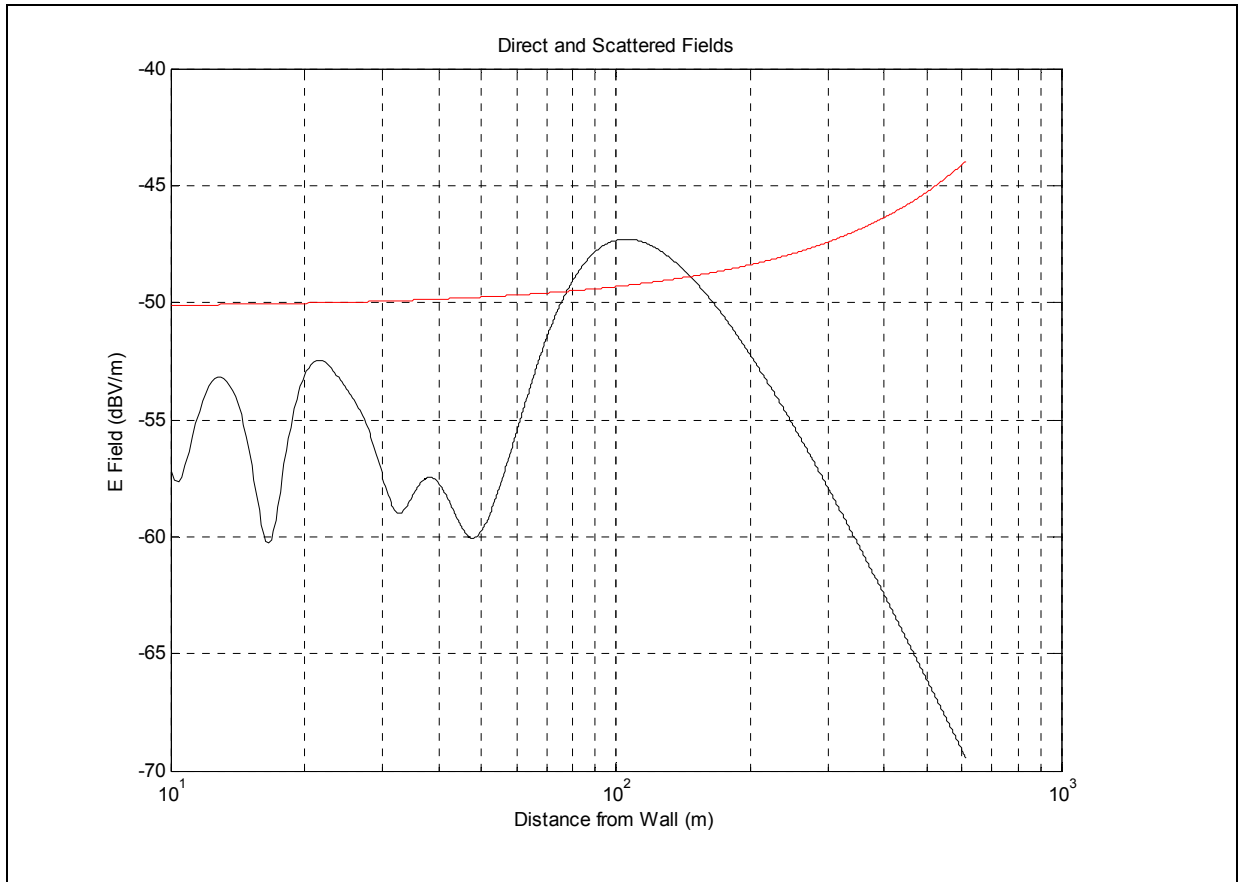


Figure 2.8 Vertical electric field magnitude, 20 m × 10 m wall, ground reflection. Red: direct field, Black: reflected field.

These figures again show a complex near zone reflection field whose magnitude is similar to that of the direct field at the mobile. However, outside of the near zone, the reflected field falls off as $1/d^2$ i.e. by 40 dB/decade. The size of the near zone, while roughly similar to that determined previously, is affected by the ground reflection so that no simple relationship is evident. It is still determined approximately by the size of the reflector.

2.3 Reflection from other surfaces

The analysis given above has focussed on the case where the reflector is a flat building wall. Many structures have more complex shapes, as do natural reflectors such as hills or trees. This section briefly considers more general structures. The scattering behaviour of a general

structure will obviously depend on its shape and each structure will behave somewhat differently.

Consider first a surface made up of a number of plane facets. In this case, to a first approximation, each facet will produce a specular reflection like the flat walls analyzed above. Each specular reflection will have a near zone and a far zone governed by its area and the wavelength. There will also be diffraction from edges but their effect is smaller than that of the specular reflections.

Consider next a smooth surface. For very short wavelengths, it can be shown [5, 6] using geometric optics that the reflected field is given by:

$$E_s = \rho \cdot E_i \cdot \sqrt{\frac{r_1 \cdot r_2}{(d + r_1) \cdot (d + r_2)}} \quad (2.19)$$

where E_i is the incident field, ρ is the reflection coefficient and r_1 and r_2 are the principal radii of curvature of the wavefronts of the reflected field. It can also be shown [5, 6] that $r_1 \cdot r_2 = r_{s1} \cdot r_{s2}$, where r_{s1} and r_{s2} are the principal radii of curvature of the surface at the reflection point. Clearly, near the surface (when $d < r_1, r_2$), the field is about $\rho \cdot E_i$ and far away, it falls off as $1/d$. It is also shown [5, 6] that, for a sphere, geometric optics gives the correct value for the far field radar cross section.

Natural structures are difficult to treat. However, some general statements can be made. Firstly, the largest scattered fields will occur near the structure. The structure can be considered as a collection of scattering objects or equivalent radiating sources. In the absence of a reflecting ground, the scattering of each element will be governed by Equation (2.1) and the scattered field varies inversely with distance from the element. If some of the scattering elements lie approximately in a plane, they will produce a specular reflection like that of a flat surface in a direction perpendicular to the plane. If a reflecting ground is present, it is well known [2, 3] that the field of a radiating element varies as $1/d^2$ where d is the distance from the radiator. This is also evident in **Figures 2.6 to 2.8** for flat wall reflectors. In the far field, the wave from the source grazes the earth and the ground

reflection coefficient goes to -1 [5]. Thus, the scattered field goes to zero far from the structure and the largest fields must be close to it. There will be a near zone but its size cannot be predicted. The magnitude of the reflected field near the structure also cannot be predicted.

The scattering from large rough surfaces is considered in [36]. The surface elevation is considered to be random with a normally distributed height variation. The average of the height variations is zero and the standard deviation of the height variations is σ_s . The reflection coefficient is taken to be -1 in the absence of the terrain height variations. It is shown that the scattered field consists of a random diffuse component and a specular component. The mean value of the specular component is smaller than for a smooth flat surface and is given by :

$$A_s = \exp\left(-0.5 \cdot \left(\frac{4 \cdot \pi \cdot \sigma_s \cdot \sin \gamma}{\lambda}\right)^2\right) \quad (2.20)$$

where σ_s is the surface roughness, λ is the wavelength and γ is the grazing angle of the wave i.e. the angle between the direction of propagation of the incident wave and the mean surface. This expression is generally taken, in practice, as the factor by which the reflected wave is reduced by the roughness of the surface. The scattered wave varies randomly with location and has a Rician distribution [36] i.e. the wave has a specular component and a component with a random amplitude and phase as a function of position. The magnitude of the specular component is calculated from Equation (2.20) above. It is shown that, as the surface gets rougher, the amplitude of the specular component decreases and that of the random component increases. At the same time, more and more of the wave power is scattered in directions other than the specular direction.

Another aspect which has not been considered so far is polarization. In the analysis of Section 2.2, the polarization of the incident field was vertical and the equivalent sources of the scattered field were vertical as well. In general, depending on the polarization of the incident wave and the slope of the reflecting surface, the polarization of the scattered wave

may be different from that of the incident wave. The greater the surface roughness, the greater is the depolarization [36].

Equation (2.20) implies that a surface of greater roughness will have a smaller average reflected signal and, therefore a generally smaller multipath distortion. Similarly, a smaller wavelength (higher frequency) will produce a similar effect. This implies that a higher frequency signal would have less multipath distortion. This seems to be borne out by experimental measurements of near zone scattering by Al-Nuaimi and Ding [23, 24] at 11 GHz (small wavelength) which show lower than predicted levels. On the other hand, the Doppler shifts due to motion would be higher and a receiver would have to track higher rates of change of the signal frequency and the multipath variations. The analysis in Section 2.2 was done for a relatively low frequency around 300 MHz because it was felt that lower Doppler rates would be more favourable for signal tracking. Further work is required in this area to determine where the greatest advantage lies.

2.4 Summary and evaluation of analysis results

The analysis of the geometry of **Figure 2.1** gives the following general results:

- The reflected near fields of a reflecting wall are of the same order as the incident field and the field at the mobile when the mobile is close to the wall.
- The fields are large only near the reflector; the near zone cross section is the wall shape and extends out to a distance which is related to the size of the wall.
- Beyond the near zone distance, the field drops off as $1/d^2$ where d is the distance from the wall.
- The magnitude of the reflected field depends on the reflection coefficient of the wall.
- The field in the near zone is very complex and highly variable with position.
- As a mobile moves in the near zone, there will be significant periodic level variations and signal distortion.

The model of **Figure 2.1** is somewhat idealized in that the ground is not always very flat, although the terrain and roads in many suburban areas are. If the terrain is not flat, the reflection properties of the ground will not be the same as those of the model. If the terrain is rough, the magnitude of the ground reflection coefficient will be less than -1 . In addition, the ground reflection may be different for the direct fields and those reflected from the structure. For example, if the reflection coefficient for the direct field is small, the direct field will tend to be larger than the reflected field and the influence of the reflection near zone of the structure will extend to a smaller distance or have little effect. If the terrain between the reflector and the mobile is rough or the reflection is otherwise obstructed, the reflected field will be larger than the direct field and the influence of the reflected field will extend to larger distances. If the reflections are reduced or obstructed for both the direct and reflected fields, the situation is like that of parts b) and c) above for an isolated reflector for which the field falls off as $1/d$ outside the near zone.

At this point, it is appropriate to re-emphasize the distinction between specular reflection and scattering. For a flat wall, there will be a direction of specular reflection which is the direction for an infinite plane reflector at the same location. For a finite wall, the reflection will mostly be contained by the wall cross-section in the near zone and, in the far zone, will have a beamwidth related to the width of the wall. For a wall of width W (or projected width for oblique incidence), the half power beamwidth (in the horizontal plane) in the far field will be about λ/W [5]. For a 10 m wide wall at broadside incidence and a wavelength of 1 m, this beamwidth is 0.1 radians = 5.7 degrees. For wider walls, the beamwidth is smaller. Most of the incident power will be scattered within this angle. However, a scatterer will scatter some power in all directions. Thus, a received signal will consist of a direct wave, specularly reflected waves and scattered waves. The specularly reflected waves represent waves within the cross-section or beamwidth of reflectors while the scattered waves represent energy scattered in all directions. The specular components have discrete delays while the scattered components have a more or less continuous distribution of delay since they come from all the scattering structures in the area, including natural terrain features.

The above analysis and the practical considerations have been validated qualitatively by several experiments which are described in the next chapter.

CHAPTER 3

EXPERIMENTAL RESULTS

3.1 General

This chapter presents measurements of a communication channel between a base station and a moving vehicle in suburban and semi-rural areas which have line-of-sight (LOS) or near LOS propagation. The objective is to provide a better understanding of the communications environment for this type of link and to validate the conclusions of Chapter 2, which presents a theoretical analysis of such a channel.

A number of experiments have been performed to characterize a mobile communications channel. The experiments consisted of setting up and running a communications link between a base station and a moving vehicle. The radios were standard line-of-sight systems with simple single carrier modulation formats. Data rates were 1 to 3 Mb/s. Link error rates were measured along with received signal spectra and signal levels. Measurements were also made in one case with a pulse transmitter. The experiments were conducted in a suburban area and a semi-rural area. All of the experiments and measurements described in this chapter have been obtained by the author, in conjunction with his colleagues from Ultra Electronics, as noted in the Acknowledgements. All conclusions derived from these results are due to the author.

The experiments were performed to validate the results derived by the author in the analysis of Chapter 2. Prior to this analysis, it had been expected that, as long as a line of sight existed between the base station and the mobile, communication would generally be possible with low error rates, although the multipath interference would degrade the receiver threshold and reduce the link range. The received signal would contain a relatively steady direct component. On the other hand, for the obstructed case, the largest component could be from a reflection and this would fluctuate, causing changes between minimum phase and non-minimum phase conditions. This would tend to produce numerous signal outages with

consequent poor link performance. It was also expected that for the line-of-sight case, the level of the direct component would be significantly larger than any single reflected component.

Contrary to the initial expectations, it was found that, even for line-of-sight conditions, there were numerous outages and severe multipath signal distortions. The link error rates were often poor and loss of timing synchronization was frequent. It was noted that, whenever the mobile approached a structure, there would be link problems, even in the semi-rural environment. The channel behaviour tended to be either good, with few errors, or bad. The bad channels were usually characterized by a single dominant reflection with small delay which produced periodic fading with significant level variations and severe signal distortion.

The next section gives some typical experimental results and an analysis of their implications.

3.2 Experimental results

3.2.1 Measurement methods

The experiments consisted of running a full duplex communications link between a base station and a moving vehicle, the scenario illustrated in **Figure 2.1**. The base station had an omnidirectional (in azimuth) vertically polarized antenna on top of a 20 m mast. The vehicle was a pickup truck with a vertical antenna mounted in the back. The base of the antenna was at a height of roughly 2 m above the ground and the length of the antenna was about 2 m. The base station and vehicle antennas were the same type, vertical dipole arrays having a nominal gain of 4 dBi. The communication links were run at frequencies in the range of 300 MHz to 400 MHz at bit rates of 1 Mb/s to 3 Mb/s using simple modulation formats. During the experiments, received error rates, received signal levels and received spectra were monitored.

Also, the mobile contained a video camera and the base station had a monitor, allowing an assessment of the structures near the mobile when the link performance was poor. In addition, in one case, a pulse transmitter was used to directly study the reflections. The link configuration is shown in **Figure 3.1**. The term BERT refers to a Bit Error Rate Test Set.

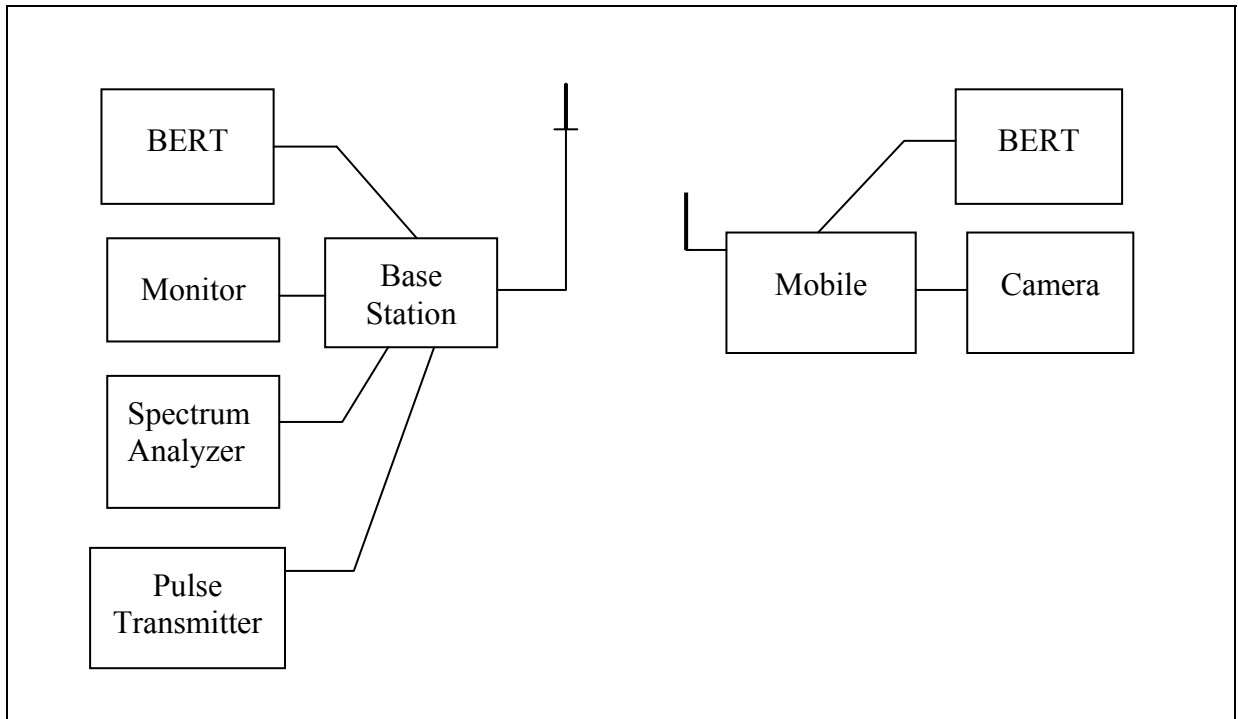


Figure 3.1 Experimental link configuration.

The experiments were run in two locations: a suburban location with a mixture of residential buildings and office buildings and a semi-rural area with single houses and small clusters of farm buildings. The link lengths ranged from about 250 m to several km. In most cases, a line of sight existed between the base station and the vehicle. Under these conditions, the received signal level was usually well above the receiver threshold and no errors would be expected due to noise.

The radios used for this experiment were digital radios transmitting and receiving continuously on different frequencies. The waveforms were simple and robust QPSK and

binary FM (CPFSK). The QPSK transmitter and receiver used matched root raised cosine filters and coherent demodulation. The binary FM transmitter used Gaussian filtering plus pre-emphasis while the receiver used Gaussian filters and limiter-discriminator detection. Block diagrams of the QPSK and binary FM receivers are shown in **Figures 3.2** and **3.3**.

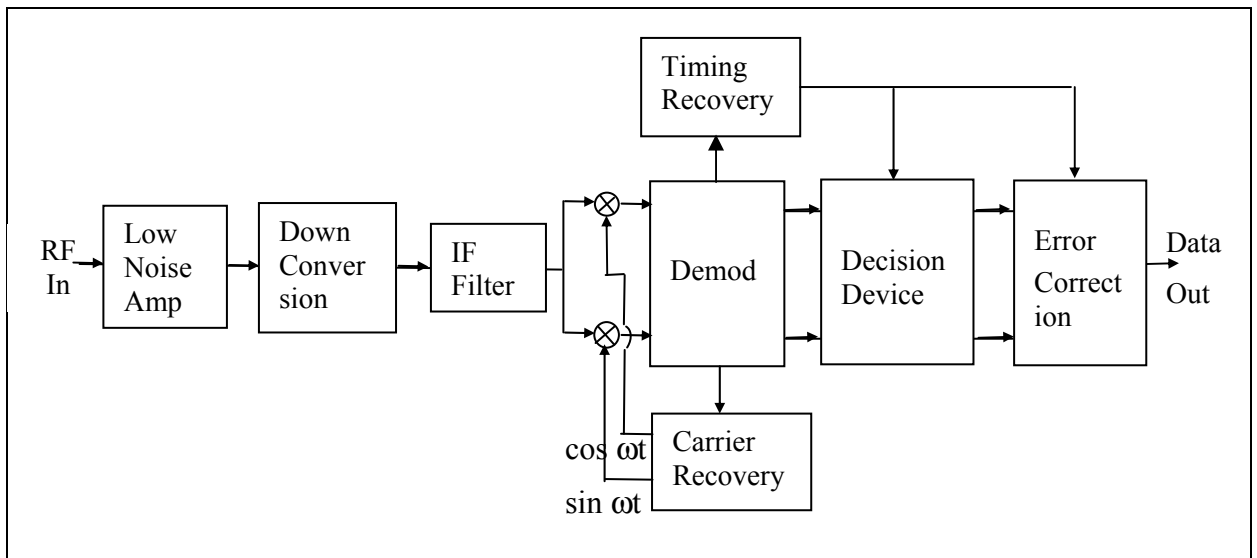


Figure 3.2 QPSK receiver.

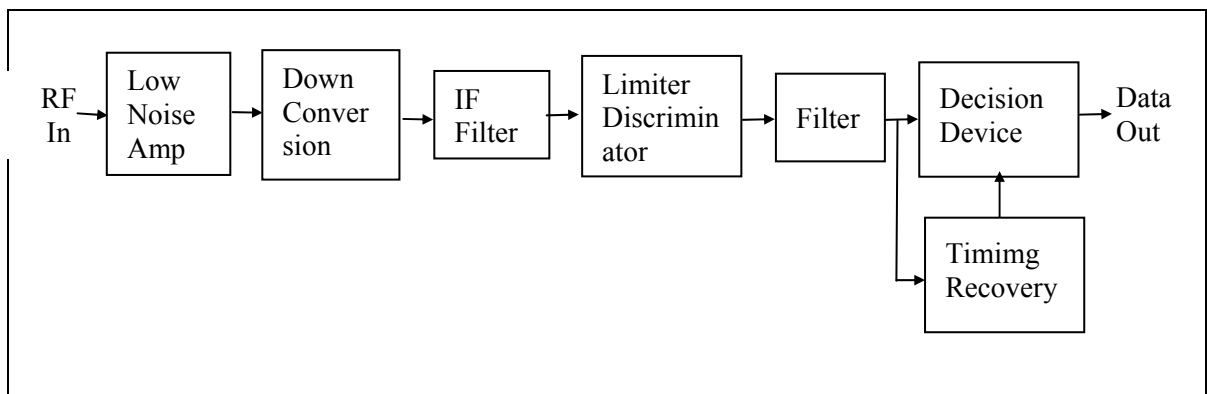


Figure 3.3 Binary FM receiver.

The transmitter output power was about 35 dBm, while the receiver thresholds for a 10^{-5} error rate in thermal noise were typically better than -90 dBm. The received signal levels were therefore generally well above threshold.

3.2.2 Results

The experimental results are divided into four sections. The first gives typical distributions of error rates. The second shows examples of measured spectra. The third illustrates measurements of received levels. The fourth shows the results of the pulse transmitter tests. These results are shown in the following sub-sections.

a) Error rate distributions

It was typically found that the link performance would be either good with few errors or very poor with high error rates and frequent loss of link synchronization. Link error rates were monitored continuously during a test run and sampled every 2 seconds. The results are summarized as a distribution of the sample values i.e. the percentage of samples with various error rates. Typical results are displayed as pie charts in **Figure 3.4** for suburban and rural runs respectively. These results were obtained with a link using binary FM modulation, a form of continuous phase FSK extensively used in military systems, at a transmitted bit rate of 1 Mb/s, although similar results were obtained with other simple modulation methods.

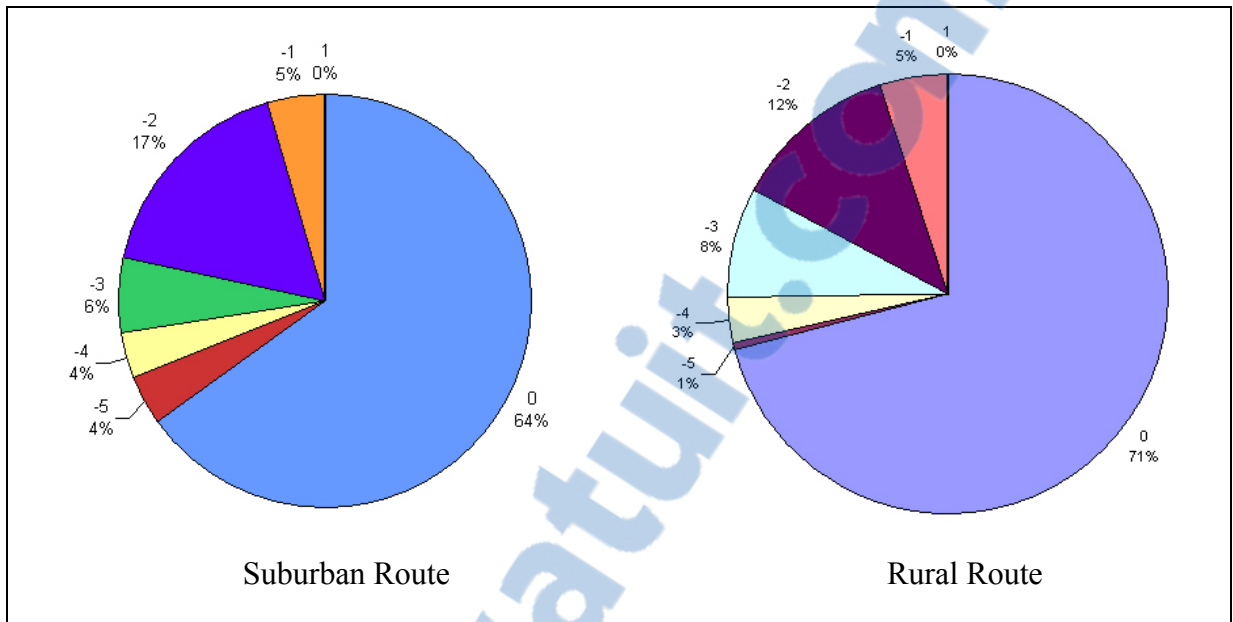


Figure 3.4 Distribution of error rates, suburban and rural links.

These charts show the percentage of the time that the error rate exponent is a given value. For example, an exponent of -4 indicates that the error rate is between 10^{-4} and 10^{-3} . Note, however, that the values 0 and 1 represent actual BER values. It can be seen that the error rate in both cases is 0 for the majority of the time but, for 1/3 or 1/4 of the time respectively, the error rate is significant.

These results are typical, with the suburban results worse than the rural, but the pattern indicates a 0 error rate for the majority of the time but significant errors for 10% to 30% or more of the time. Error rates greater than 10^{-1} likely represent loss of synchronization of timing recovery. These runs were for short routes with the maximum range less than about 2 km. On longer routes, the percentage of time with 0 error rate is smaller. It was also noted that results for the base station to mobile and mobile to base station were very similar, as would be expected due to reciprocity.

The results show that there are many locations where there is little multipath and other areas where multipath interference is very high. For a simple modulation like binary FM, it is

reasonable to assume that a 0 error rate implies that the interference is at least 10 to 15 dB below the desired signal since the signal levels are well above the receiver thresholds. On the other hand, an error rate above 10^{-2} implies an interference level within a few dB of the desired signal.

This type of behaviour for a wireless channel, i.e. either very good or bad, has been noted by other authors, e.g. [34]. In the present study, it was noted that most of the “bad” areas were close to buildings. When the mobile unit approached a structure, the error rate would increase and there would be losses of timing synchronization. A typical situation is illustrated in the sketch of **Figure 3.5**. The transmitter was about 250 m from the mobile and the mobile was in the parking lot of a commercial building. When the mobile was close to the building within the area where the reflection from the front wall would be, the link transition between these areas was quite sudden.

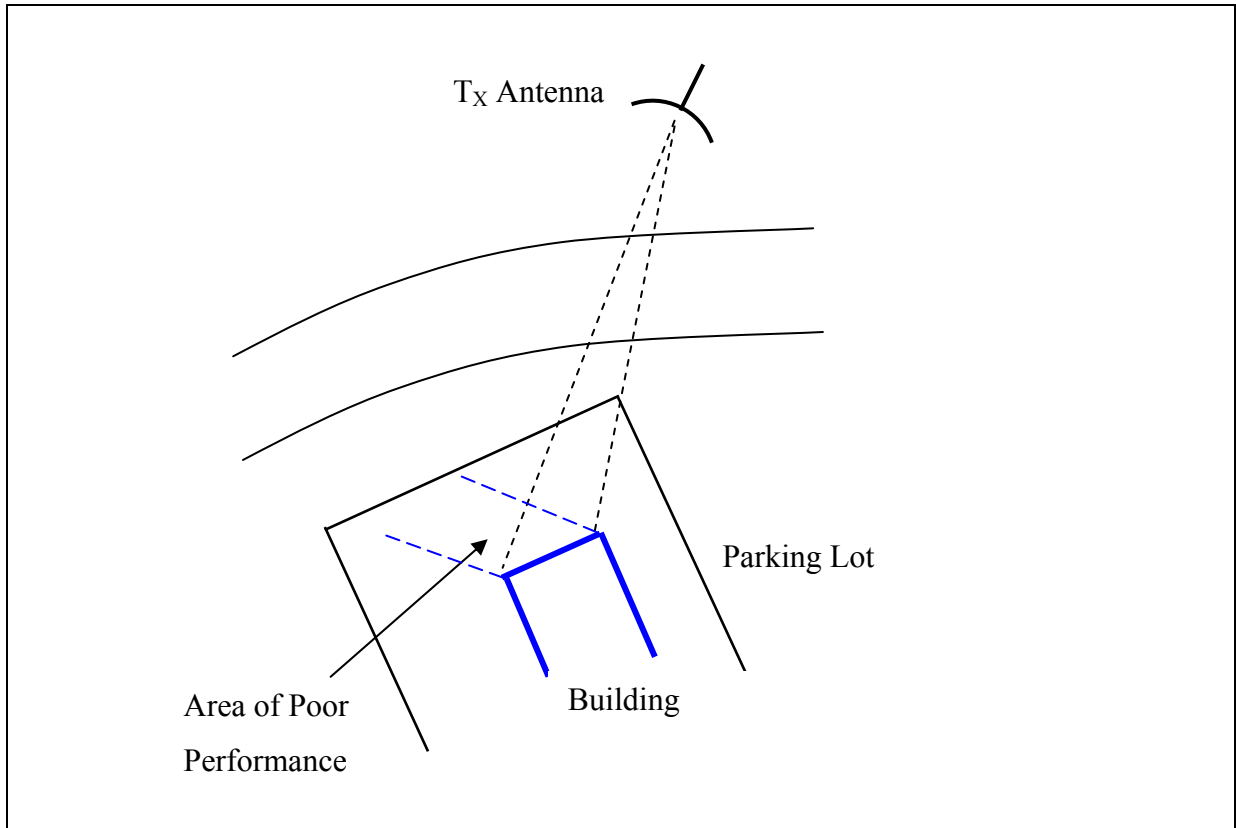


Figure 3.5 Mobile close to a building.

b) Spectrum measurements in bad areas

During the test runs, received spectra were monitored continuously using a spectrum analyzer. Spectra were recorded throughout the run to capture typical responses, especially when the mobile entered a “bad” area. Sampling was done manually so that the number of recordings is not large but the recorded spectra are very representative. Most measurements were made at the base station but the spectra at the mobile were found to be similar.

Measurements were made both at RF frequency and at the receiver IF frequency. In the first case, the spectrum analyzer was used as a receiver directly and was preceded by a low noise amplifier. In the second case, the radio receiver was used and measurements were made using a spectrum analyzer at the IF frequency of 140 MHz. **Figures 3.6 to 3.10** show typical spectra.

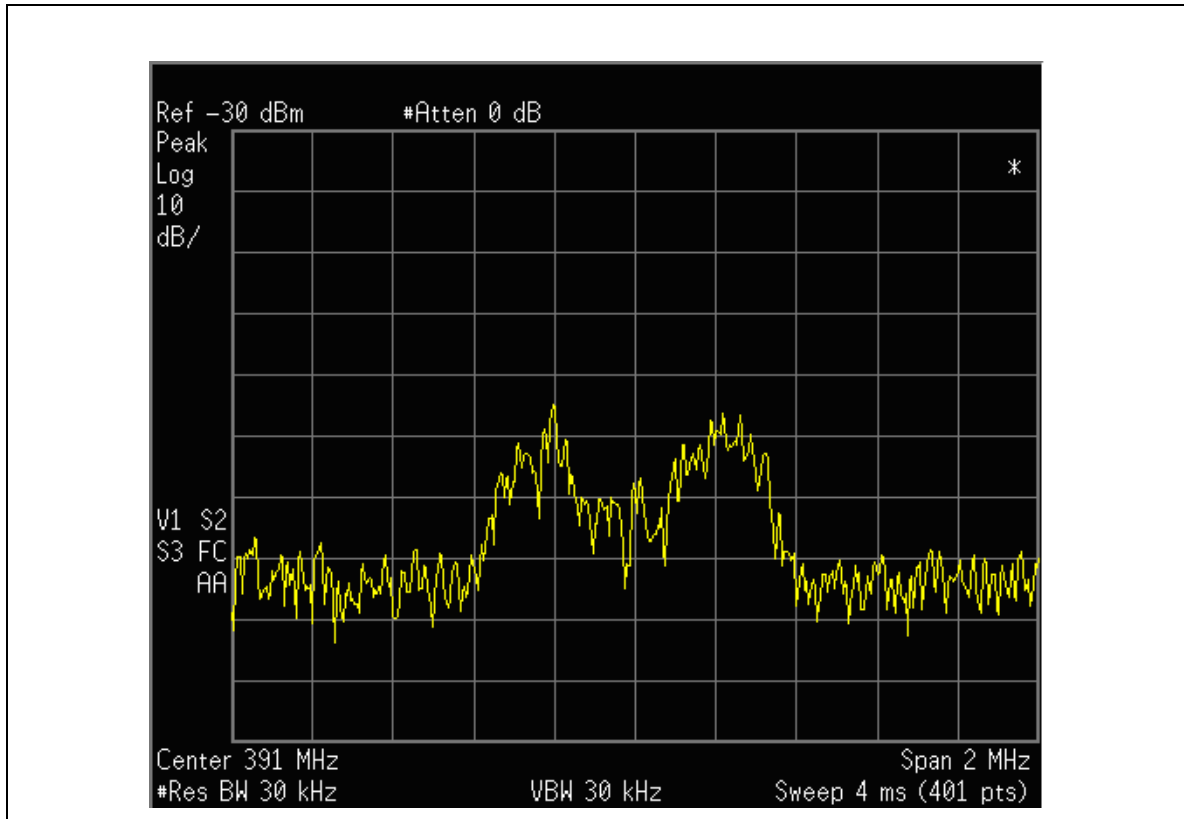


Figure 3.6 RF spectrum (18 February 2005).

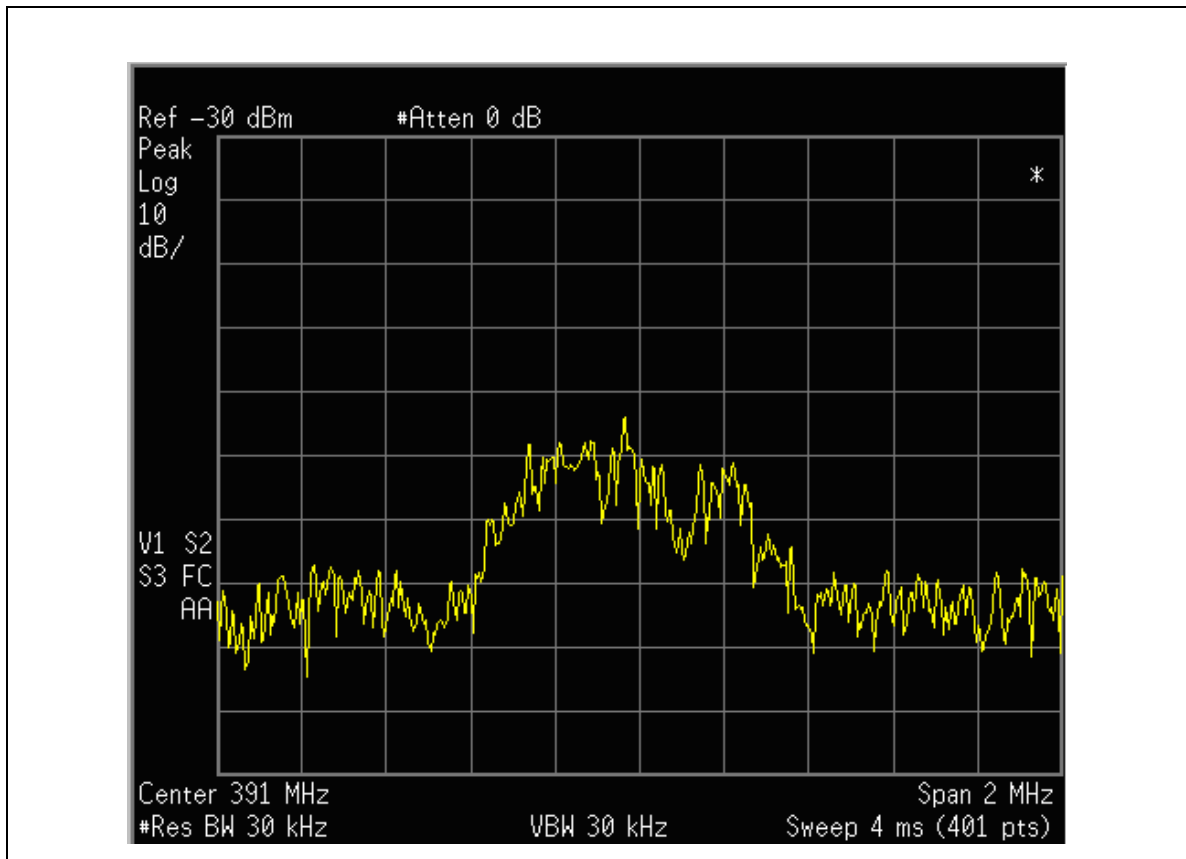


Figure 3.7 RF spectrum (18 February 2005).

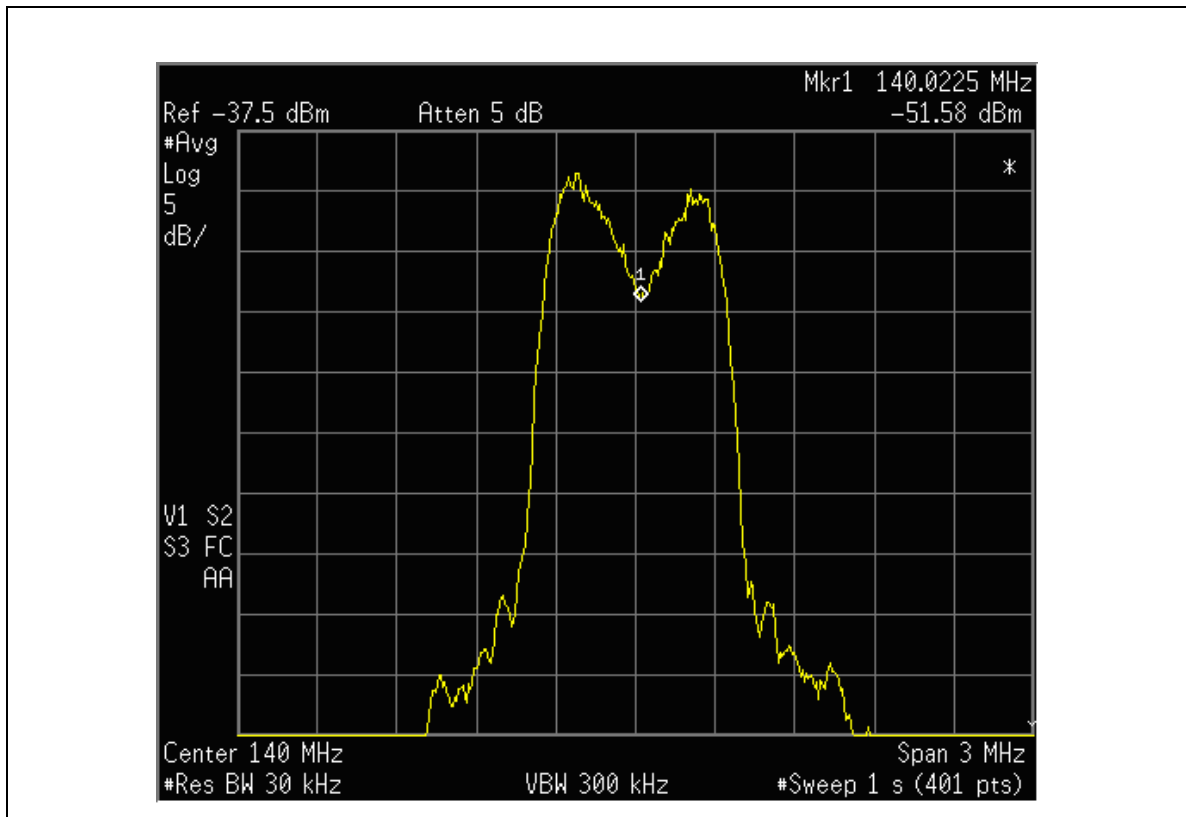


Figure 3.8 IF spectrum (18 February 2005).

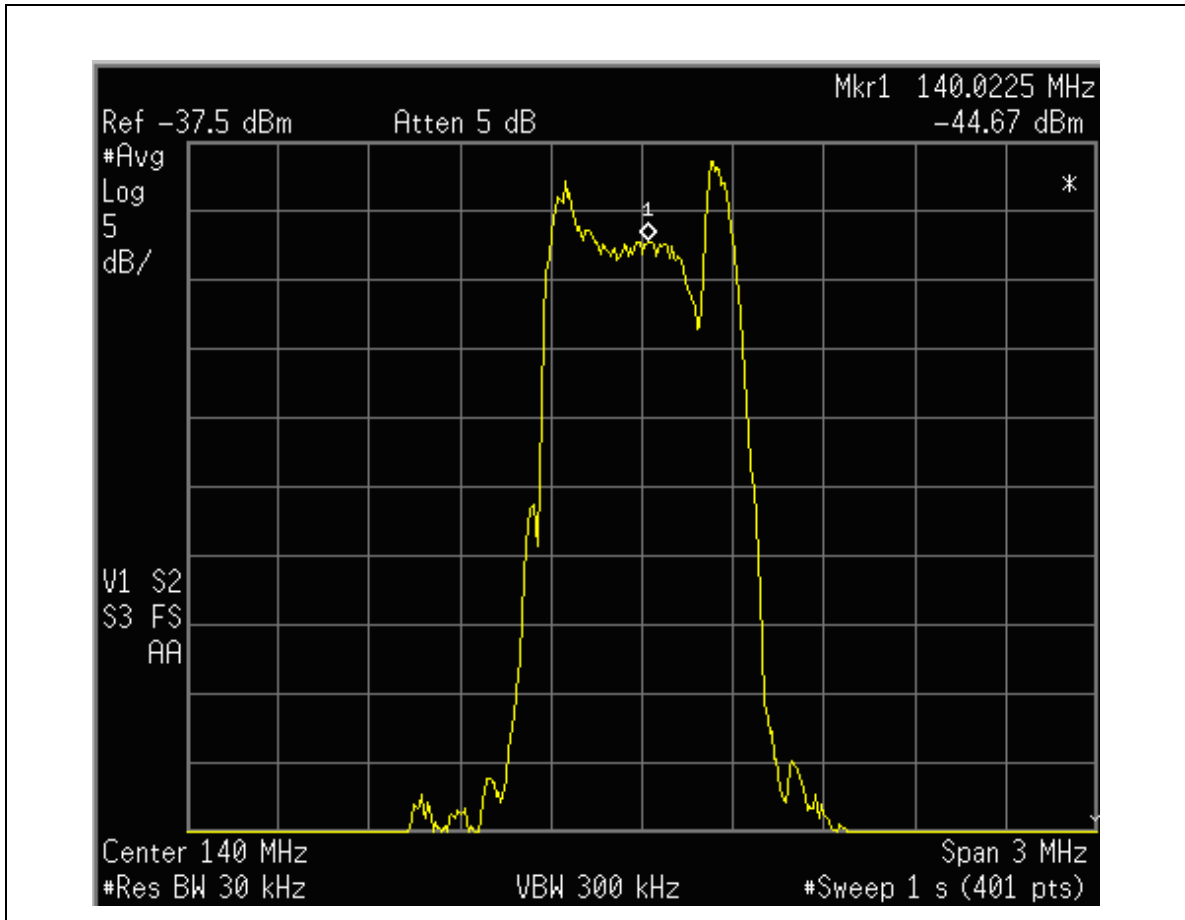


Figure 3.10 IF spectrum (18 February 2005).

The spectra of **Figures 3.6 to 3.9** show very significant distortion with a large notch in the spectrum, indicating a single dominant reflection. **Figure 3.10** has a more complex distortion than a single notch, indicating more than one reflection. All of these figures represent bad channels.

The spectrum obtained from the spectrum analyzer has only amplitude information and therefore represents the power spectrum of the positive frequency portion of the received signal around the carrier frequency. The envelope of the autocorrelation of the received signal can be obtained from the inverse Fourier transform of this power spectrum, treating the spectrum as a lowpass spectrum centered on 0 frequency. Let the displayed lowpass power spectrum be $V(f)$. Then, the complete power spectrum is:

$$V_1(f) = V(f - f_0) + V(-f - f_0) \quad (3.1)$$

Taking the inverse Fourier transform gives:

$$U_1(\tau) = U(\tau) \cdot e^{j2\pi f_0 \tau} + U^*(\tau) \cdot e^{j2\pi f_0 \tau} \quad (3.2)$$

where $U_1(\tau)$ is the autocorrelation function of the complete waveform and $R(\tau)$ is the inverse Fourier transform of $V(f)$. Let $U(\tau) = U_p(\tau) + jU_q(\tau)$. Then, the envelope of the autocorrelation function is:

$$|U(\tau)| = \sqrt{U_p^2(\tau) + U_q^2(\tau)} \quad (3.3)$$

However, if a bandpass signal consists of a sum of delayed replicas with distinct delays, amplitudes of the delayed components can often be determined. Assume a bandpass signal consisting of the sum of 3 components, the direct signal and 2 delayed components.

$$y_b(t) = \sum_{i=0}^2 a_i \cdot x_b(t - t_i) \cdot \cos(2 \cdot \pi \cdot f_0 \cdot (t - t_i) + \beta(t - t_i) + \varphi_i) \quad (3.4)$$

where $x_b(t)$ is the amplitude modulation, $\beta(t)$ is the phase modulation and φ_i is a phase shift. The t_i are delays with $t_0 = 0$.

The autocorrelation function $U_{y_b}(\tau) = E(y_b(t+\tau) \cdot y_b^*(t))$ will be a bandpass function whose envelope has 4 peaks: at $t = 0, t_1, t_2$ and $|t_1 - t_2|$ as well corresponding peaks at negative delay values. The peaks will be distinct as long as $|t_1 - t_2|$ is not equal to t_1 or t_2 and the 4 peaks do not overlap (due to the finite bandwidth of the modulated signal). The relative amplitudes of the envelope peaks are given by:

$$\begin{aligned} 0: & \quad |a_0|^2 + |a_1|^2 + |a_2|^2 \\ t_1: & \quad |a_0 \cdot a_1| \\ t_2: & \quad |a_0 \cdot a_2| \\ |t_1 - t_2|: & \quad |a_1 \cdot a_2| \end{aligned} \quad (3.5)$$

Thus, the magnitudes and delays of the delayed reflected components can often be determined from the envelope of the autocorrelation function given by Equation 3.5. However, the minimum delay which can be distinguished is limited by the bandwidth of the signal modulation.

A number of spectra have been analyzed in this way and are shown below. The spectrum and its corresponding autocorrelation envelope are shown in the same figure. The autocorrelation function has been obtained by a discrete inverse Fourier transform (IDFT). The spectral data had 401 points and a 401 point IDFT was used as well. No smoothing or windowing has been used on the spectral data prior to inverse Fourier transformation. In this experiment, the time resolution of the measurement system is not very good due to the relatively low bandwidth of the signal. Windowing would widen the peaks of the time domain displays and degrade the time resolution further.

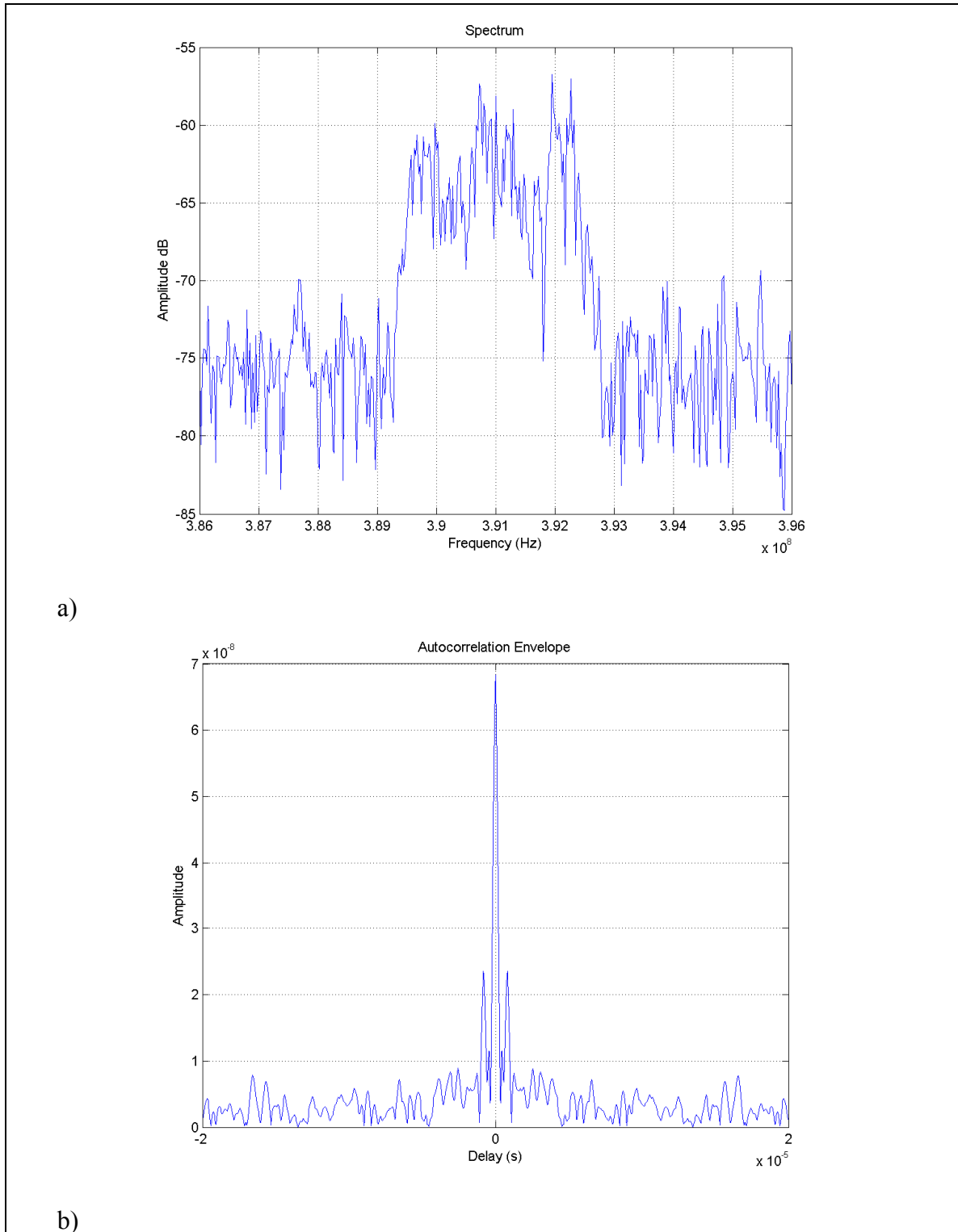


Figure 3.11 Spectrum analysis (a & b).

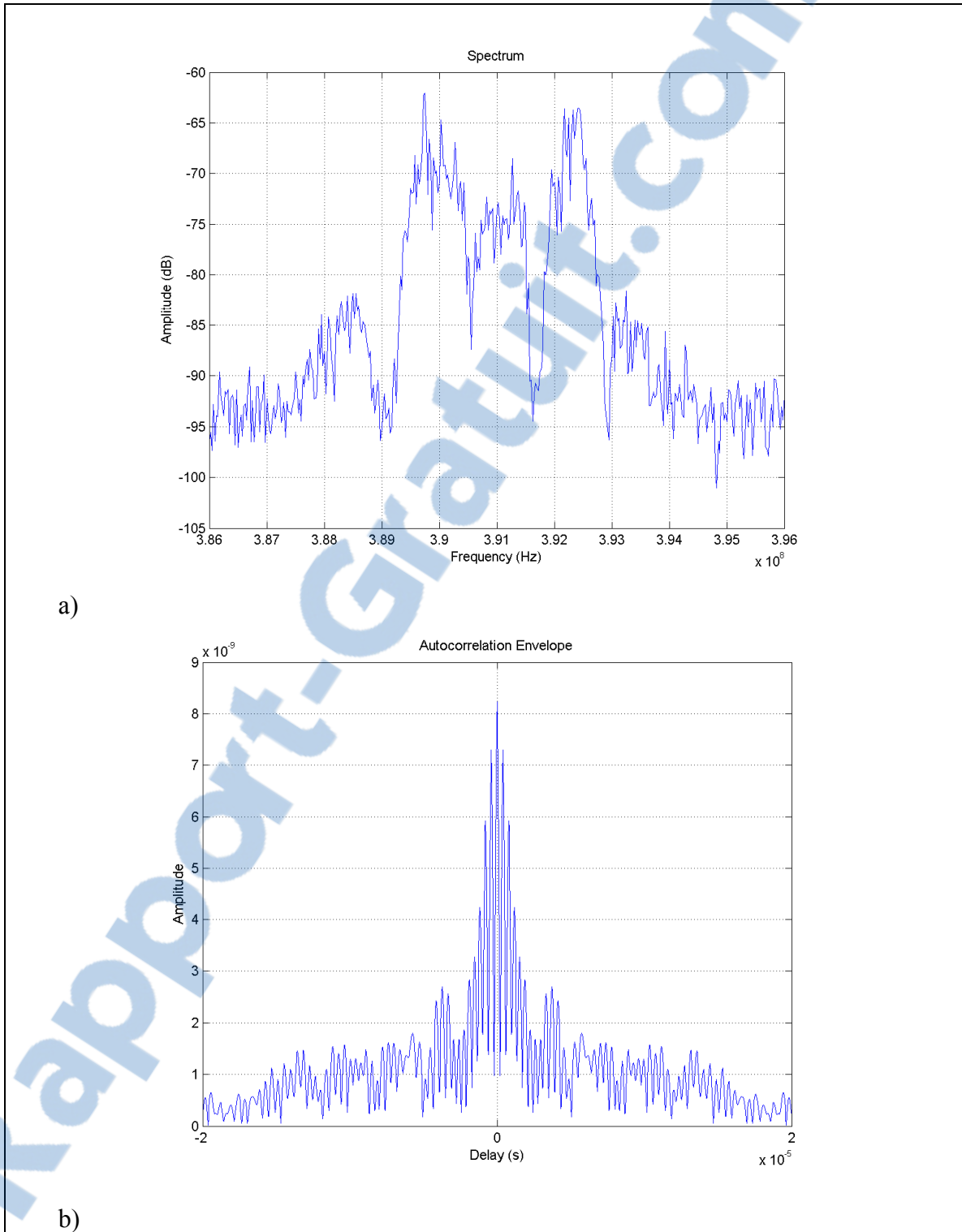


Figure 3.12 Spectrum analysis (a & b).

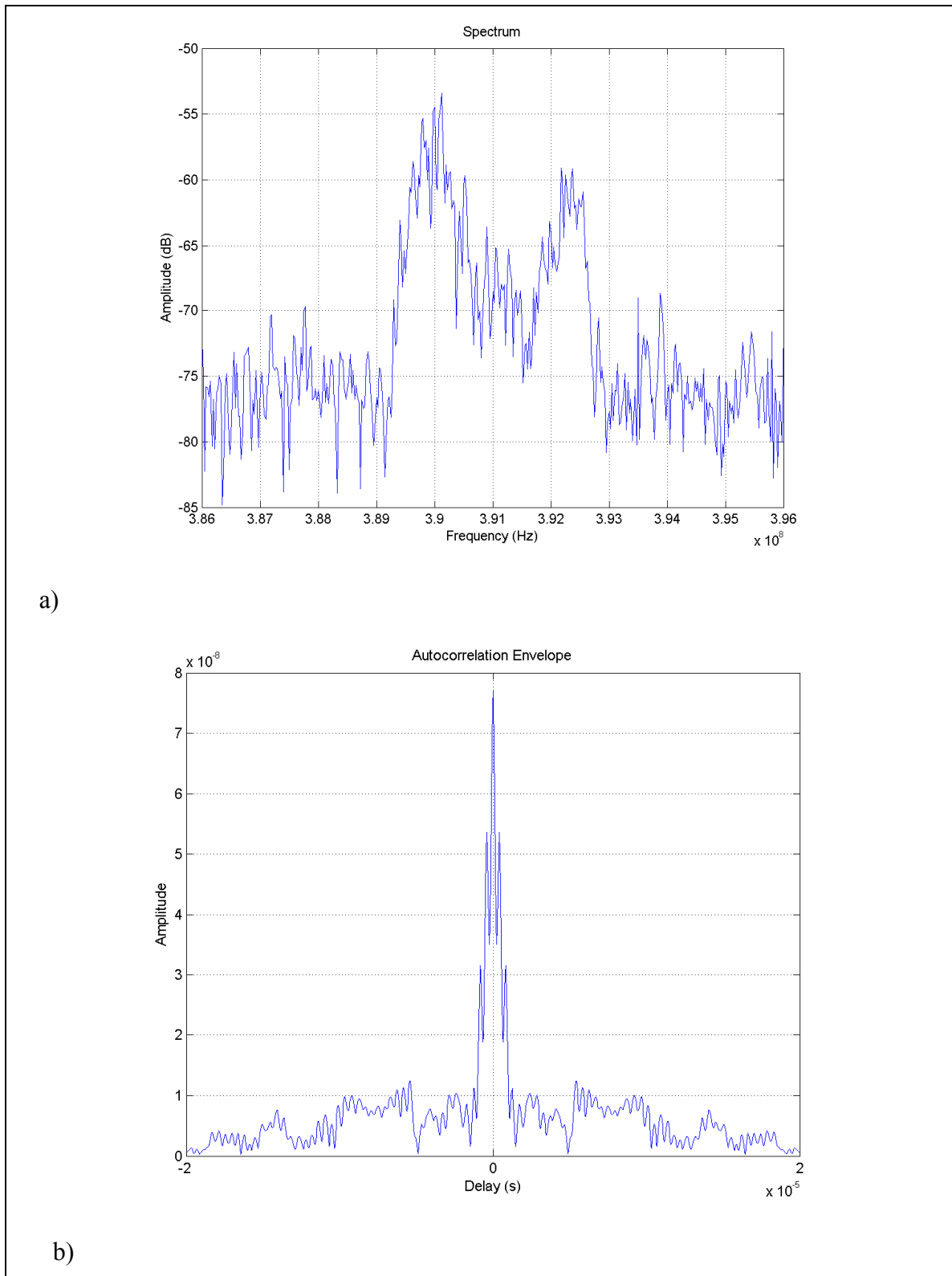


Figure 3.13 Spectrum analysis (a & b).

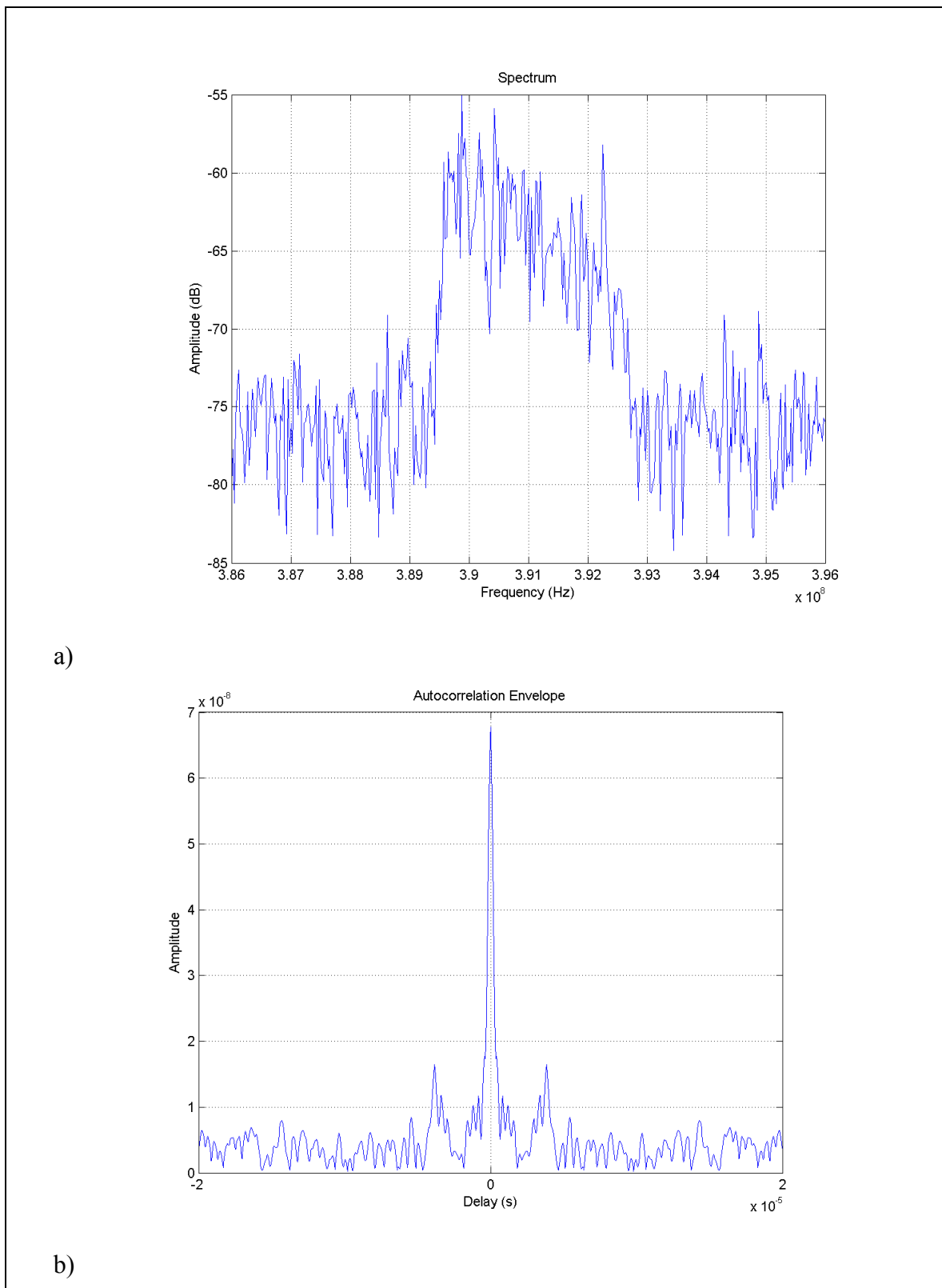


Figure 3.14 Spectrum analysis (a & b).



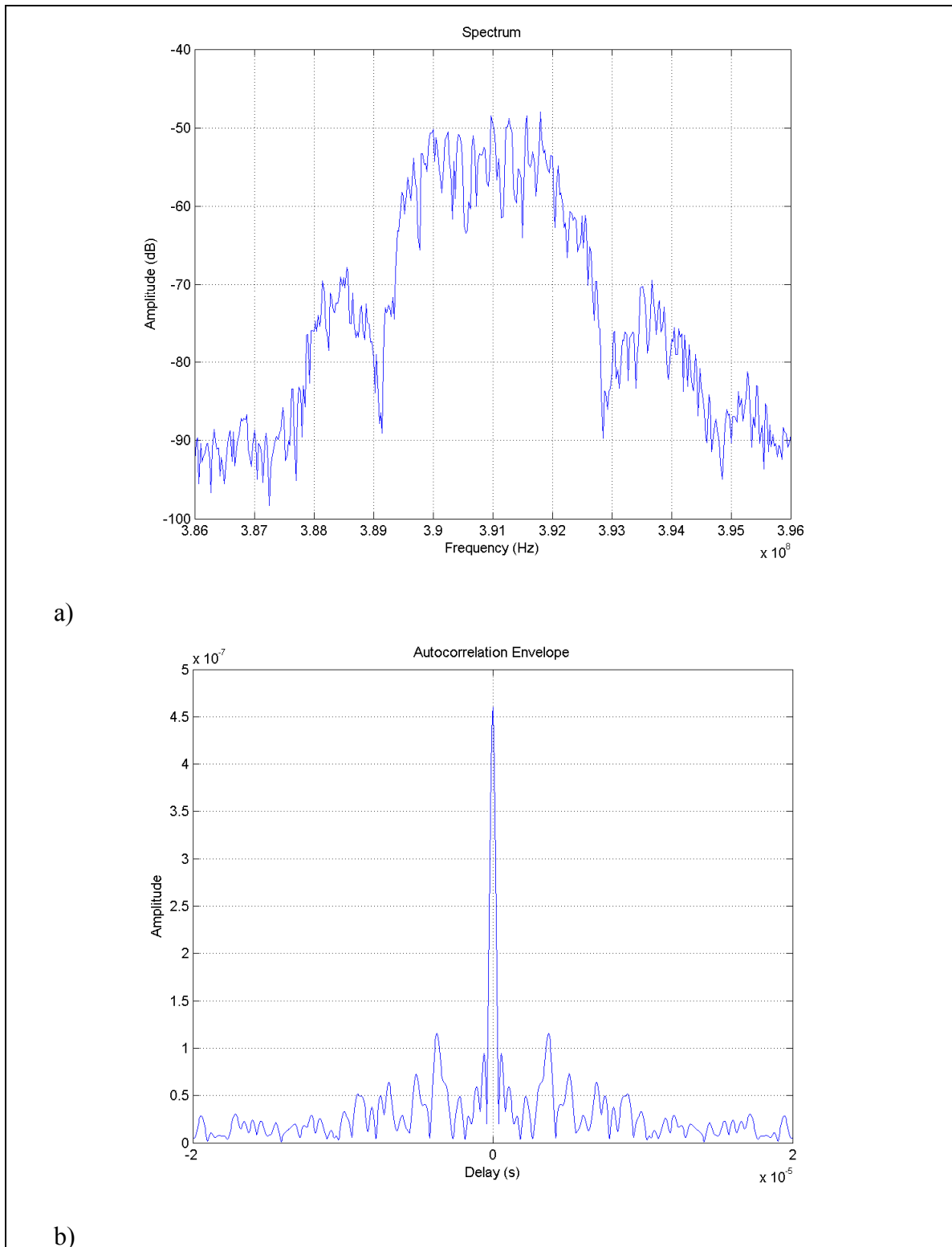


Figure 3.15 Spectrum analysis (a & b).

In **Figure 3.11**, there is only one significant reflection with a delay of 0.82 μs and an estimated amplitude of 0.4 relative to the main component.

In **Figure 3.12**, there are a number of reflections, with at least one being of high amplitude. The simple analysis does not apply here.

In **Figure 3.13**, there are 2 significant reflections, with delays of 0.43 μs and 0.82 μs . Again, the simple analysis does not apply since the difference in delay between the two reflected components will fall on the first reflected component and make it impossible to determine an accurate value of amplitude for the first reflected component. However, the reflections are a significant percentage of the main signal.

In **Figure 3.14**, there is only one relatively small reflected component visible at a delay of 3.8 μs . However, the significant slope of the spectrum indicates that a large reflection of very small delay is present but cannot be distinguished in the autocorrelation due to the bandwidth of the modulation. Its delay is a small fraction of a microsecond and the fact that the spectrum drops by 10 dB over its width indicates that the relative reflection amplitude is greater than 0.5. (For a single reflection with a relative amplitude b , the peak to peak variation in channel frequency response is $(1-b)/(1+b)$).

In **Figure 3.15**, the signal spectrum appears almost undistorted, with perhaps a small reflection at a delay of 3.7 μs and a relative amplitude of about 0.27. Other smaller reflections are present at delays of 0.6 μs and 5.1 μs . There is either no large reflection or it is not visible because it has very short delay, with the channel frequency response nulls symmetrically located around the center frequency.

The graphs show the range of results which were observed. Many spectra did not have extreme distortion while others showed only a single notch or tilt, indicating that there was probably a single dominant reflection. The delay of this reflection was usually less than about 1 μs . However, sometimes, there were spectra with several equally spaced notches,

indicating a reflection with longer delays. Occasionally, there were very distorted spectra with several reflections.

Figures 3.11 to 3.15 show that analysis of signal spectra can sometimes, but not always, give an indication of the magnitudes of reflections present in the received signal.

c) Level measurements

Some test runs were made to measure received signal level using a spectrum analyzer set to zero span mode (i.e. sweeping in time at a fixed frequency). The resolution bandwidth of the analyzer was set large enough to capture most of the received signal energy. The video bandwidth was selected to smooth the signal, consistent with the sweep rate. Generally, it was set equal to or slightly less than the resolution bandwidth.

Measurements were made both at RF frequency and at the receiver IF frequency. In the first case, the spectrum analyzer was used as a receiver directly and was preceded by a low noise amplifier. In the second case, the radio receiver, with the RF AGC disabled, was used and measurements were made using a spectrum analyzer at the IF frequency of 140 MHz. The signal on the link was a 1 Mb/s QPSK modulation.

Some typical measurements are illustrated in the figures below for both RF and IF measurements. These measurements were made on the rural route but similar results were observed during the suburban tests.

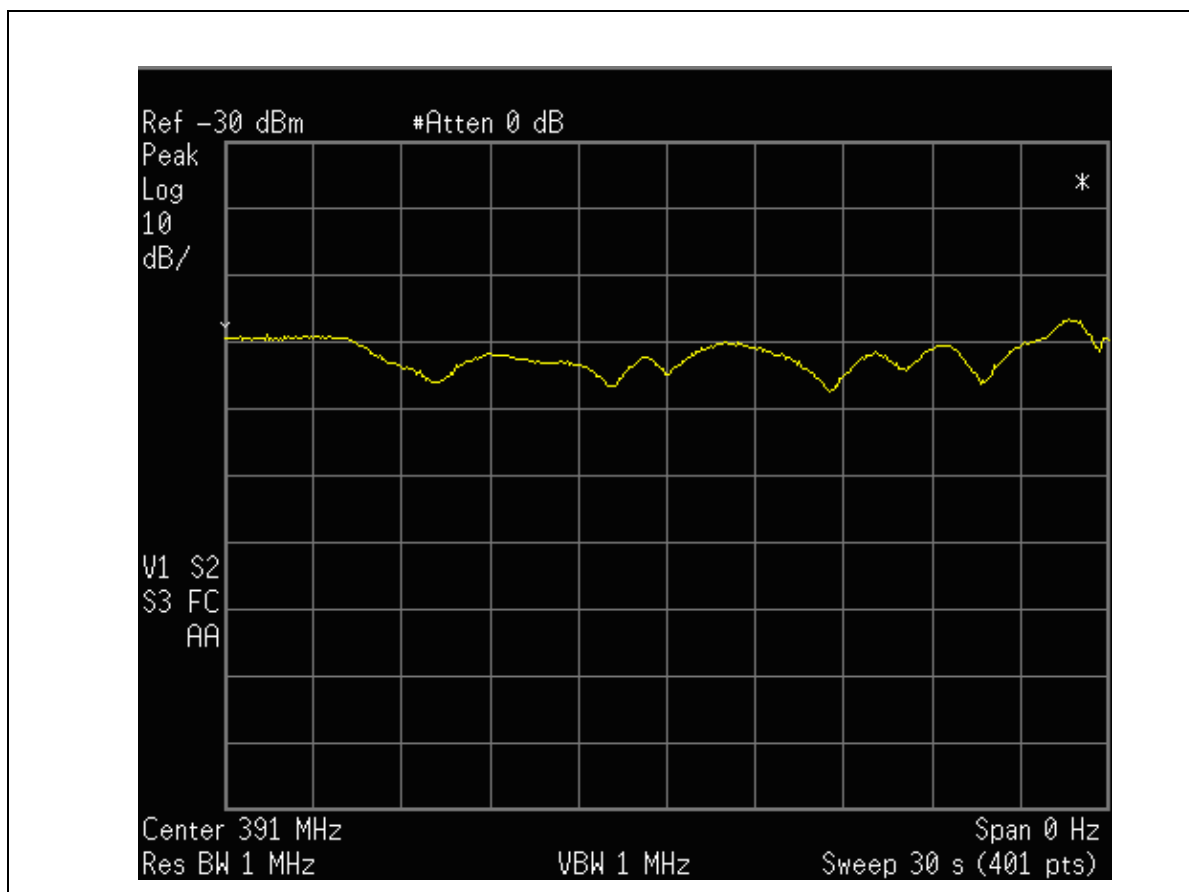


Figure 3.16 RF level variation with time, slow random variations (18 February 2005).

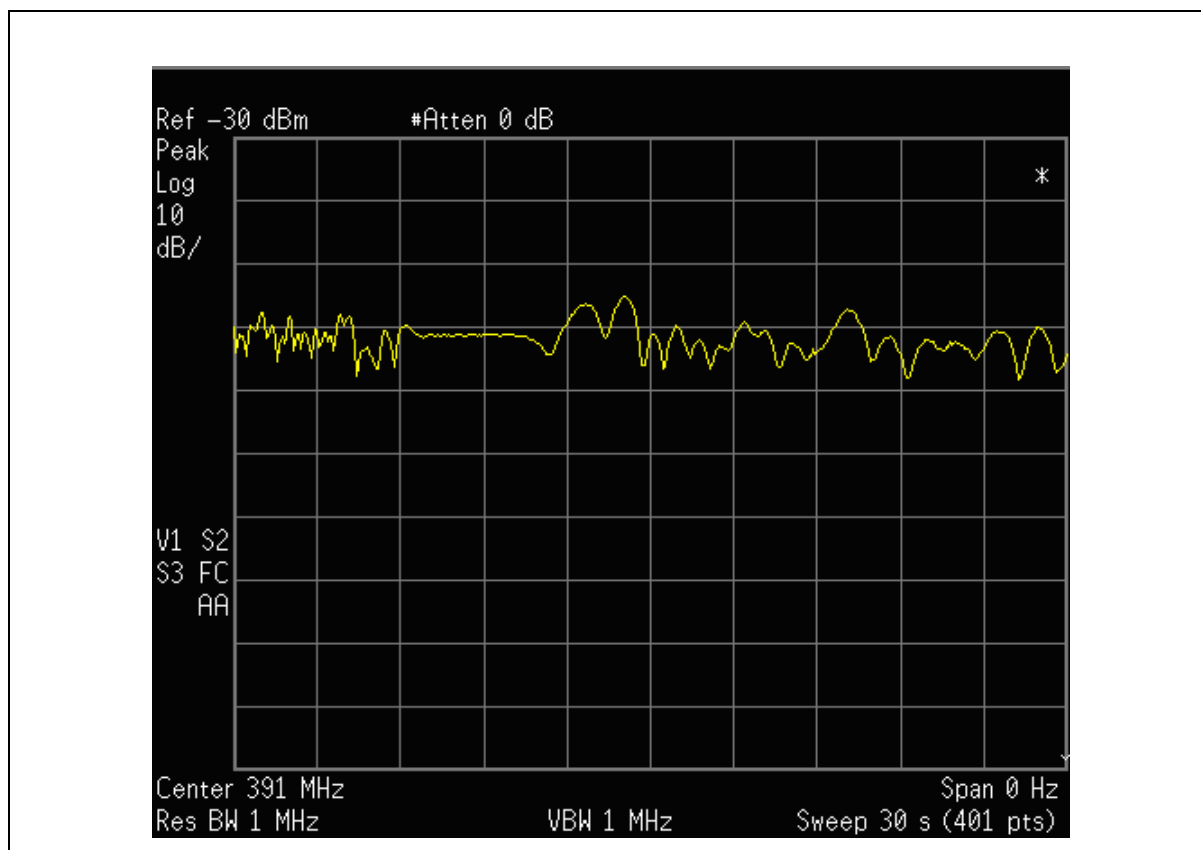


Figure 3.17 RF level variation with time, random variations (18 February 2005).

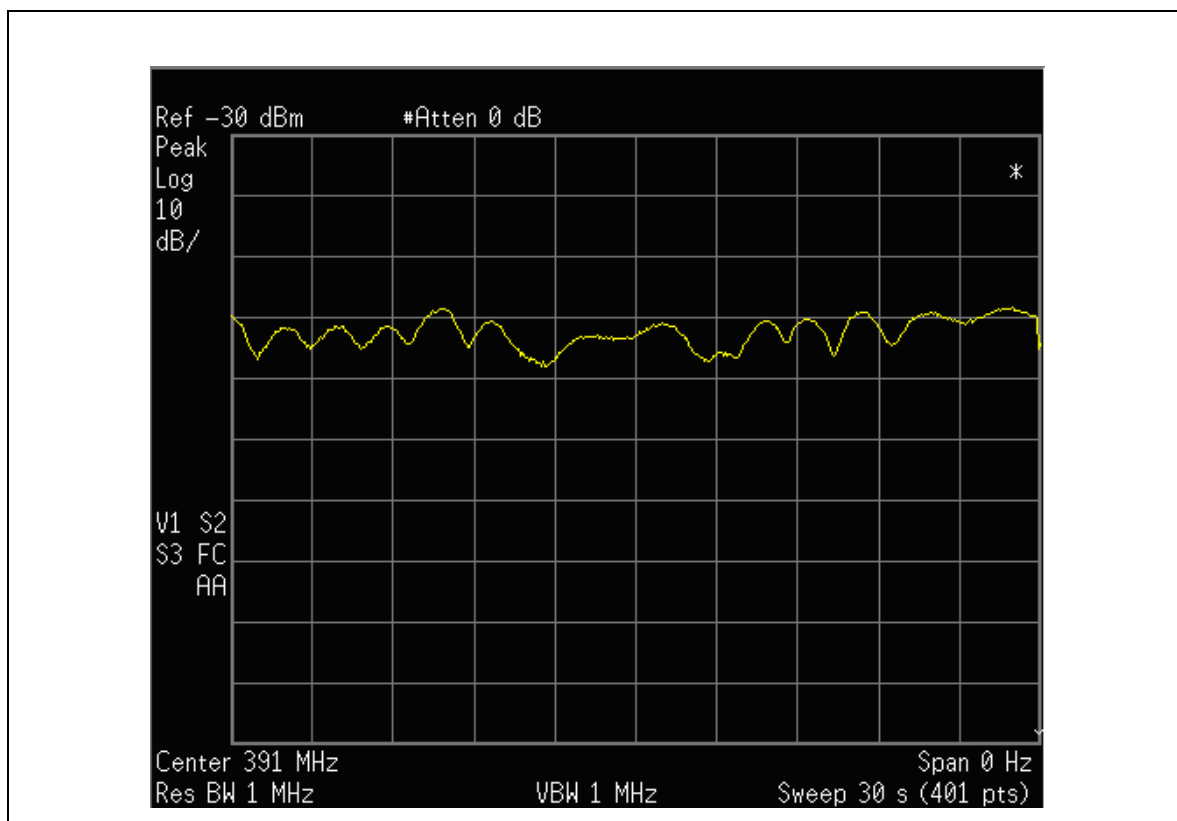


Figure 3.18 RF level variation with time, small single reflection (18 February 2005).

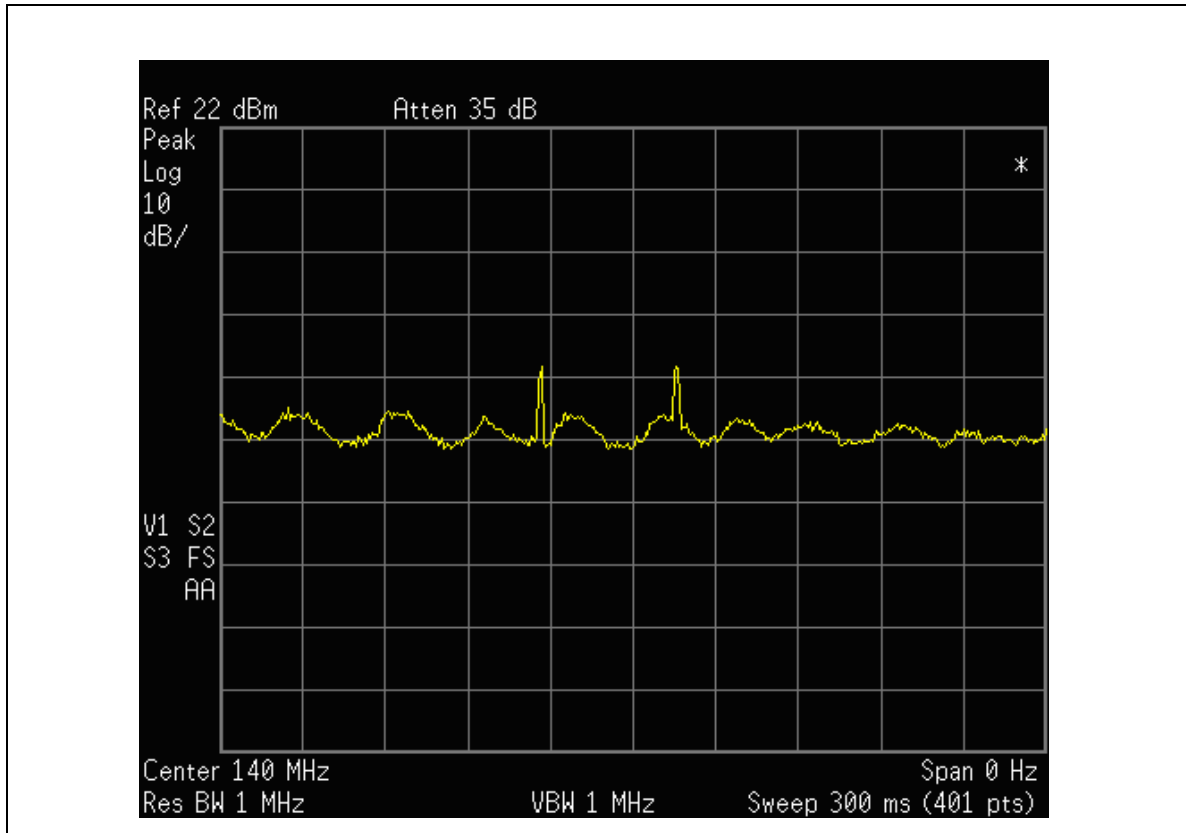


Figure 3.19 RF level variation with time, small single reflection (18 February 2005).

Figure 3.16 and **Figure 3.17** show small random variations of received level. **Figure 3.18** shows small variations of about 4 dB peak to peak which are partly periodic with a rate of about 2 sec. This shows the presence of a small reflection with a small Doppler shift of about 0.5 Hz. The last of the four figures, **Figure 3.19**, shows periodic variations of about 4 dB peak to peak with a period of about 30 ms, which corresponds to a reflection with a Doppler shift (relative to the direct received signal) of about 33 Hz. The two spikes are believed to be impulsive interference and are not related to the signals being measured.

Figures 3.20 to **3.26** show IF level measurements. It should be noted that the IF and RF level measurements are showing the same phenomenon. The IF measurements were made for areas where greater variation of level was expected. The sweep speeds are therefore higher. Most of the RF measurements have a sweep speed of 3 sec/division whereas most of the IF measurements have a sweep speed of 0.1 sec/division.

The measurements were made with resolution bandwidths of 1 MHz and 5 MHz. Those using 5 MHz show a “Meas Uncal” indication, which is generated automatically by the spectrum analyzer. For this setting, there is a slight error in amplitude measurement which is not significant for the signal parameters being measured.

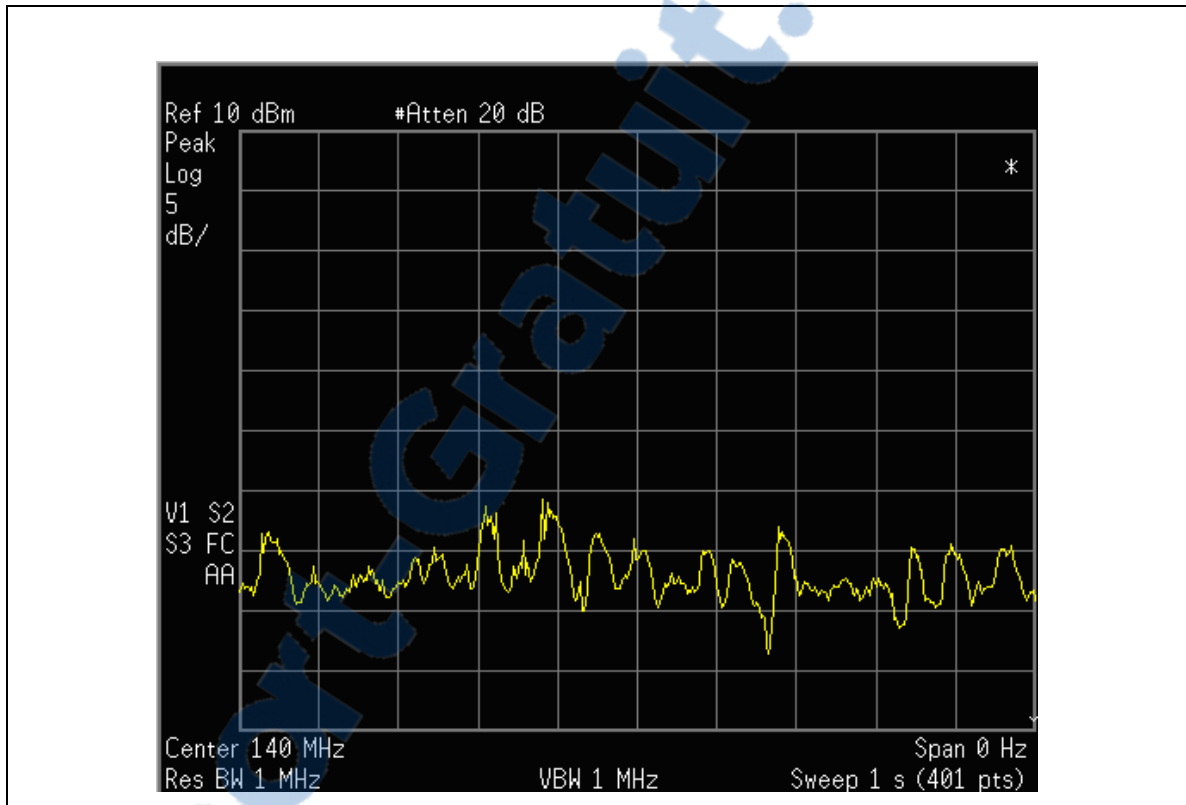


Figure 3.20 IF level variation with time (18 February 2005).

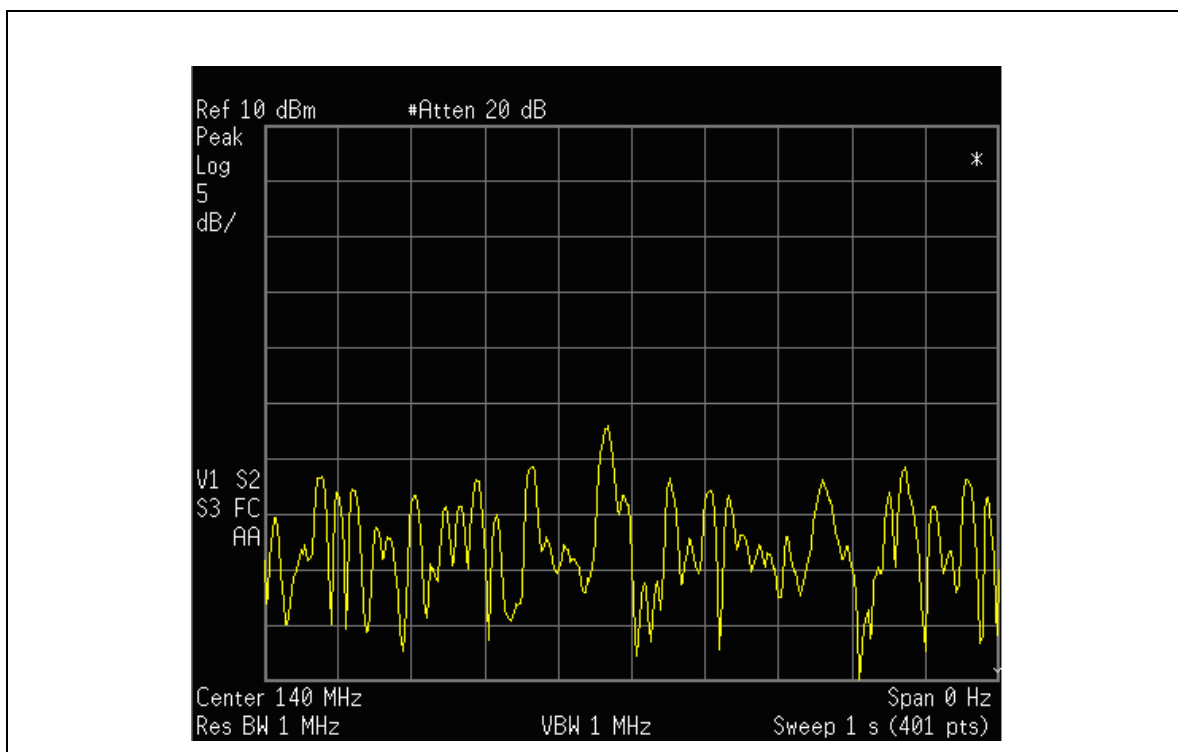


Figure 3.21 IF level variation with time (18 February 2005).

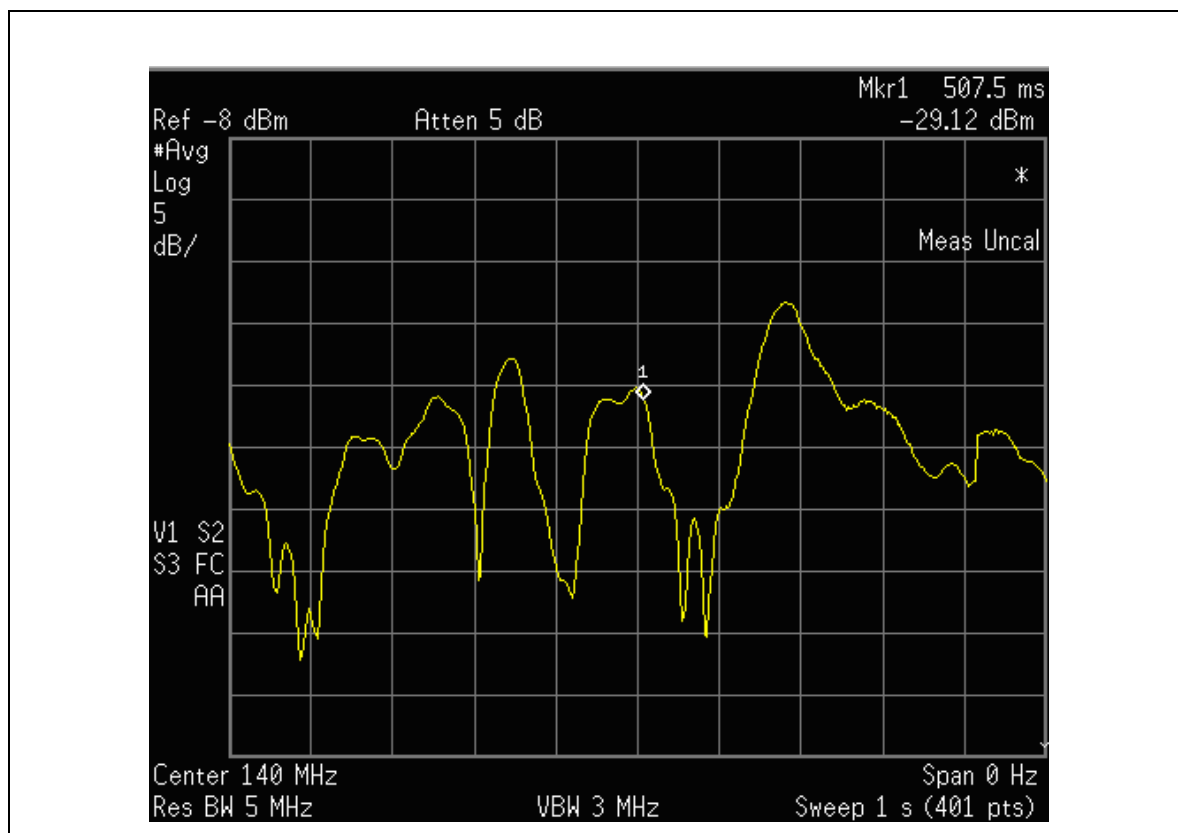


Figure 3.22 IF level variation with time (18 February 2005).

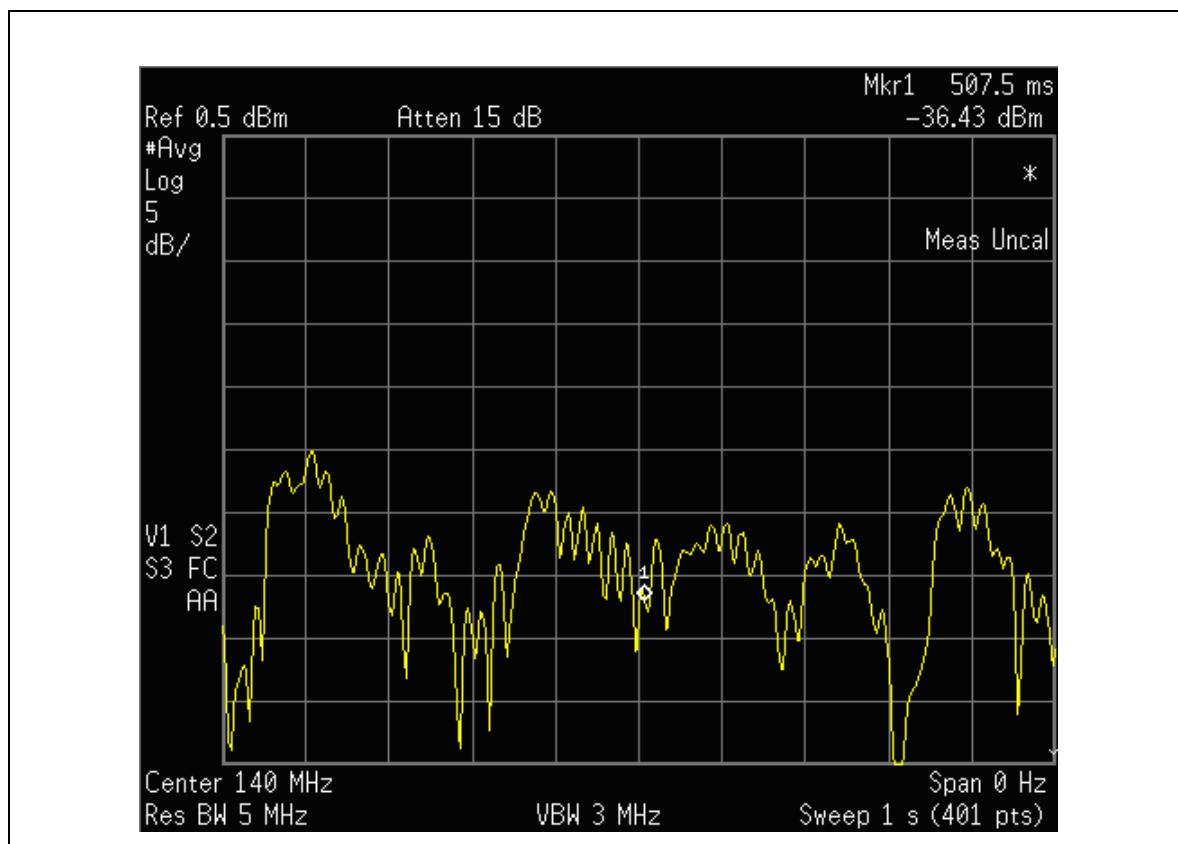


Figure 3.23 IF level variation with time (18 February 2005).

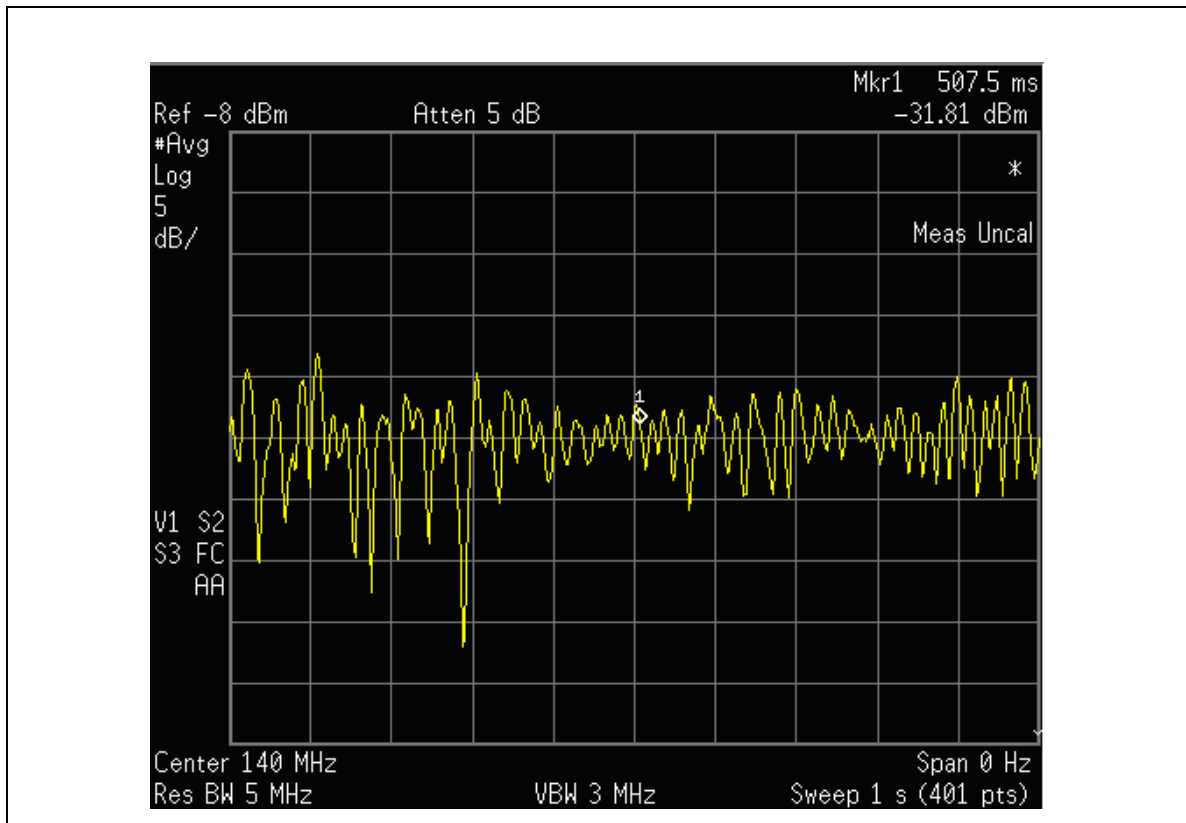


Figure 3.24 IF level variation with time (18 February 2005).

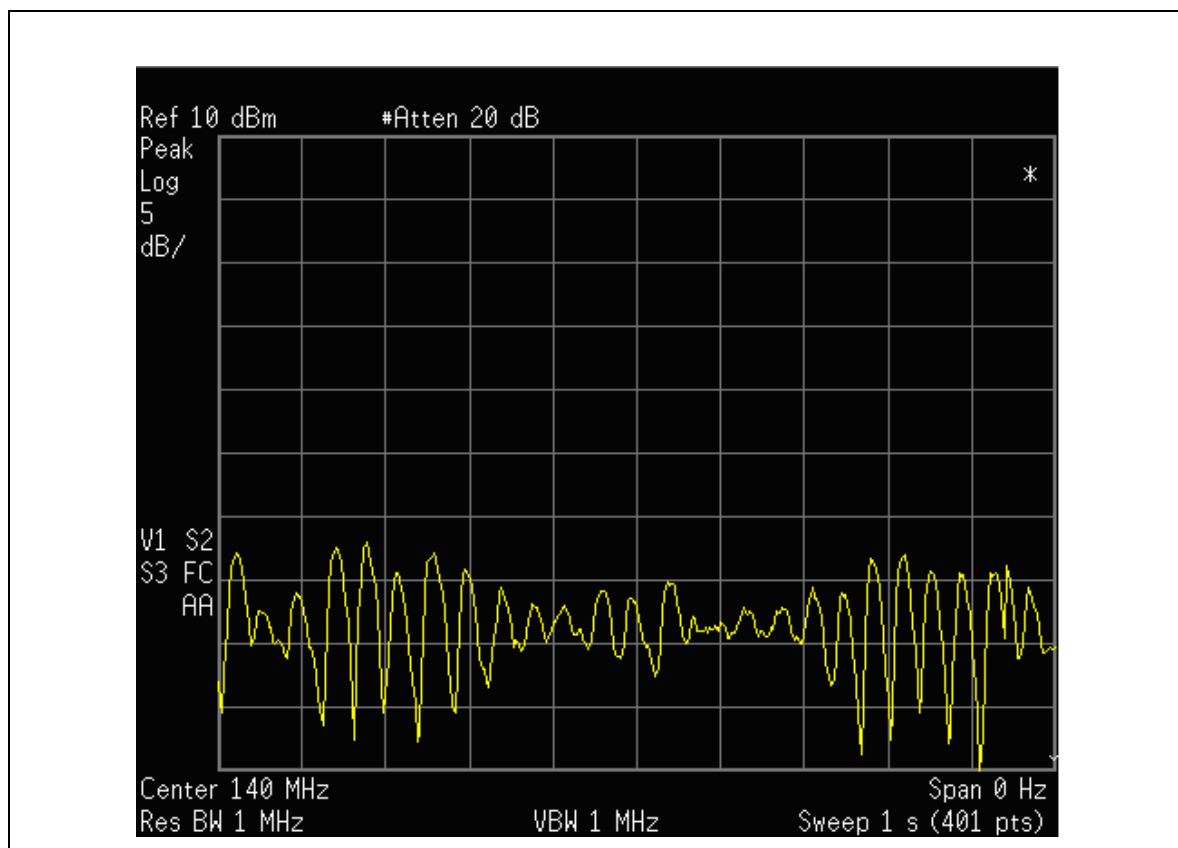


Figure 3.25 IF level variation with time (18 February 2005).

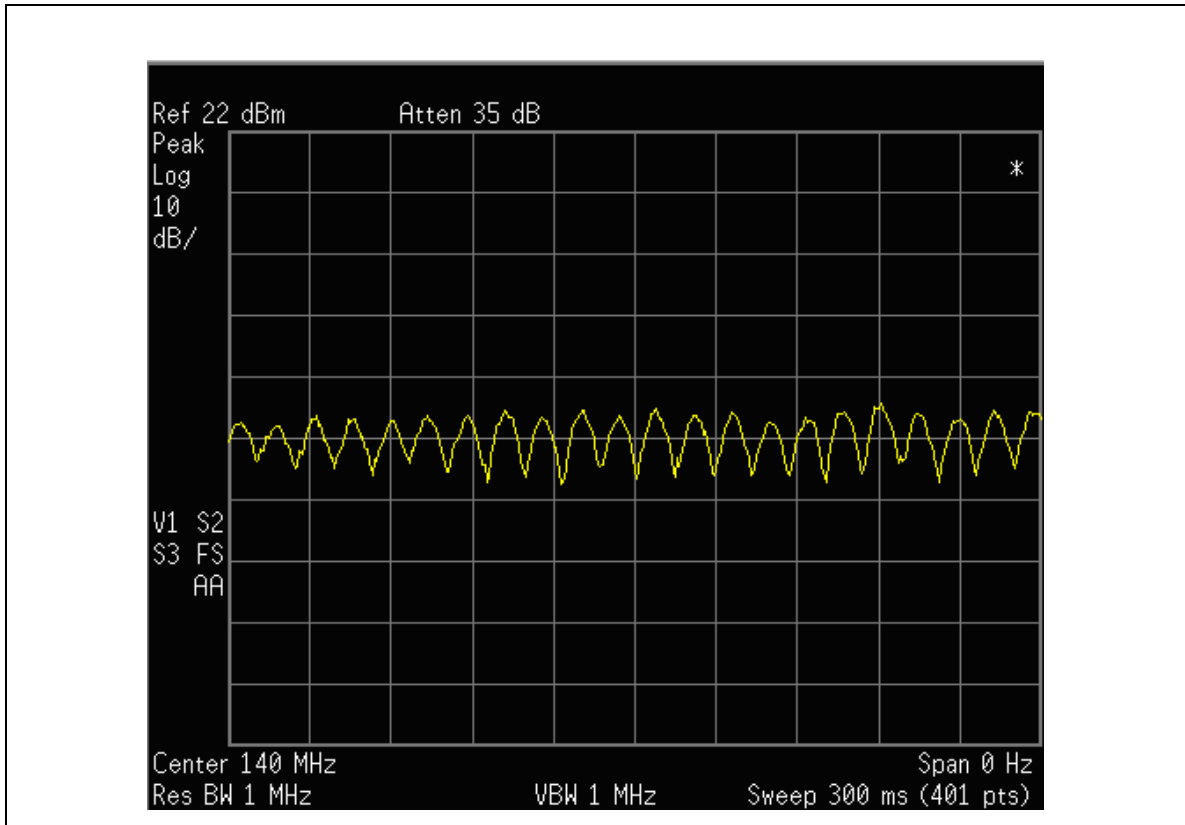


Figure 3.26 IF level variation with time (18 February 2005).

Figure 3.20 and **Figure 3.21** show fairly rapid random amplitude variations. **Figure 3.22** shows a slower random variation while **Figure 3.23** has a combination of slow and rapid variations, with the latter apparently from a single reflection. **Figure 3.24** and **Figure 3.25** show very rapid variations with deep notches in which the variations are mostly due to a single reflection. The periods of the rapid variations are about 16 ms and 40 ms respectively. The apparent modulated character of these waveforms is interesting and requires further study. They appear to indicate that the magnitude of the reflection is changing. **Figure 3.26** shows a very regular rapid 10 dB peak to peak variation with a period of 15 ms, which represents a single reflection with a Doppler shift of 66 Hz.

The RF and IF level measurements illustrated by **Figures 3.16** to **3.26** are representative of what was seen in both the suburban and rural test runs. In terms of error rate performance, for the cases of random or slow variations, the error rate was usually zero or small.

However, those cases of rapid periodic variations greater than about 10 dB peak to peak almost always represented “bad” areas for error rate performance, with frequent losses of timing synchronization.

The fact that there are deep fading notches of up to about 15 dB in the presence of a single dominant reflection is very significant. For a CW or narrow bandwidth signal, a reflection of the same amplitude can null the signal completely. A single reflection with a delay T will produce periodic notches in the frequency domain with a spacing of $1/T$. However, in this case, the signal bandwidth is about 500 KHz. If the notches were spaced by 500 KHz or less, they would not null out the whole spectrum and the fade depth would not be large. Thus, to produce deep fades, the notch spacing must be much greater than 500 KHz. In fact, it can be shown that a 15 dB fade for a 1 Mb/s QPSK signal requires a notch spacing of 2.5 MHz and a reflection amplitude close to that of the direct signal. The reflection delay is therefore about 0.4 μ s and the corresponding path length difference is about 120 m. This delay is less than the symbol periods of the signals used for this experiment.

The analysis of Chapter 2 demonstrates that, for broadside reflection from a building wall, a near zone exists within which the reflected signal is large and outside of which, the reflection amplitude falls off quickly. For a 10 m x 10 m wall, this near zone extends out about 100 m. For broadside reflection, a path length difference of 120 m corresponds to a distance of 60 m from the wall. Thus, the observed behaviour is consistent with the theoretical analysis.

d) Pulse transmitter measurements

For these measurements, a pulse transmitter was used to study reflections directly. A spectrum analyzer set to zero span mode and triggered on large received pulses was used as a receiver. The pulse width was 1 μ s and the frequency was 391 MHz. The pulse repetition period was 40 μ s. The resolution bandwidth was set to capture most of the signal energy while the video bandwidth was set to provide as much smoothing as possible consistent with the signal bandwidth and the sweep rate.

The test was performed on a portion of the rural route which was known to give poor performance during the error rate and spectrum measurements. **Figures 3.27 to 3.35** below show the results of this test.

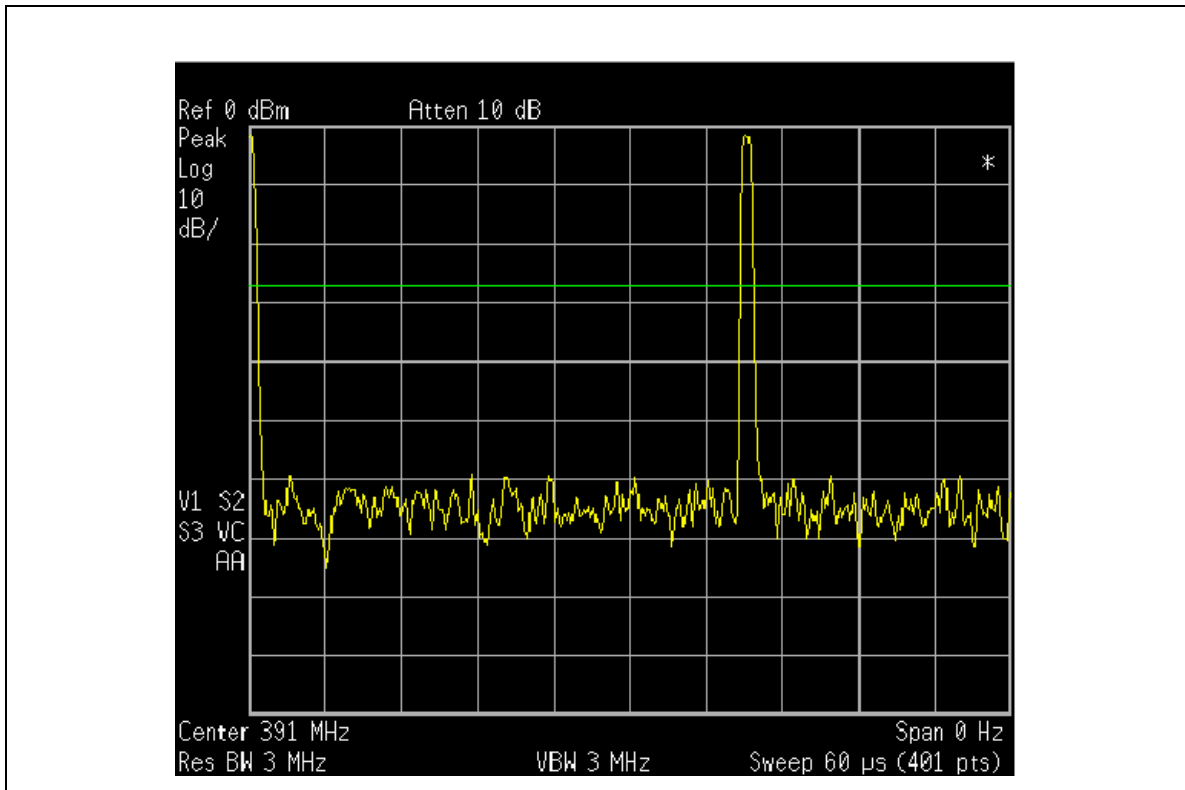


Figure 3.27 Transmitted pulses (reference) (23 December 2004).

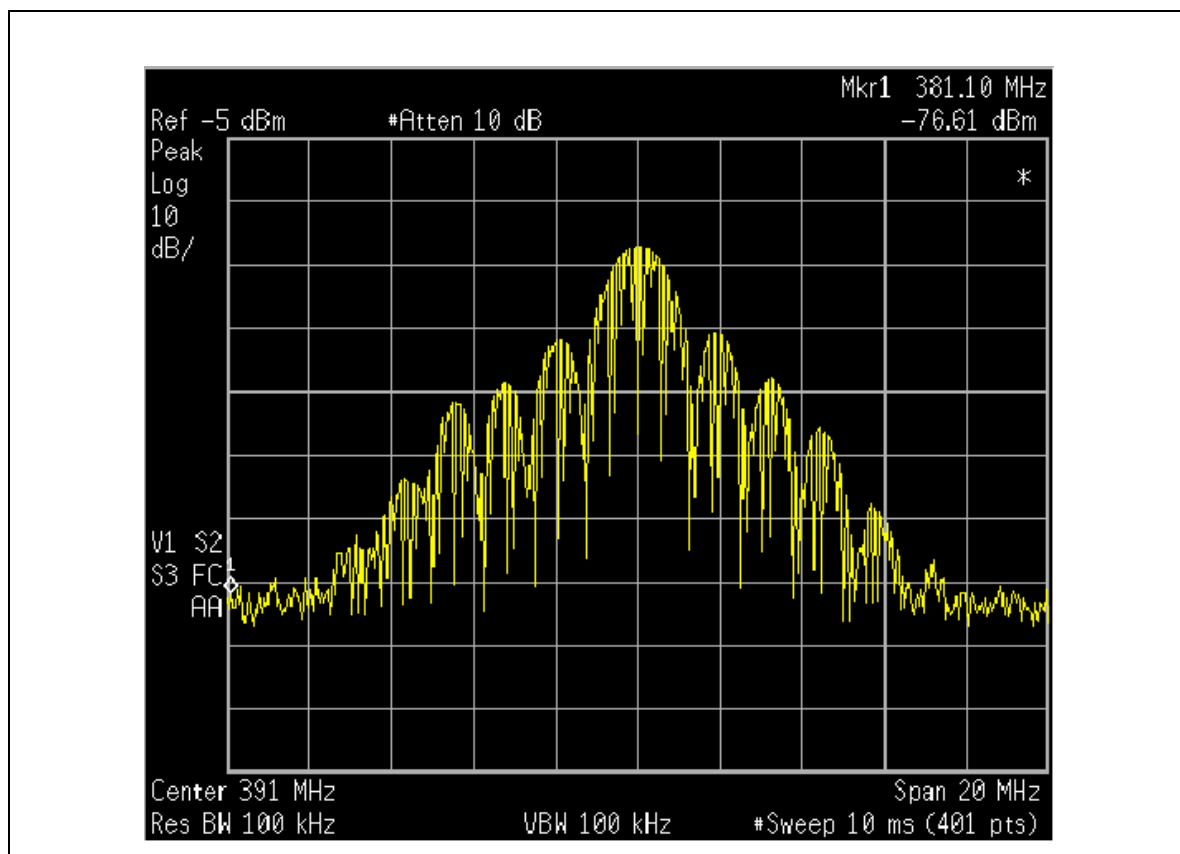


Figure 3.28 Transmitted pulse spectrum (23 December 2004).

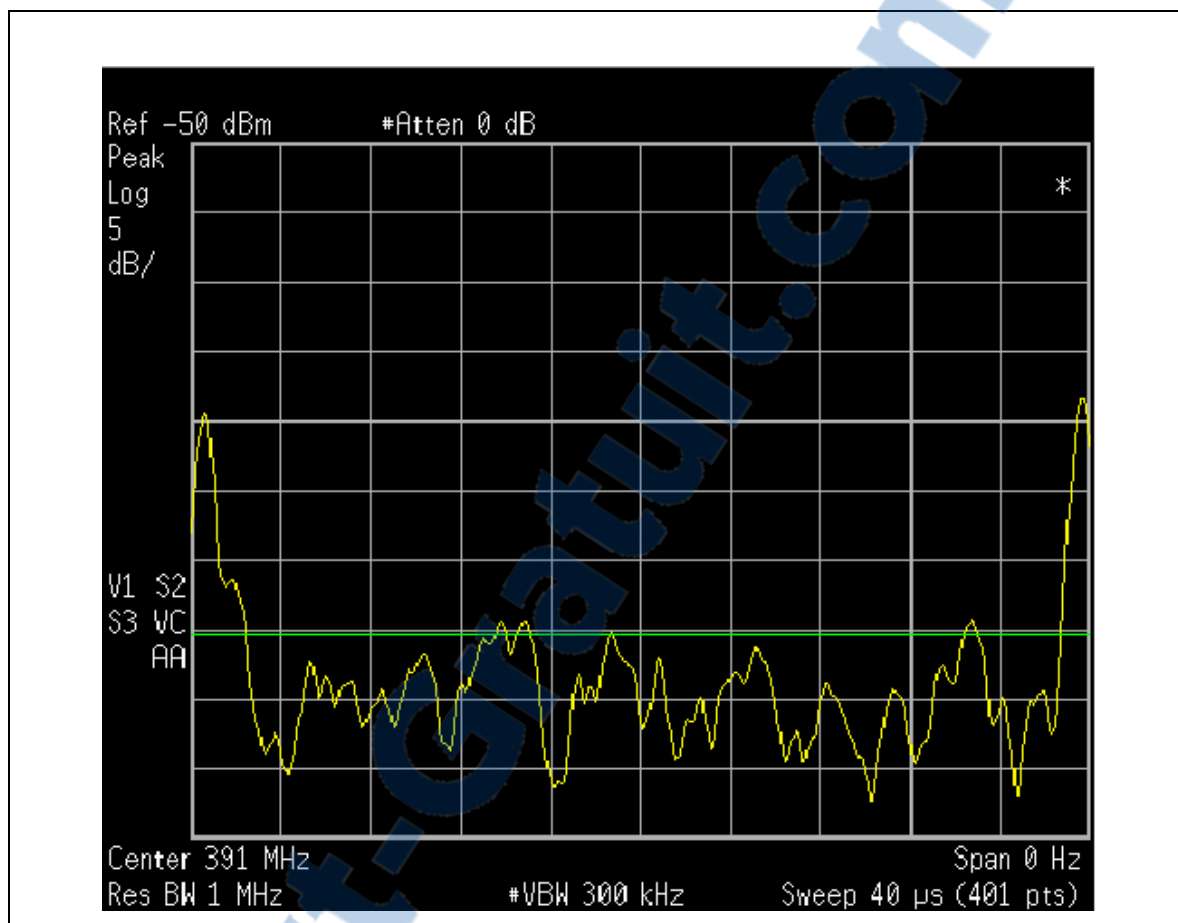


Figure 3.29 Received pulse (23 December 2004).

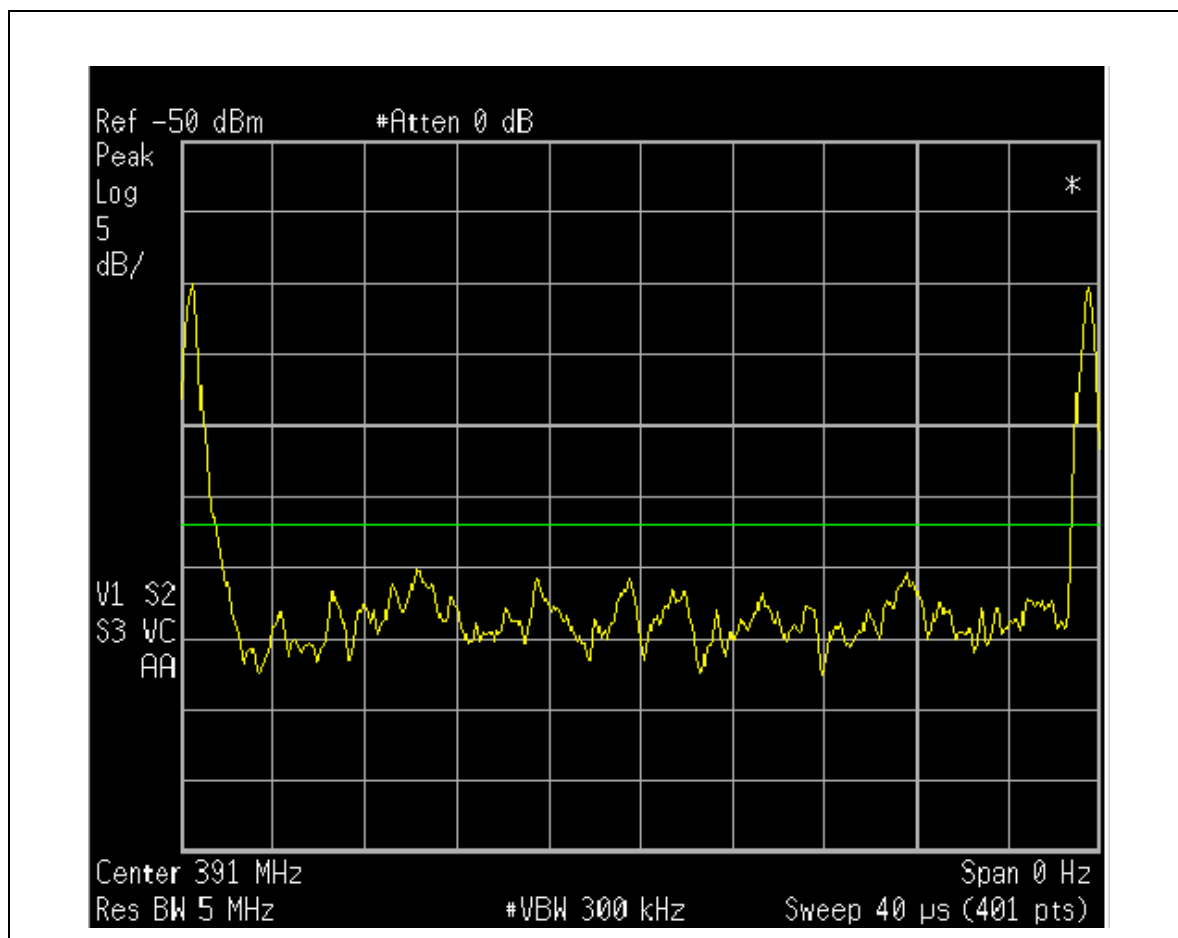


Figure 3.30 Received pulse (23 December 2004).

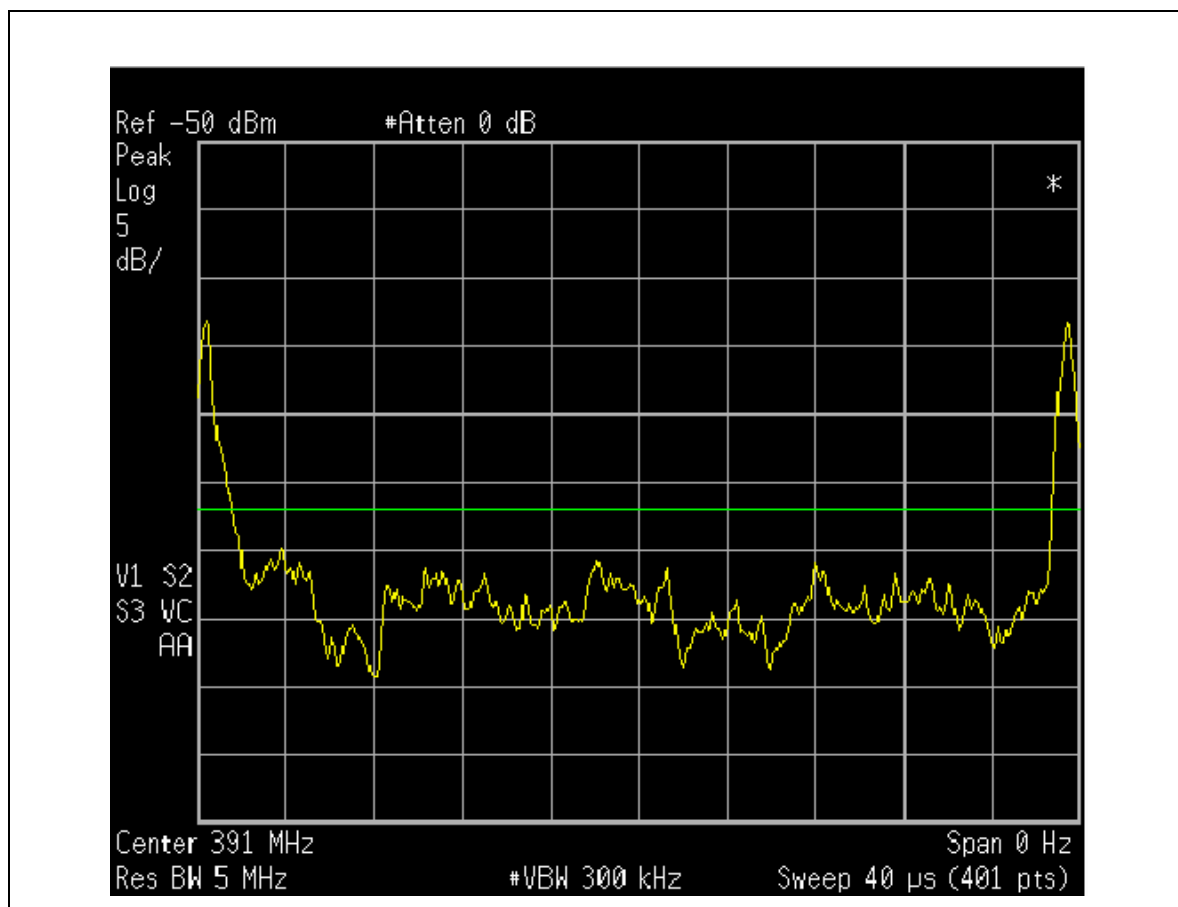


Figure 3.31 Received pulse (23 December 2004).

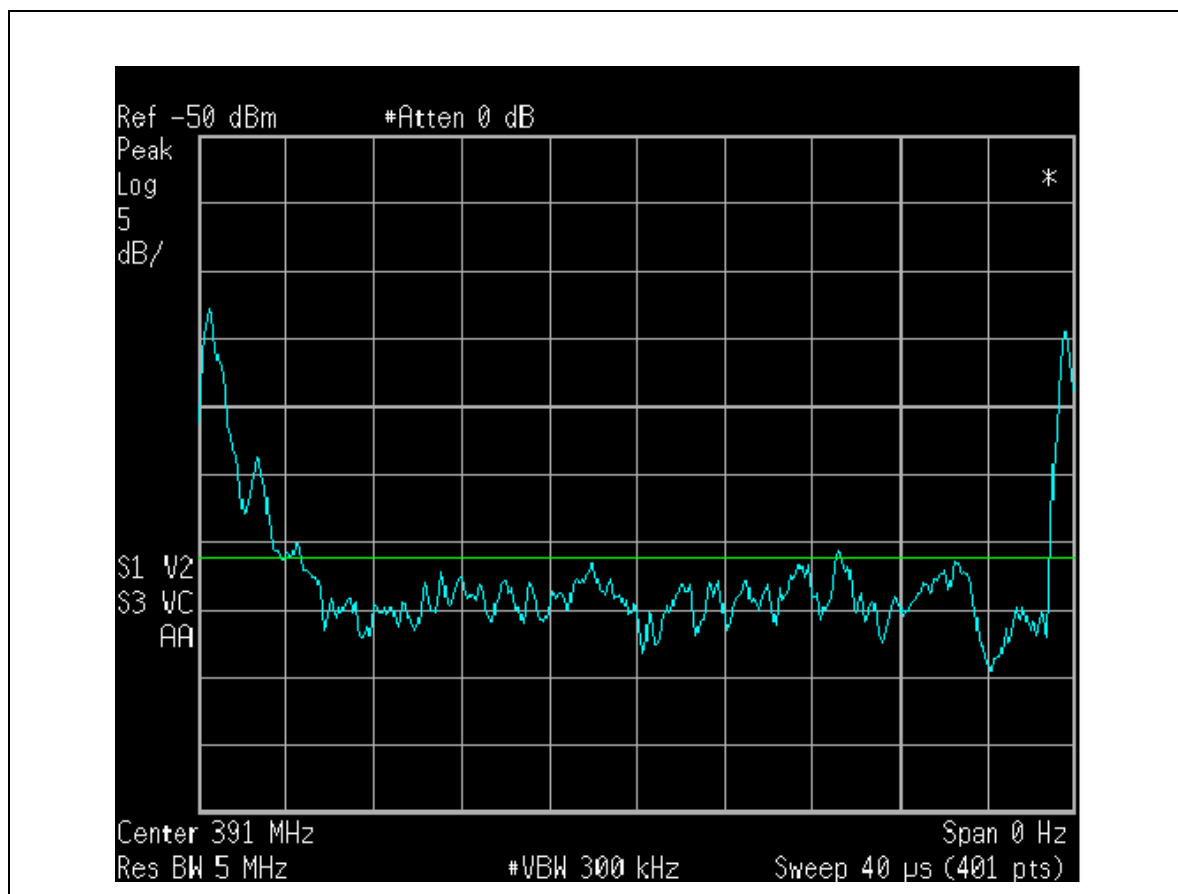


Figure 3.32 Received pulse (23 December 2004).

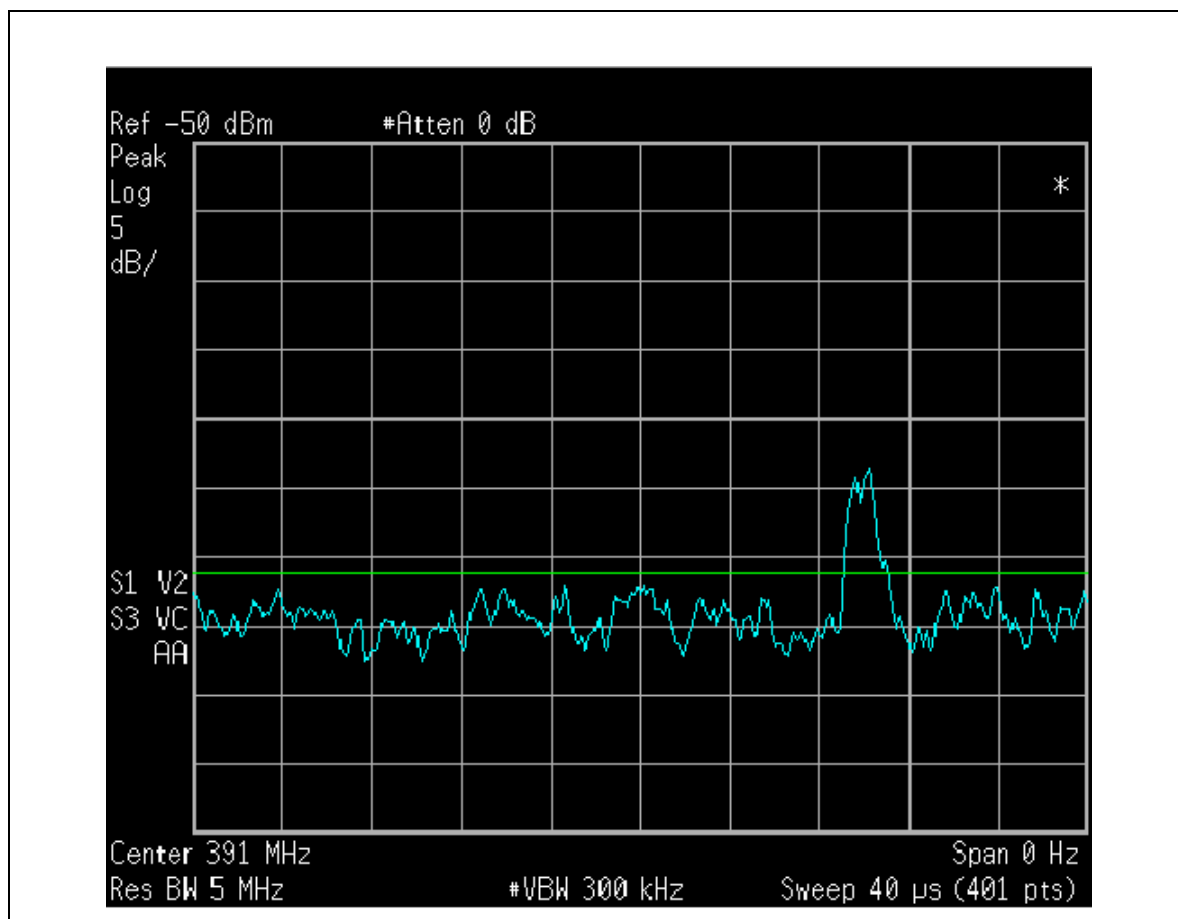


Figure 3.33 Received pulse (23 December 2004).

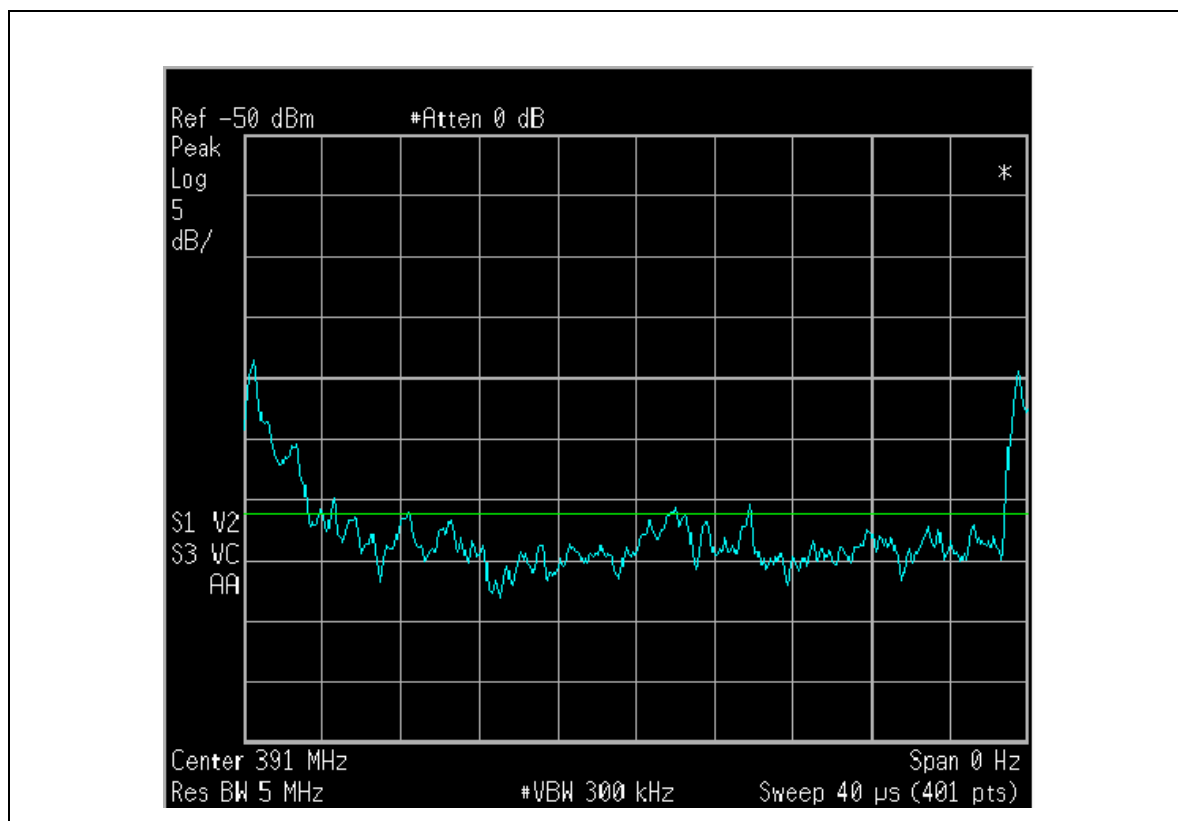


Figure 3.34 Received pulse (23 December 2004).

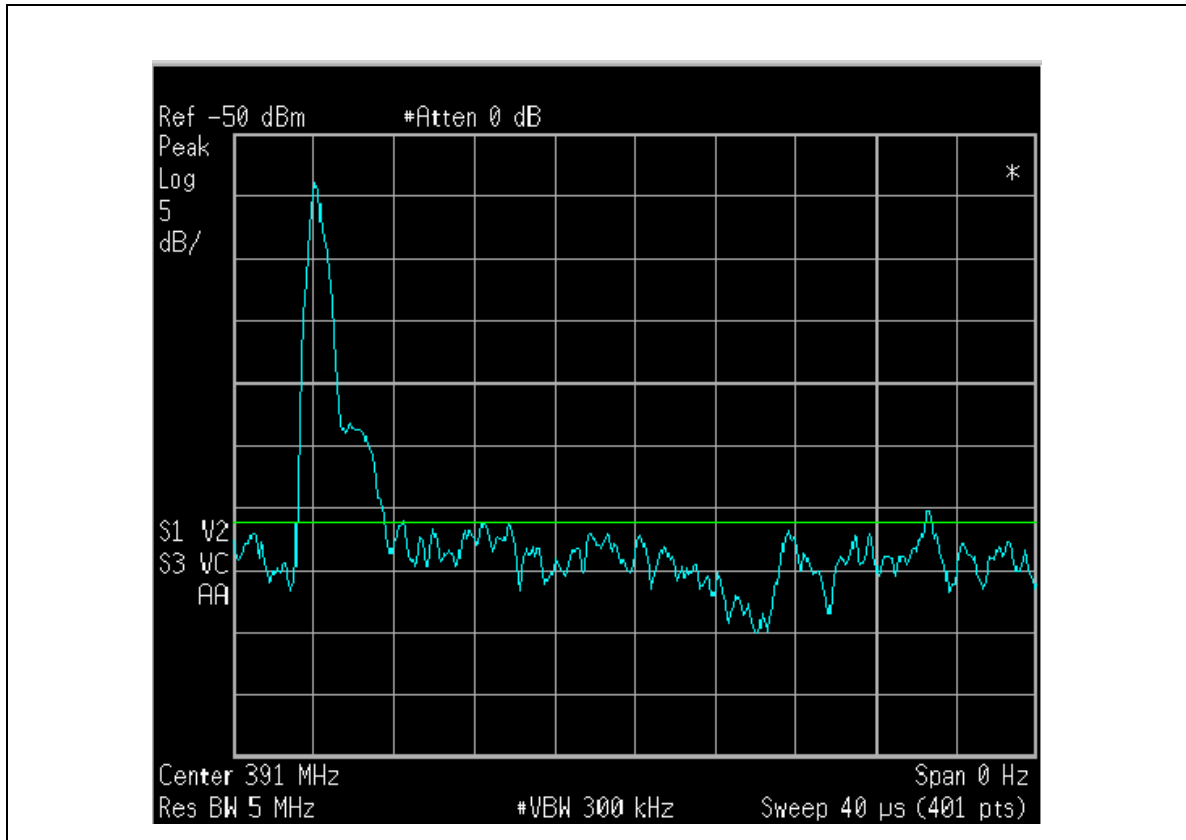


Figure 3.35 Received pulse (23 December 2004).

Figure 3.27 shows the reference pulse shape. The bandwidth of the analyzer has been set at 3 MHz for both resolution and video bandwidth to minimize the rise time. **Figure 3.28** shows the pulse spectrum. **Figures 3.29 to 3.35** show various received pulses with video bandwidth settings to give a rise time (10% to 90%) of around 1 μ s in order to smooth out noise effects. This gives a time resolution of around 1 μ s. This is not ideal to accurately measure reflections with a sub microsecond delay but it is still possible to detect short delay pulses. The noise floor in the figures is due to the equipment, not the reflections.

The received pulses were continuously monitored and recorded at times which showed a representative behaviour. The recording was initiated manually.

A number of the figures show a thickening of the main received pulse which indicates the presence of a reflection with a delay of 1 μ s or less and a level which is within 5 dB of the main pulse. **Figure 3.33** shows two pulses where the second is about 1 μ s after the first and 1 dB higher. One case, which was not recorded, showed 4 pulses of equal levels within 4 μ s. Many of the figures also show smaller pulses at delays of 2 to 3 μ s and levels of -10 dB or less.

3.2.3 Summary and analysis of experimental results

These results indicate that, for the environments studied, the signal distortions are often due to a single dominant reflection. It has been observed that, in “bad areas”, a large reflection is usually present and that this dominant reflection has an amplitude similar to that of the direct path. The presence of this reflection produces deep periodic fades as the mobile moves, causing a poor link performance with a high error rate and usually a loss of synchronization. There are also other smaller reflections. Furthermore, the delay of the dominant reflection is often short: less than 1 μ s. The second smaller reflection, where it exists, has a delay of a few microseconds.

CHAPTER 4

APPLICATIONS

4.1 Propagation models for practical channels

The ideas of Chapters 2 and 3 can be used to construct models for mobile communication channels in many types of environments. In general, a mobile moves throughout a defined region which contains reflecting structures such as buildings which usually have flat walls. For a given base station location, each structure will have one or perhaps two associated near zones (from two walls) in which the reflected fields are large; in many cases of the same order as the direct field at the mobile. It should be noted that if either the direct or reflected field is much larger than the other, it is easier to correct the channel degradations. If the fields are of similar magnitude, the channel degradations are much greater and more difficult to correct. Outside the near zones, the reflected field falls off rapidly and its influence is reduced.

The area in which the mobile moves will contain locations which are in the near zones of reflecting structures and other locations which are not. In rural areas, the sizes of the near zones are small and less numerous. The near zone may extend several hundred meters out from building walls. In suburban areas, the buildings are larger and more numerous. Therefore, the near zones are also larger and occupy a larger fraction of the area. In urban areas, the buildings are large and the density is high. Most locations are likely in one or more near zones of buildings. In this case, the near zones will extend far from the buildings and the reflections with significant magnitudes can have large delay spreads. This explains the greater delay spreads seen in urban areas. It should be recalled, however, that we consider only situations where there is line-of-sight. Locations which are obstructed will have greater channel degradations.

One other characteristic of urban areas deserves mention. Since the near zones tend to be large, they may include other buildings, which implies that multiple reflections cannot be ignored. This effect is not considered here.

In the present context, these concepts are used to construct a channel model for the rural and suburban cases. A two-state model is appropriate here. For some locations, the mobile will not be in any near zones and the channel will have small degradations which can, for most purposes, be ignored. This is a good state. For other locations, the mobile will be in a near zone and there will be a reflected field which is taken to have the same magnitude as the direct field. The delay of the reflected field will be relatively small since the size of the near zone is small i.e. several hundred meters. Thus, the maximum delay is around 1 μs or less. There may be other smaller reflections present but they can be modelled as an additional reflection whose magnitude is at least 10 dB below that of the direct path. The delay of this reflection can be taken as 3 to 4 μs (refer to experimental results of Chapter 3). It should be noted that this model is close to that of the SUI model for suburban locations [30]. The fractions of the operating area which represent good and bad locations depend on the building density.

4.2 Estimation of link availability

The concepts in this work can be applied to estimate the fraction of the locations which will experience a degradation of signal quality or will have an outage. It has been shown that the worst case reflection is one which is similar in magnitude to that of the desired signal and that this will occur near structures.

Consider again the case of the flat reflecting wall which was shown in **Figure 2.1**. The wall has height H , width W and area A and its normal is here assumed to be oriented at an angle θ to the direction of propagation of the signal from the base station. The wall will have a near zone with a width equal to $W \cdot \cos \theta$. The projected area is $A \cdot \cos \theta$ and the near zone distance (based on Equation 2.9) will then be about:

$$d_0 = \frac{A \cdot \cos \theta}{\lambda} \quad (4.1)$$

where λ is the wavelength. In this case, d_0 is the distance from the wall to the mobile, taken along a line from the reflection point on the wall to the mobile. Note that the distance is assumed to be taken from the center of the wall but the near zone distance is generally much greater than the wall dimensions so this does not represent a large error.

This is an approximation for the following reasons. Based on the discussion of Section 2.2 c), the equation will be an over-estimate when one of the wall dimensions is much smaller than the other. When the angle θ approaches 90° , the effective wall width goes to zero and the height is no longer important. Thus, when the angle increases beyond about 60° , the equation becomes increasingly inaccurate. Also, Equation 2.9 does not consider ground reflection but the near zone is, in any case, not precisely defined. Keeping in mind these caveats, it is believed that the equation provides a reasonable approximation of the near zone distance and will be used here.

The delay difference between the direct signal and the reflected signal can be calculated from the geometry of **Figure 4.1** below. The distance from the base station to the reflection point on the wall is R_b and the distance from the wall to the mobile is R_m . The distance from the base station to the mobile is R_{bm} .

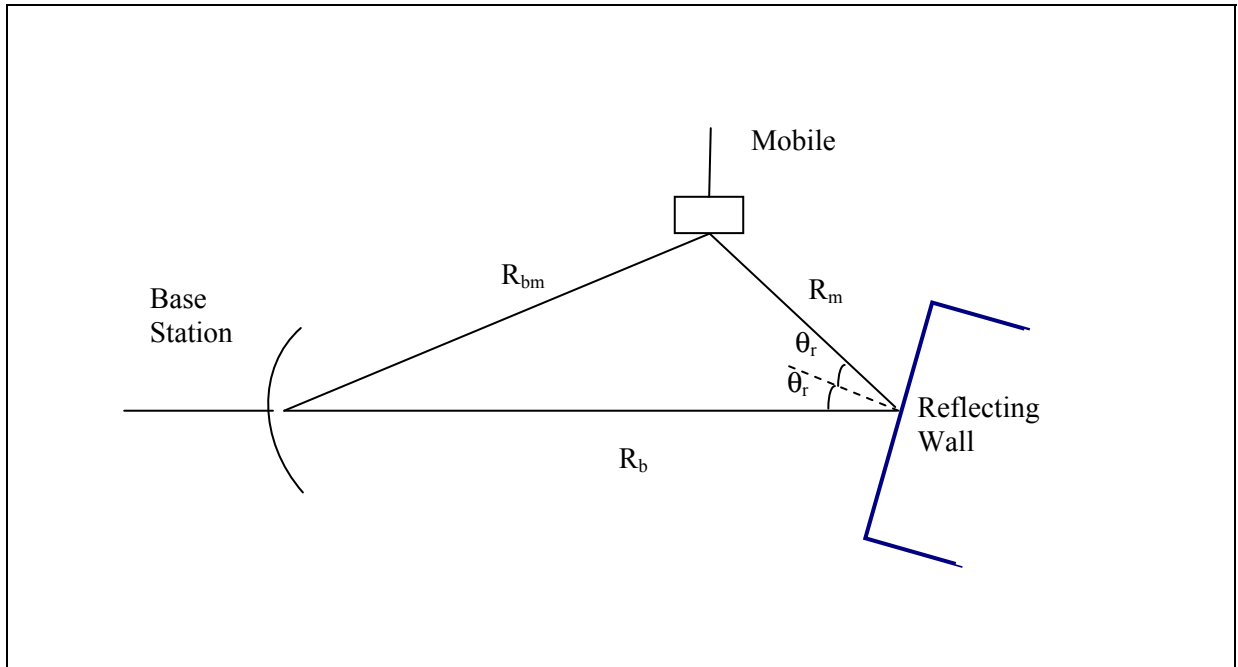


Figure 4.1 Reflection delay geometry.

The distance difference ΔR between the direct and reflected waves is given by:

$$\Delta R = R_b + R_m - \sqrt{R_b^2 + R_m^2 - 2 \cdot R_b \cdot R_m \cdot \cos(2 \cdot \theta_r)} \quad (4.2)$$

And the delay difference is then:

$$\tau = \frac{\Delta R}{c} \quad (4.3)$$

where c is the speed of light. In general, the distance to the base station is much greater than the near zone distance from the wall. Thus, Equation 4.2 can be simplified to:

$$\tau \approx 2 \cdot R_m \cdot \frac{\cos^2 \theta_r}{c} \quad (4.4)$$

The first condition for a link outage is that the mobile must be in the near zone i.e. $R_m < d_0$. In Chapter 5, it is shown that some systems are able to compensate for reflections whose relative delay is greater than a symbol period of the transmitted signal. For example, DS spread spectrum systems whose transmitted spreading code symbol period is less than the reflection delay are able to resolve echoes and greatly reduce the effects of reflections. Non-

spread modulations with short symbol periods are also theoretically capable of good performance in the presence of reflections. In such cases, another condition for an outage is that $\tau < 1/R_s$ where R_s is the symbol period of the modulation. To get an outage, the mobile must be in the near zone of the reflecting wall AND the delay difference must be less than the symbol period of the modulation. Then, from Equations 4.1 and 4.4, the conditions for a link outage are:

$$R_m < \frac{c}{2 \cdot R_s \cdot \cos(2 \cdot \theta_r)} \quad (4.5)$$

and

$$R_m < \frac{A \cdot \cos \theta_r}{\lambda} \quad (4.6)$$

If the symbol period is long or the incidence angle is large, the entire near zone is potentially an outage area. The part of the near zone outside the delay constraint is not an outage area. If the symbol period is small and the incidence angle is small, the delay constraint will determine the size of the outage area. Of course, the width of the outage area is approximately the projected wall width perpendicular to the direction of propagation of the reflected wave.

These concepts allow the potential outage areas, and therefore the areas where system coverage is available, to be determined. The approach is illustrated in **Figure 4.2**, which shows a typical layout of buildings on a street grid. All of the buildings within the line of sight (or with only a slight obstruction) of the base station are first identified. Then, the reflection angles and near zone distances for each reflecting wall are calculated. A delay constraint can be added, if required, for each near zone. In this way, all of the areas where there is likely to be an outage, i.e. areas with high reflections, can be mapped. The area can be further restricted to those in which the mobile can move (streets and parking lots). The fraction of this area which falls within the zones where an outage can occur will determine the percent outage time. If the route of the mobile is known, the percent outage time can be estimated from the distances which fall within the outage zones.

The analysis above has been applied to line-of-sight situations. However, this methodology can also be applied to diffracted waves if the diffraction angle is shallow. For example, this type of analysis could be applied to a wave diffracted over a low roof with a large open area on the other side.

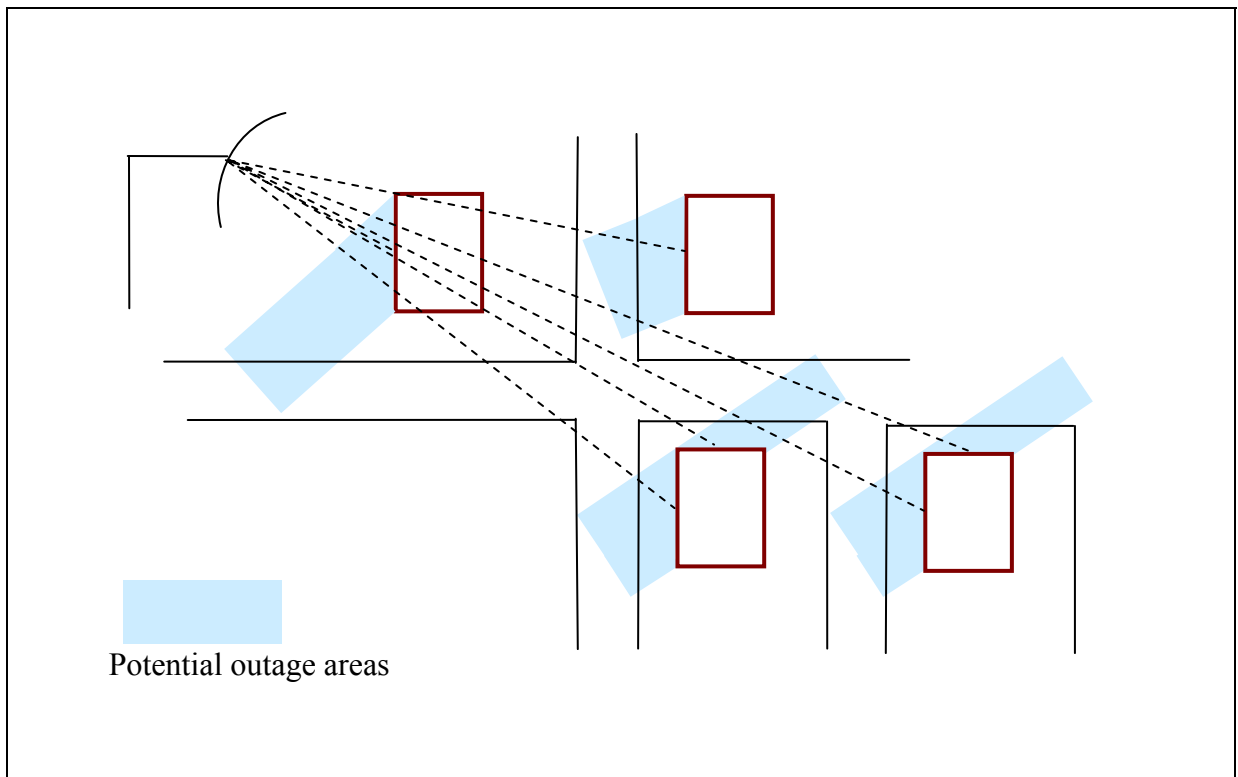


Figure 4.2 Outage area estimation.

Systems are often characterized by their coverage i.e. the areas where service with acceptable performance is possible. In general, outages can occur either due to low signal levels or high reflections. The outage areas considered in this study are areas of high signal level since they have line-of-sight or near line-of-sight. They would often be considered areas of good performance based on an analysis of propagation loss. However, the presence of reflections indicates that these areas likely have poor performance and should not be considered areas of system coverage.

It has been stated previously (Chapter 2) that, if the ground reflected wave from either the building or the base station is not present, the effective near zone will be affected. For example, if the ground reflection from the base station is blocked, while that from the building reflection is not, the effective near zone would be smaller since the signal reflected by the building would be smaller until the mobile was very close to the building. If the situation is reversed, the effective near zone could be much bigger since the signal reflected by the building would not be partially cancelled by its ground reflection. The locations of fences, for example, must be taken into account in this regard.

4.3 Example of outage area prediction

The methods outlined can be used to estimate theoretically the BER results shown in **Figure 3.3**. Specifically, the route driven by the mobile to produce this result can be analyzed using satellite images. The areas where the signal quality is poor can be determined and the distances for which they intersect the route taken by the mobile can be found. The fraction of the route for which the signal is poor and data errors occur can be compared to the outage fraction shown in the pie chart.

The overall route is an 11 km circuit in a semi-rural area as shown in **Figure 4.3**. The location of the base station is shown in the figure. The height of the antenna mast is 20 m. The radio equipment is that of Chapter 3.

The mobile travelled around the circuit at a speed of 40 to 50 km/hr. Taking an average of 45 km/hr, the speed is about 12.5 m/s. The link error rate was sampled every 2 s, i.e. every 25 m. The data rate was 1 Mb/s. The sampling rate therefore permits the detection of low error rates approaching 10^{-6} but gives a reasonable resolution of error rate versus location.

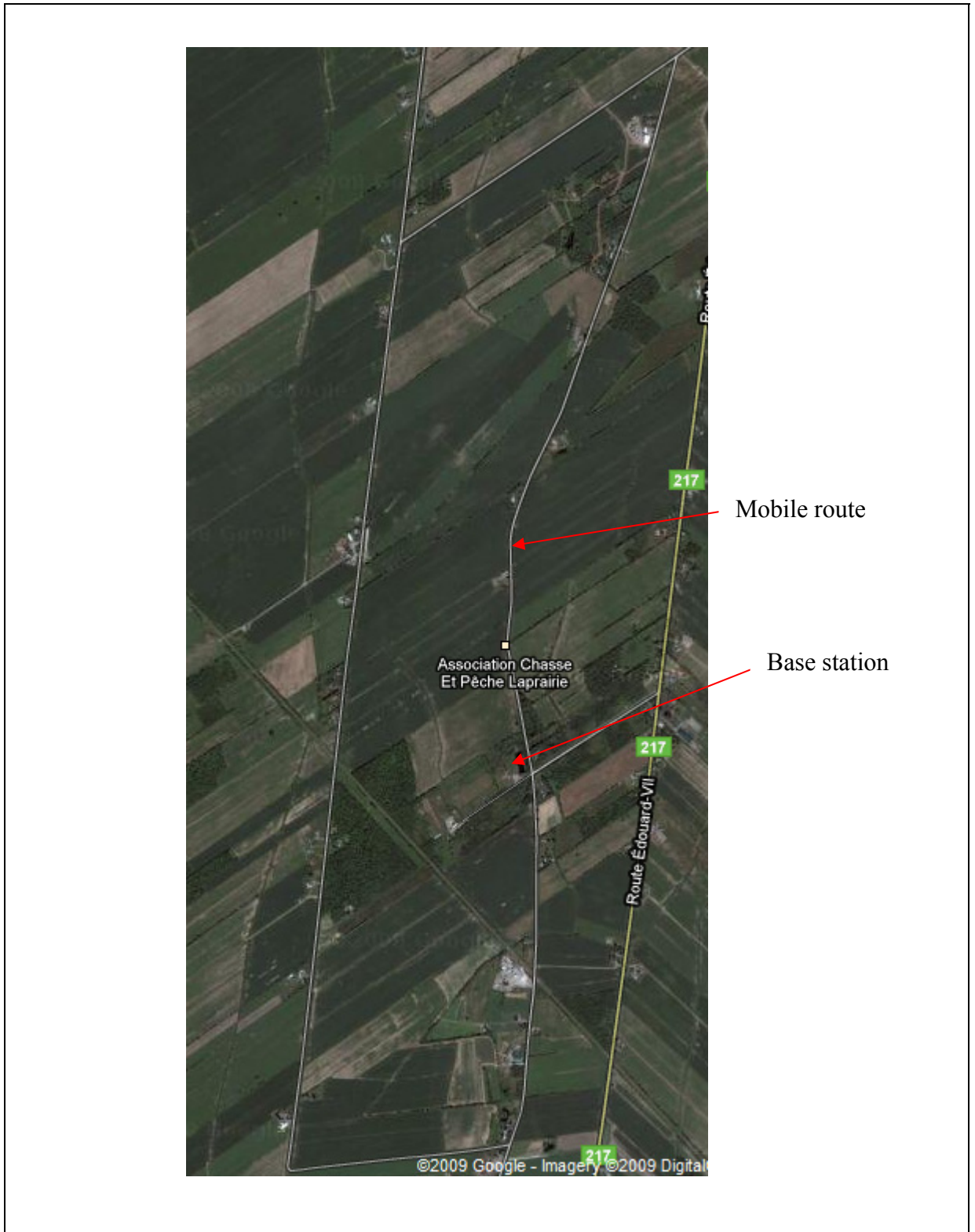


Figure 4.3 Test route of the mobile (© Google 2009).

A number of individual houses and clusters of farm buildings are located beside the road. In addition, there are stands of trees as well as individual trees. The maximum link distance is about 3 km and usually much less. In most places along the route, the signal levels are high. Line-of-sight or near line-of-sight is available in most places along the route. However, in one area directly behind the base station, signal levels are extremely low because the signal path is blocked by a large area of trees which end close to the road and there is also an old railway embankment between the base station and the mobile. In this area, the signal is too low for communication.

During the test, it was noted that the errors or link synchronization loss occurred whenever the mobile approached buildings or stands of trees which were close to the road. Therefore, it is possible using satellite images to estimate where link errors would occur, based on the direction of the base station, the directions of reflections from buildings and the presence of stands of trees close to the road, which could reflect signals toward the mobile. The widths of buildings in the area are at least 10 m so that the near zone distance is around 100 m or more. Thus, any near zone area which intersects the route of the mobile will produce an outage area. In addition, as noted, there was one area of very low signal level. **Figures 4.4 to 4.8** show successive parts of the route, starting at the top (North end) and ending at the bottom (South end), at larger magnifications. The images show the buildings and trees along the route. These figures also indicate the lengths of road which are expected to be outage areas. It should be noted that some reflectors appear in two images but the corresponding outage distance is given in only one image. The directions of reflection from buildings can be estimated from **Figure 4.3**.

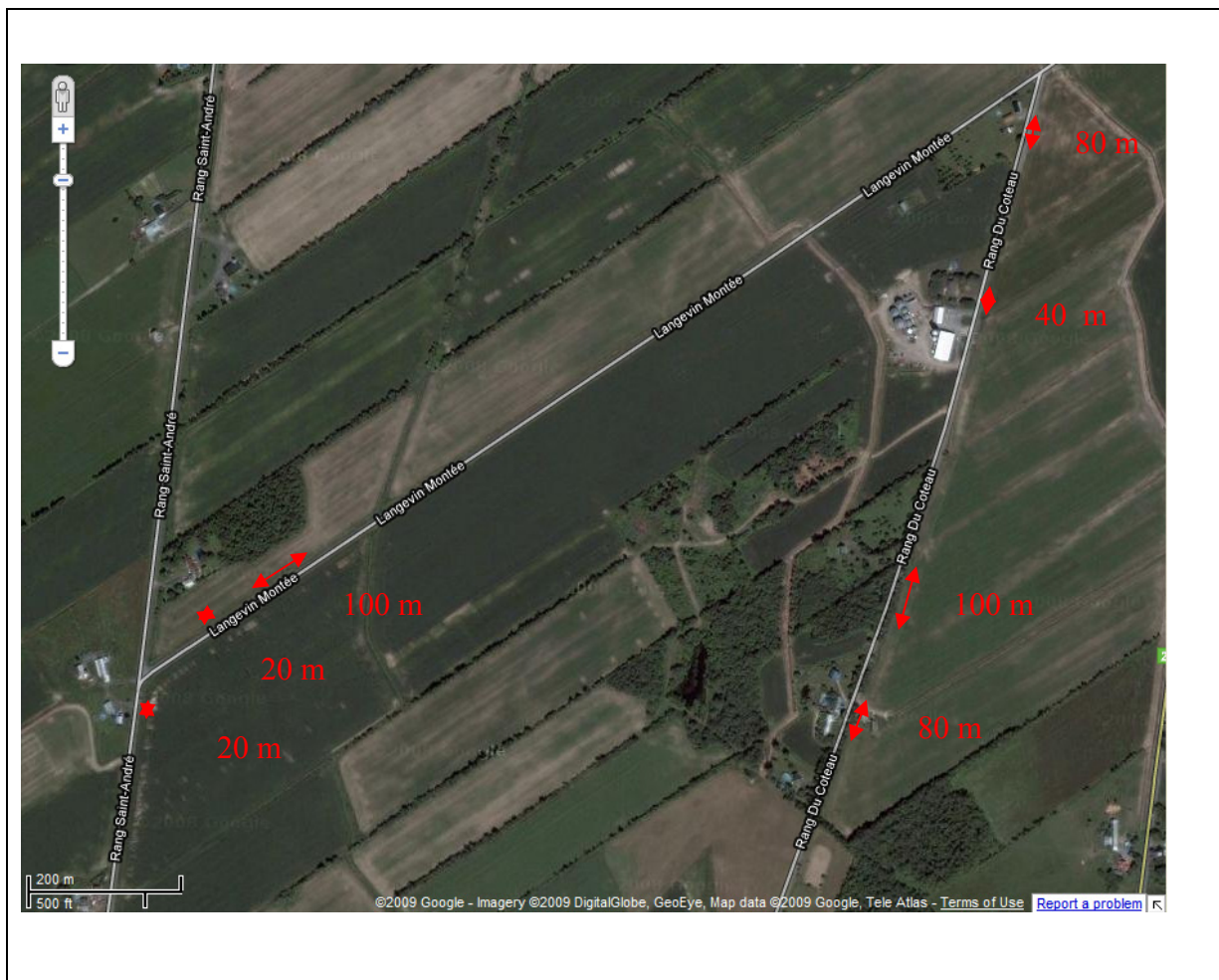


Figure 4.4 Magnified mobile route 1 (© Google 2009).

In **Figure 4.4**, the total distance which is judged to be within the near zones of reflectors is 440 m. Of this total, 200 m is due to houses while 240 m is due to stands of trees.



Figure 4.5 Magnified mobile route 2 (© Google 2009).

In **Figure 4.5**, the total distance which is judged to be within the near zones of reflectors is 445 m. Of this total, 400 m is due to houses while 45 m is due to stands of trees.



Figure 4.6 Magnified mobile route 3 (© Google 2009).

In **Figure 4.6**, the total distance which is judged to be within the near zones of reflectors is 745 m. Of this total, 530 m is due to houses while 215 m is due to stands of trees.



Figure 4.7 Magnified mobile route 4 (© Google 2009).

In **Figure 4.7**, the total distance which is judged to be within the near zones of reflectors is 740 m. Of this total, 140 m is due to houses while 600 m is due to a large stand of trees very close to the road. This stand of trees, along with the railway embankment behind them blocks the propagation path and produces a very low signal level in this area. This is the only area with a low signal level along the route.



Figure 4.8 Magnified mobile route 5 (© Google 2009).

In **Figure 4.8**, the total distance which is judged to be within the near zones of reflectors is 180 m. All of the reflectors are from houses.

The total length of the route is 10.9 km. Adding the lengths of the outage areas along the route, it is calculated that 23.4% of the circuit should produce errors or more serious link problems; 13.3% due to reflections from houses, 4.6% due to reflections from trees and 5.5% due to low signal levels caused by blockage by trees. The measured outage percentage from **Figure 3.3** is 29%. It is believed that the difference is due to the presence of numerous

individual trees close to the road. It is possible that each tree could produce a short burst of errors which would be detected by the error counters. In **Figure 3.3**, 4% of error samples had low error rates of 10^{-4} to 10^{-5} , which represents 20 to 200 errors over a 2 s period for a data rate of 1 Mb/s. If a tree produces an error rate of 0.1, a burst of 200 errors would be produced over a time period of 2 ms. For a vehicle moving at 12.5 m/s, this represents a distance of 0.025 m. Thus, very small areas of high reflection could produce noticeable error rates.

CHAPTER 5

EFFECTS OF SINGLE DOMINANT REFLECTION ON SIGNAL MODULATION

5.1 General

The previous analysis and experimental results show that, in areas where the channel is very poor, there tends to be a single dominant reflection. In this section, the effects of such a reflection on several typical modulation methods are studied. A signal reflection can be considered as a type of interference and the general effects of interference are well known: they increase the signal to noise ratio required for demodulation for a specified error probability. Alternatively, signal reflections can be considered to modify the spectrum of a received signal. These approaches are well known. Here, the emphasis will be on consideration of more detailed problems such as the effects on timing and carrier recovery as well as using these standard analysis techniques to determine how to minimize the effects of the reflection.

For this model, as the mobile moves in areas of good propagation, the link performance will be good, with few errors. The received field magnitude will vary slowly. However, as it approaches a near zone, the reflected field increases rapidly until it is of a similar magnitude to the direct field. The total field will then oscillate rapidly in magnitude and phase as the direct and reflected waves add and cancel due to the vehicle motion. The rate at which the level changes depends on the mobile speed and the path geometry (Doppler effect). The signal may switch between a minimum phase and non-minimum phase type. In this situation, the link performance will likely be poor, with numerous errors and perhaps loss of synchronization. When the mobile passes out of the near zone, the level oscillations decrease rapidly and the link performance returns to normal.

The proposed propagation model consists of a direct wave, a reflected wave of similar magnitude and short delay and a second small reflection of larger delay. It is important to determine the effects of this model on typical digital modulation waveforms. This will be

done here in a general and qualitative way, followed by a more detailed analysis. In this work, only continuous transmission systems using single antennas are considered. Antenna diversity is not considered in detail but is briefly discussed in Section 5.9.

We consider mainly the effect of the larger, shorter delay, reflection whose effect is to put notches into the channel frequency response. The notches are spaced in frequency by $1/\tau$ where τ is the relative delay of the reflection. The depth of the notches depends on how close the magnitudes of the direct and reflected signals are. If the mobile is moving, the notches also move in the frequency domain.

The effects on a signal modulation depend on the signal bandwidth. If the signal bandwidth is much less than the notch spacing i.e. the reflection delay is small relative to the modulation symbol period, then the signal level will vary according to its carrier frequency relative to the notch. If the frequency is at the peak of the channel response, the signal level is high and the signal distortion is small. As a notch moves closer to the carrier frequency, the signal level fades. When the signal carrier frequency is very close to the notch, the level is very small and the distortion will be very great. At this point, there may be numerous errors on the link or the link may be lost. The overall effect is similar to flat fading, in which the signal will be lost for a certain percentage of the time. The fading rate will depend on the speed of the mobile. The only remedy for this situation is coding and interleaving where the interleaver depth must encompass a number of fades. This implies that the required interleaver depth is a function of vehicle speed, which may not be a practical solution for low speeds as the interleaver becomes too large. Diversity would also help in this situation but is not considered in detail here as this analysis deals with the effects on a single receiver.

If the signal bandwidth is much greater than the notch spacing, the received signal level will not fade (at least due to reflection multipath) but some parts of the spectrum will always be lost. However, in this case, a number of solutions are possible. For example, a system which transmits very short pulses, such as ultra wideband (UWB) can overcome the reflections if the pulse width is shorter than the reflection delay. Similarly, a direct sequence spread

spectrum system whose chip period is less than the reflection delay can also work. An OFDM system is another potentially suitable candidate but the system design must take into account the dynamic behaviour of the multipath.

A higher bandwidth signal will, in principle, be better able to tolerate reflections as long as the delay is above a certain value. However, the higher the bandwidth, the lower the range of the system since a higher received level is required for low error rates. This implies a trade-off between range and reflection tolerance.

The reflection delay depends on the mobile position relative to the reflector and the location and size of the near zone. In general, the larger the bandwidth of the signal, the closer the mobile will be able to come to the reflector. The following sections contain a more detailed analysis of some of the effects of multipath.

5.2 Mathematical models of modulated signals

Modulated signals are narrowband bandpass signals which can be expressed as [42]:

$$s(t) = p(t) \cdot \cos(\omega_0 \cdot t) - q(t) \cdot \sin(\omega_0 \cdot t) \quad (5.1)$$

Where ω_0 is the radian center frequency of the carrier. This can be written in the equivalent form [41]:

$$s(t) = \text{Re}\{[p(t) + j \cdot q(t)] \cdot e^{j \cdot \omega_0 \cdot t}\} \quad (5.2)$$

This represents a phasor of varying amplitude and phase rotating with a radian frequency ω_0 .

The analytic signal associated with $s(t)$ is [42]:

$$z(t) = p(t) + j \cdot q(t) \quad (5.3)$$

This is a baseband signal which represents the complex envelope of the bandpass signal i.e. the real and complex parts represent the in-phase and quadrature components of the signal. The Equation (5.3) is completely general but, in this thesis, the signals are generally quadrature amplitude modulated (QAM) signals where $p(t)$ and $q(t)$ are of the form [42]:

$$p(t) = \sum_{n=-\infty}^{\infty} a_n u(t - n \cdot T) \quad (5.4)$$

$$q(t) = \sum_{n=-\infty}^{\infty} b_n u(t - n \cdot T) \quad (5.5)$$

where n is the symbol number, a_n and b_n are discrete levels, $u(t)$ is the basic pulse shape and T is the symbol interval.

5.3 Delay and doppler effects

The delayed signal $s(t-\tau)$ is:

$$s(t - \tau) = \text{Re}\{[p(t - \tau) + j \cdot q(t - \tau)] \cdot e^{j\omega_0(t-\tau)}\} \quad (5.6)$$

which corresponds to the analytic signal:

$$z_1(t, \tau) = [p(t - \tau) + j \cdot q(t - \tau)] \cdot e^{-j\omega_0\tau} \quad (5.7)$$

The quantity $-\omega_0\tau$ corresponds to an angle of rotation. Thus, the delay τ produces a delay in the complex envelope as well as a rotation of the complex envelope. The delay τ can be written as:

$$\tau = \frac{r_{tr}}{c} \quad (5.8)$$

where r_{tr} is the distance that the ray travels between transmitter and receiver (including reflections) and c is the speed of light. When the distance changes, the rotation angle changes with time. In most ground based mobile applications, accelerations are small and the distance r_{tr} can be written:

$$r_{tr} = r_0 + v \cdot t \quad (5.9)$$

where r_0 is a constant and v is a velocity. In this case, the phase angle is:

$$\theta_r(t) = -\frac{\omega_0 \cdot r_0}{c} - \frac{\omega_0 \cdot v \cdot t}{c} \quad (5.10)$$

The term $-\omega_0 r_0/c$ is a constant phase while the term $\omega_0 vt/c$ is a phase that varies linearly with time. If $\omega_0 = 2\pi f_0$, then the variable term corresponds to a frequency shift:

$$f_d = f_0 \cdot \frac{v}{c} \quad (5.11)$$

which is called the Doppler shift [9]. The frequency shift is positive when the distance between the transmitter and receiver decreases and negative when it increases.

5.4 Effect of reflections on modulated signals

When the received signal consists of a desired signal and a series of reflections, it is described by the equation:

$$r_r(t) = \sum_{n=-\infty}^{\infty} a_{rn} \cdot z_1(t, \tau_n) \quad (5.12)$$

Where the a_{rn} are complex coefficients, the τ_n are delays and the function z_1 is as defined in Equation (5.7). This thesis deals with communication between a fixed base station and a mobile which is assumed to be moving with a fixed velocity. Thus, the received signal can be written as:

$$r_r(t) = \sum_{n=-\infty}^{\infty} a_{rn} \cdot [p(t - \tau_n) + j \cdot q(t - \tau_n)] \cdot e^{-j \cdot (2 \cdot \pi \cdot f_{dn} \cdot t + \theta_{0n})} \quad (5.13)$$

where it has been assumed that the delays are varying linearly with time to produce a fixed phase offset and a fixed Doppler frequency offset for each reflected component. The first component is taken to be the direct signal and the others reflections. The direct signal is arbitrarily taken as a reference; the delay and Doppler shift of this signal are ignored and only the relative delays and Doppler shifts of the other components considered. Thus, Equation (5.13) can be written as:

$$r_r(t) = a_0 \cdot [p(t) + j \cdot q(t)] + \sum_{n=-\infty}^{\infty} a_{rn} \cdot [p(t - \Delta \tau_n) + j \cdot q(t - \Delta \tau_n)] \cdot e^{-j \cdot (2 \cdot \pi \cdot \Delta f_{dn} \cdot t + \Delta \theta_{0n})} \quad (5.14)$$

where the Δ indicates a relative value referenced to the direct component.

In general, the complex coefficients a_{rn} , and the delays τ_n are variable as the mobile moves. However, if the mobile is moving over a small area, these quantities can be considered as fixed [11]. In this case, only the rotation angles $2\pi \Delta f_{dn} t$ are variable. Also, the data rates of the communication links for this study are in the range of several Mb/s while the relative Doppler frequency offsets are below 100 Hz. Therefore, the rotation angles $2\pi \Delta f_{dn} t + \Delta \theta_{0n}$ vary much more slowly than the modulation which carries the information and can be considered as fixed over many modulation symbols.

As an illustration, consider a carrier frequency of 400 MHz (approximately the same as the largest frequency used for the measurements). For a vehicle speed of 100 Km/hr, the Doppler shift would be 28 Hz. A QPSK signal with a data rate of 1 Mb/s would have a symbol period of 2 μ s and the rotation of the signal phasor during this time period is 0.02°. The rotation would be 1° during a time period of 50 symbols. During a 1 symbol time period, the vehicle would move 0.056 mm and the delay would change by a negligible amount over a symbol period.

Thus, the received signal can be considered to consist of the desired signal plus a series of delayed versions of the desired signal which are also rotated in phase. The delays are fixed. The phase rotations vary linearly with time depending on the relative Doppler rates of the desired signal and the delayed reflections.

An important factor about the relative delays between the desired signal and the reflections is the size of the delays relative to the symbol period of the signal. If the data symbols are independent and the delays are greater than the symbol period, the interference looks like separate independent interferers and the reflected signals can, in principle, be resolved. However, if one or more of the delays are less than the symbol period, the corresponding reflections cause distortion of the desired signal and a reduction in average signal level when the relative phases of the components are such that cancellation occurs.

The effect of the delayed reflections is to produce intersymbol interference in the desired received signal. For a classical receiver with symbol by symbol detection, the effect will be to degrade the bit error probability of the demodulated signal. A conceptual model for a standard classical receiver (e.g. [42, 43, 44]) for digital signals was shown in **Figure 3.1** and is reproduced in **Figure 5.1** below for convenience. The front end provides low noise amplification and down conversion to a lower IF frequency. The demodulator includes down conversion to DC, matched filtering and a decision process to recover the data. The demodulation is generally coherent and therefore includes a carrier recovery function which tracks the carrier of the received signal. There is also a timing recovery function which

tracks the symbol timing of the signal and provides a symbol clock which times the decision process i.e. it determines when the demodulated signal is sampled.

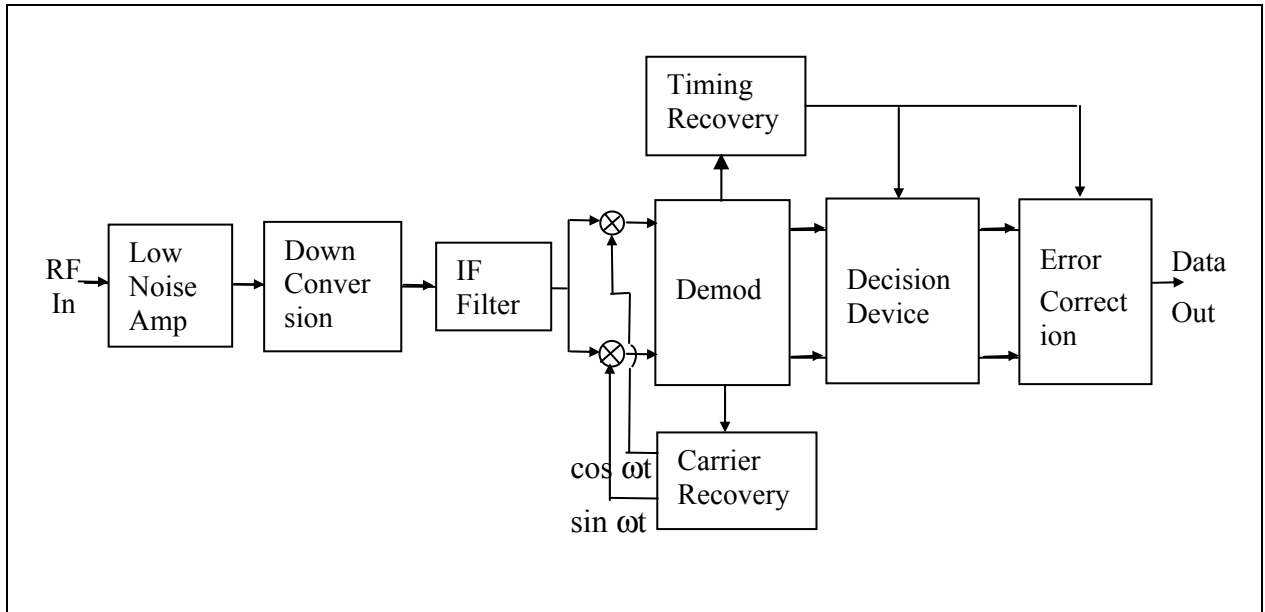


Figure 5.1 Standard receiver model.

A brief discussion of the performance of more general receiver structures in the presence of multipath is given in Section 5.9.

For a QAM type signal, the decision process consists of a sampling of the in-phase and quadrature components followed by a hard decision process or a soft decision process and forward error correction decoding [42]. The effects of interference produce errors in this decision process when the interference is too large. In general, the effects are limited to those time periods for which the interference is large.

However, if the interference is able to affect the carrier recovery or timing recovery processes, the effects can last considerably longer because these functions are generally performed by specialized phase locked loops with very narrow bandwidths, which react relatively slowly. Once disturbed or forced out of lock, these loops may take many milliseconds to recover. For a 1 Mb/s data stream, 10 ms represents 10000 bits.

Even more serious problems may occur for some older types of serial multiplexing equipment connected to a radio receiver. Such equipment operates on a continuous data stream and usually takes the recovered timing from the radio to process the data. If the timing loses synchronism with the data stream, the external equipment loses synchronism as well and must resynchronize before it can resume proper operation. Thus, such equipment will suffer an outage as well and this will add to the time for which the data is not usable. Serial digital multiplexing equipment usually requires that the incoming data and timing signals are synchronous, even if the data itself contains errors. This is generally described as a requirement for “bit count integrity” i.e. the number of data bits in a specified time period must correspond to the number of clock cycles in this period. No “cycle slips” of the timing (either gains or losses of cycles) are permitted for proper operation of the equipment. It should be noted, however, that newer IP, LAN or packet based equipment would not have this requirement for bit count integrity since each packet is processed independently.

It is apparent that the effects of interference can cause even greater problems than to produce errors in the data stream itself if it can cause the loss of synchronism of the carrier recovery process and, especially, the timing recovery process. The theory of Chapter 2 and the measurements of Chapter 3 have shown that there is often a single dominant multipath interferer. Thus, in this work, we focus on the effects of multipath interference with a single dominant reflection on the carrier recovery and timing recovery processes in a typical coherent demodulator of a QPSK receiver. Most of the measurements of Chapter 2 were made with a QPSK system. It is also felt that QPSK would be more likely to be used for a mobile system than a more complex QAM modulation because a complex QAM system would be much more susceptible to multipath interference. A complex QAM system needs a much higher signal to noise ratio for equivalent error rate performance [43] and would therefore be more susceptible to multipath interference as well. Such a system also requires a precise AGC, which would also be affected by interference.

5.5 Effects of single dominant reflection on signal spectrum

For a single reflection, Equation 5.14 simplifies to:

$$r_r(t) = a_0 \cdot [p(t) + j \cdot q(t)] + \sum_{n=-\infty}^{\infty} a_1 \cdot [p(t - \Delta\tau_1) + j \cdot q(t - \Delta\tau_1)] \cdot e^{-j \cdot (2\pi \cdot \Delta f_{d1} \cdot t + \Delta\theta_{01})} \quad (5.15)$$

The expression $2\pi\Delta f_{d1}t + \Delta\theta_{01}$ represents a slow phase variation with time over many modulation symbols. As a first approximation, it can be considered constant. Thus, taking a Fourier transform of Equation 5.14 gives approximately:

$$R_r(f) \approx a_0 \cdot [P(f) + j \cdot Q(f)] + a_1 \cdot [P(f) + j \cdot Q(f)] \cdot e^{-j \cdot (2\pi \cdot \Delta f_{d1} \cdot t + \Delta\theta_{01})} \cdot e^{-j \cdot 2\pi \cdot f \cdot \Delta\tau_1} \quad (5.16)$$

or

$$R_r(f) \approx [P(f) + j \cdot Q(f)] \cdot (a_0 + a_1 \cdot e^{-j \cdot (2\pi \cdot \Delta f_{d1} \cdot t + \Delta\theta_{01})} \cdot e^{-j \cdot 2\pi \cdot f \cdot \Delta\tau_1}) \quad (5.17)$$

The frequency response of the channel is given by:

$$F(f) \approx (a_0 + a_1 \cdot e^{-j \cdot (2\pi \cdot \Delta f_{d1} \cdot t + \Delta\theta_{01})} \cdot e^{-j \cdot 2\pi \cdot f \cdot \Delta\tau_1}) \quad (5.18)$$

where $2\pi\Delta f_{d1}t + \Delta\theta_{01}$ is a slowly varying phase. For a given value of a_1 , this represents a notch filter with a period of $1/\Delta\tau_1$ in the frequency domain. The rate of change of the notch frequency with time is $\Delta f_{d1}/\Delta\tau_1$ in Hz/sec. Without loss of generality we set $a_0 = 1$ and $\Delta\theta_{01} = 0$. Also, a_1 is assumed real since a phase term can be taken into the exponential. The maximum frequency response is $1 + |a_1|$ while the minimum is $1 - |a_1|$. Thus, for values of the reflection coefficient close to 1, the notch can be deep. The width of the notch is proportional to $1/\Delta\tau_1$.

If the notch is moving, it will periodically hit the signal spectrum and cause distortion. If the delay $\Delta\tau_1$ is much less than a symbol period, the notch will be wider than the signal spectrum and the signal level will be significantly reduced when the notch hits the signal frequency

and the signal will be distorted. When the notch does not hit the signal spectrum, the signal will not be affected. If the delay is greater than a symbol period, there will always be a notch somewhere in the signal spectrum and perhaps more than one. The signal level will not vary greatly but the signal will always be distorted.

5.6 Effects of single dominant reflection on receiver synchronization

5.6.1 Aspects of synchronization

The signals under consideration in this work are continuous transmission QAM types, especially QPSK which is emphasized here. These signals require coherent demodulators for optimum demodulation. The measurements of Chapter 3 were made mostly with coherent QPSK demodulators. Thus, synchronization (i.e. carrier and timing recovery) of such a system is considered here.

The received signal consists of a series of symbols equally spaced in time. Each symbol shape is a pulse defined by the overall system filtering, which is assumed here to be a raised cosine shape [42] with an excess bandwidth of 25%. The raised cosine filter produces a pulse shape with zero intersymbol interference on that symbol; neighbouring symbols have no effect.

In order to demodulate this signal, the carrier signal must be recovered and the signal down converted to DC to produce in-phase and quadrature components corresponding to the real and imaginary components of the analytic signal of Equation (5.3). Also, the symbol timing must be recovered. In the absence of interference, the instants corresponding to the centres of the symbols must be determined. The signal components are sampled at the centres of the symbols and the data recovered. In the presence of multipath interference, the optimum sampling instant may not be in the centre of the symbol; a better strategy for a classical receiver is to sample at the maximum eye opening [42].

Carrier and timing synchronization of coherent demodulators is a well known field and many methods to accomplish this are described in the literature [42, 43, 44]. Meyr [43] gives a general framework for analyzing synchronization and detection for non-fading and fading channels. A number of references also treat the effects of multipath fading on carrier recovery [50, 51] and timing recovery [51, 52, 53]. However, these references generally treat flat fading [50 51] or multipath where the delay spreads are small fractions of a symbol [53]. Brandao [52], who treats the optimization of the sampling timing instants to minimize the bit error rate, states that the degradation of timing recovery due to multipath and cochannel interference is large. Carrier synchronization in the context of CDMA systems is treated, for example, by Van Nee [54]. Boyer [54] states that the optimum timing for frequency selective fading channels is an open question and treats the performance difference due to setting the timing reference on the first or largest multipath components. An indoor propagation delay distribution is used in [55].

The objective of the present work is to determine how the synchronization is affected by multipath interference with a single dominant reflection having different amplitudes, delays and reflection angles. Such an analysis has not been found in the literature. In particular, it is important to judge whether synchronization is maintained in the presence of multipath.

A timing recovery function for a QPSK signal typically has the form shown in **Figure 5.2**.

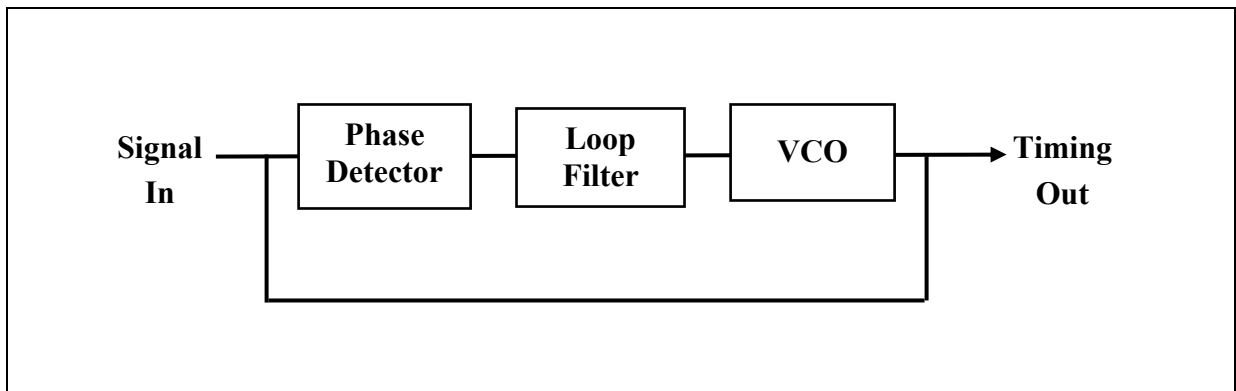


Figure 5.2 Typical timing recovery function for QPSK.

This structure is a phase locked loop which tracks the average symbol positions of the received signal. A typical phase detector for timing recovery in a classical receiver forms the derivative of the squared magnitude of the signal and averages this quantity over corresponding time instants in a number of successive symbols [42]. For a symbol time $0 < t < T$, the phase detector forms the quantity:

$$P_d(t) = E\left\{\frac{d(p^2(t) + q^2(t))}{dt}\right\} \quad (5.19)$$

where the expectation E indicates averaging over all symbols. Such a detector is maximum likelihood for the whole channel. In practice, the averaging is done over a large number of symbols. For the assumed system filtering, the phase detector characteristic approximates a sine wave, as determined from a system simulation i.e.

$$P_d(t) \approx K_d \cdot \sin\left[2 \cdot \pi \cdot \left(0.5 - \frac{t}{T}\right)\right] \quad (5.20)$$

where K_d is the phase detector constant. It can be shown analytically that, when the system filtering is Nyquist, the phase detector characteristic of Equation 5.19 is, in fact, a sine wave. Analyses for similar situations are performed by Meyr et al [43] and Gardner [56].

The best estimate of the timing instant occurs when the phase detector output is zero i.e. when $t = T/2$. The loop constants and filter parameters are chosen to track the assumed dynamics of the incoming signal. It should be noted that the timing recovery function depends only on the signal magnitude and therefore, does not depend on having a correct carrier phase i.e. the timing can be recovered before the carrier phase has been correctly synchronized.

A carrier recovery function is also typically implemented as a phase locked loop but the phase detector estimates the error in the recovered carrier. In a data aided carrier recovery loop, the phase error is estimated by the phase difference between the recovered signal and

the nearest correct symbol location [42]. The phase error is averaged over many symbols. The loop acts to reduce the average phase error to 0. A QPSK constellation is shown in **Figure 5.3**.

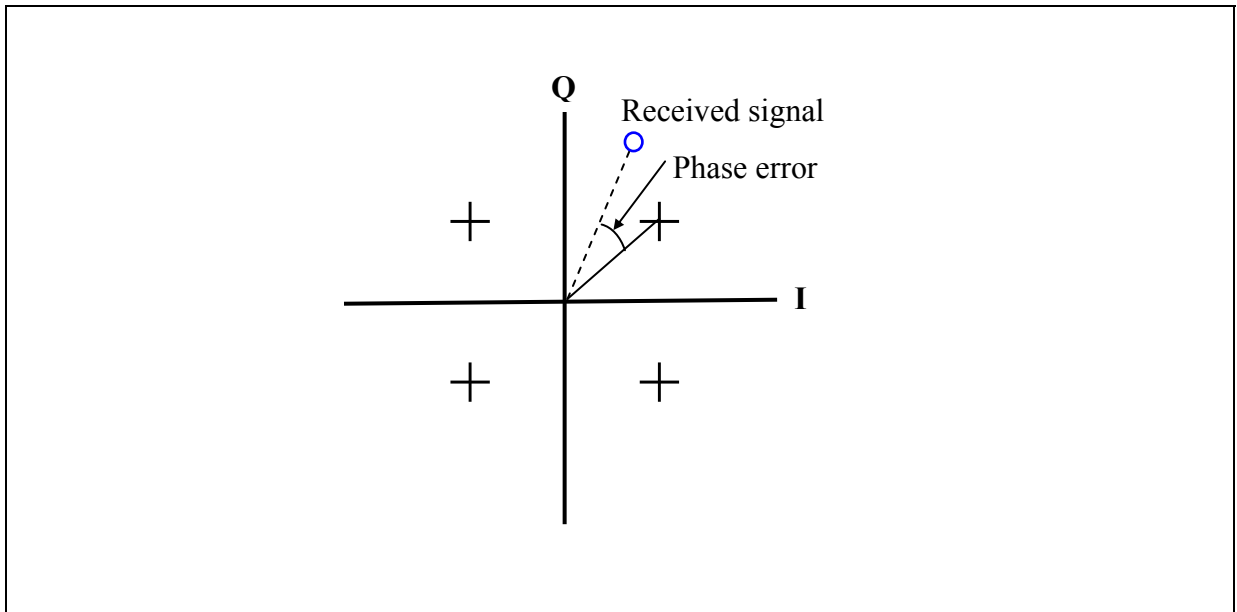


Figure 5.3 QPSK constellation.

The phase detector for this system is periodic with a period of $\pi/2$ since there are 4 symbol locations. The recovered carrier therefore has a 4 fold ambiguity, which is typically resolved either by differential decoding or by detection of known sequences within the data stream. The resolution of the ambiguity is not the main focus of this work and is not considered further.

In a classical coherent receiver, the carrier recovery function is used to generate a carrier which down-converts the received signal to DC. The in-phase and quadrature signal components are then sampled in the middle of the symbol period by the recovered timing signal.

5.6.2 Steady state timing and carrier recovery phase errors due to single reflection

A first analysis of the effects of a single reflection on the timing and carrier synchronization has been performed by the author by means of simulation. The simulation implements Equation 5.14 with a single reflection having a fixed phase shift. The timing phase is estimated from Equation 5.19 where $P_d(t) = 0$. The carrier phase error for each symbol is determined from the in-phase and quadrature sample values at the timing phase. The simulation is performed for 1024 symbols with 32 samples per symbol. The timing recovery phase detector characteristic and the carrier phase error are averaged over 1024 symbols. The overall channel filtering is a raised cosine with 25% excess bandwidth.

The above process has been repeated with different reflection delays, different reflection amplitudes and different reflection phases. The results have been plotted by the author in a series of graphs in the Annex. For each reflection delay, the carrier or timing phase error is plotted as a function of reflection amplitude and phase. Recall that, as the mobile moves over a small area, the reflection magnitude will stay fixed and the phase will rotate. Thus, phase errors of the recovered timing and carrier will have a periodic variation with time (and mobile position). Delays are plotted up to two symbol times. Beyond this, the effects are mostly random since the data symbols are assumed to be independent.

The Annex shows the average timing phase error as a function of reflection amplitude and phase. The relative amplitudes range from 0 to 1 and the phases from $-\pi$ to π . For small amplitudes, the timing phase errors are also small and tend to be sinusoidal. However, as the amplitudes approach 1, the timing phase errors become significant and tend to be very non-linear with reflection angle. The phase errors tend to have two values, with very rapid transitions between them at certain reflection phase angles. One value of phase error is about 120 degrees while the other is about -40 degrees. When the delay exceeds 1 symbol, the two delay values are -120 degrees and 40 degrees. At the same time, the peak phase detector output varies widely in magnitude. The peak phase detector output affects the parameters of the phase locked loop. When it is low, the loop becomes underdamped and tends toward

instability. When the peak phase detector output is low, it is low regardless of the phase error. Thus, the loop cannot respond correctly to phase errors. These effects cause the recovered timing to be very unreliable when the magnitude of the reflection approaches one.

The preceding discussion of the peak phase detector output has omitted any consideration of the operation of the automatic gain control (AGC) in a practical receiver. A receiver always has an AGC system because signal variations with link range can be very great. The speed of the AGC has a great effect on the peak phase detector output. If the AGC speed is fast enough to track the signal level variations, the peak phase detector output will not be greatly changed and the preceding discussion will not apply. However, if the AGC is too slow, it will not respond to fast level variations and the simulation results will apply.

Clearly, the operation of the timing recovery is greatly affected by the presence of large reflections and also by other details of the system design such as the AGC. It can therefore be expected that timing recovery in the presence of large reflections, especially with low delays, will be unreliable.

Annex 1 also shows the average carrier phase errors. Again, the relative amplitudes range from 0 to 1 and the phases from $-\pi$ to π . When the reflection delay is very small, the peak carrier phase error approaches 90 degrees for reflection magnitudes approaching one. For larger delays, the peak errors are smaller but still significant. It should be noted as well that a data aided carrier phase detector for QPSK will have a range of ± 45 degrees since the constellation points are spaced by 90 degrees. Thus, any phase error beyond 45 degrees will be incorrectly interpreted by the phase detector. The tracking loop will then get incorrect information and will not be able to track correctly. The stability of the carrier recovery loop will be degraded and the tendency to lose lock will be increased.

Also shown in Annex 1 is the variation of the received signal power. For large reflections with low delays, when the reflection phase is zero, the peak signal is 6 dB greater than normal while the minimum signal can be deeply faded. Very low delays correspond to the

case of flat fading. As the delay increases, the variation in the signal is decreased, even when the reflection phase is 180 degrees. When the delay exceeds one symbol period, the variation is not large. This corresponds to the notches in the channel frequency response being spaced by less than the signal bandwidth.

5.7 Direct sequence spread spectrum systems

It has been seen that large reflections cause problems for standard modulation systems. For delays greater than a symbol, the reflection looks like random interference because the data symbols are assumed to be independent. For delays less than a symbol, the reflection causes distortion of the signal and potentially fading if the delay is small enough. It is therefore useful to reduce the effective level of the reflections. Direct sequence (DS) spread spectrum systems offer a way to do this because a reflection with a delay greater than the chip period of the spreading code looks like an independent interferer. When the signal is despread, the desired signal is recovered while the reflection looks like noise.

DS systems are treated in detail in a large number of texts [42, 46, 47]. The data symbols with a rate of R_S are combined with a high rate spreading code of rate R_C and modulated onto a carrier. The modulation is assumed to be QPSK for simplicity. The effective bandwidth of the spread signal is R_C , where R_C is the chip (symbol) rate of the spreading code. The spreading codes are designed to look random i.e. there is a low correlation between any two chips.

At the receiver, the signal is despread by a multiplicative process which leaves the unspread modulated signal having a bandwidth of R_S . Suppose that the received signal consists of a desired signal plus a reflection having a delay greater than the chip period and a relative amplitude of α_I . The result of the despreading operation will be that the desired signal keeps the same amplitude while its bandwidth is reduced to R_S . The reflection, however, while keeping the same relative amplitude, will still have a bandwidth of approximately R_C because code chips are approximately uncorrelated. The desired signal can then be filtered by a filter

of bandwidth R_s and the power of the reflection will be reduced by a factor of R_s/R_c (the process gain of the system). Thus, the reflection of relative amplitude α_l will appear as a noise having a relative power of $\alpha_l^2 R_s/R_c$. The effective power of the reflection is reduced by the process gain of the despreading operation. If the signal to noise ratio is high enough, the effect of the reflection is negligible. Error correction coding can also be applied to remove any remaining errors.

When the delay is less than a chip period, the reflection will appear partially correlated to the desired signal during the despreading process. Part will appear as uncorrelated noise and part will cause distortion of the direct signal component.

The effect of a simple DS system is therefore to allow the mobile to come closer to a reflective structure than with a non-spread modulation. When the delay of the reflection is less than the length of the spreading code chip, the reflection begins to have a significant effect but the chip period is typically much less than that of the modulation symbol period. The disadvantage of the DS system is that it requires much more bandwidth than a non-spread modulation.

A more complex type of DS receiver is a RAKE receiver [42], in which the different reflected components are tracked by the system. They then have their delay differences compensated and all the components are added. This type of receiver is typically used in a CDMA cellular base station [57]. The delay components are referred to as “fingers”. Usually, 5 fingers are tracked. This type of system is more complex than the simple DS receiver but has much better performance. However, the time resolution of the system is still one spreading code chip period. If the delay of the reflected component is less than 1 chip period, signal distortion will still result.

5.8 OFDM systems

An OFDM signal has features which enable it to withstand multipath to a greater extent than a single carrier modulation. An OFDM signal consists of many small subcarriers spaced at precisely the symbol rate to maintain orthogonality [48]. For each symbol, every subcarrier is modulated with an amplitude and phase, usually with a QAM constellation. Typical QAM constellations are BPSK, QPSK, 16 QAM and 64 QAM. Each symbol also has a cyclic prefix (guard time), which is a repeated portion of the end of the symbol. In this way, as long as the delay spread of the multipath is less than the length of the cyclic prefix, there will be no intersymbol interference since there will always be a clear time period equal to the symbol length which can be demodulated.

The demodulator removes any frequency offset (for example due to Doppler shifts) and synchronizes with the symbol times. Then an FFT is performed on the symbol and each subcarrier recovered. The subcarrier amplitude and phase are converted into information bits.

In order to correctly recover the amplitude and phase of each subcarrier, an amplitude and phase reference is required. For this purpose, a number of subcarriers are allocated for pilot subcarriers with known amplitude and phase values. Pilot subcarriers may occur on every symbol or on some of the symbols.

The amplitudes and phases of the pilots are recovered and used as amplitude and phase references. The phase and amplitude shifts introduced by the channel for each subcarrier are estimated from the pilot values by an interpolation process.

The demodulator must remove Doppler frequency offsets, recover the symbol timing, estimate the channel response and make a decision on the symbol value of each subcarrier. The following sub-sections briefly consider these subjects, with the main emphasis on recovery of the data.

a) Doppler effects

The demodulator must estimate the frequency errors of the received signal and try to remove them. Frequency errors can be due to oscillator tolerances or vehicle motion. If there is no multipath, frequency correction should be straightforward and there will, in principle, be no degradation due to Doppler effects.

If there is static multipath, the channel does not change with time but the received signal is not flat across the frequency band and there may be errors in the frequency correction. In this case, there will be a performance degradation due to interference between the subcarriers [48]. If there is dynamic multipath due to vehicle motion, there may be a variable frequency correction error, also producing a degradation for the same reason. It is assumed here that the Doppler shifts are sufficiently corrected to achieve acceptable performance.

b) Symbol timing recovery

Symbol timing recovery can be performed in various ways [48], such as correlation of the cyclic prefix with the end of the symbol. It is assumed that, as long as the cyclic prefix is long enough to cover the multipath delay spread, symbol timing recovery performance should be acceptable.

c) Channel estimation and tracking

When multipath is present, the channel frequency response is no longer flat and the amplitude and phase of the subcarriers will vary in time and across the symbol frequency range. The demodulator must estimate this variation to correctly demodulate the signal. Also, both the main component and the multipath reflections have Doppler frequency errors due to mobility.

The estimation of the pilots can be regarded as a sampling process. There must be enough pilot subcarriers and symbols containing pilots to permit the unambiguous recovery of the pilot samples under the given delay spread and Doppler spread. It is also assumed here that this condition is fulfilled.

d) Data recovery

Each subcarrier is modulated with a QAM signal, which is typically BPSK, QPSK, 16 QAM or 64 QAM (for example in the WiMAX system [58, 59]). To recover the data, the nominal subcarrier level and phase must be known so that slicing levels can be set for the demodulator. The pilot subcarriers are used for this purpose and it is assumed that the channel is correctly tracked. The level of each subcarrier varies with symbol time and subcarrier frequency according to the channel frequency response given by Equation 5.18. The value α_0 is taken as 1 and α_l is assumed to be between 0 and 1. The magnitude response can then be between + 6 dB and $-\infty$.

For the environments considered in this work, the received signal is likely to be far above the thermal noise level. Thus, assuming that the channel is tracked, the error rate performance of this demodulator will be determined by how far above the noise floor each subcarrier is. In general, unless the relative delay of the reflection is very small, some of the subcarriers will fall into the notch but most will have a sufficient signal to noise ratio to provide good performance. Typical OFDM implementations have forward error correction coding and interleaving [48, 58] which will remove most of the errors on the subcarriers with low signal to noise ratio. The code rate can be chosen to trade off error reduction against system capacity. It should be noted that OFDM systems such as those specified by [58] have been designed specifically to provide good performance in a multipath environment.

e) Summary of OFDM performance

Based on the above considerations, it can be concluded that an OFDM system generally has better multipath performance than a single carrier system with a classical demodulator which performs symbol by symbol detection. The only possible exception may be for cases in which the mobile is very close to a reflecting wall. In this case, the entire signal would be periodically faded and no system would have good performance.

In a multipath environment, when a notch is induced into the signal spectrum, the spectrum is distorted. For a single carrier system with a classical demodulator, this produces distortion on all of the symbols. For an OFDM system, on the other hand, the notch only degrades the symbols on some of the subcarriers and error correction coding with interleaving can recover most of the errors.

The following section looks at the performance of some other receivers for single carrier systems.

5.9 Performance of other receivers

In assessing the effects of multipath on single carrier systems, most of the discussion in this thesis has dealt with classical receivers which use symbol by symbol detection without additional attempts to compensate for the multipath. However, other approaches have also been used and analyzed in the literature. They include sequence detection, equalization and antenna diversity. These types of receivers are briefly considered in this section.

a) Sequence detection

The optimum receiver for channels with a non-flat frequency response is a Maximum Likelihood Sequence Detector (MLSD) [42, 60]. This type of receiver would typically be implemented using the Viterbi algorithm [42]. The performance of this type of receiver can

be characterized by the concept of the minimum Euclidean distance between two sequences, [42]. The square of the distance between two signals is, for the case where the noise is white Gaussian noise, the integral of the magnitude squared of the difference between the signals [42]. The minimum distance is the smallest value between all pairs of possible signals.

Consider a system which transmits blocks of data in the presence of multipath interference from a single reflection. When the multipath delay is much less than a symbol period, the signal energy of a block may be increased, if the spectrum notch is outside the signal spectrum or reduced if the notch falls within the spectrum. In the latter case, the energy may be greatly reduced if the delay is small. The minimum distance varies directly with the signal energy. Therefore, a notch in the spectrum will reduce the system performance, even with an optimum demodulator. However, Proakis [42] shows that, for a case where the delay is equal to a symbol period, the minimum distance is proportional to the sum of the powers of the direct and reflected signal components. This will also be the case for delays greater than a symbol period as the reflection will appear as random interference. Lucky [60] states in his review paper that the Viterbi algorithm, in most cases, uses all the available signal energy and effectively removes the effects of intersymbol interference. Thus, it can be concluded that the MLSD will have reduced performance when the multipath produces a notch in the signal spectrum (short delay with the worst case reflection phase) but will have better performance than for the direct signal alone when the delay is greater than a signal period.

One important point regarding the MLSD is that the channel response is assumed to be known. Thus, tracking of the channel is required for this scheme.

b) Equalization

Equalizers try to compensate for the effects of intersymbol interference due to multipath. Linear equalizers try to correct the channel frequency response. Decision feedback equalizers have a linear portion for precursors and a decision feedback portion which use decisions

which have already been made. Both types generally try to minimize the mean squared error of the received signal at the sampling instants.

Linear equalizers generally do not perform well when channel spectrum nulls are present [42, 60] as they try to produce a very high gain at these frequencies which enhances the noise. Decision feedback equalizers have better performance with spectral nulls and their mean squared error remains finite under these conditions [60]. However, equalizers are, in general, considered to be sub-optimal [42, 60]. A summary of modern approaches to equalization is given by Osman and Ucan [61].

c) Antenna diversity

Antenna diversity is generally described in the context of multipath with very short delays which produce flat fading [42]. In this case, if two (or more) antennas have independent fading, their outputs can be linearly combined to reduce the probability of fading in the energy of the combined signal. Proakis [42] describes the maximal ratio combiner, which weights and adds the antenna outputs together to maximize the overall signal to noise ratio.

In general, MLSD can also be applied to the outputs of two (or more) antennas. Usually, the antennas on the mobile are not separated by more than a few wavelengths. Thus, the signal magnitudes of the direct signals are approximately the same at all antennas. Similarly, the magnitudes of the reflected components are approximately the same at all antennas and the delays of the reflected components relative to those of the direct components are also approximately the same at all antennas. However, the carrier phase of each component will be different at each antenna.

The performance of such a diversity system can also be characterized in terms of an overall minimum Euclidean distance. The square of the overall minimum Euclidean distance is just the sum of the squares of the minimum Euclidean distances of each antenna output. If the relative delays of the reflected components are small and the relative carrier phases are such that more than one antenna output has cancellation, the minimum distance may be degraded.

In most cases, even with small delays, the minimum distance should be somewhat enhanced. However, if the relative delays are more than a symbol period, the square of the overall minimum distance will be proportional to the sum of the powers of all of the direct and reflected components and the overall performance will be significantly enhanced.

CONCLUSIONS

A typical line of sight mobile communication scenario has been presented and analyzed in order to characterize the channel behaviour for suburban and semi-rural areas. Based on the physics of reflection and scattering from flat walls, several key points about the behaviour of this propagation scenario have emerged.

- 1) There exists a near zone extending outward from the reflecting structure in the direction of specular reflection. The field within this near zone is similar in magnitude to that of the direct wave at the mobile.
- 2) Beyond a certain near zone distance, the reflected field drops rapidly with distance from the structure, often as $1/d^2$ when there is a reflecting ground plane.
- 3) The near zone distance depends on the size of the reflecting wall. A very rough measure, for the case of broadside incidence, is the area divided by the wavelength.

These points have been used to explain many of the aspects of the behaviour of mobile communication channels. They have also been used to develop a model for the case of suburban and rural communications which, incidentally, is close to that of the corresponding SUI model. The behaviours of some typical modulation formats in the presence of this model have been examined in a qualitative way.

The thesis has also presented the results of measurements on suburban and semi-rural communications links which were carried out to validate the results of the theoretical analysis. These measurements are in agreement with the theoretical analysis which shows that, for the types of areas which were studied, there were generally two types of behaviour: a good state and a bad state. In the good state, there is little channel distortion and the error rates are small or zero. In the bad state, there is significant distortion with high error rates and general poor performance. In this state, there tends to be a single dominant reflection

whose amplitude is close to that of the desired signal and whose maximum delay is around 1 μ s or less. There may be other smaller reflections present but they can be modeled as an additional reflection whose magnitude is at least 10 dB below that of the direct path. The delay of this reflection can be taken as 3 to 4 μ s.

The effects of this type of communication channel on modulated signals have been studied by analyzing various aspects of the performance of several typical modulation methods for the case where there is a single dominant reflection. It is shown that the timing and carrier recovery functions of a coherent QPSK receiver will be greatly affected by the reflection when the reflection amplitude approaches that of the desired signal. In fact, it is likely that synchronization will be lost under these conditions. Steady state timing and carrier recovery phase errors have been studied by simulation.

Direct sequence spread spectrum systems and OFDM systems were also examined briefly. A DS system is able to discriminate between the desired signal and the reflections as long as the reflected component delay is greater than the code chip period. If the process gain of the system is large enough, the effects of the reflection can be greatly reduced, particularly if coding is used as well. A RAKE type receiver can obtain even better performance because reflected components can be tracked. The effects of this type of channel model on OFDM systems have been considered. It has been shown that, if the channel can be tracked, OFDM systems with coding offer much better performance than a single-carrier system with classical symbol by symbol demodulation. For very short delay spreads, the situation approaches flat fading and all types of systems will suffer degraded performance during the fade.

In summary, this thesis has shown, by analysis, measurement and simulation that near line-of-sight channels in suburban and semi-rural areas can cause very severe distortions in standard signal modulations because of the presence of multipath reflections. It has been shown that there is usually a single dominant reflection which can approach the level of the desired signal within the near zone of a building wall. The reflection can cause a severe periodic fading and signal distortion which can lead to the loss of synchronization of classical

coherent receivers. A system design for this application requires special features to combat this type of behaviour. DS or OFDM systems offer much better performance than a classical single-carrier system.

Other receiver structures have also been addressed. Maximum likelihood sequence detection can make use of the power in both the direct signal and the reflection. Diversity can also enhance performance.

ANNEX

QPSK TIMING AND CARRIER RECOVERY SIMULATIONS

This Annex provides the results of the timing and carrier recovery simulations described in Section 5.6.2. Steady state timing and carrier phase errors are displayed as a function of reflection level, phase and delay for the case of a single dominant reflection.

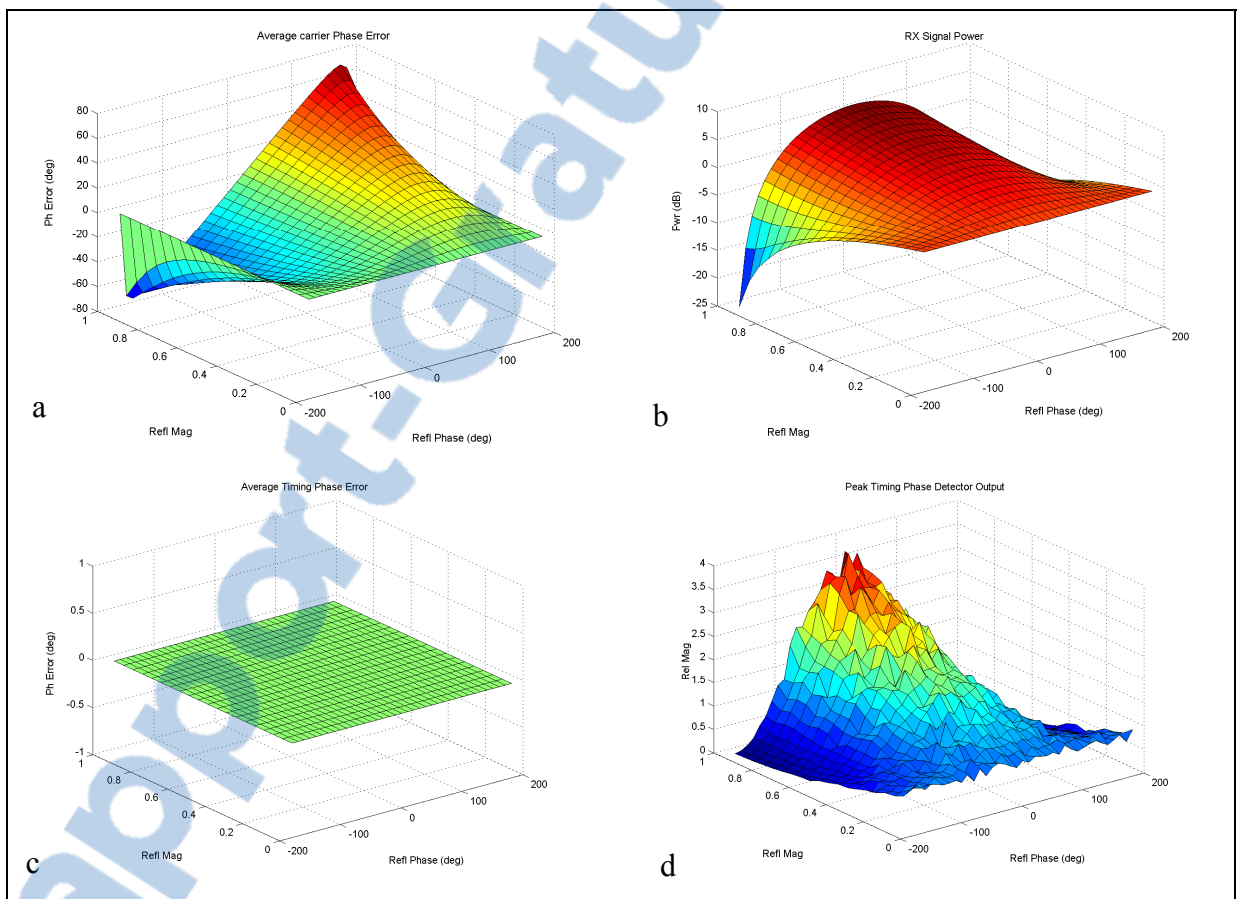


Figure A.1 Delay 0.0 symbols. a) average carrier phase error; b) received signal power; c) average timing phase error; d) peak timing phase detector output.

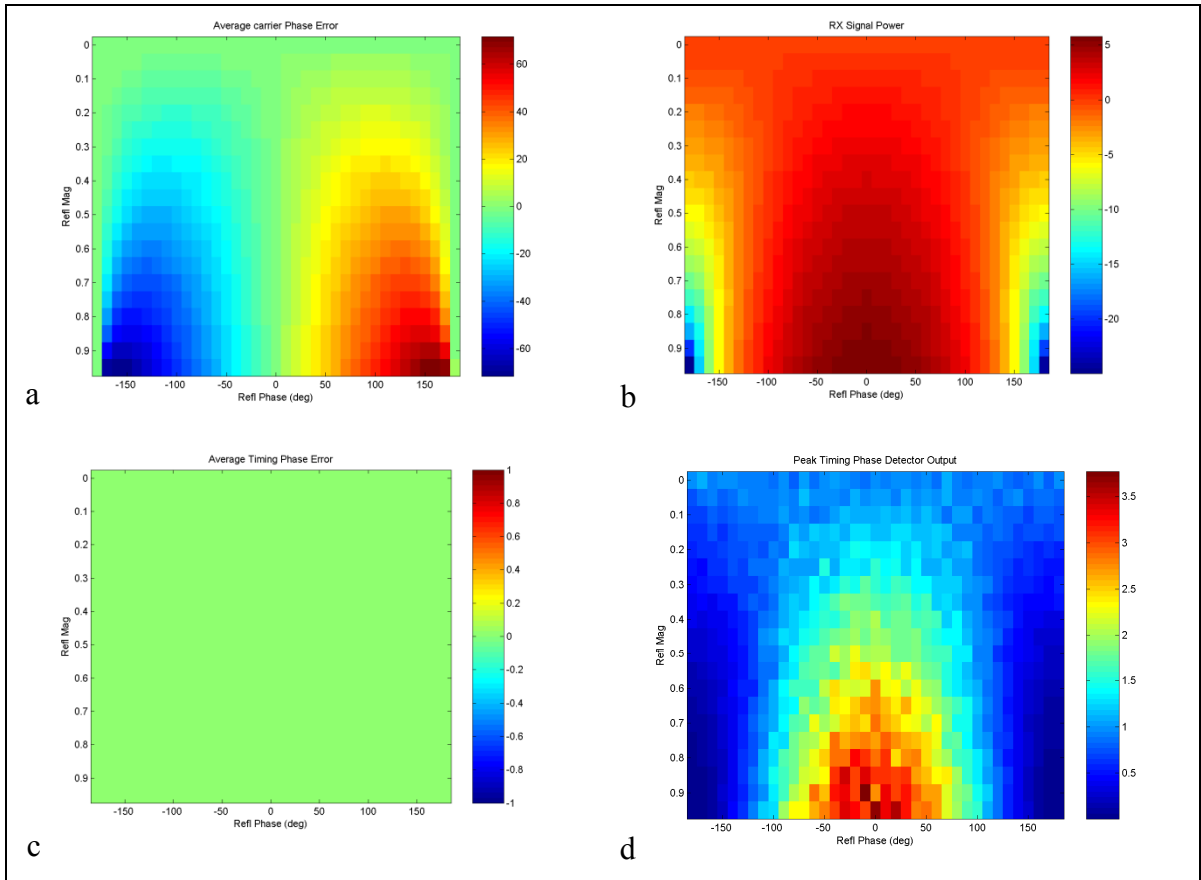


Figure A.2 Delay 0.0 symbols. a) average carrier phase error; b) received signal power; c) average timing phase error; d) peak timing phase detector output.

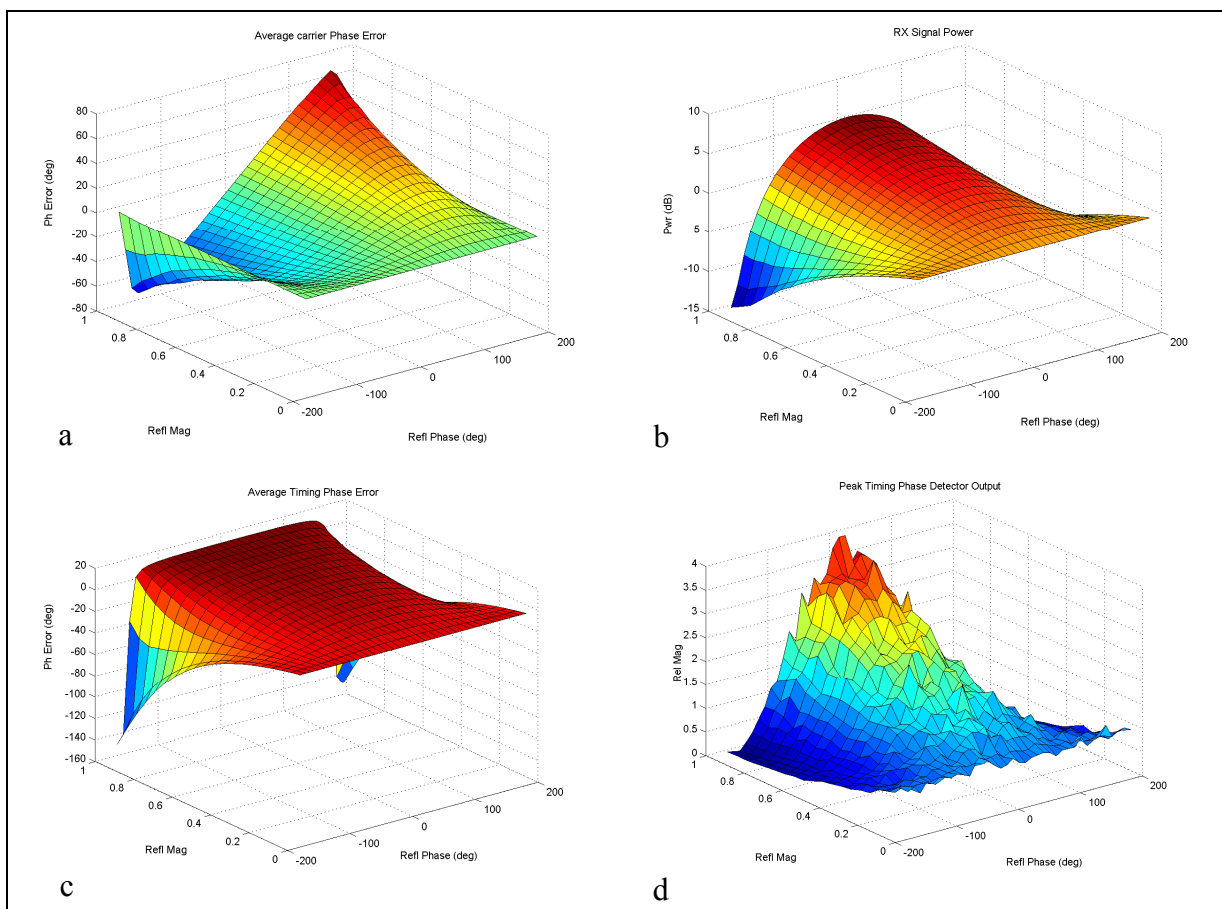


Figure A.3 Delay 0.1 symbols. a) average carrier phase error; b) received signal power; c) average timing phase error; d) peak timing phase detector output.



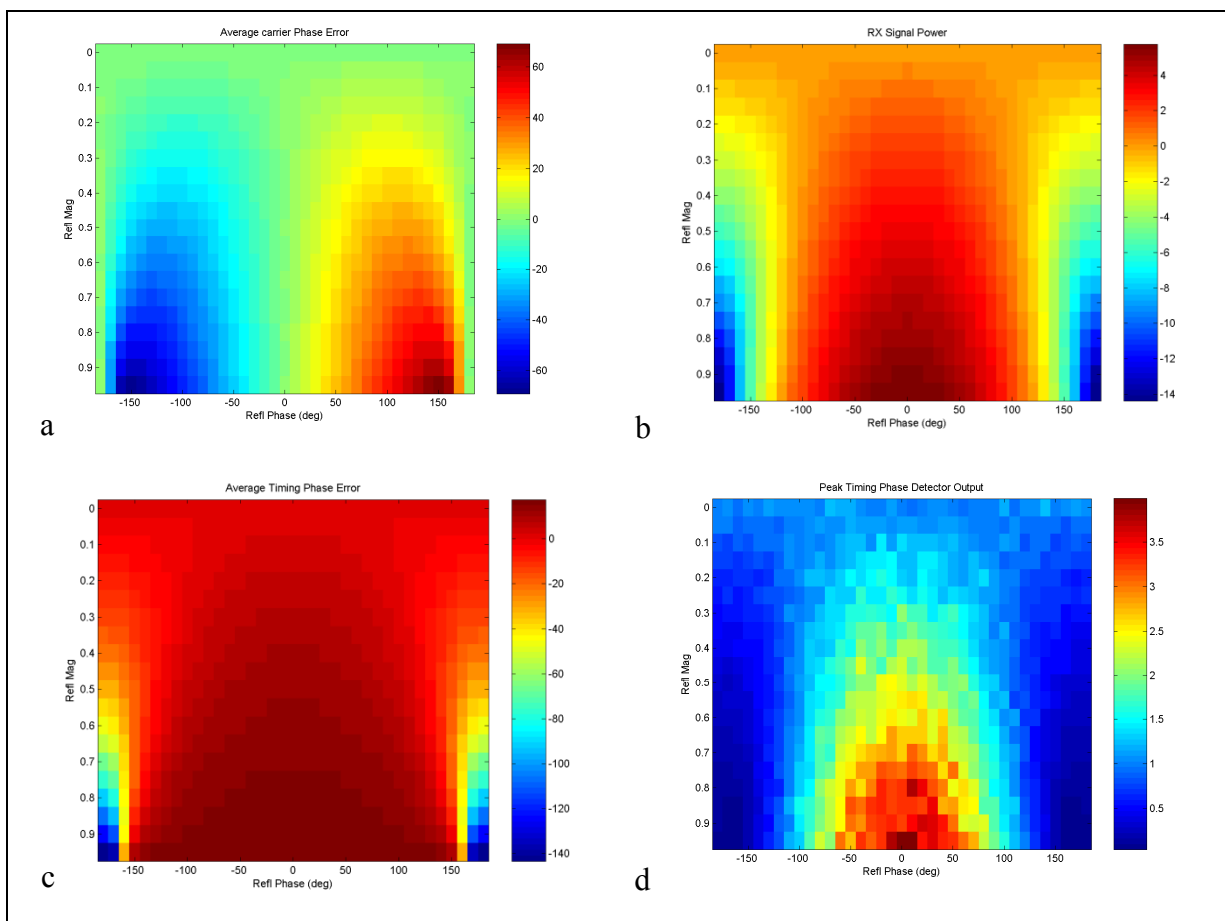


Figure A.4 Delay 0.1 symbols. a) average carrier phase error; b) received signal power; c) average timing phase error; d) peak timing phase detector output.

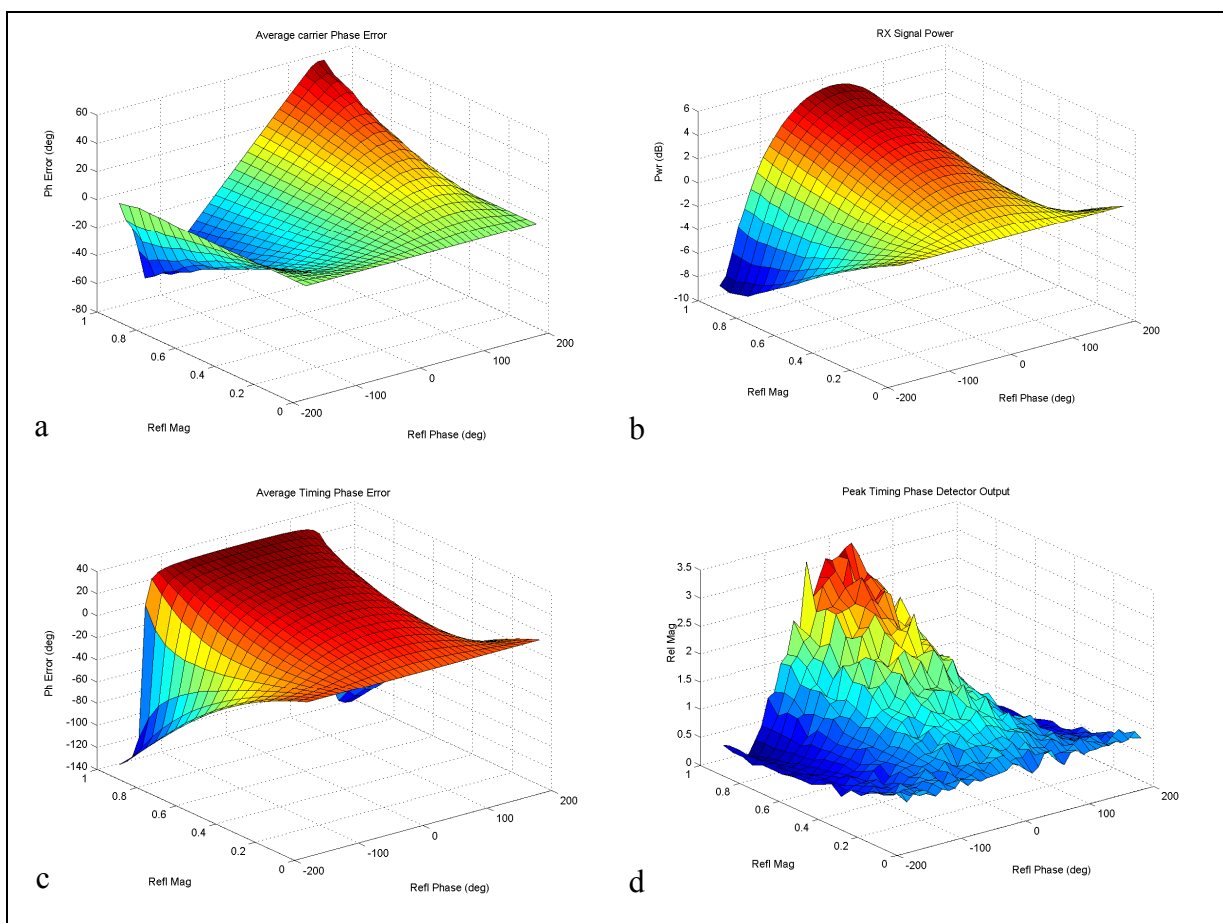


Figure A.5 Delay 0.2 symbols. a) average carrier phase error; b) received signal power; c) average timing phase error; d) peak timing phase detector output.

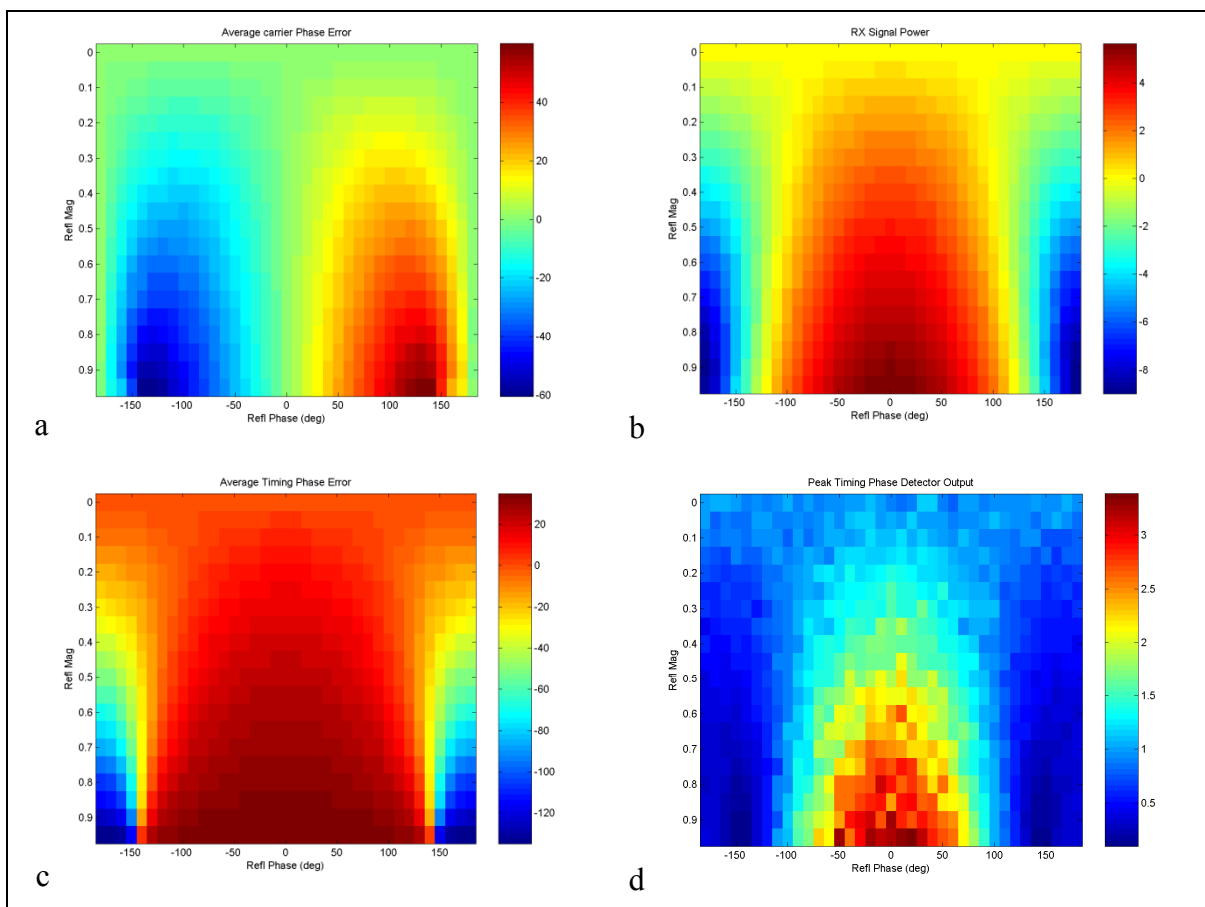


Figure A.6 Delay 0.2 symbols. a) average carrier phase error; b) received signal power; c) average timing phase error; d) peak timing phase detector output.

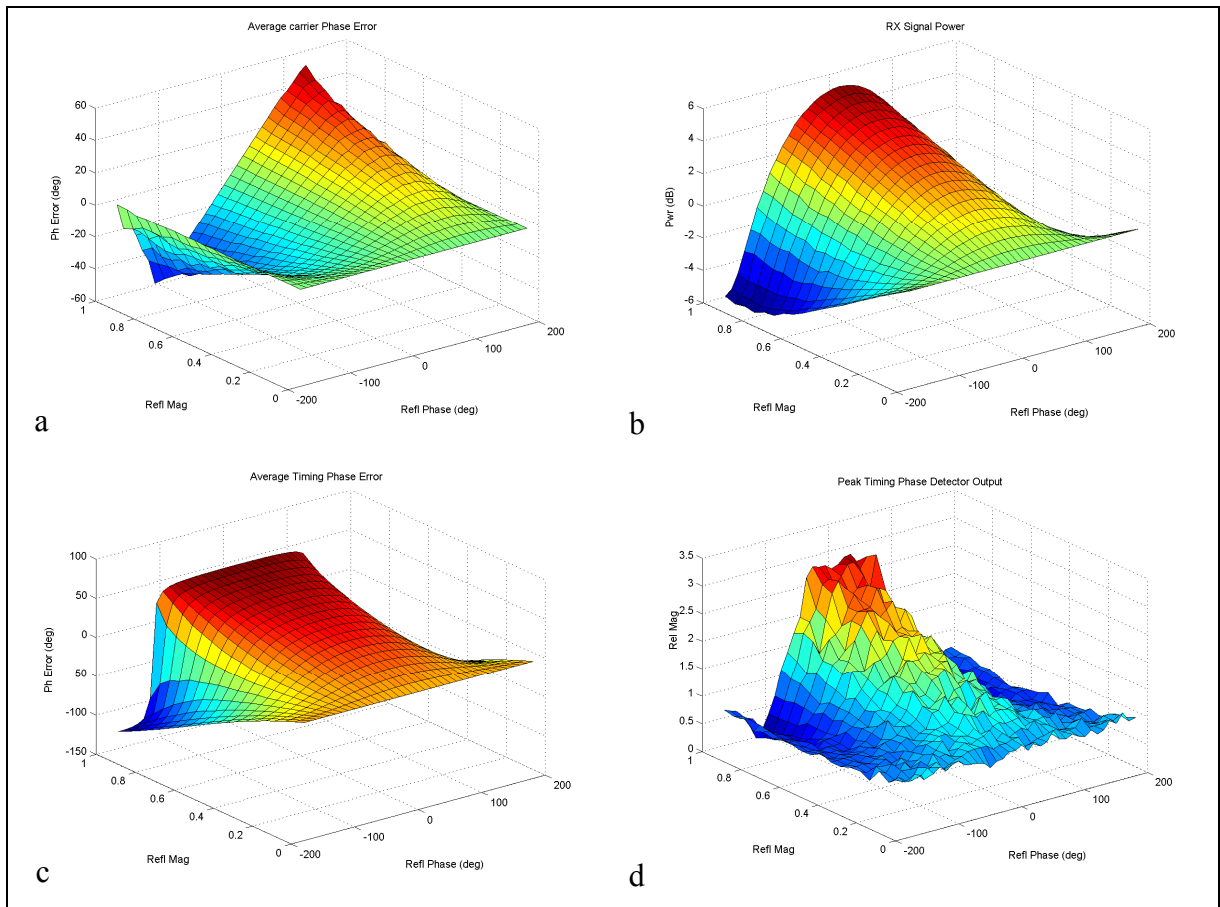


Figure A.7 Delay 0.3 symbols. a) average carrier phase error; b) received signal power; c) average timing phase error; d) peak timing phase detector output.

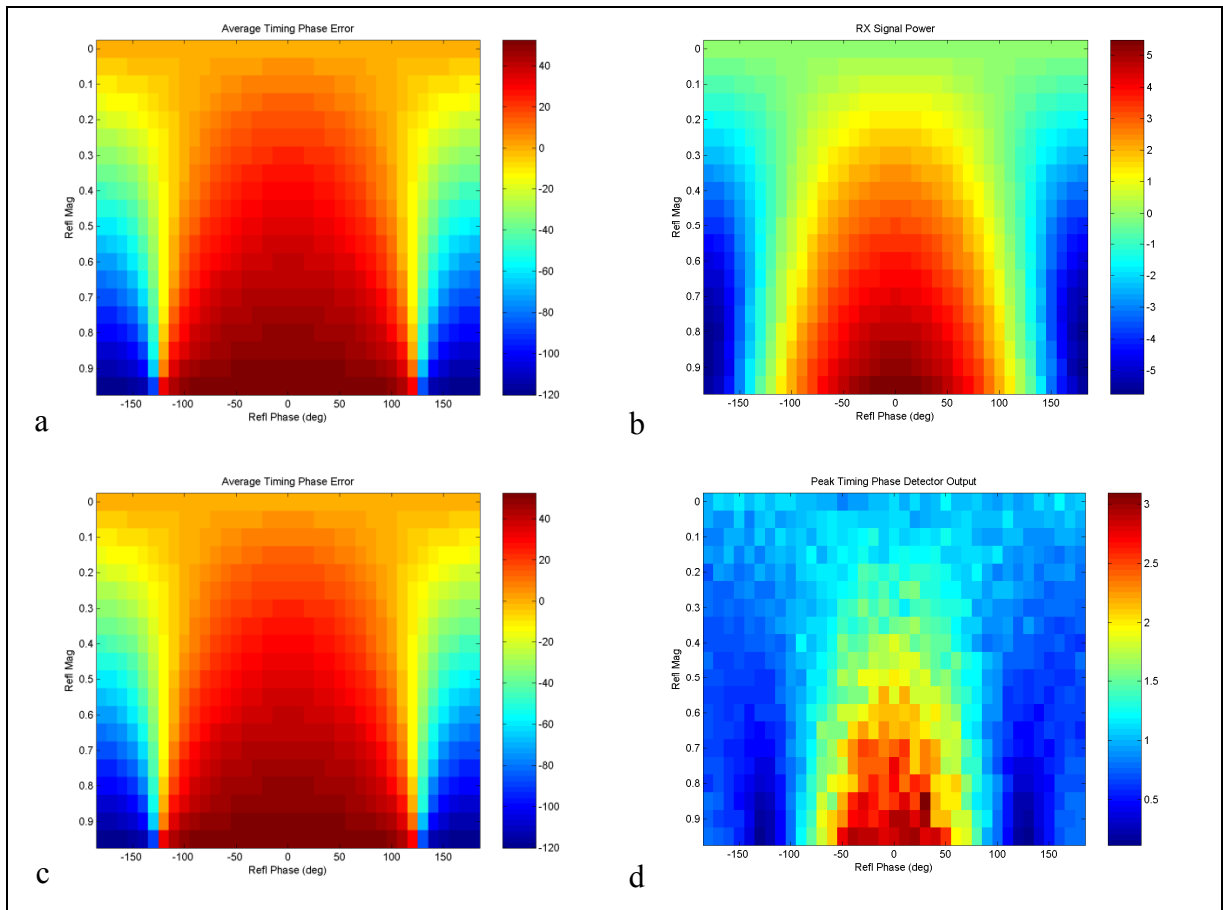


Figure A.8 Delay 0.3 symbols. a) average carrier phase error; b) received signal power; c) average timing phase error; d) peak timing phase detector output.

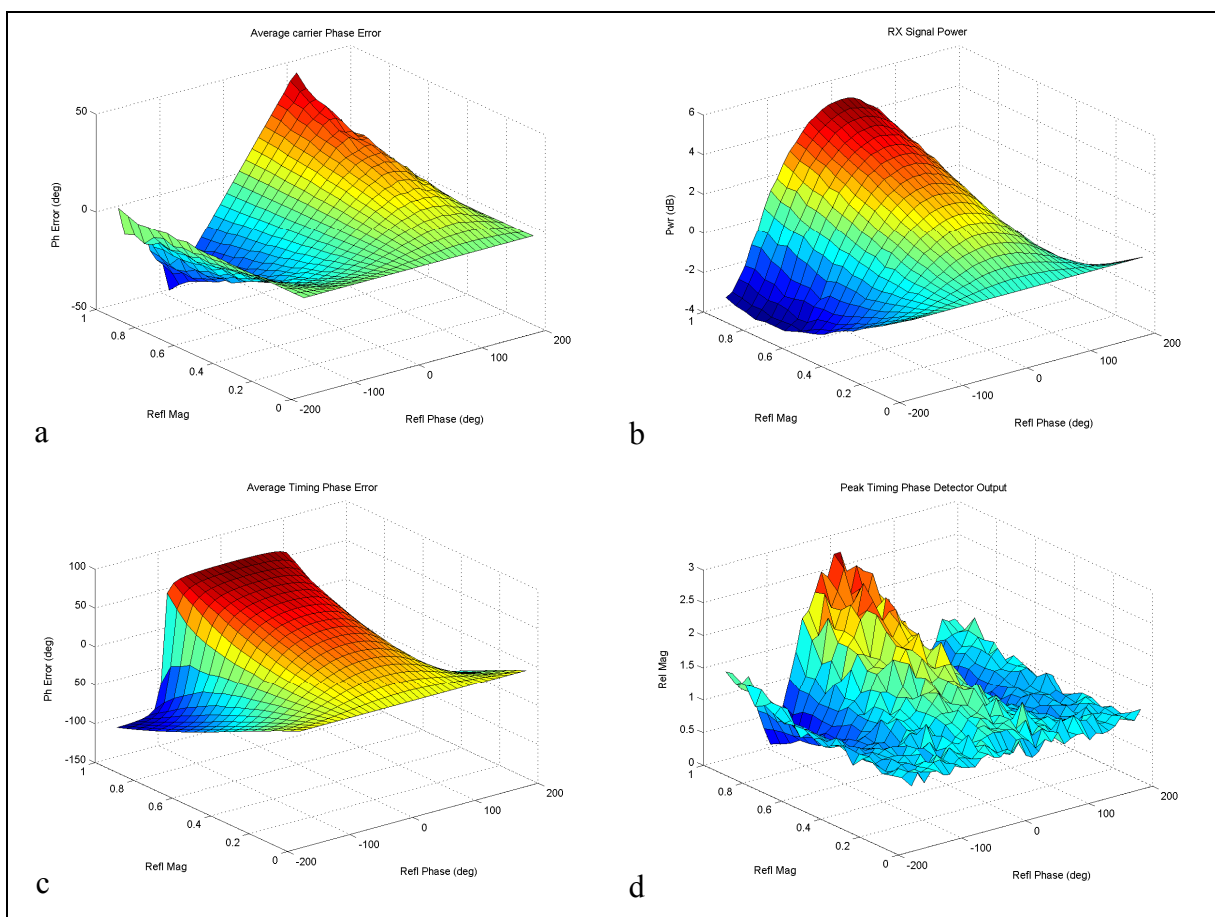


Figure A.9 Delay 0.4 symbols. a) average carrier phase error; b) received signal power; c) average timing phase error; d) peak timing phase detector output.

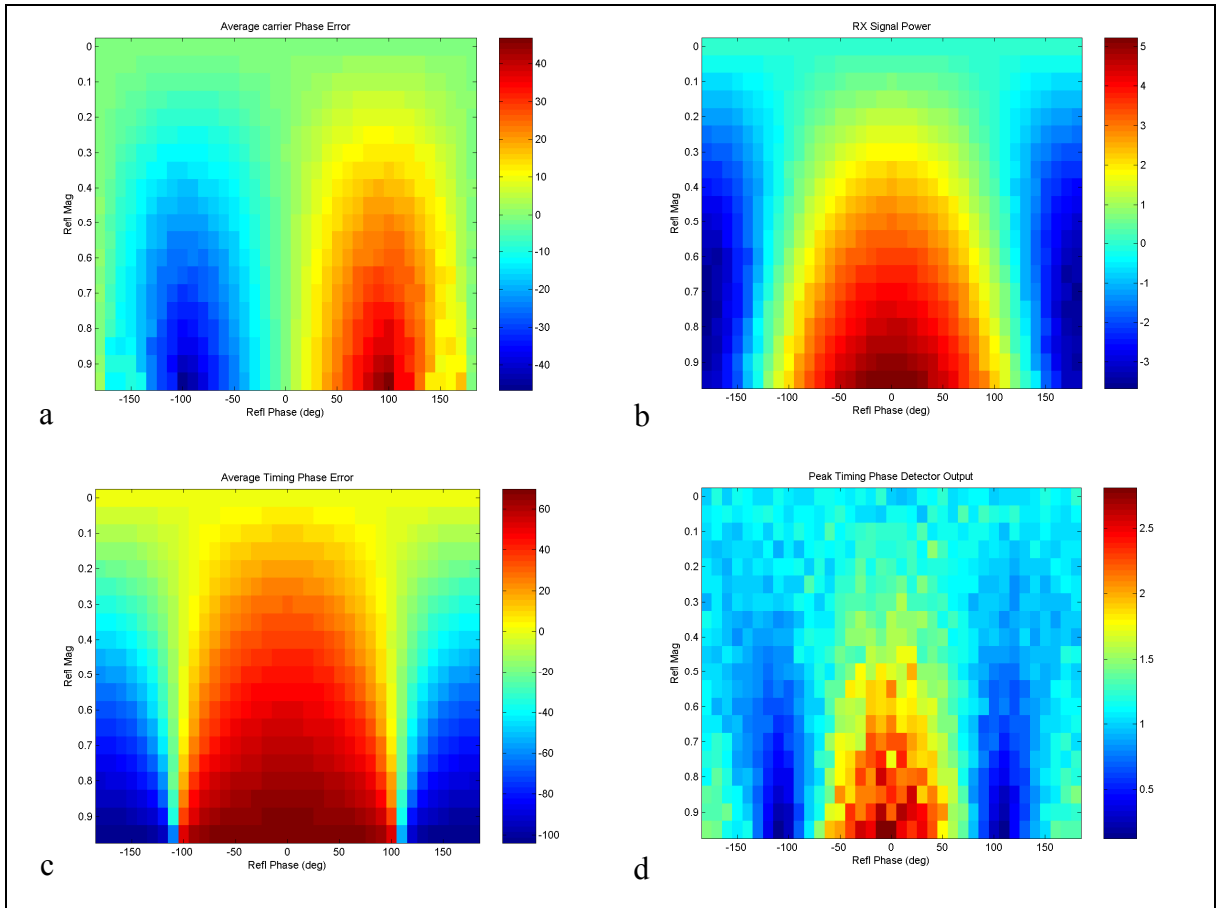


Figure A.10 Delay 0.4 symbols. a) average carrier phase error; b) received signal power; c) average timing phase error; d) peak timing phase detector output.

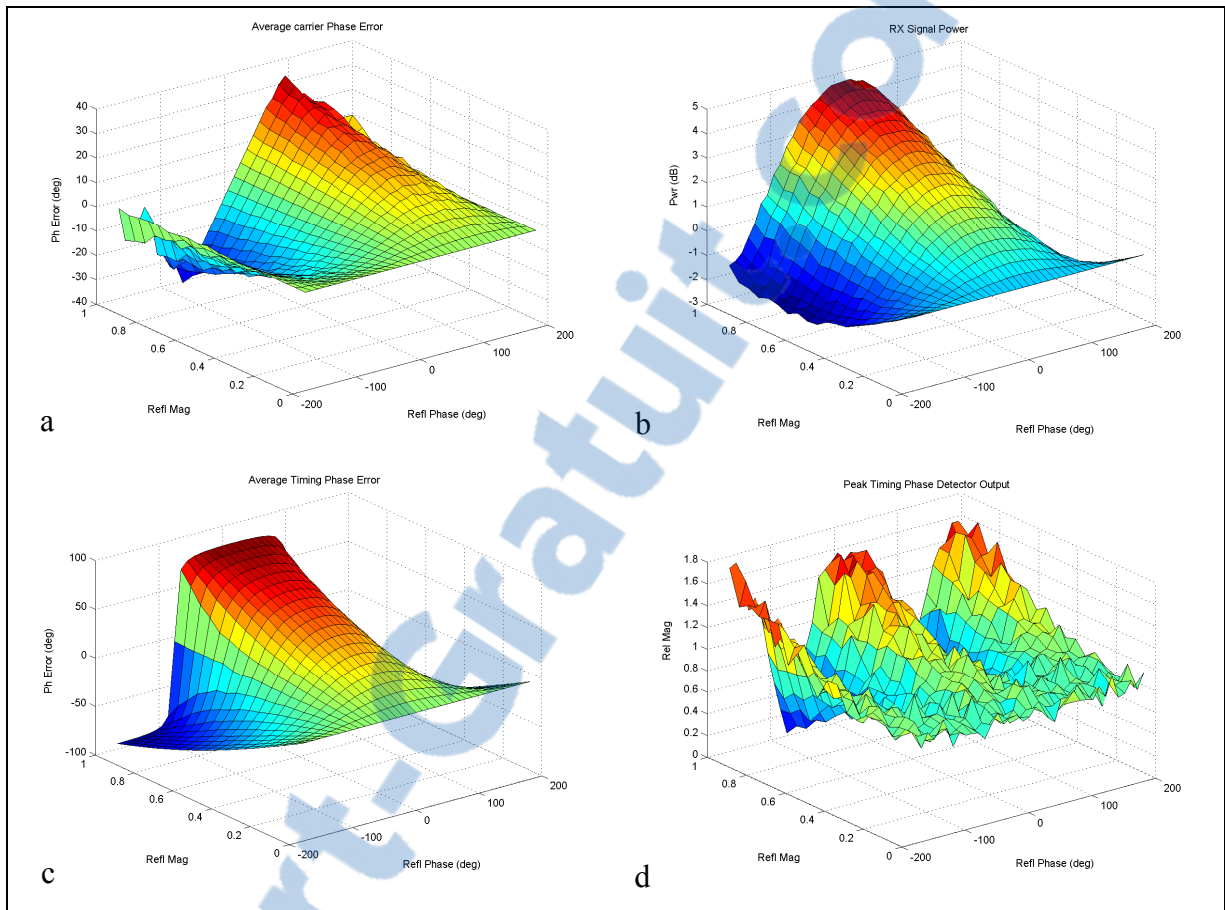


Figure A.11 Delay 0.5 symbols. a) average carrier phase error; b) received signal power; c) average timing phase error; d) peak timing phase detector output.

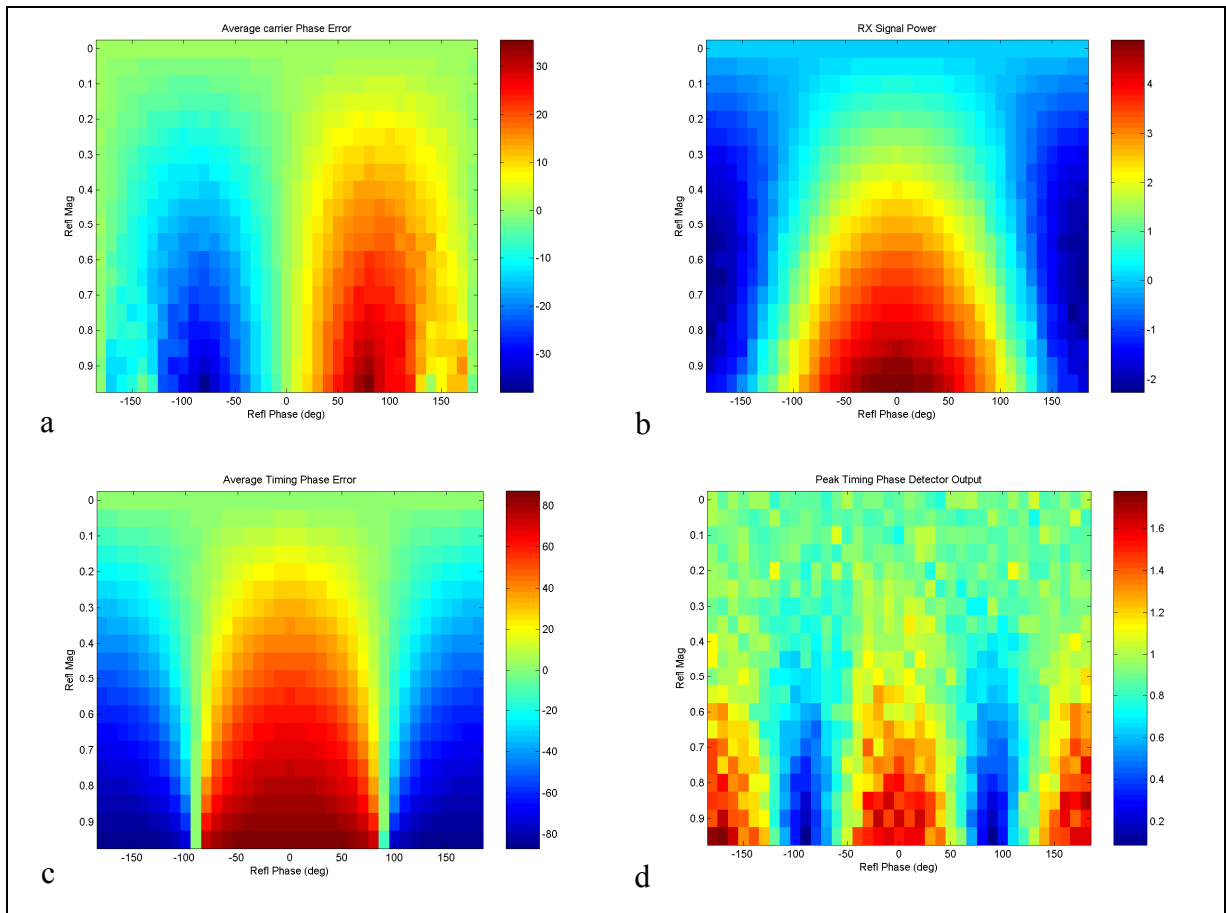


Figure A.12 Delay 0.5 symbols. a) average carrier phase error; b) received signal power; c) average timing phase error; d) peak timing phase detector output.

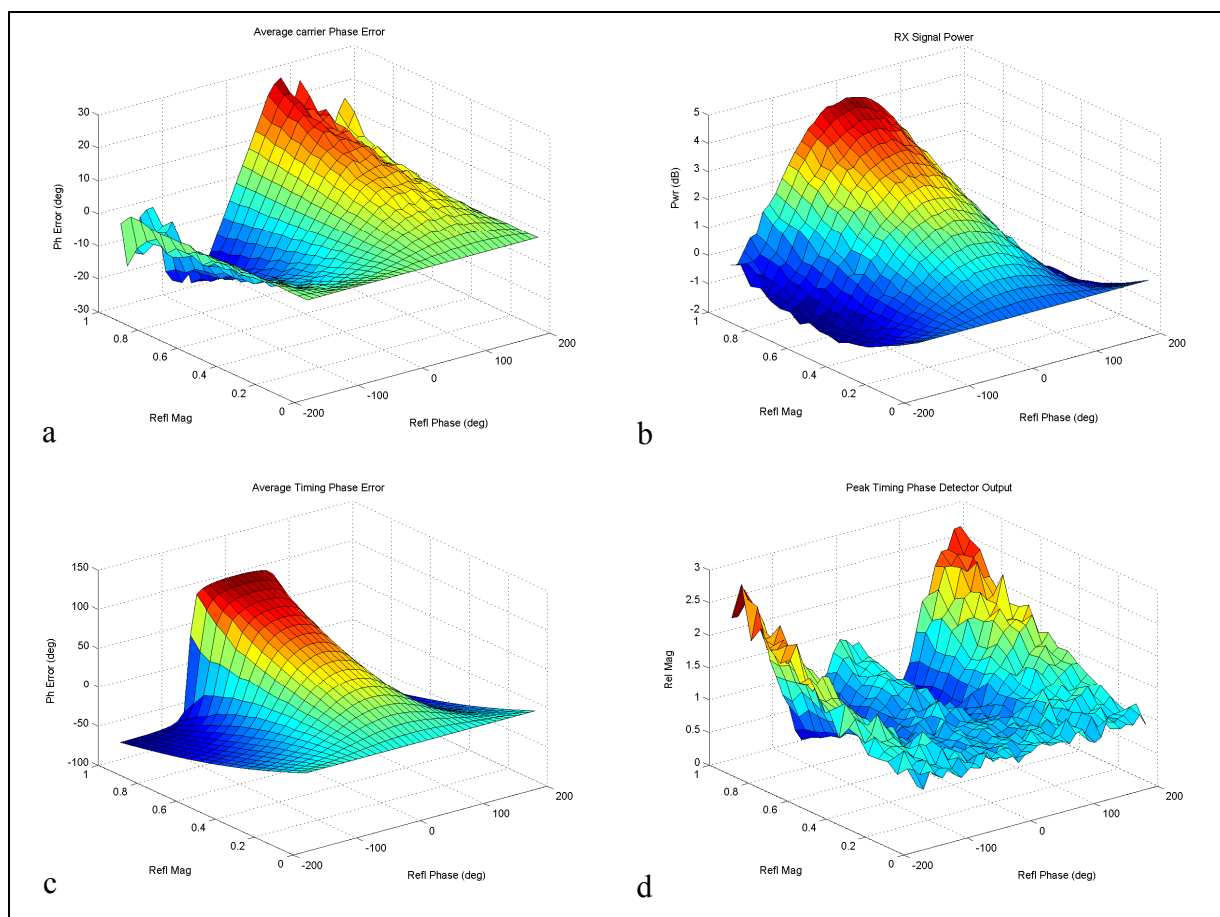


Figure A.13 Delay 0.6 symbols. a) average carrier phase error; b) received signal power; c) average timing phase error; d) peak timing phase detector output.



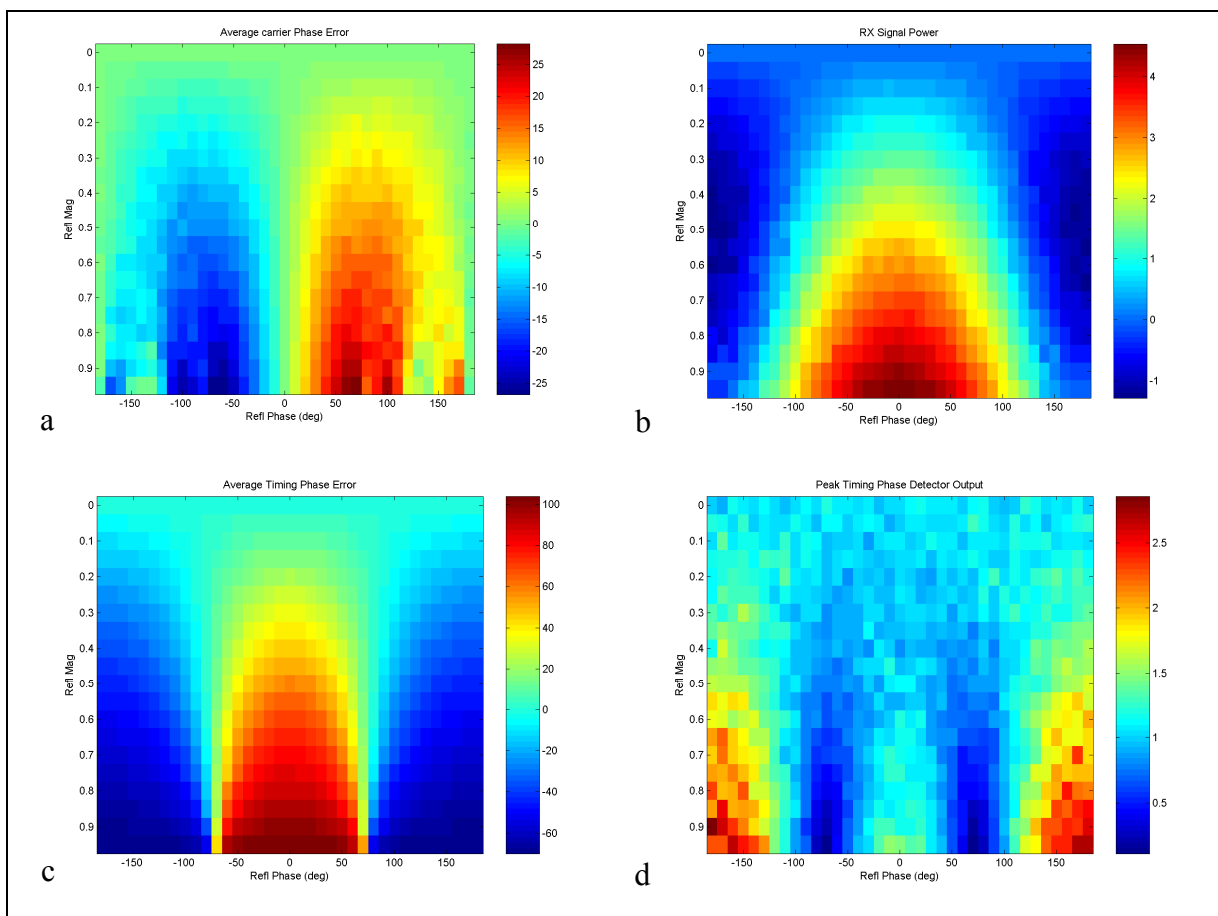


Figure A.14 Delay 0.6 symbols. a) average carrier phase error; b) received signal power; c) average timing phase error; d) peak timing phase detector output.

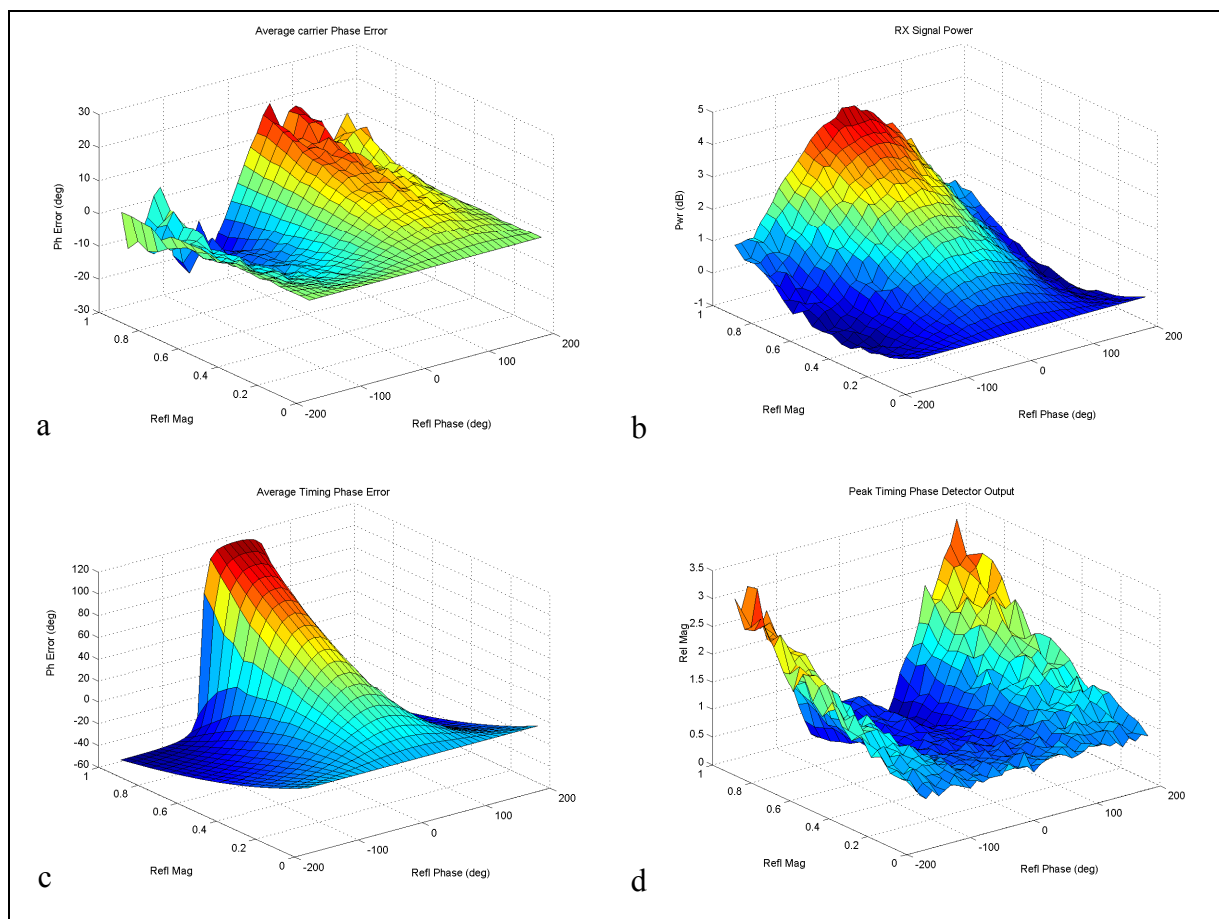


Figure A.15 Delay 0.7 symbols. a) average carrier phase error; b) received signal power; c) average timing phase error; d) peak timing phase detector output.

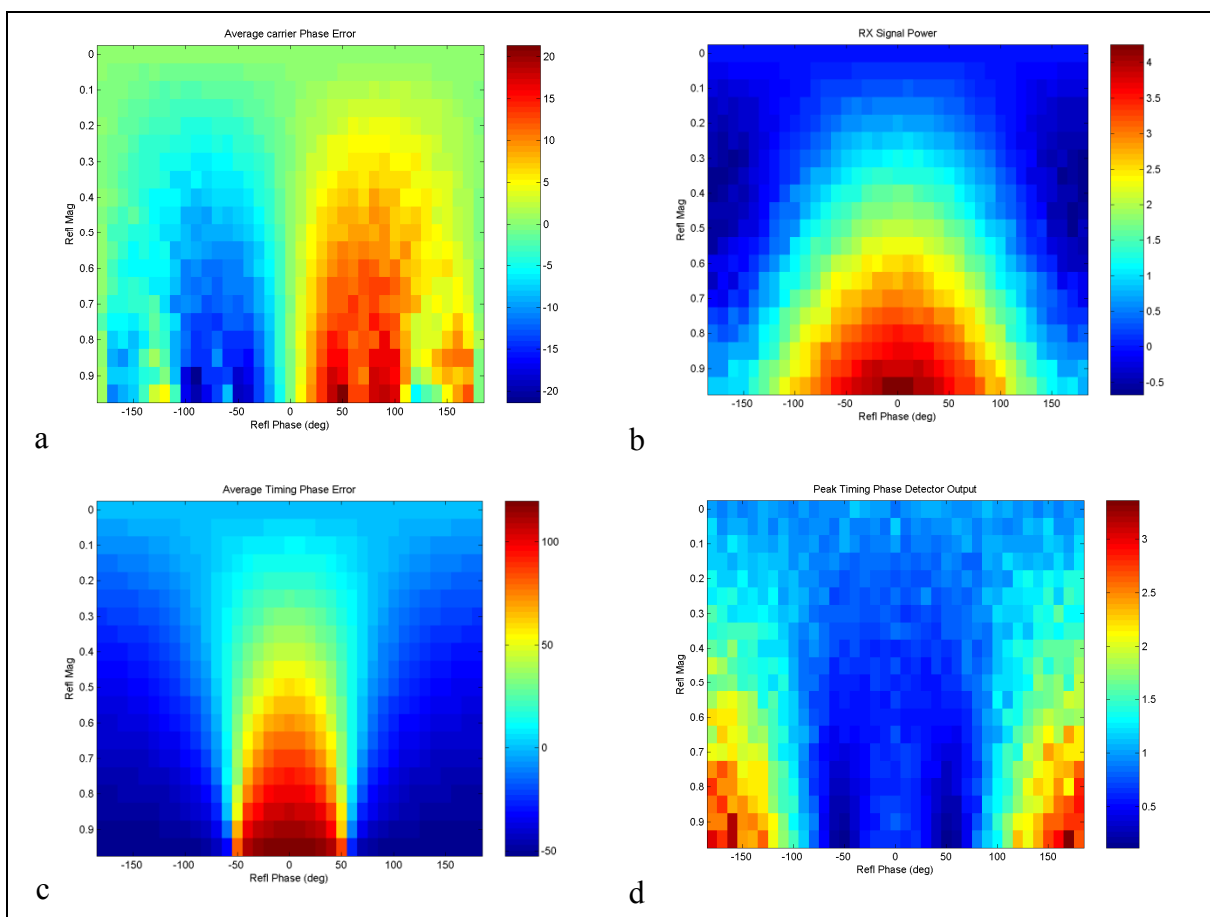


Figure A.16 Delay 0.7 symbols. a) average carrier phase error; b) received signal power; c) average timing phase error; d) peak timing phase detector output.

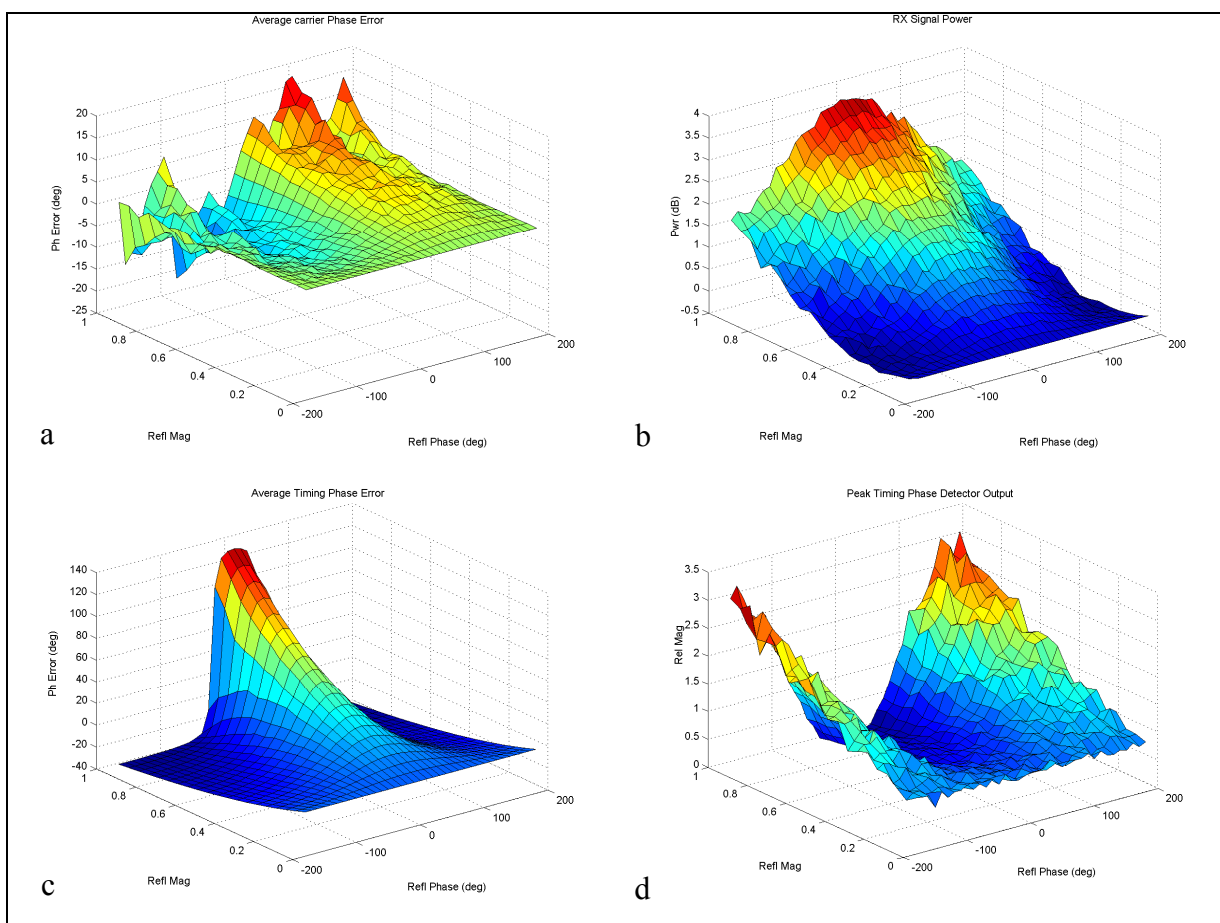


Figure A.17 Delay 0.8 symbols. a) average carrier phase error; b) received signal power; c) average timing phase error; d) peak timing phase detector output.

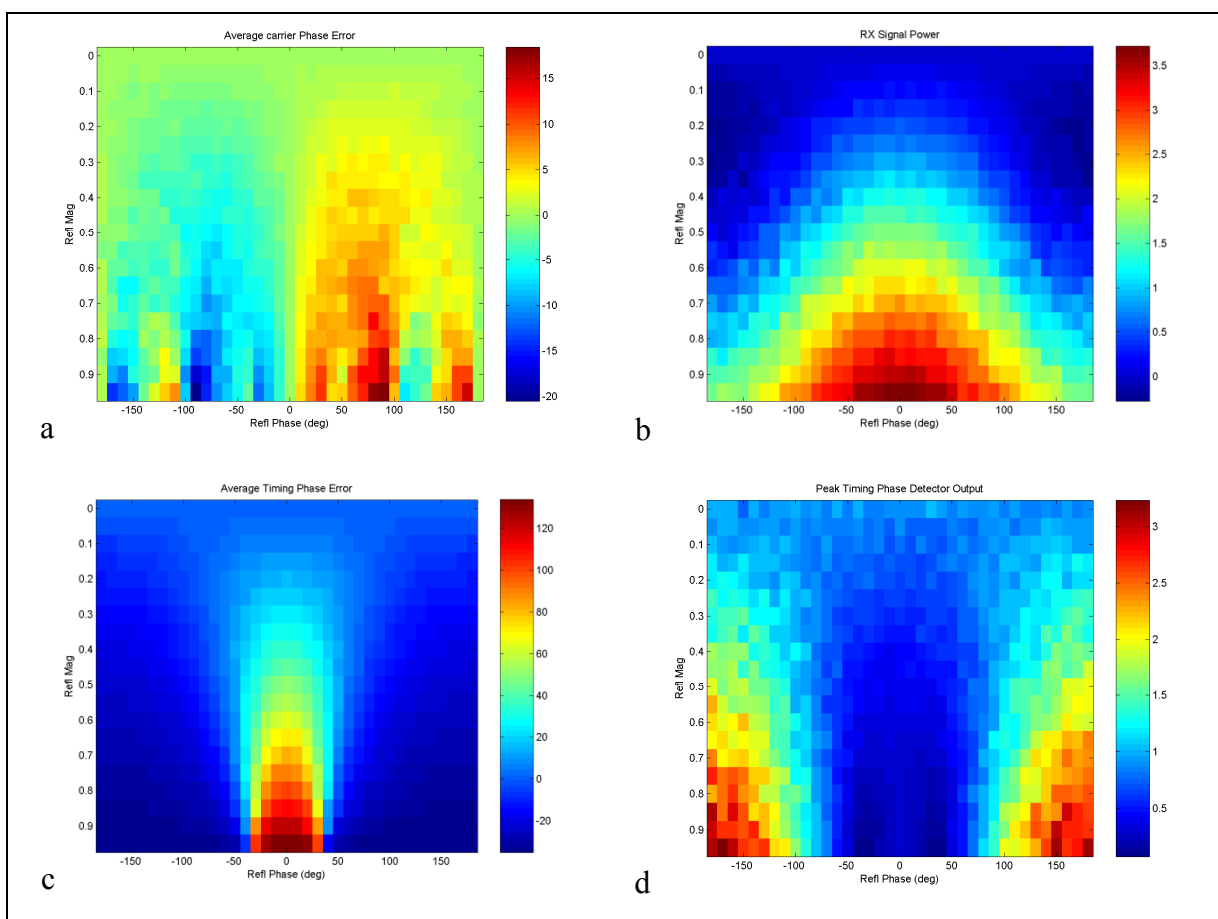


Figure A.18 Delay 0.8 symbols. a) average carrier phase error; b) received signal power; c) average timing phase error; d) peak timing phase detector output.

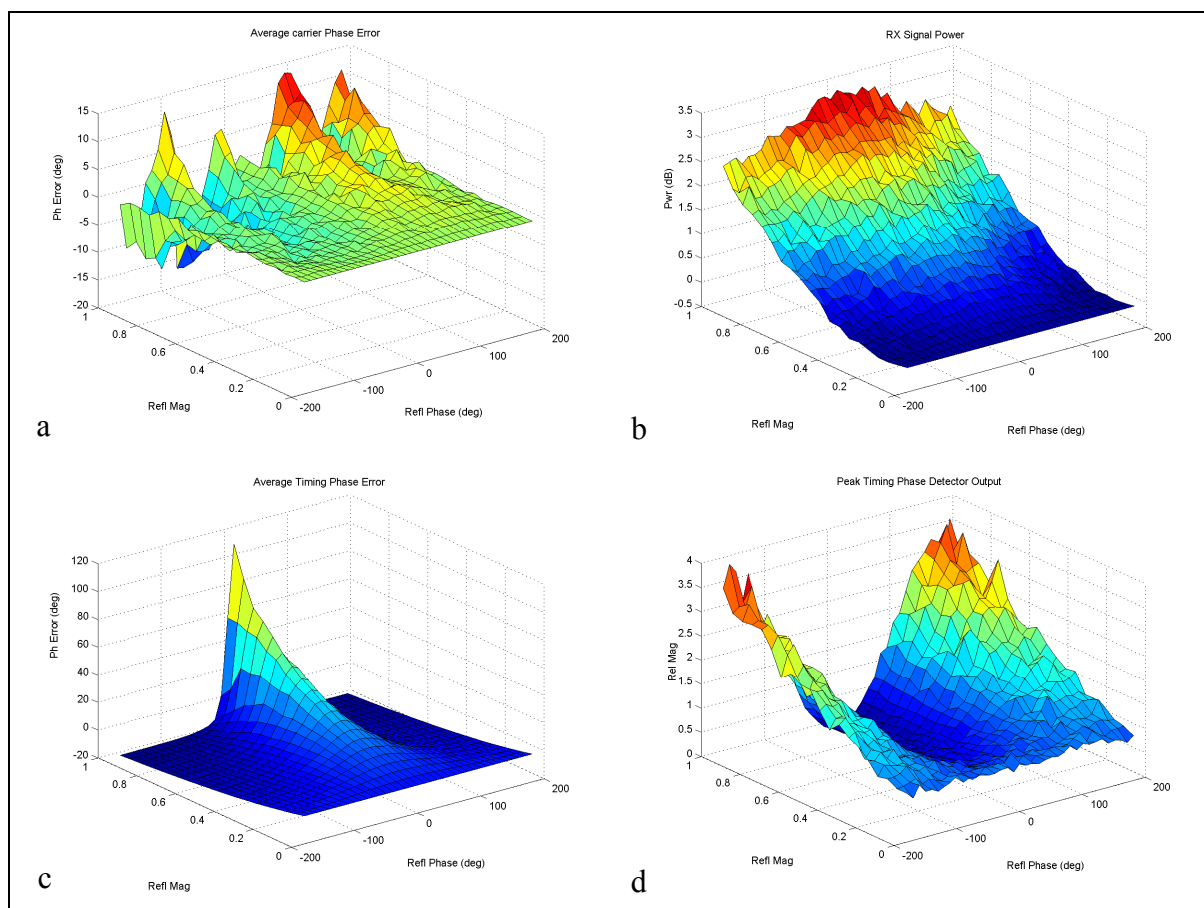


Figure A.19 Delay 0.9 symbols. a) average carrier phase error; b) received signal power; c) average timing phase error; d) peak timing phase detector output.

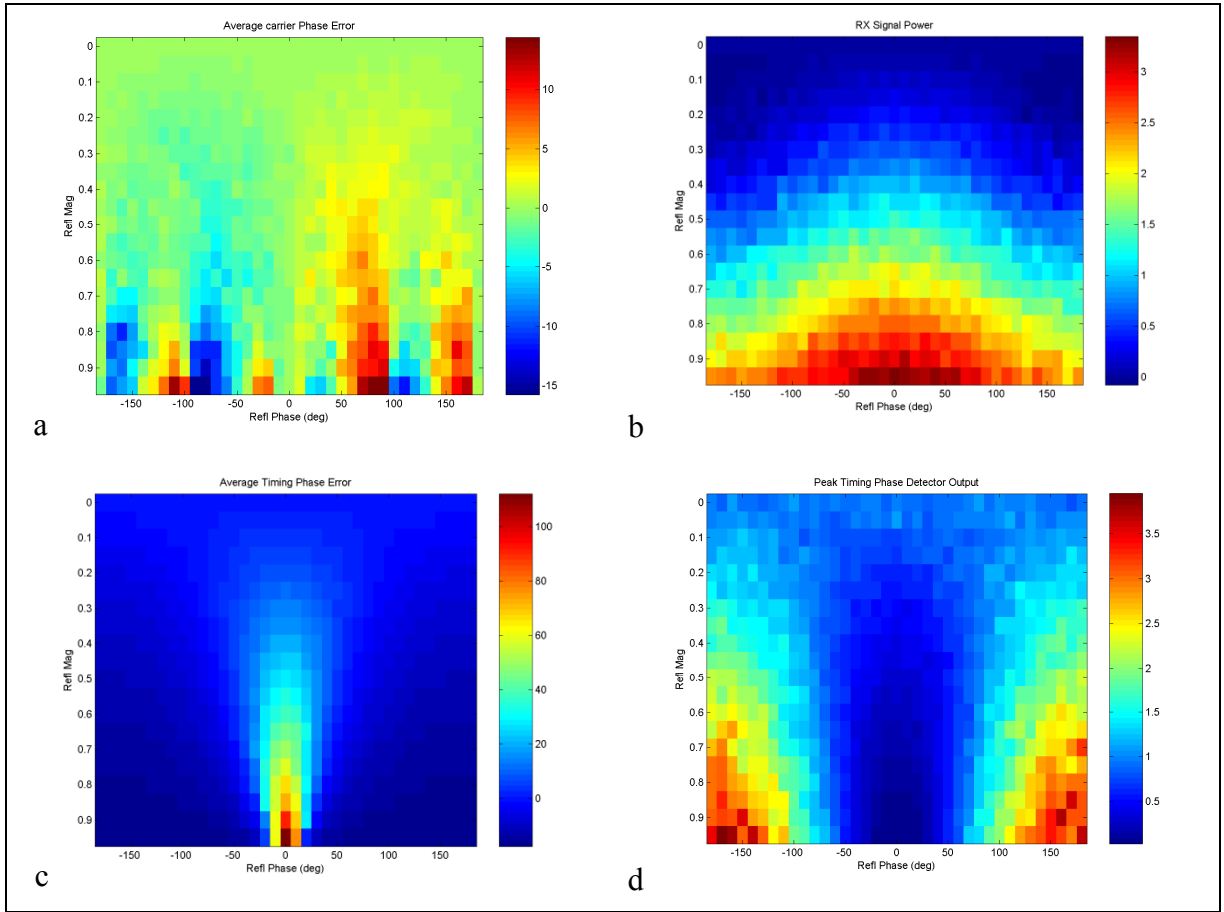


Figure A.20 Delay 0.9 symbols. a) average carrier phase error; b) received signal power; c) average timing phase error; d) peak timing phase detector output.

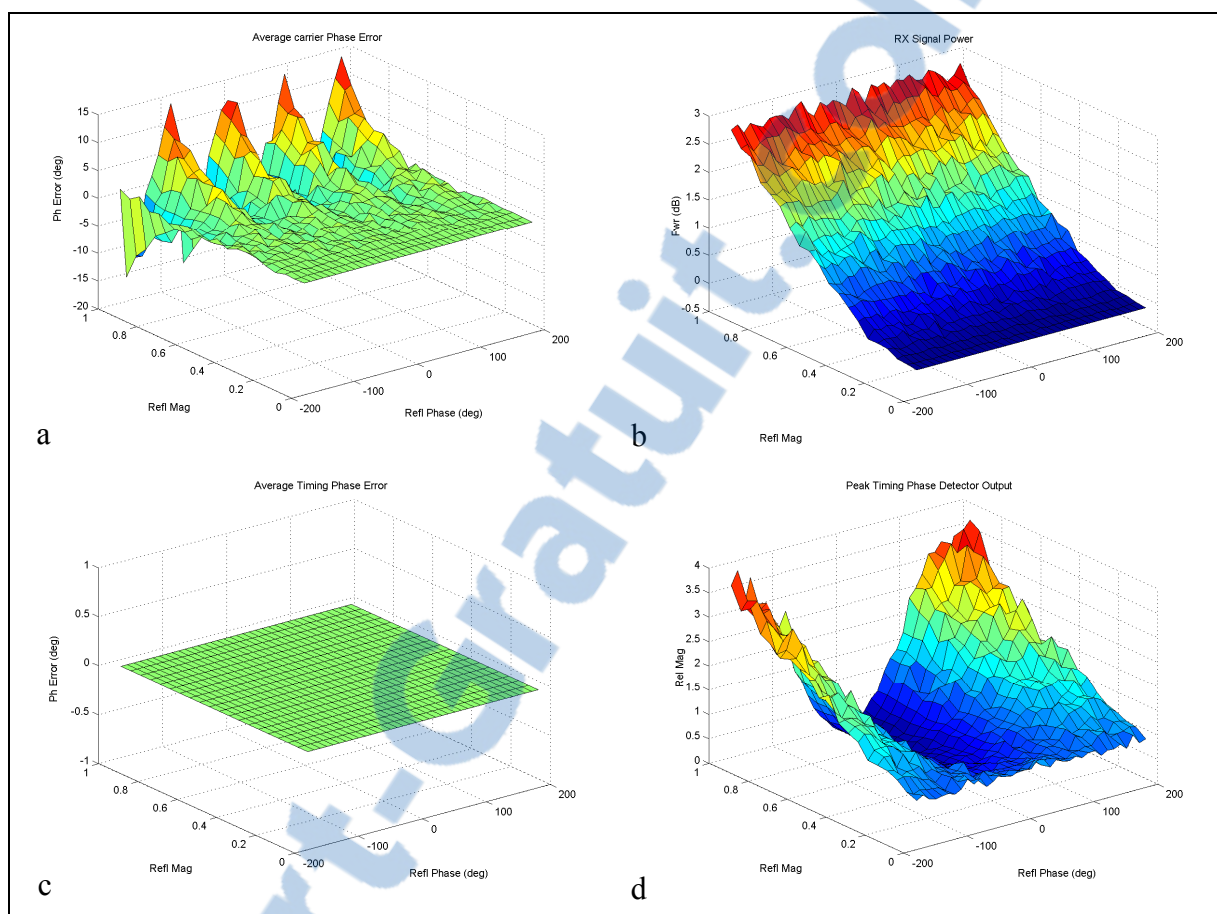


Figure A.21 Delay 1.0 symbols. a) average carrier phase error; b) received signal power; c) average timing phase error; d) peak timing phase detector output.

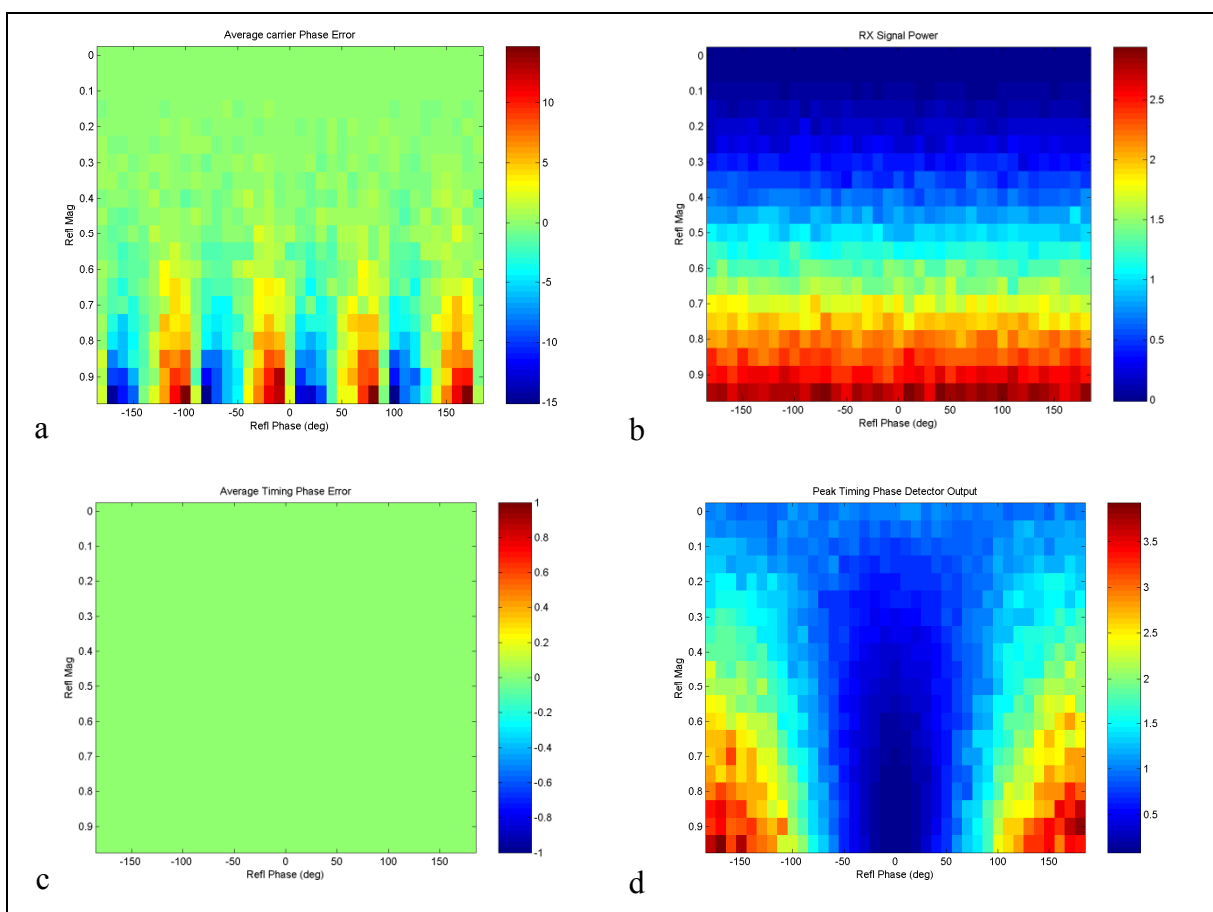


Figure A.22 Delay 1.0 symbols. a) average carrier phase error; b) received signal power; c) average timing phase error; d) peak timing phase detector output.

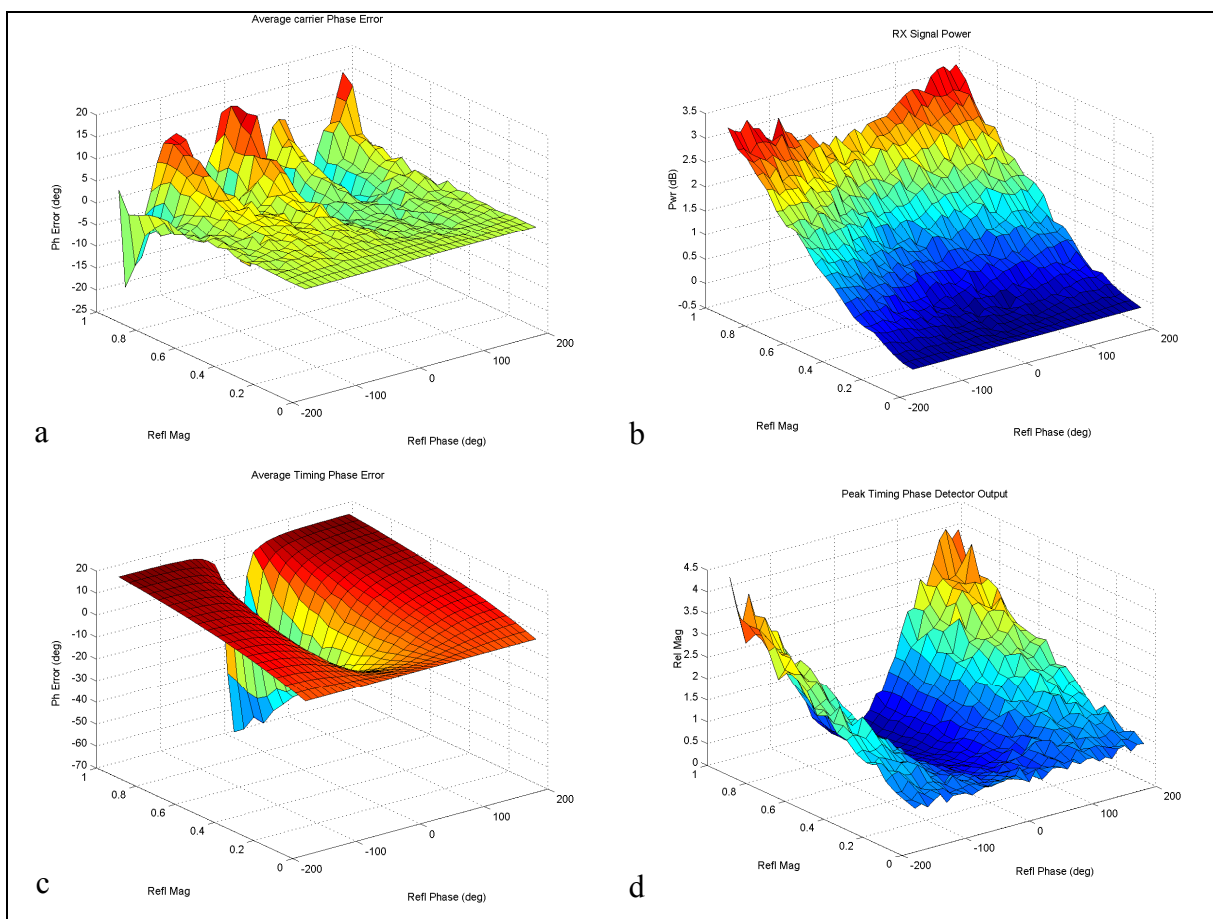


Figure A.23 Delay 1.1 symbols. a) average carrier phase error; b) received signal power; c) average timing phase error; d) peak timing phase detector output.



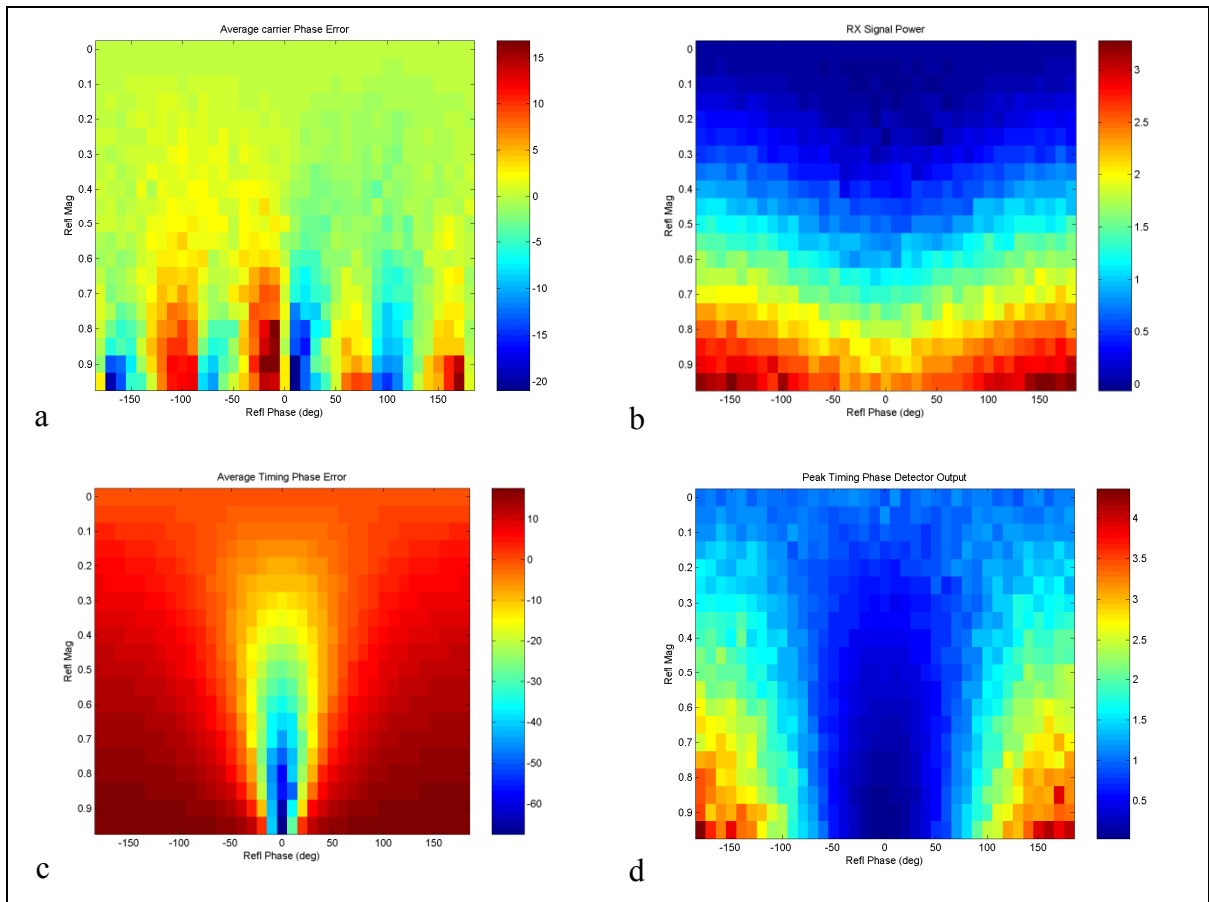


Figure A.24 Delay 1.1 symbols. a) average carrier phase error; b) received signal power; c) average timing phase error; d) peak timing phase detector output.

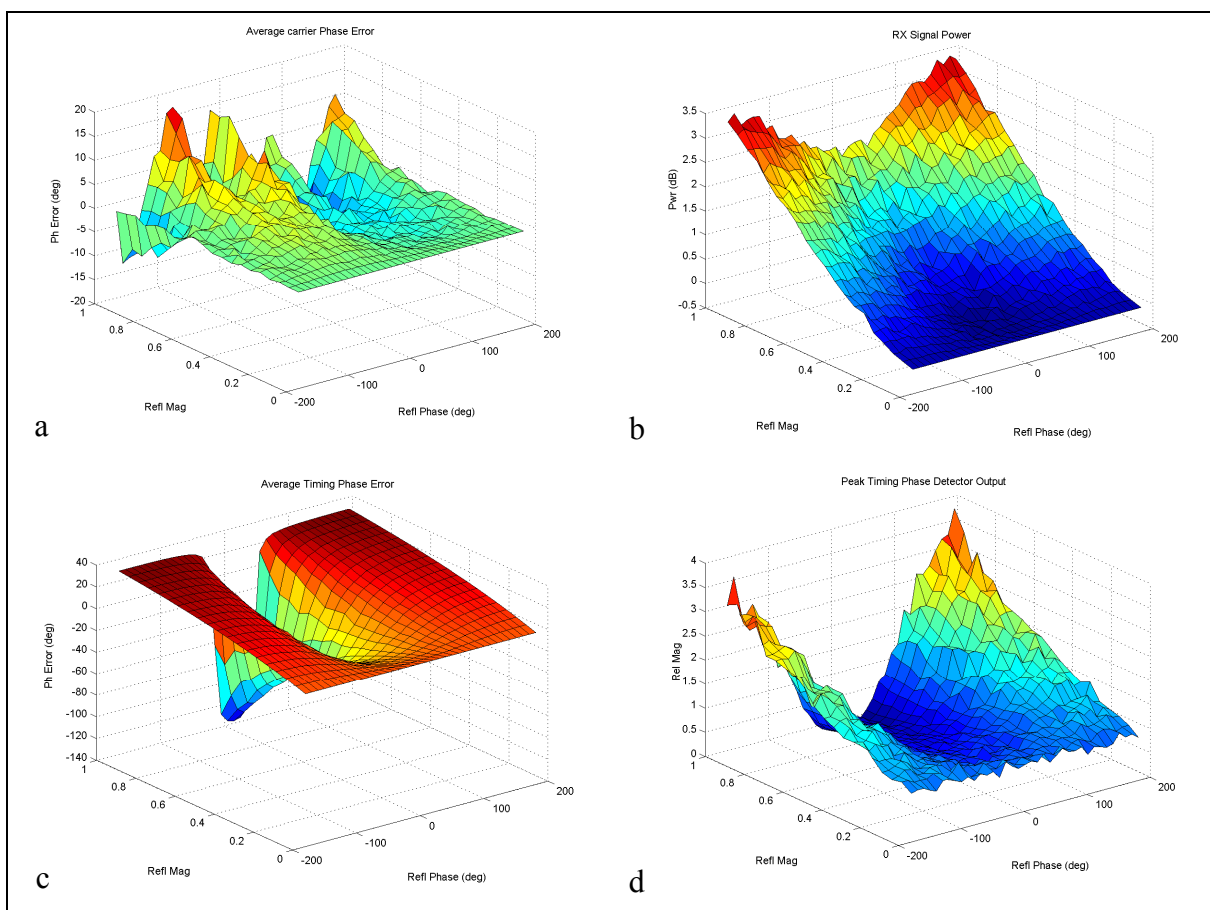


Figure A.25 Delay 1.2 symbols. a) average carrier phase error; b) received signal power; c) average timing phase error; d) peak timing phase detector output.

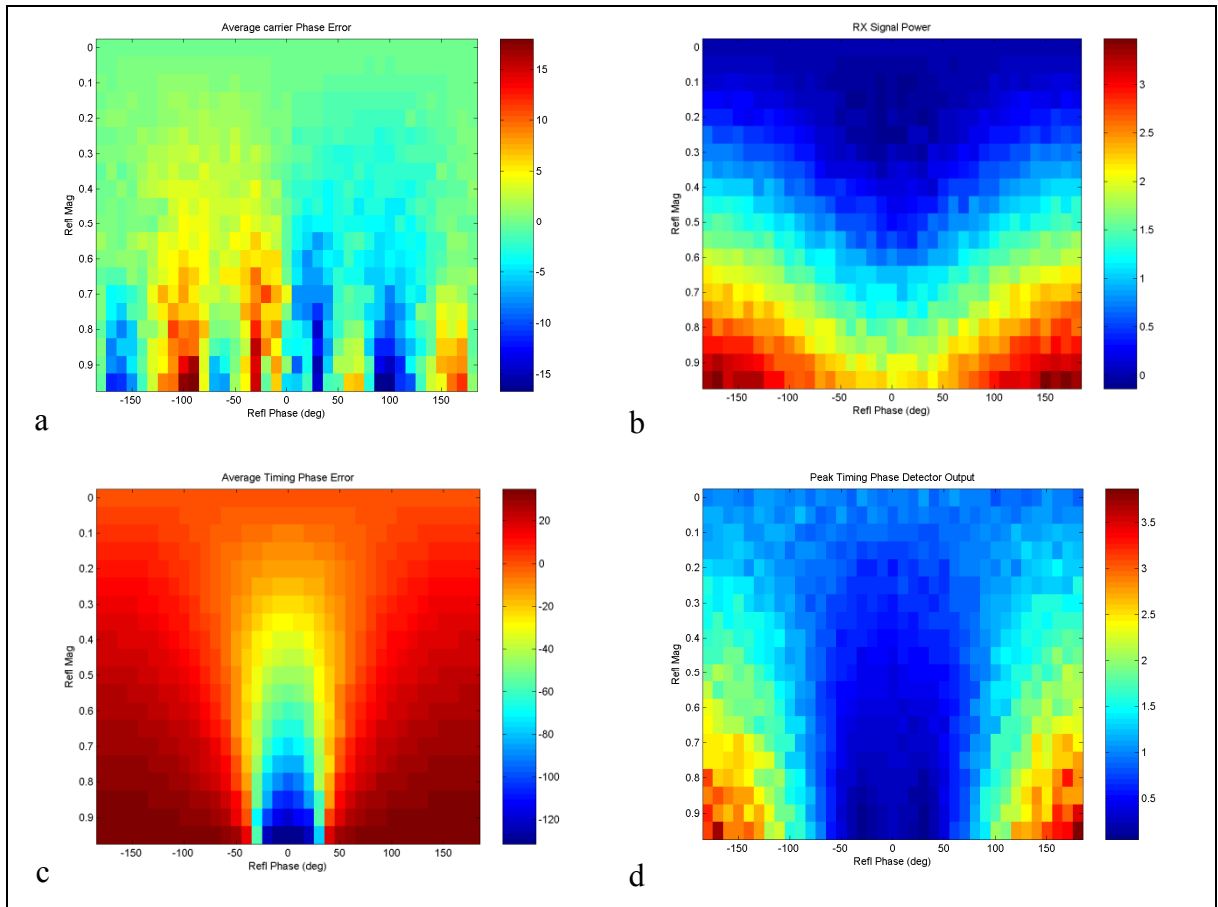


Figure A.26 Delay 1.2 symbols. a) average carrier phase error; b) received signal power; c) average timing phase error; d) peak timing phase detector output.

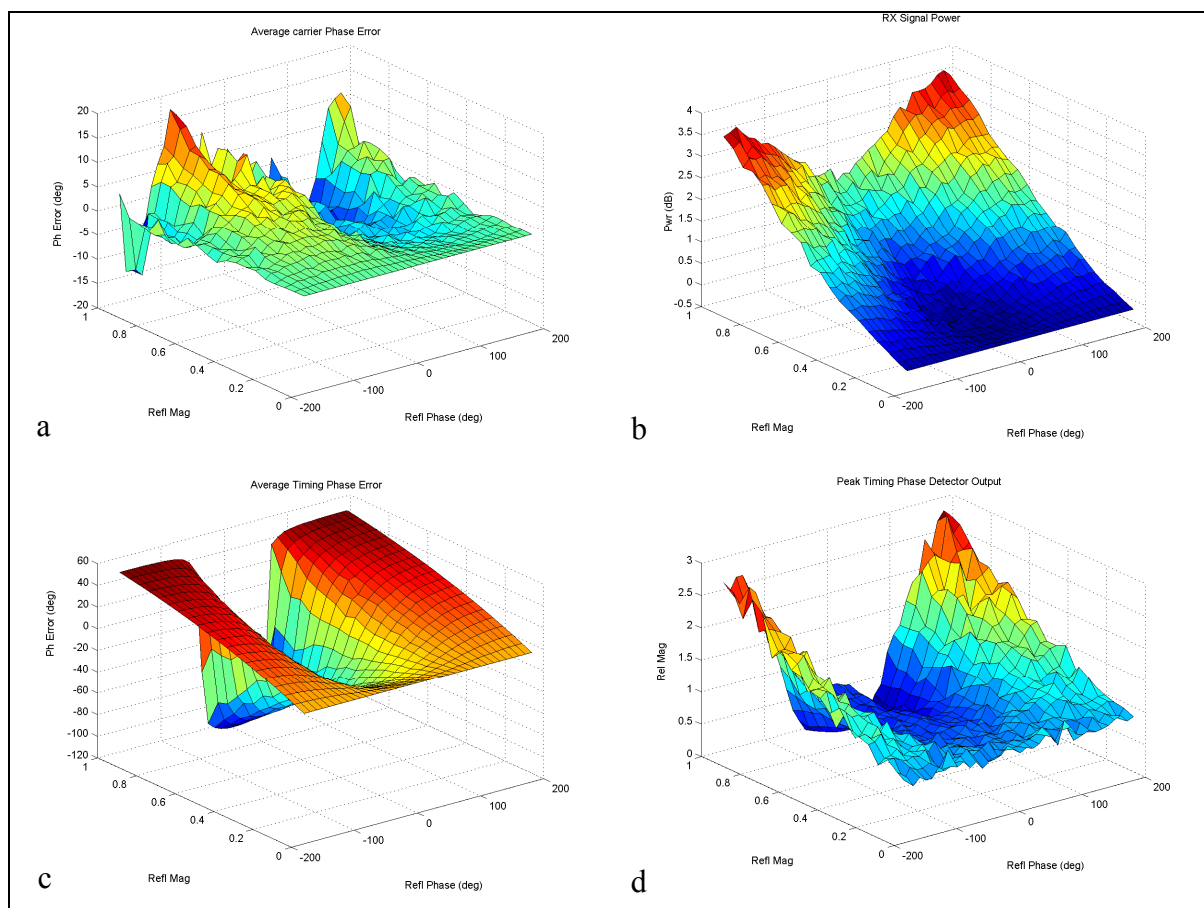


Figure A.27 Delay 1.3 symbols. a) average carrier phase error; b) received signal power; c) average timing phase error; d) peak timing phase detector output.

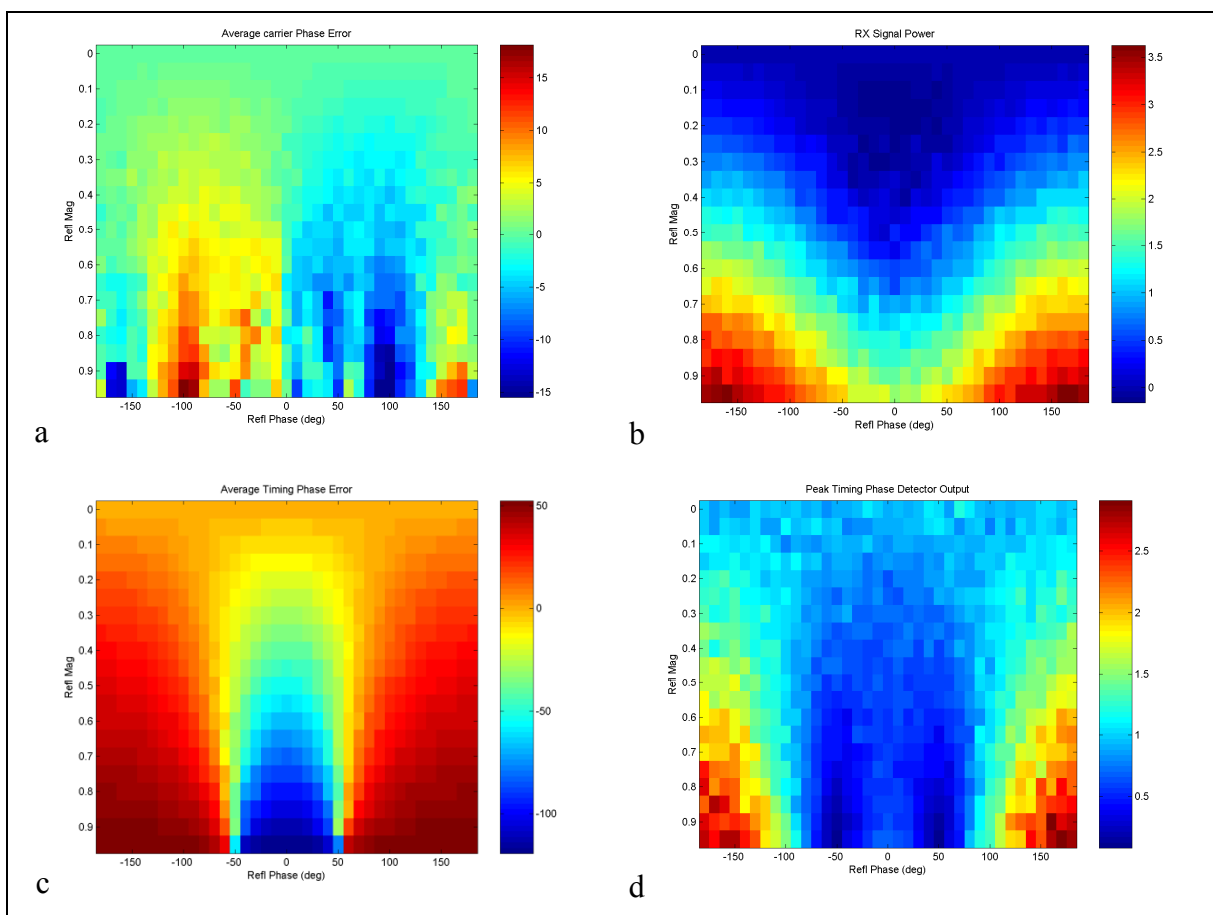


Figure A.28 Delay 1.3 symbols. a) average carrier phase error; b) received signal power; c) average timing phase error; d) peak timing phase detector output.

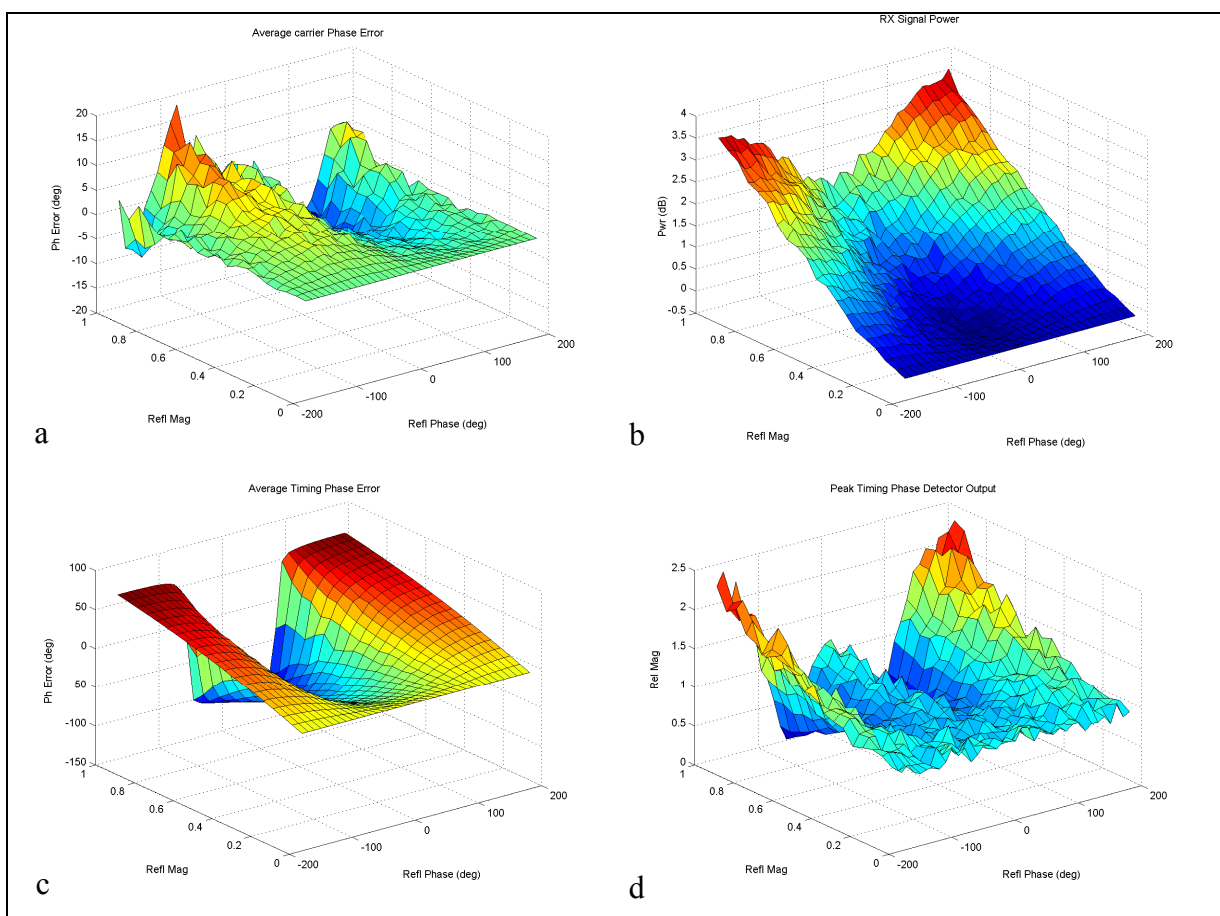


Figure A.29 Delay 1.4 symbols. a) average carrier phase error; b) received signal power; c) average timing phase error; d) peak timing phase detector output.

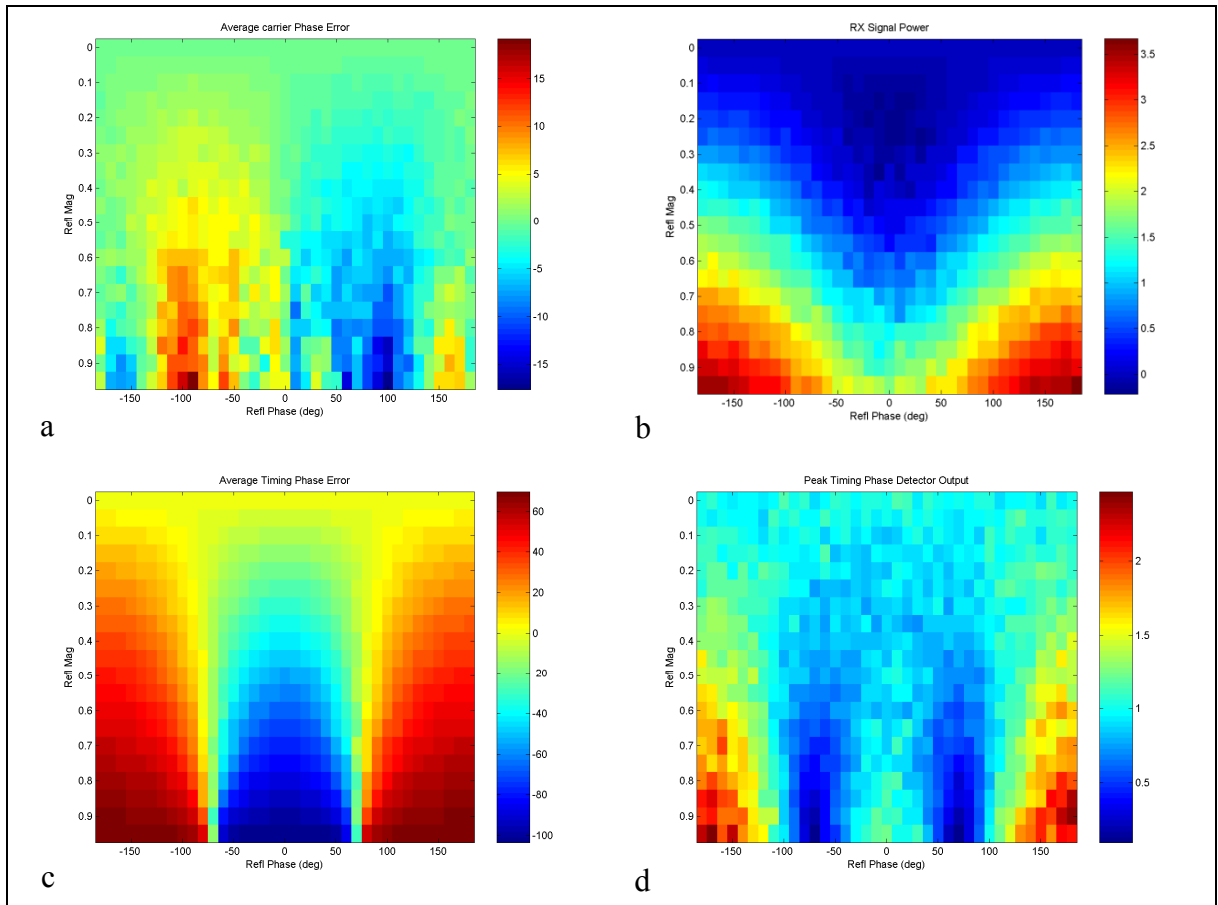


Figure A.30 Delay 1.4 symbols. a) average carrier phase error; b) received signal power; c) average timing phase error; d) peak timing phase detector output.

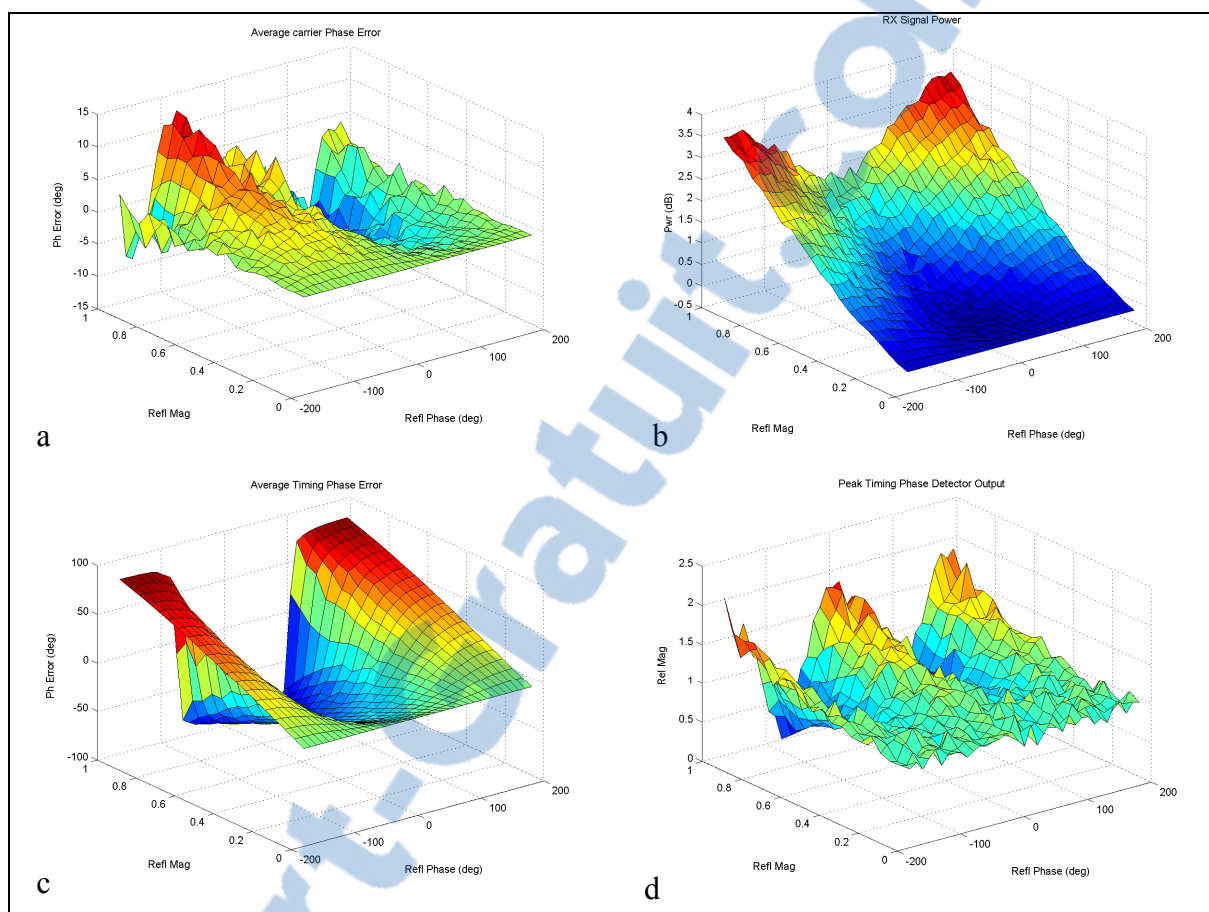


Figure A.31 Delay 1.5 symbols. a) average carrier phase error; b) received signal power; c) average timing phase error; d) peak timing phase detector output.

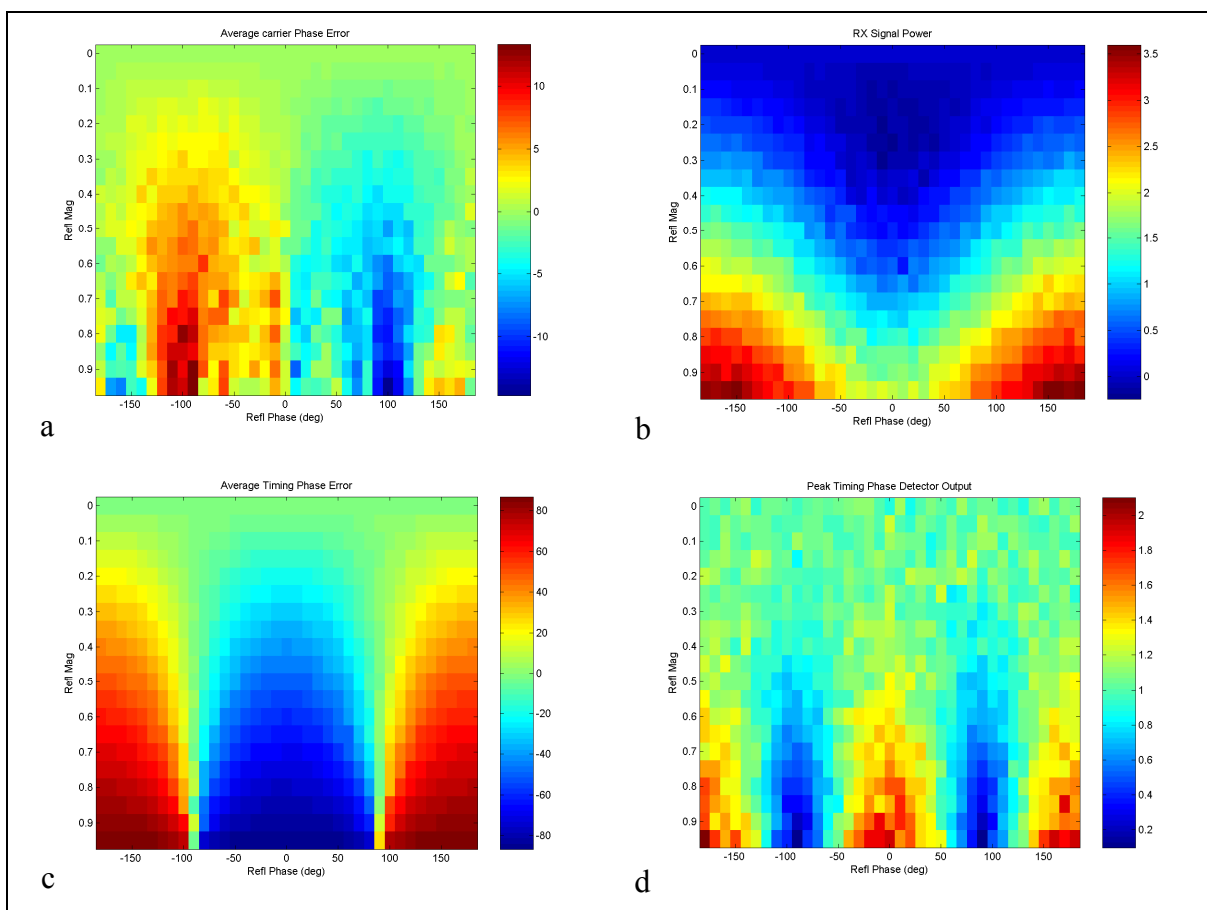


Figure A.32 Delay 1.5 symbols. a) average carrier phase error; b) received signal power; c) average timing phase error; d) peak timing phase detector output.

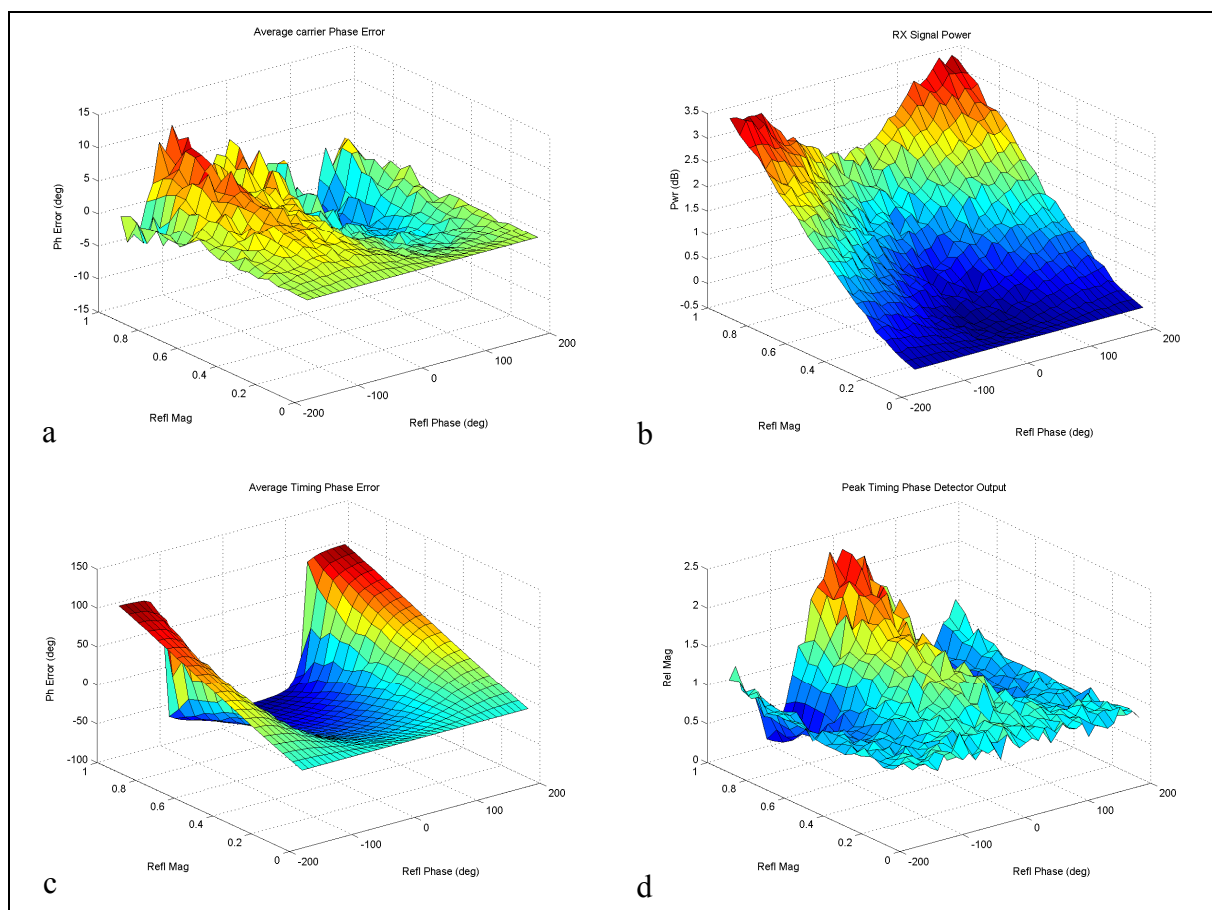


Figure A.33 Delay 1.6 symbols. a) average carrier phase error; b) received signal power; c) average timing phase error; d) peak timing phase detector output.



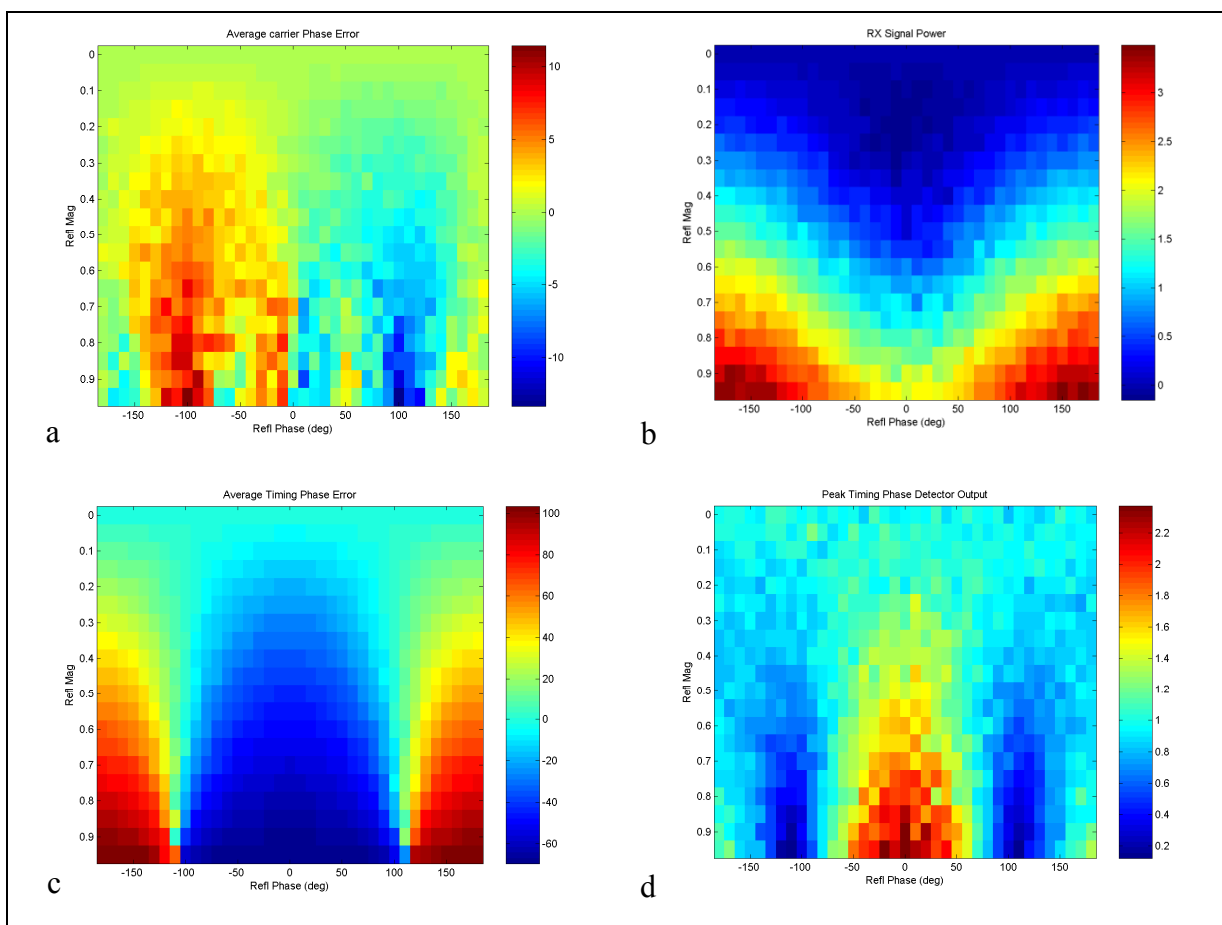


Figure A.34 Delay 1.6 symbols. a) average carrier phase error; b) received signal power; c) average timing phase error; d) peak timing phase detector output.

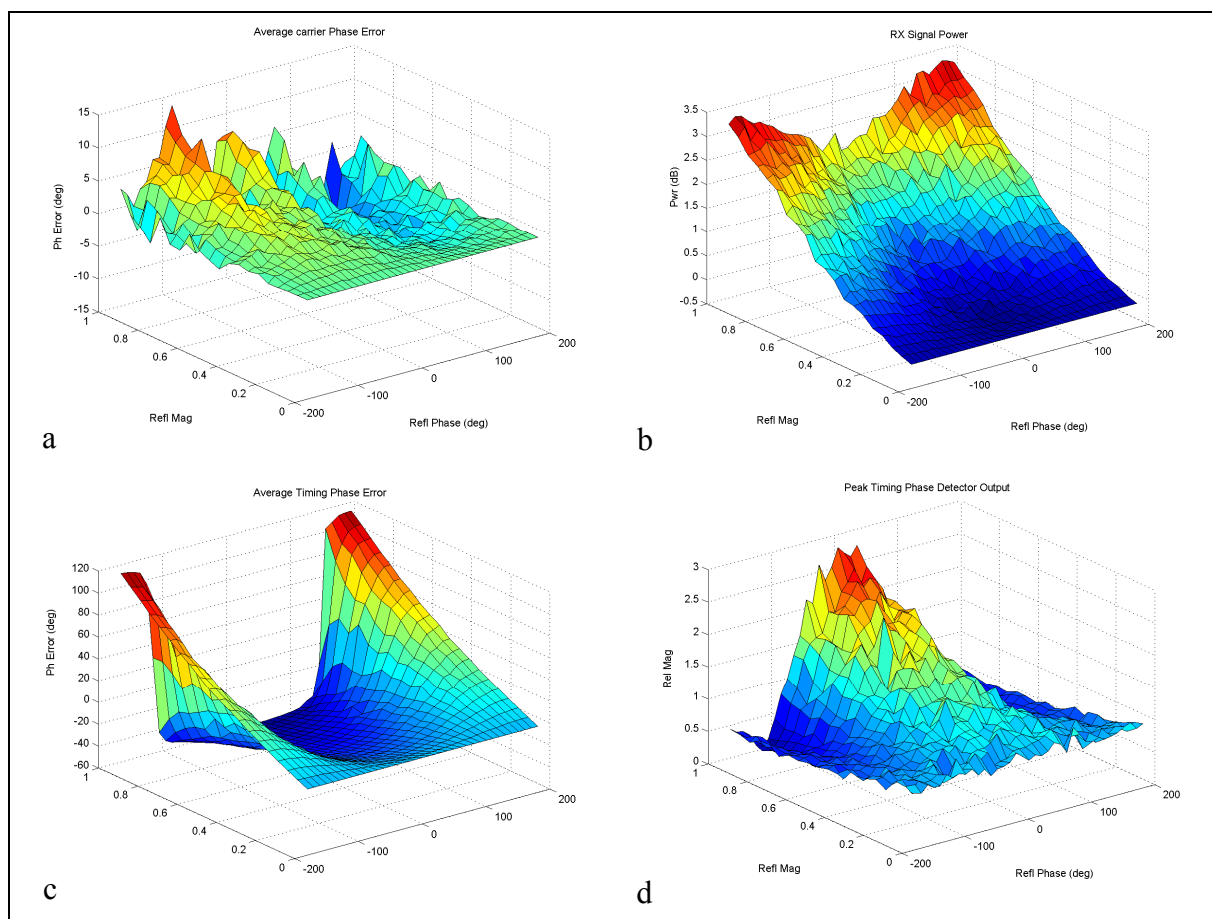


Figure A.35 Delay 1.7 symbols. a) average carrier phase error; b) received signal power; c) average timing phase error; d) peak timing phase detector output.

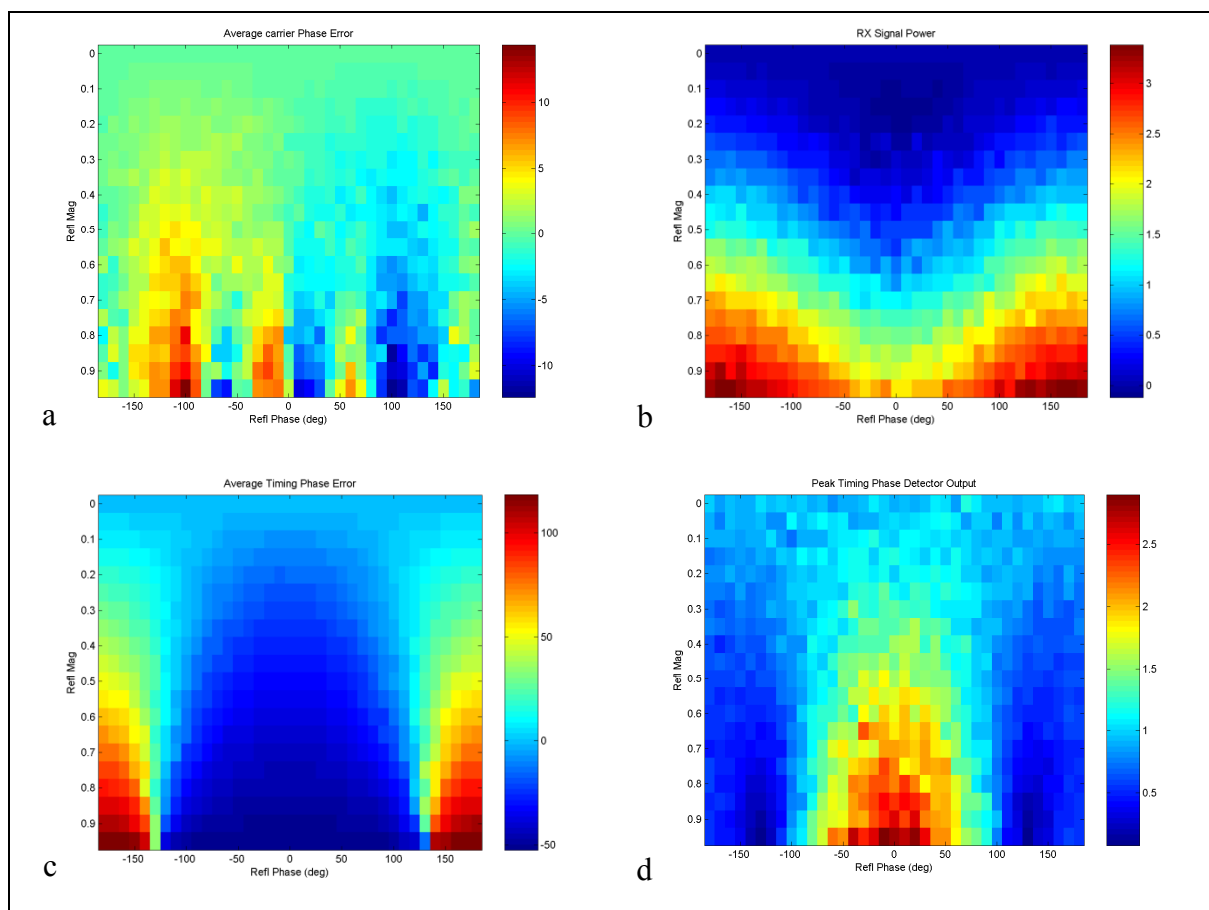


Figure A.36 Delay 1.7 symbols. a) average carrier phase error; b) received signal power; c) average timing phase error; d) peak timing phase detector output.

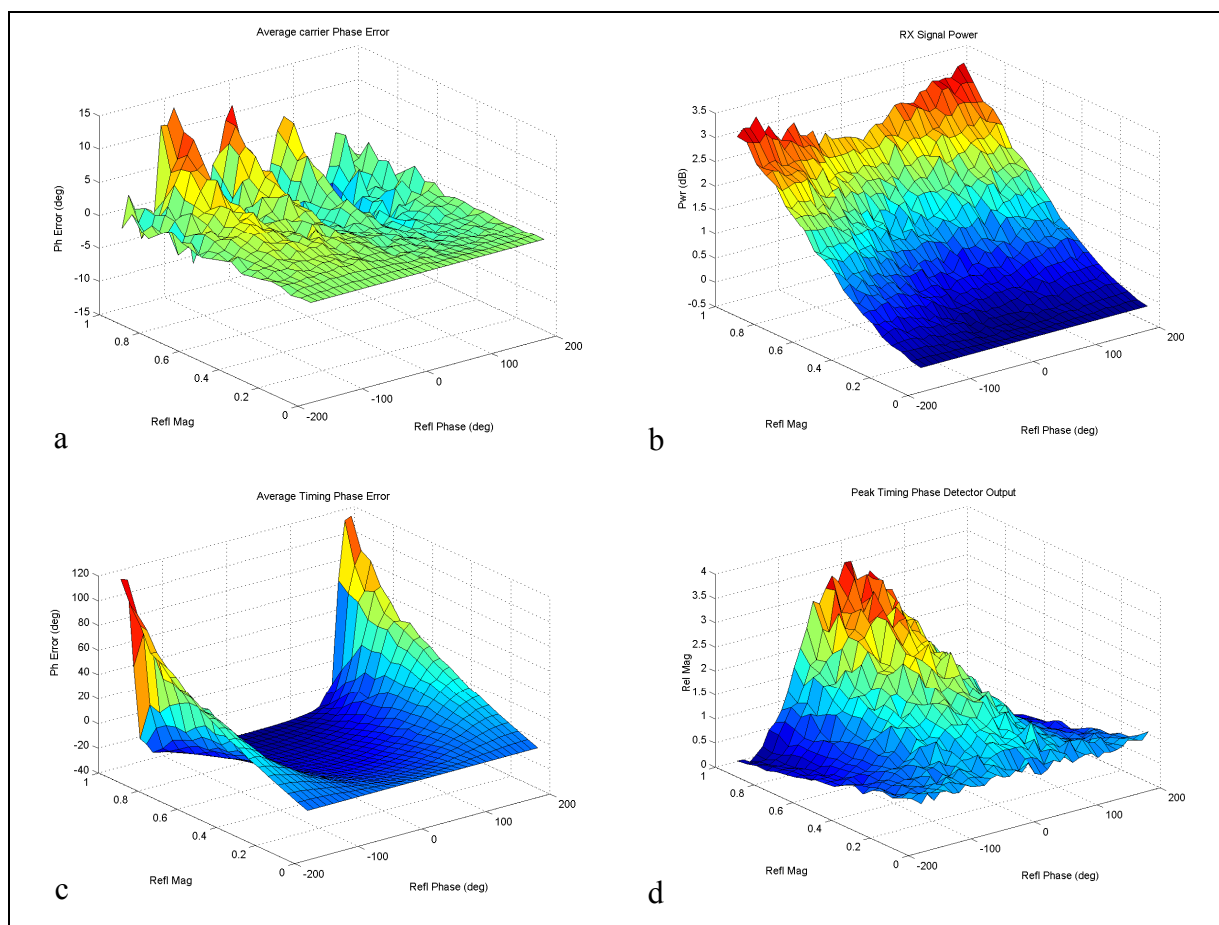


Figure A.37 Delay 1.8 symbols. a) average carrier phase error; b) received signal power; c) average timing phase error; d) peak timing phase detector output.

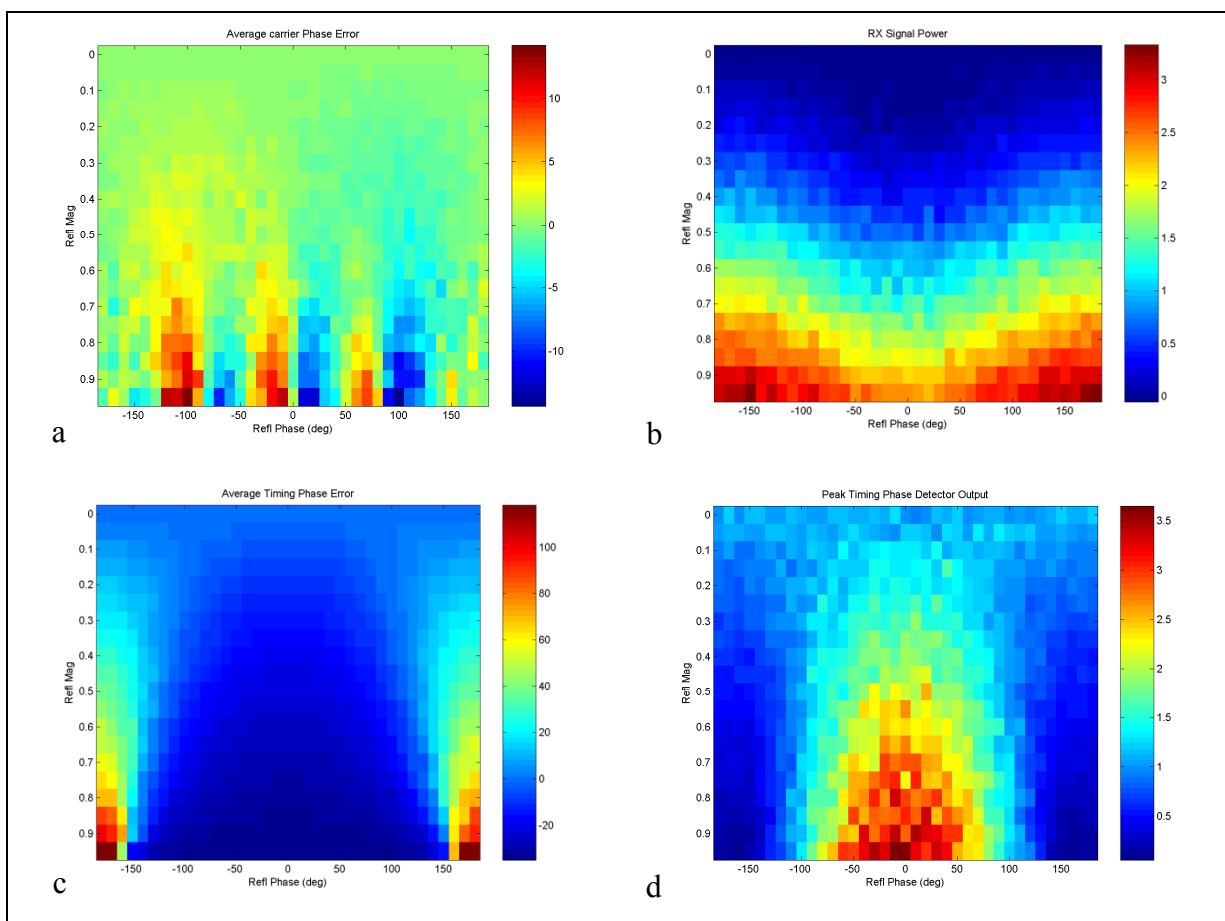


Figure A.38 Delay 1.8 symbols. a) average carrier phase error; b) received signal power; c) average timing phase error; d) peak timing phase detector output.

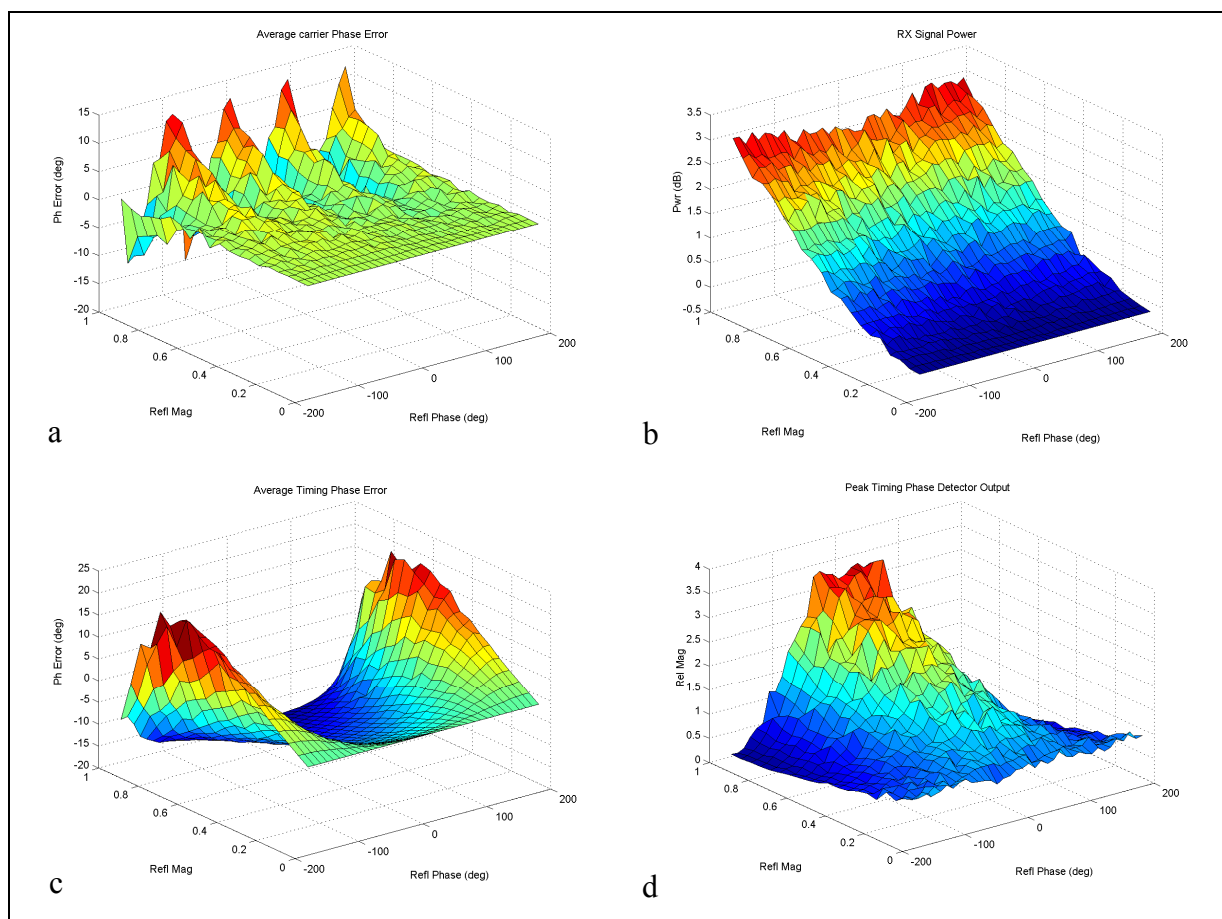


Figure A.39 Delay 1.9 symbols. a) average carrier phase error; b) received signal power; c) average timing phase error; d) peak timing phase detector output.

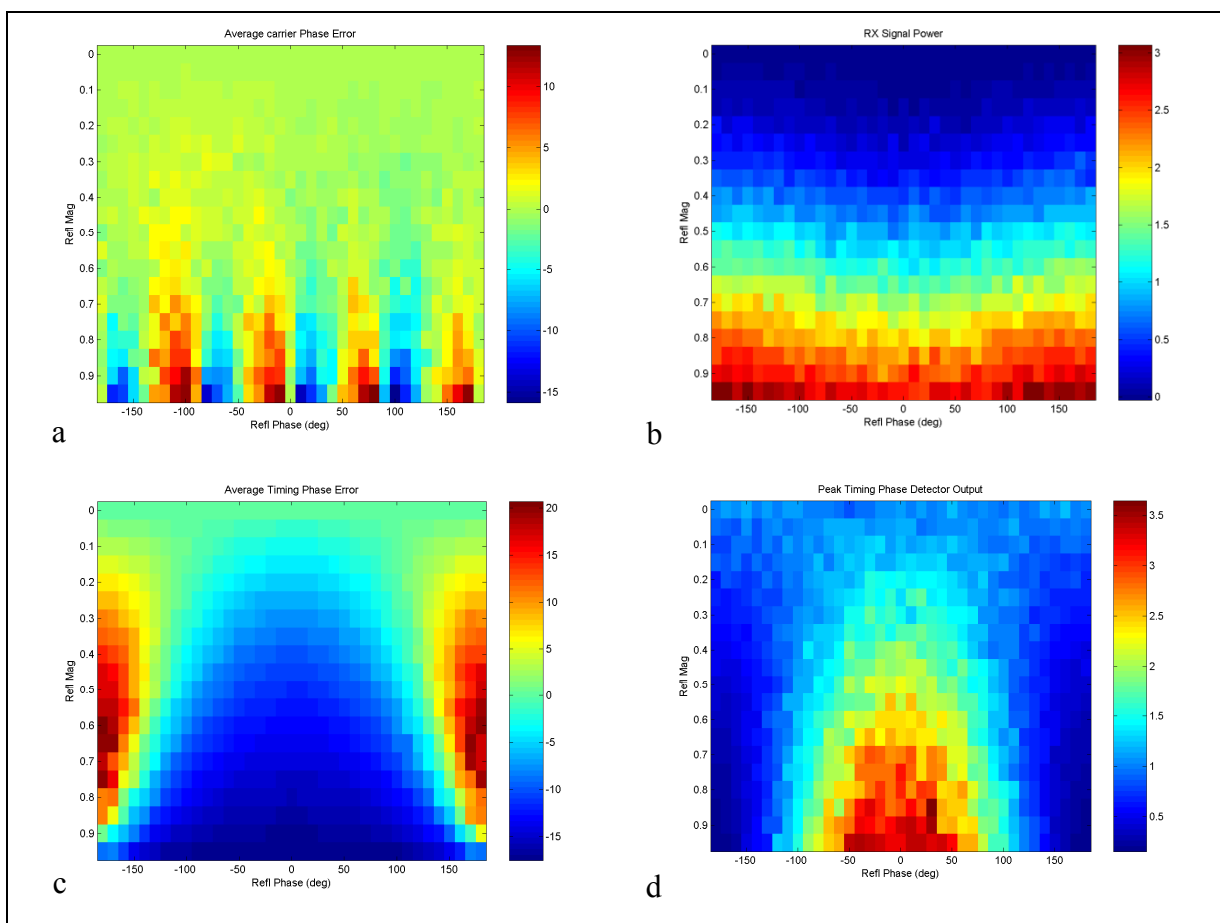


Figure A.40 Delay 1.9 symbols. a) average carrier phase error; b) received signal power; c) average timing phase error; d) peak timing phase detector output.

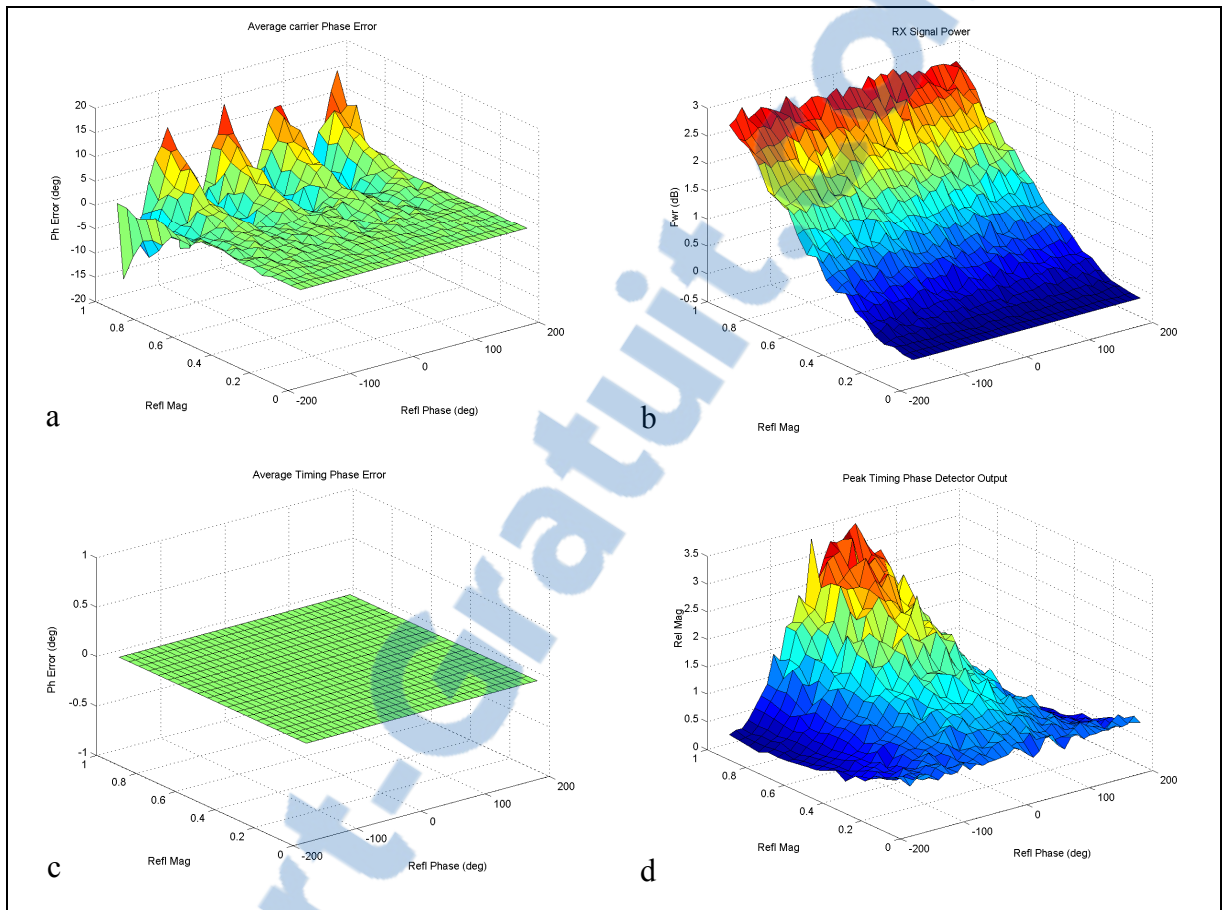


Figure A.41 Delay 2.0 symbols. a) average carrier phase error; b) received signal power; c) average timing phase error; d) peak timing phase detector output.

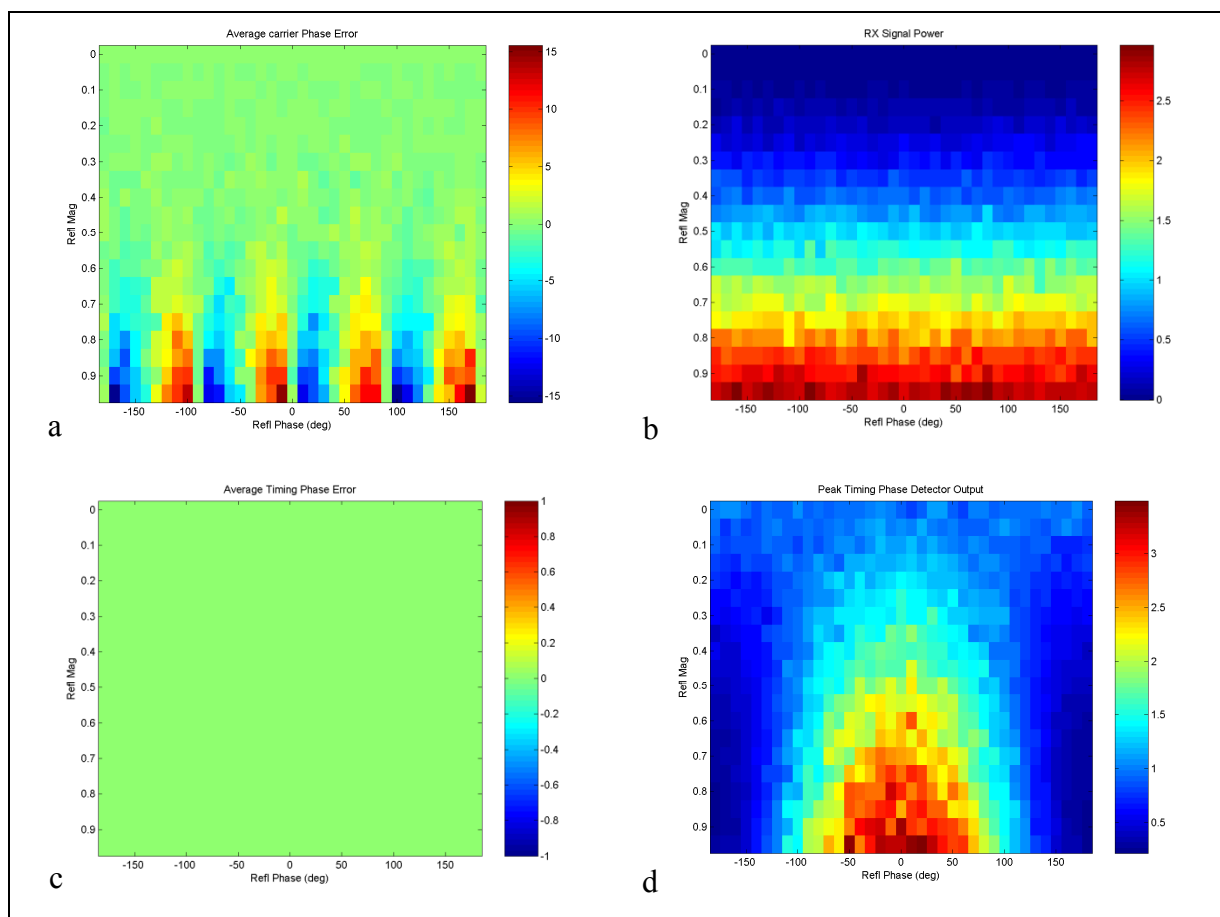


Figure A.42 Delay 2.0 symbols. a) average carrier phase error; b) received signal power; c) average timing phase error; d) peak timing phase detector output.

REFERENCES

- [1] Balanis, Constantine A. 1982. "Antenna Theory Analysis and Design". Harper & Row, Publishers, New York, pp 63 – 65.
- [2] Bullington, Kenneth. 1947. "Radio Propagation at Frequencies Above 30 Megacycles". Proceedings of the IRE, vol. 35, Oct. 1947, pp. 1122 – 1136.
- [3] Egli, John J. 1957. "Radio Propagation Above 40 MC Over Irregular Terrain". Proceedings of the IRE, vol.45, Oct. 1957, pp. 1383 – 1391.
- [4] Deygout, Jacques. 1966. "Multiple Knife-Edge Diffraction of Microwaves". IEEE Transactions on Antennas and Propagation, vol. AP-14, no. 4, July 1966, pp. 480 – 490.
- [5] Balanis, Constantine A. 1989. "Advanced Engineering Electromagnetics". John Wiley & Sons, 1989, pp. 180 – 220.
- [6] McNamara, D. A., Pistorius, C. W. I., Malherbe, J. A. G. 1990. "Introduction to the Uniform Geometrical Theory of Diffraction". Artech House, 1990.
- [7] Freeman, Roger L. 1987. "Radio System Design for Telecommunications (1 – 100 GHz)". John Wiley & Sons, 1987
- [8] White, Robert F. 1970. "Engineering Considerations for Microwave Communications Systems". Lenkurt Electric Co. Inc., June 1970.
- [9] Lee, William C. Y. 1982. "Mobile Communications Engineering". McGraw-Hill Inc., 1982.
- [10] Bertoni, Henry L. 2000. "Radio Propagation for Modern Wireless Systems". Prentice Hall PTR. New Jersey, 2000.
- [11] Durgin, Gregory D. 2003. "Space-Time Wireless Channels". Prentice Hall PTR, New Jersey, 2003
- [12] Constantinu, C. C., Mughal, M. J. 2005. "On the Modeling of Reflected Energy From Building Faces in Microcellular Mobile Radio Planning Tools". IEEE Transactions on Antennas and Propagation, Vol. 53, No. 8, August 2005.
- [13] Van Dooren, G. A. J. 1994. "A Deterministic Approach to the Modelling of Electromagnetic Wave Propagation in Urban Environments". PhD Thesis, Technische Universiteit Eindhoven, March 29, 1994.
- [14] Bertoni, H. L., Pongsalamane, P., Chen, Z. 2002. "Defining and Computing the Diffuse Scattering Coefficient for Building Surfaces". Proceedings of the XXVII th

General Assembly of the International Union of Radio Science, p. 1407, August 2002.

- [15] Kleintz, Michael. 1992. "Diffraction of Microwaves at Rectangular Facades of Buildings With and Without Ground Reflections Fresnel-Kirchhoff Approximation" Deutsche Forschungsanstalt fuer Luft- und Raumfahrt, Oberpfaffenhofen (Germany), November 1992.
- [16] Sun, Q. Tan, S. Y., Teh, Kah C. 2005. "Analytical Formulae for Path Loss Prediction in Urban Street Grid Microcellular Environments"
- [17] Xu, Ying, Tan, Qiwu, Erricolo, Danilo, Uslenghi, Peirgeorgio L. E. 2005. "Fresnel-Kirchhoff Integral for 2-D and 3-D Path Loss in Outdoor Urban Environments". IEEE Transactions on Antenna and Propagation, Vol. 53 No. 11, November 2005.
- [18] Jiang, L., Tan, S. Y. 2004. "Simple geometrical-based AOA model for mobile communication Systems". Electronics Letters, Vol. 40, No. 19, 16th September, 2004.
- [19] Xu, Y., Tan, Q., Erricolo, D., Uslenghi, P. L. E. 2004. "Experimental verification of a 3-D propagation model based on Fresnel-Kirchhoff integral". IEEE Antennas and Propagation Society International Symposium, June 2004.
- [20] Xu, Y., Tan, Q., Erricolo, D., Uslenghi, P. L. E. 2003. "3D propagation in urban environments using Fresnel-Kirchhoff integrals". 2003 IEEE Topical Conference on Wireless Communication Technology. 2003.
- [21] Tan, S. Y., Tan, M. Y., Tan, H. S. 2000. "Multipath Delay Measurements and Modeling for Interfloor Wireless Communications". IEEE Transactions on Vehicular Technology, Vol. 49, No. 4, July 2000.
- [22] Tan, S. Y., Tan, H. S. 1997. "An Improved Three-Dimensional Propagation Model and Measurements for Indoor Wireless Communication Systems". 10th International Conference on Antennas and Propagation, IEE, April, 1997.
- [23] Ding, M. S., Al-Nuaimi, M. O. 1996 "Characterisation of building reflection and scatter of microwaves using Fresnel-Kirchhoff diffraction theory". 26th European Microwave Conference. September 1996.
- [24] Al-Nuaimi, M. O., Ding, M. S. 1994. "Prediction Models and Measurements of Microwave Signals Scattered from Buildings". IEEE Transactions on Antennas and Propagation, Vol. 42, No. 8, August 1994.
- [25] Gutierrez-Meana, J., Las-Heras, F., Martinez-Lorenzo, J. A., Martinez, D., Campos, A. "Radio Coverage Analysis in Urban Scenarios with PO". IEEE International Symposium on Antennas and Propagation and USNC/URSI meeting, July 2008.

- [26] Peters, Len Jr., Lentz, R. 1971. "Near-Zone Scattering". Communications, IEEE Transactions on Antennas and Propagation, September 1971.
- [27] Burdette, E. C., Ryan, C. E. Jr. 1974. "Near-Zone Scattering by Plates, Cylinders, and Cones". Communications, IEEE Transactions on Antennas and Propagation, November 1974.
- [28] Cox, D. C. 1973. "910 MHz Urban Mobile Radio Propagation: Multipath Characteristics in New York City". IEEE Transactions on Communications, Vol. 21, November 1973.
- [29] Erceg, V., Hari, K. V. S. et al. 2001. "Channel Models for Fixed Wireless Applications". Technical Report, IEEE 802.16 Broadband Wireless Access Working Group, January 2001.
- [30] Saleh, A., Valenzuela, R. A. 1987. "A statistical model for indoor multipath propagation". IEEE Journal of Selected Areas in Communications, Vol. 5, February, 1987.
- [31] Ertel, R. B., Cardieri, P., Sowerby, K. W., Rapaport, T. S., Reed, J. H. 1998. "Overview of Spatial Channel Models for Antenna Array Communication Systems". IEEE Personal Communications, February 1998, pp 10 – 22.
- [32] Liberti, J. C., Rapaport, T. S. 1996. "A Geometrically Based Model for Line-of-Sight Multipath Radio Channel". Vehicular Technology Conference, Atlanta, 1996, pp 844-848.
- [33] Rummler, W. D., Coutts, R. P., Linger, M. 1986 "Multipath Fading Channel Models for Microwave Digital Radio". IEEE Communications Magazine, November 1986.
- [34] Applied Signal Technology Inc. 1996. "Results of Laboratory and Field Measurements of Propagation Effects for On-the-Move High Capacity Trunk Radio. Applied Signal Technology Inc., November 1996.
- [35] Born, Max, Wolf, Emil. 1980. "Principles of Optics, Electromagnetic Theory of Propagation Interference and Diffraction of Light, Sixth Edition". Pergamon Press, 1980.
- [36] Beckmann, Petr, Spizzichino, Andre. 1987. "The Scattering of Electromagnetic Waves from Rough Surfaces". Artech House, 1987.
- [37] Crispin, J. W. Jr., Siegel, K. M. 1968. "Methods of Radar Cross-Section Analysis". Academic Press, 1968.

- [38] Henderson, Floyd M., Lewis, Anthony J. 1998. "Principles and Applications of Imaging Radar, Manual of Remote Sensing, Third Edition, Vol. 2". John Wiley & Sons, Inc. 1998.
- [39] Ulaby, F. T., Elachi, C. (Editors). 1990. "Radar Polarimetry for Geoscience Applications". Artech House Inc. 1990.
- [40] Van Valkenburg, M. E. (Editor-in Chief). 1983. "Reference Data for Engineers: Radio, Electronics, Computer, and Communications, Eighth Edition". SAMS, Prentice Hall Computer Publishing, 1983 pp. 32-7, 32-8.
- [41] Westman, H. P. (Editor). 1972. "Reference Data for Radio Engineers, Fifth Edition". Howard W. Sams & Co. Inc. 1972 pp. 25-46 to 25-48.
- [42] Proakis, John G. 2001. "Digital Communications, Fourth edition". McGraw Hill, 2001.
- [43] Meyr, Heinrich, Moeneclay, Marc, Fechtel, Stefan A. 1998. "Digital Communication Receivers". John Wiley & Sons Inc. 1998.
- [44] Haykin, Simon. 2001. "Communication Systems, Fourth Edition". John Wiley & Sons Inc. 2001
- [45] Franks, L. E. 1980. "Carrier and Bit Synchronization in Data Communication – A Tutorial Review". IEEE Transactions on Communications, Vol. COM-28, No. 8, August 1980, pp 1107 – 1121.
- [46] Dixon, R. C. 1976. "Spread Spectrum Systems". John Wiley & Sons Inc, 1976.
- [47] Simon, Marvin K., Omura, Jim K., Scholtz, Robert A., Levitt, Barry K. 1985. "Spread Spectrum Communications". Computer Science Press, 1986.
- [48] Schulze, Henrik, Lueders, Christian, 2005. "Theory and Applications of OFDM and CDMA, Wideband Wireless Applications". John Wiley and Sons, Ltd., 2005.
- [49] Schelkunoff, S. A. 1943. "Electromagnetic Waves". D. Van Nostrand Co. Inc. 1943, pp366 – 367.
- [50] Fitch, T. A. 1986. "The Effects of Rayleigh Distributed Multipath Fading on Carrier Recovery Performance". 36th IEEE Vehicular Technology Conference, 1986, pp 252 – 255.
- [51] Gini, Fulvio, Giannakis, Georgios B. 1998. "Frequency Offset and Symbol Timing Recovery in Flat-Fading Channels: A Cyclostationary Approach". IEEE Transactions on Communications 1998 Vol. 46, No. 3, March 1998, pp. 400 – 411.

- [52] Brandao, T., Lopes, L. B., McLernon, D. C. 1994. "Method for Timing Recovery in Presence of Multipath Delay and Interference". *Electronics Letters*, No. 30, pp. 1028 – 1029.
- [53] Chuang, Justin C. I. 1987. "The Effects of Multipath Delay Spread on Timing Recovery". *IEEE Transactions on Vehicular Technology*, Vol. VT-35, No. 3, August 1987, pp. 135 – 140.
- [54] Van Nee, R. D. J. 1993. "Spread Spectrum Code and Carrier Synchronization Errors Caused by Multipath and Interference". *IEEE Transactions on Aerospace and Electronic Systems*, Vol. 29, No. 4, October 1993, pp. 1359 – 1365.
- [55] Boyer, P. 2004. "Performance Based on Selective Multipath Reception". *IEEE Transactions on Communications*, Vol. 52, No.2, February 2004.
- [56] Gardner, Floyd M. 1986. "A BPSK/QPSK Timing-Error Detector for Sampled Receivers". *IEEE Transactions on Communications*, Vol. COM-34, No. 5, May 1986, pp. 423 – 429.
- [57] <http://wireless.per.nl/reference/chapter05/cdma/rake.htm> (Part of JPL Reference Website on Wireless Communication <http://wireless.per.nl/reference/about.htm>) 2009
- [58] IEEE. 2004. "IEEE 802-16-2004 - IEEE Standard for Local and Metropolitan Area Networks Part 16: Air Interface for Fixed Broadband Wireless Access Systems". Institute of Electrical and Electronics Engineers, 2004.
- [59] Wang, F., Ghosh, A., Sankaran, C., Fleming, P. J. "Mobile WiMAX Systems: Performance and Evolution". *IEEE Communications Magazine*, October, 2008.
- [60] Lucky, Robert W. 1973. "A Survey of the Communication Theory Literature: 1968 – 1973". *IEEE Transactions on Information Theory*, Vol. IT-19, No. 5, November 1973, pp. 725 – 739.
- [61] Osman, O., Ucan, O. N., "Contemporary Coding Techniques and Applications for Mobile Communications". CRC Press, 2009.